Dark Matter, Inflation and Baryogenesis in Supersymmetric extensions of the Standard Model

Ernestas Pukartas

Physics

Department of Physics

Lancaster University

Oct 2014

A thesis submitted to Lancaster University for the degree of Doctor of Philosophy in the Faculty of Science and Technology

Declaration

This thesis is my own work and no portion of the work referred to in this thesis has been submitted in support of an application for another degree or qualification at this or any other institute of learning.

Acknowledgements

I would like to thank all the people without whom this work would never have seen the light of day.

I feel enormously indebted to my supervisor Dr. Anupam Mazumdar, my mentor and friend, for his patience, tenacity, effort and words of encouragement in times of despair. Thank you for the multitude of fruitful conversations we shared, the interesting projects offered and for the freedom I was given during my studies.

I am very grateful to all the collaborators I had the pleasure of working with. Csaba Balázs, Celine Bœhm, Sofiane Boucenna, Sayantan Choudhury, Jonathan Da Silva, Bhupal Dev, Graham White deserve special mention.

Further thanks to the members of our cosmology group: Amjad Ashoorioon, Aindriú Conroy, Konstantinos Dimopoulos, David Lyth, John McDonald, Saleh Qutub, Arron Rumsey, Philip Stephens, Spyridon Talaganis, Ilia Teimouri and Lingfei Wang. You are the reason my time at Lancaster was so enjoyable.

To say that I feel a heartfelt gratitude to my parents and Rasa, my fiancé, would be an understatement. Any attempt to express my appreciation for your lifelong and manifold support would be incomplete.

Ačiū Jums!

Finally, I would like to extend my gratitude to STFC and Lancaster University for funding me throughout my studies.

List of Abbreviations

AMS – Alpha Magnetic Spectrometer

AMSB – Anomaly Mediated SUSY Breaking

ATIC – Advanced Thin Ionization Calorimeter

BSM – Beyond Standard Model

CMB – Cosmic Microwave Background

CKM Matrix – Cabibbo–Kobayashi–Maskawa Matrix

CMSSM – Constrained MSSM

DD – Direct Detection

d.o.f. – degree of freedom

(C)DM – (Cold) Dark Matter

EW – Electroweak

Fermi–LAT – Fermi Large Area Telescope

GMSB – Gauge Mediated SUSY Breaking

GR – General Relativity

GUT – Grand Unified Theories

ID – Indirect Detection

LEP – Large Electron–Positron Collider

LH – Left Handed

LHC – Large Hadron Collider

LKP – lightest Kaluza–Klein particle

LSP – Lightest Supersymmetric Particle

MSSM – Minimal Supersymmetric Standard Model

NLSP – Next–to–LSP

NMSSM – Next–to–Minimal MSSM

NUHMII – MSSM with non Universal Higgs Masses

PAMELA – Payload for Antimatter Matter Exploration and Light-Nuclei Astrophysics

PQ limit/symmetry/mechanism – Peccei–Quinn limit/symmetry/mechanism

p19MSSM – phenomenological MSSM with 19 free input parameters

RGE – Renormalization Group Equation

RH – Right Handed

SD – Spin Dependent

SI – Spin Independent

SM – Standard Model

SUSY – Supersymmetry

VEV – Vacuum Expectation Value

WIMP – Weakly Interacting Massive Particle

Abstract

This thesis reviews building blocks of the supersymmetric particle physics models and how the Standard Model (SM) drawbacks can be addressed within this framework. In particular, the emphasis is put on exploring the regions, where the neutralino ($\widetilde{\chi}_1^0$) dark matter (DM), gauge invariant inflation and electroweak baryogenesis could coexist.

We chose a few benchmark points within the minimal supersymmetric SM (MSSM) with non–universal Higgs masses to illustrate how the allowed regions for the DM relic abundance and the particle physics constraints could possibly pin down the masses of supersymmetric inflaton candidates, m_ϕ, and the vacuum expectation value (VEV) of the inflaton field at the beginning of inflation ϕ_0. Similarly, we probed the MSSM augmented with singlino component, NMSSM, to find how the requirement to achieve first order electroweak phase transition constraint NMSSM free parameters and what the subsequent implications on the DM phenomenology and supersymmetric inflation are.

Since certain direct detection (DD) searches hint at the light $\widetilde{\chi}_1^0$ DM, complementary studies were carried out to explore the lower bounds on DM mass, which yielded $m_{\widetilde{\chi}_1^0} \gtrsim 10$ GeV within phenomenological MSSM (pMSSM) and $m_{\widetilde{\chi}_1^0} \gtrsim 1$ GeV within NMSSM setup.

Contents

Chapter 1

Introduction

One of the most successful theories in physics, the Standard Model of Particle Physics, has recently been further bolstered by the discovery of the fundamental Higgs scalar in the ATLAS [1] and CMS [2] detectors at the Large Hadron Collider (LHC). However, the SM is also known to have a number of drawbacks. The origin of neutrino masses [3, 4, 5], inflation [6, 7, 8], existence of DM [9, 10] and the necessity of a strong first order electroweak (EW) phase transition in order to generate matter antimatter asymmetry [11, 12] are examples where the SM fails. Moreover, metastable EW vacuum [13], fine–tuning of the Higgs scalar mass, strong CP problem and the smallness of the Θ parameter [14, 15] in the kinetic gauge term of the SM Lagrangian, which is constrained by the neutron dipole moment, render the theory even less appealing.

Probably the most compelling theory, that has a potential to resolve the aforementioned issues, is Supersymmetry (SUSY). SUSY is a spacetime symmetry between bosons and fermions. With the help of a fermionic SUSY generator, every fermion (boson) of the SM is turned into boson (fermion). The emergence

of additional degrees of freedom (d.o.f.), collectively dubbed as sparticles, have many profound implications. They alter equations that govern the energy dependence of the gauge couplings in a way that allows their unification at the GUT scale [1]. The quadratic divergences, appearing in the Higgs mass corrections due to coupling to fermions, are cancelled by the Higgs scalar coupling to their respective supersymmetric counterparts, leaving only logarithmic corrections and thus stabilizing its mass. The necessity to stabilize the proton against decay, leads to the introduction of a discrete symmetry that also makes the lightest supersymmetric particle (LSP) stable. In the regions of the parameter space of SUSY models, where the LSP is colour and electrically neutral, it becomes a natural DM candidate. Moreover, certain condensates made up of sparticles can be identified as inflaton candidates.

In this thesis we concentrate on trying to explain DM, inflation and baryogenesis in a coherent fashion within the SUSY framework.

• *Dark Matter*: The evidence for DM comes from various astrophysical observations such as the galaxy rotation curves [10], gravitational lensing [16, 17, 18], velocity dispersion of galaxies in galaxy clusters and superclusters [19, 20, 21]. Another well known example used as a proof for DM existence is the bullet cluster. It consists of two colliding galaxy clusters passing through each other. After the collision, hot X-ray emitting gas that dominates baryonic matter in clusters slows and separates from their respective clusters. However, the lensing maps show that the dominant mass component remains concentrated around the galaxies rather than intergalactic gas [22, 23, 24]. It is important to mention though,

[1] The GUT scale, often denoted as $\Lambda_{\rm GUT}$, is the scale where the strong and EW forces are of the same strength. In SUSY models $\Lambda_{\rm GUT} \simeq 10^{16}$ GeV. To compare, the LHC is now probing physics at 10^4 GeV.

that lensing maps of the bullet cluster can also be explained in modified gravity theories by scaling the gravitational constant with an interpolation function and adding ordinary SM neutrinos of 2 eV mass as a hot DM [25]. From studies of the cosmic structure formation on large scales it is known that the DM has to be non–relativistic otherwise those structures either would have been washed out during their formation or would be of a different size as compared to what we observe [26, 27]. Here we will concentrate on the most popular DM candidate within SUSY – the lightest neutralino $\widetilde{\chi}_1^0$. There are three main methods of how the neutralino could be detected: collider searches, direct and indirect detection (DD/ID) experiments. Since the neutralino interacts very weakly, the sign of it in the collider detectors would be a large missing energy. DD experiments rely on registering very rare interactions between the DM particles and the nucleons in the detector. In fact, the SI nucleon–$\widetilde{\chi}_1^0$ scattering cross section can be schematically written as $\sigma^{SI} \propto [f_p Z + f_n(A-Z)]^2$, where Z is atomic number of the active material in detector, A is number of nucleons and $f_{p(n)}$ is the relative coupling strength of DM to the protons (neutrons). From here follows, that in order to have a bigger chance of interaction, large amount of active material in the detectors is needed. Finally, the ID experiments, that are either orbit or ground based, try to register the excesses and anomalies in the cosmic rays, such like an increase of positrons or antiprotons, or look for the γ–rays that could be identified as the decay or annihilation products of the DM.

• *Inflation*: Inflation is conceived to explain such observationally well established facts like why our Universe is so close to flat, why the CMB is smooth to about 1 part in 100,000 even though today the size of the Hubble horizon at the time of decoupling corresponds to $\sim 1^\circ$ and therefore any two patches separated by larger

angle were causally disconnected, or why we do not see the magnetic monopoles, that are predicted by the GUT theories [6, 7, 8]. The inflaton is a scalar field and, as such, Higgs stands out as the only viable candidate from the SM perspective. In SUSY, the inflaton scalar candidate can be identified as a condensate of squarks or sleptons along the certain D–flat directions of the scalar potential[1] [28, 29]. Lifting these flat directions by the soft breaking and non–renormalizable terms allows one to construct an inflationary potential with an inflection point that governs the dynamics of the inflaton in the Early Universe and yields the right values for the cosmological observables such as: the Hubble expansion rate of the Universe $\mathcal{H}$, the amplitude of density perturbations in the CMB δ_H, the spectral tilt of the CMB power spectrum n_s and tensor–to–scalar ratio r.

• *Baryogenesis:* The necessity for BSM physics in order to explain the matter antimatter asymmetry comes from the fact that within the SM, it requires the Higgs to be lighter than 46 GeV [30], which is in disagreement with the experimental bounds [31, 32]. Moreover, the only source of the CP–violation in SM is the CKM (Cabibbo–Kobayashi–Maskawa) matrix [33, 34], which is not enough to yield the total matter antimatter asymmetry. Finally, in SM framework, the EW phase transition is not strongly first order. In this thesis we will show that strongly first order phase transition can be achieved within NMSSM, as the new SM gauge singlet provides more flexibility and the order parameter is then determined by the singlet sector and becomes independent of the SM–like Higgs mass.

In the collider searches, SM particles are accelerated to the high energies, and if this would turn out to be enough to excite SUSY d.o.f. then they would

[1] F and D–flat directions are explained in Section 4.4.1.

cascade decay into the lighter particles, that could be traced directly, or by the excess of missing energy, see [35, 36, 37, 38, 39, 40, 41] and references therein. Unfortunately, there have been no positive detection signals in the experimental searches and, as it stands now, SUSY hasn't been found [31, 32]. The fact that SUSY particles haven't been observed implies that they must be much heavier than their SM partners. Actually, LEP (Large ElectronPositron Collider) already ruled out sleptons lighter than ∼100 GeV, and LHC pushed the scale of squarks up to 2 TeV [1] [42]. This in turn pushes the SUSY scale higher and makes it a more fine–tuned theory [2]. Currently, SUSY models that respect universality conditions at the GUT scale, such as for example mSUGRA or CMSSM[3], attract less attention and those with the input at the low scale, like pMSSM (also called SUSY without prejudice), NMSSM and others are more actively investigated.

Here we will try to build a unified picture within a SUSY framework that would encompass DM, inflation and baryogenesis, meanwhile satisfying all known constraints imposed by cosmology, particle physics, DD and ID experiments.

The thesis is organised in the following manner. In Chapter 2, the building blocks of the Standard Model and the mechanism of EW phase transition are reviewed. Besides the stunning success and predictive power of the SM, we will also elaborate on some of the phenomena, which are already briefly mentioned in the beginning of the introduction, as they clearly point out limitations of the

[1] It should be noted that the exclusion limits are often model and/or analysis dependent and in many cases can be avoided to a certain extent. Generic bounds on the scale of SUSY are often given within CMSSM framework. In order to simplify analysis the universality conditions and hierarchies, especially between LSP and next–to–LSP (NLSP) are assumed. Great simplification also can be achieved by tuning the spectrum of sparticles (like for e.g. in natural or split SUSY cases), thus excluding many decay/annihilation channels. See for example [31, 32, 42, 43, 44, 45] and references therein.

[2] A way to parametrize fine–tuning will be discussed in Section 4.4.4.

[3] More discussion on mSUGRA and CMSSM can be found in Section 4.5.1.

theory. In Chapter 3, we review the standard model of cosmology, problems with the Big Bang theory and how inflation could resolve them. In the next, Chapter 4, the theory of supersymmetry is analysed. Starting with SUSY algebra and its implications we later move on to understand the key principles in building the supersymmetric toy model. Afterwards, the MSSM and its various extensions and modifications are discussed. In Chapter 5, the latest theoretical and experimental advances in the DM searches are covered. At the end of this chapter the possibility of light neutralino DM is explored trying to explain the positive signal claims of some DD experiments. In Chapter 7, the gauge invariant supersymmetric inflaton candidates are introduced. The idea of how the Higgs mass can directly pin down the mass of the inflaton and the scale of inflation is presented and developed in great detail. Finally, in Chapter 8, baryogenesis is discussed. The model that is explored puts tight constraints on some of the parameters that directly control the mass of the neutralino and the top quark mass. This immediately has many of the phenomenological consequences, most importantly via DM relic abundance and Higgs physics. Finally, we explore the parameter space of the next–to–minimal MSSM, where all three phenomena: strongly first order phase transition, DM and inflation coexist.

Chapter 2

Standard Model of Particle Physics

Thus far the Standard Model is one of the most successful theories in physics. It accurately describes elementary particles and the three fundamental forces – strong, weak and electromagnetic, that govern the interactions amongst the matter particles. The SM model is constructed by collecting all the renormalizable terms in the Lagrangian, which respect invariance under the Lorentz symmetry and the postulated $SU(3)_c \times SU(2)_L \times U(1)_Y$ gauge group transformations [46, 47, 48]. In principle, non–renormalizable terms could also be added, but they would not bear any phenomenological contribution at the low scale due to their suppression by $1/\Lambda^n$ prefactor, where Λ is the scale of new physics and n can be determined by power counting. Some of the biggest successes of the SM are the prediction of the muon anomalous magnetic moment, the existence of the top quark, τ neutrino, and the recently discovered Higgs scalar. Nevertheless, by now there is plenty of evidence that this is just an effective theory and that a

more fundamental one should be realised in nature [49, 50]. In this chapter, we will review the building blocks of the SM, the mechanism of the EW symmetry breaking, how radiative corrections can break the symmetry and observations that are difficult or even impossible to explain within SM framework.

2.1 Constructing the Standard Model

The gauge group of a SM model is $SU(3)_c \times SU(2)_L \times U(1)_Y$. The $SU(3)_c$ symmetry controls interactions of the coloured particles and thus describes quantum chromodynamics and the $SU(2)_L \times U(1)_Y$ refers to the EW part that gets broken during EW symmetry phase transition in the following manner:

$$SU(2)_L \times U(1)_Y \to U(1)_{em}. \tag{2.1}$$

Index L means that the nature differentiates between left and right handed particles. In other words, the LH fermions are assigned the so called weak isospin quantum number and transform non–trivially under the weak interactions whereas the RH fermions are treated as singlets. To accommodate this experimentally well established fact the particle content of the standard model is chosen to be:

$$\begin{aligned}
Q_{i,L} &= \begin{pmatrix} u_L \\ d_L \end{pmatrix}, \begin{pmatrix} c_L \\ s_L \end{pmatrix}, \begin{pmatrix} t_L \\ b_L \end{pmatrix}, \\
u_{i,R} &= u_R, c_R, t_R, \\
d_{i,R} &= d_R, s_R, b_R, \\
L_{i,L} &= \begin{pmatrix} \nu_{e,L} \\ e_L \end{pmatrix}, \begin{pmatrix} \nu_{\mu,L} \\ \mu_L \end{pmatrix}, \begin{pmatrix} \nu_{\tau,L} \\ \tau_L \end{pmatrix}, \\
e_{i,R} &= e_R, \mu_R, \tau_R,
\end{aligned} \tag{2.2}$$

where subscripts L and R show the handedness of a particle and $i = 1, 2, 3$ denotes generation indices. The $SU(N)$ group has $N^2 - 1$ generators, and thus the gauge fields corresponding to each generator of $SU(3)_c \times SU(2)_L \times U(1)_Y$ are:

$$\begin{aligned} SU(3)_L &\to G^1_\mu, G^2_\mu, ...G^8_\mu, \\ SU(2)_L &\to W^1_\mu, W^2_\mu, W^3_\mu, \\ U(1)_Y &\to B_\mu. \end{aligned} \tag{2.3}$$

The field strength tensors take the following form:

$$\begin{aligned} G^i_{\mu\nu} &\equiv \partial_\mu G^i_\nu - \partial_\nu G^i_\mu + g_3 f^{abc} G^b_\mu G^c_\nu, \\ W^i_{\mu\nu} &\equiv \partial_\mu W^i_\nu - \partial_\nu W^i_\mu + g_2 f^{abc} W^b_\mu W^c_\nu, \\ B_{\mu\nu} &\equiv \partial_\mu B_\nu - \partial_\nu B_\mu. \end{aligned} \tag{2.4}$$

The last terms in $G^i_{\mu\nu}$ and $W^i_{\mu\nu}$ arise from the fact that unlike $B_{\mu\nu}$ those fields are non–Abelian. Complete SM Lagrangian can be split into the following parts:

$$\mathcal{L}_{\text{SM}} = \mathcal{L}_{\text{gauge}} + \mathcal{L}_{\text{dynamical}} + \mathcal{L}_{\text{Yukawa}} + \mathcal{L}_{\text{Higgs}}, \tag{2.5}$$

where $\mathcal{L}_{\text{gauge}}$ is the gauge kinetic term, $\mathcal{L}_{\text{dynamical}}$ describes matter particles' interactions with gauge bosons, $\mathcal{L}_{\text{Yukawa}}$ generates masses of the fermions and $\mathcal{L}_{\text{Higgs}}$ is responsible for generating masses for gauge bosons and the Higgs scalar itself. The gauge kinetic term then has the form:

$$\mathcal{L}_{\text{gauge}} = -\frac{1}{4} B_{\mu\nu} B^{\mu\nu} - \frac{1}{4} W^l_{\mu\nu} W^{l,\mu\nu} - \frac{1}{4} G^k_{\mu\nu} G^{k,\mu\nu}, \tag{2.6}$$

where $l = 1, 2, 3$ and $k = 1, 2, ...8$. The field strength tensors can be constructed using covariant derivatives in the following relation:

$$F_{\mu\nu} = -\frac{i}{g}[D_\mu, D_\nu]. \tag{2.7}$$

The coupling of matter fields to gauge bosons occurs through the kinetic terms of the form $\mathcal{L}_{\text{dynamical}} \supset i\bar{\Psi}\not{D}\Psi$, where $\bar{\Psi} = \Psi^\dagger\gamma^0$ is the Dirac adjoint, Ψ denotes the particles listed in 2.2 and $\not{D} \equiv \gamma^\mu D_\mu$. In the Weyl or chiral basis γ^μ is written as:

$$\gamma^\mu = \begin{pmatrix} 0 & \sigma^\mu \\ \bar{\sigma}^\mu & 0 \end{pmatrix}. \tag{2.8}$$

D_μ is called the covariant derivative whose form depends on the handedness of Ψ and the quantum numbers under which it is charged, for eg:

$$D_\mu \begin{pmatrix} \nu_{e,L} \\ e_L \end{pmatrix} = \left[\partial_\mu - ig_2\frac{\boldsymbol{\sigma_a}}{2}\mathbf{W_\mu^a} - ig_1 Y_L B_\mu\right]\begin{pmatrix} \nu_{e,L} \\ e_L \end{pmatrix},$$

$$D_\mu e_R = [\partial_\mu - ig_1 Y_e B_\mu]e_R,$$

with $Y_L = -1/2$ and $Y_e = 1$. Another important part of the SM Lagrangian is the portion that contains Yukawa terms. Once the Higgs field develops a VEV, fermions acquire mass proportional to Yukawa coupling of the form $\mathcal{L}_{\text{Yukawa}} \supset y\bar{\Psi}H\Psi$, where H is the $SU(2)_L$ Higgs doublet, $H = \frac{1}{\sqrt{2}}\begin{pmatrix} H^+ \\ H^0 \end{pmatrix}$.

2.2 The Higgs mechanism

The Higgs field H is a complex $SU(2)$ doublet with 4 degrees of freedom. After EW symmetry breaking, three of them are absorbed to give the masses for the $W^\pm$ and Z bosons, while the remaining d.o.f. is just an ordinary Higgs [51, 52, 53]. The Lagrangian of the Higgs field H is made of a kinetic and potential terms and can be written as:

$$\mathcal{L}_{\text{Higgs}} = (D^\mu H)^\dagger(D_\mu H) - V(H), \tag{2.9}$$

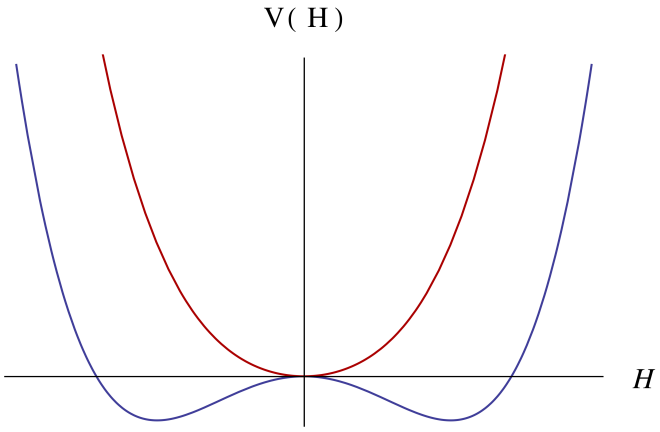

Figure 2.1: EW symmetry is unbroken if $\mu > 0$ in the Higgs potential (red) and it is broken if $\mu < 0$ (blue) [51].

where:

$$V(H) = \frac{1}{2}\mu|H|^2 + \frac{\lambda}{4}|H|^4, \tag{2.10}$$

and D_μ is the covariant derivative for the Higgs doublet:

$$D_\mu \to \partial_\mu - ig_2\frac{\boldsymbol{\sigma_a}}{2}\mathbf{W_\mu^a} - i\frac{g_1}{2}B_\mu, \tag{2.11}$$

where σ_a are the Pauli matrices – generators of a SU(2) group. Vector boson masses arise from the kinetic part of Eq. (2.9) which can be expanded as:

$$\begin{aligned} |D_\mu H|^2 &= |(\partial_\mu - ig_2\frac{\boldsymbol{\sigma_a}}{2}\mathbf{W_\mu^a} - i\frac{g_Y}{2}B_\mu)|^2 \\ &= \frac{1}{2}\left|\begin{pmatrix} \partial_\mu - \frac{i}{2}(g_1W_\mu^3 + g_2B_\mu) & -\frac{ig_1}{2}(W_\mu^1 - iW_\mu^2) \\ -\frac{ig_1}{2}(W_\mu^1 + iW_\mu^2) & \partial_\mu + \frac{i}{2}(g_1W_\mu^3 - g_2B_\mu) \end{pmatrix}\begin{pmatrix} 0 \\ v+H \end{pmatrix}\right|^2 \\ &= \frac{1}{2}(\partial_\mu H)^2 + \frac{1}{8}g^2(v+H)^2|W_\mu^1 + iW_\mu^2|^2 + \frac{1}{8}(v+H)^2|g_2W_\mu^3 - g_1B_\mu|^2. \end{aligned} \tag{2.12}$$

Expressing vector bosons $W^\pm$ as:

$$W_\mu^\pm = \frac{1}{\sqrt{2}}(W_\mu^1 \mp W_\mu^2), \tag{2.13}$$

their masses become $m_{W^\pm} = \frac{g_2 v}{2}$. The fields W^3_μ and B_μ mix amongst themselves to produce a neutral Z_μ boson and a photon A_μ:

$$\begin{pmatrix} A_\mu \\ Z_\mu \end{pmatrix} = \begin{pmatrix} \cos\theta_W & \sin\theta_W \\ -\sin\theta_W & \cos\theta_W \end{pmatrix} \begin{pmatrix} B_\mu \\ W^3_\mu \end{pmatrix}, \tag{2.14}$$

or:

$$\begin{aligned} A_\mu &= \cos\theta_W B_\mu + \sin\theta_W W^3_\mu, \\ Z_\mu &= -\sin\theta_W B_\mu + \cos\theta_W W^3_\mu, \end{aligned} \tag{2.15}$$

where θ_W is the Weinberg or weak mixing angle which at the scale of M_Z in modified minimal subtraction scheme ($\overline{\text{MS}}$) is given as $\sin^2\theta_W = 0.23126 \pm 0.00005$ at 1σ confidence level [54]. Writing

$$\cos\theta_W = \frac{g_2}{\sqrt{g_2^2 + g_1^2}} \qquad \text{and} \qquad \sin\theta_W = \frac{g_1}{\sqrt{g_2^2 + g_1^2}}, \tag{2.16}$$

from Eq. (2.12) one can see that the field Z_μ can be written as $Z_\mu = \frac{1}{\sqrt{g_2^2+g_1^2}}(g_2 W^\mu_3 - g_1 B_\mu)$ and acquires mass $m_Z = \sqrt{g_2^2 + g_1^2}\frac{v}{2}$, while the A_μ remains massless.

2.3 Effective potential

In the next four sections, we will explore how quantum corrections can be responsible for symmetry breaking. In order to do this, we introduce the concept of an effective potential, along with techniques, which will prove useful at the evaluation stage. Afterwards, a one–loop correction to the tree level potential of the massless ϕ^4 scalar theory will be calculated. Finally, the necessity of renormalization group equations (RGE) in computing the potential will be explained.

In these sections, discussions from refs. [55, 56, 57, 58] are closely followed.

2.4 Functional methods in QFT

This part of discussion gives a short overview of the functional methods that are used in quantum field theory while discussing transition amplitudes and the effective potential.

The vacuum to vacuum amplitude in presence of external sources, $J(x)$, can be calculated using generating functional of correlation functions, $Z[J]$:

$$\langle \phi(x_1)...\phi(x_n)\rangle = \frac{(-i)^n}{Z[J]} \frac{\delta^n Z[J]}{\delta J(x)_1 ... \delta J(x_n)}\bigg|_{J=0}, \tag{2.17}$$

where the current $J \equiv J(x)$ is a source for the field $\phi(x)$ and $Z[J]$ has a standard path integral representation. Generating functional for connected correlation functions, $W[J]$, is related to $Z[J]$ via:

$$W[J] = -i \ln Z[J]. \tag{2.18}$$

The effective action is then defined as a Legendre transformation:

$$\Gamma[\phi_c] = W[J(x)] - \int J(x)\phi_c(x) d^4x, \tag{2.19}$$

where a classical expectation value of $\phi(x)$ in the presence of the source $J(x)$ is defined as:

$$\phi_c(x) \equiv \frac{\delta W[J(x)]}{\delta J(x)}. \tag{2.20}$$

Variation of $\Gamma[\phi]$ with respect to the field can then be calculated to be:

$$\frac{\delta\Gamma[\phi_c(x)]}{\delta\phi_c(x)} = \frac{\delta W[J(x)]}{\delta J(x)}\frac{\delta J(x)}{\delta\phi_c(x)} - J(x)\frac{\delta\phi_c(x)}{\delta\phi_c(x)} - \phi_c(x)\frac{\delta J(x)}{\delta\phi_c(x)} = -J(x). \quad (2.21)$$

From here we see that in the absence of external sources, i.e. when $J(x) = 0$, we have that:

$$\frac{\delta\Gamma[\phi_c(x)]}{\delta\phi_c(x)} = 0. \quad (2.22)$$

The functional $\Gamma[\phi_c(x)]$ can be expanded in a following way [55, 56, 57]:

$$\Gamma[\phi_c(x)] = \int d^4x[-V_{\text{eff}}(\phi_c(x)) + X(\phi_c(x))(\partial\phi_c(x))^2 + Y(\phi_c(x))(\partial\phi_c(x))^4 + ...].$$

In the translational invariant theory (i.e. $\phi_c(x)$ is constant) the terms containing derivatives vanish and we are left with:

$$\Gamma[\phi_c(x)] = -\int d^4x[V_{\text{eff}}(\phi_c(x))]. \quad (2.23)$$

Using condition in Eq. (2.22) leads to:

$$\left.\frac{\delta\Gamma[\phi_c(x)]}{\delta\phi_c(x)}\right|_{J(x)=0} = 0 = -V'_{\text{eff}}(\phi_c(x)). \quad (2.24)$$

Therefore, we see that a VEV of a field $\phi_c(x)$ can be found by minimizing V_{eff} which is then nothing else but the effective potential. Another way to expand effective action is to write [55, 56, 57]:

$$\Gamma[\phi_c(x)] = \sum_{n=0}^{\infty}\frac{1}{n!}\int d^4x_1...d^4x_n\phi_c(x_1)...\phi_c(x_n)\Gamma^{(n)}(x_1...x_n), \quad (2.25)$$

where $\Gamma^{(n)}$ is the sum of all one particle irreducible graphs i.e. Feynman diagrams

that cannot be split in two by cutting a single propagator line. Fourier transforming $\Gamma^{(n)}(x_1...x_n)$ and using the definition of Dirac delta function one arrives at [55]:

$$\Gamma[\phi_c(x)] = \sum_{n=0}^{\infty} \frac{1}{n!} \phi_c^n(x) \Gamma^{(n)}(p_i = 0) \int d^4x. \tag{2.26}$$

Comparing this to the expression in Eq. (2.23) it is easy to see that effective potential can be calculated using:

$$V_{\text{eff}}(\phi_c(x)) = -\sum_{n=0}^{\infty} \frac{1}{n!} \phi_c^n(x) \Gamma^{(n)}(p_i = 0). \tag{2.27}$$

2.5 One–loop effective potential

In this section, we will calculate the one–loop contribution to the effective potential for the ϕ^4 theory, whose Lagrangian density is given by:

$$\mathcal{L} = \frac{1}{2}(\partial^\mu \phi)(\partial_\mu \phi) - \frac{1}{2} m^2 \phi^2 - \frac{\lambda}{4!} \phi^4, \tag{2.28}$$

where the non–derivative part is the negative tree level potential of the ϕ^4 theory, $-V_0(\phi_c)$. One particle irreducible diagrams at one–loop level are depicted in Fig. 2.2. In order to summate diagrams, we need to recall the Feynman rules for the scalar theory. The n–th diagram has n propagators and vertices. Propagators contribute:

$$\int \frac{d^4p}{(2\pi)^4} \left(\frac{i}{p^2 - m^2 + i\epsilon} \right)^n. \tag{2.29}$$

For n vertices we have a factor $(-i\lambda/2)^n$ where the 2 in the denominator is a combinatorial factor, due to the fact that the diagram remains the same when two external legs are interchanged. Then there is then a symmetry factor of $1/(2n)$,

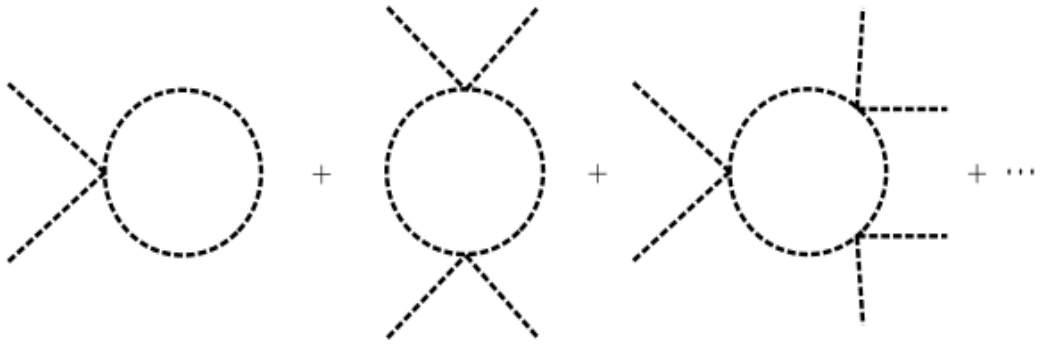

Figure 2.2: Diagrams contributing to the one–loop effective potential in the ϕ^4 theory [57].

as external legs can start anywhere on a circle. The factor $(2n)!$ arises because there are precisely that many ways to reshuffle $2n$ legs on a circle. Therefore, $\Gamma^{(2n)}(p=0)$ can be expressed as:

$$\Gamma^{(2n)}(p=0) = \frac{(2n)!}{(2n)} \int \frac{d^4p}{(2\pi)^4} \left(\frac{\lambda/2}{p^2 - m^2 + i\epsilon} \right)^n . \tag{2.30}$$

Inserting this into the expression for the effective potential and using Taylor series expansion for $\ln(1-x)$:

$$-\sum_{n=1}^{\infty} \frac{x^n}{n} = \ln(1-x) \qquad \text{with} \qquad x \equiv \frac{\lambda\phi_c^2/2}{p^2 - m^2 + i\epsilon}, \tag{2.31}$$

we have:

$$\begin{aligned} V_1(\phi_c) &= -\sum_{n=1}^{\infty} \frac{1}{(2n)!} \Gamma^{(2n)}(p=0)\phi_c^{2n} \\ &= i\sum_{n=1}^{\infty} \frac{1}{(2n)!} \frac{(2n)!}{(2n)} \int \frac{d^4p}{(2\pi)^4} \left(\frac{\lambda\phi_c^2/2}{p^2 - m^2 + i\epsilon} \right)^n \\ &= i\sum_{n=1}^{\infty} \frac{1}{2n} \int \frac{d^4p}{(2\pi)^4} \left(\frac{\lambda\phi_c^2/2}{p^2 - m^2 + i\epsilon} \right)^n \\ &= -\frac{i}{2} \int \frac{d^4p}{(2\pi)^4} \ln\left(1 - \frac{\lambda\phi_c^2/2}{p^2 - m^2 + i\epsilon} \right). \end{aligned} \tag{2.32}$$

With the help of a Wick rotation, the four momentum in Euclidean space can be expressed as $p_E = (-ip^0, \mathbf{p})$ which implies that $p_\mu p^\mu = p^2 = (p^0)^2 - \mathbf{p}^2 = -p_E^2$ (where (-,+,+,+) metric signature in Minkowski space is assumed). Inserting this into expression for the one–loop contribution to the effective potential one arrives at:

$$V_1(\phi_c) = \frac{1}{2}\int \frac{d^4p_E}{(2\pi)^4} \ln\left(1 + \frac{\lambda\phi_c^2/2}{p_E^2 + m^2}\right). \tag{2.33}$$

A ϕ_c–dependent effective mass can be calculated from Eq. (2.28):

$$m^2(\phi_c) = \frac{d^2V_0(\phi_c)}{d\phi_c^2} = m^2 + \frac{\lambda}{2}\phi_c^2. \tag{2.34}$$

Substituting it back to Eq. (2.33) and dropping the subscript "E", the one–loop correction to the effective potential looks like:

$$V_1(\phi_c) = \frac{1}{2}\int \frac{d^4p}{(2\pi)^4} \ln(p^2 + m^2(\phi_c)), \tag{2.35}$$

where the fact that $p^2 + m^2(\phi_c) - \lambda\phi_c^2/2 = 0$ with $p^2 = -m^2$ has to be used.

2.5.1 Renormalization of the effective potential

In this section, we will analyse a renormalization of the one-loop effective potential for a massless ϕ^4 theory, in order to see how radiative corrections can be responsible for symmetry breaking. We start by writing a Lagrangian for a quartically interacting massless scalar particle, which includes the renormalization counterterms:

$$\mathcal{L} = \frac{1}{2}(\partial_\mu\phi)(\partial^\mu\phi) - \frac{\lambda}{4!}\phi^4 + \frac{A}{2}(\partial_\mu\phi)(\partial^\mu\phi) - \frac{B}{2}\phi^2 - \frac{C}{4!}\phi^4, \tag{2.36}$$

where A, B, C are the counterterms for the field, mass and coupling renormalization respectively.

The first step in the calculation is to integrate the expression (2.35) from zero to infinity. The problem though is that this integral is ultraviolet divergent. The standard approach is to first regularize the theory by integrating the integrand up to a cut–off scale $p^2 = \Lambda^2$. We then take the limit $\Lambda \to \infty$, resulting in the Λ–dependent terms being absorbed into counterterms.

By using several integral identities and neglecting the vanishing terms when $\Lambda \to \infty$, the effective potential in Eq. (2.35) becomes [57]:

$$V_1(\phi_c) = \frac{m^2(\phi_c)}{32\pi^2}\Lambda^2 + \frac{m^4(\phi_c)}{64\pi^2}\left(\ln\frac{m^2(\phi_c)}{\Lambda^2} - \frac{1}{2}\right). \tag{2.37}$$

Using Eq. (2.34) to replace $m^2(\phi_c)$ in the above expression the total one–loop effective potential including counterterms becomes:

$$V(\phi_c) = \frac{B}{2}\phi_c^2 + \frac{\lambda + C}{4!}\phi_c^4 + \frac{\lambda\Lambda^2}{64\pi^2}\phi_c^2 + \frac{\lambda^2\phi_c^2}{256\pi^2}\left(\ln\frac{\lambda\phi_c^2}{2\Lambda^2} - \frac{1}{2}\right). \tag{2.38}$$

As mentioned in the beginning of this section, we are analysing the ϕ^4 theory for a massless scalar particle. As such, a renormalization condition for a mass, evaluated at renormalization scale $\phi_c = 0$, should be zero, i.e.

$$m^2(\phi_c) = \left.\frac{d^2V(\phi_c)}{d\phi_c^2}\right|_{\phi_c=0} = 0. \tag{2.39}$$

It is easy to see from Eq. (2.38), only the first and third terms contribute, giving

$$B = -\frac{\lambda\Lambda^2}{32\pi^2}. \tag{2.40}$$

Because of the logarithm behaviour, we can not choose the renormalization scale for λ at $\phi_c = 0$, however, we can choose an arbitrary scale $\hat{\mu}$ such that

$$\left.\frac{d^4V(\phi_c)}{d\phi_c^4}\right|_{\phi_c=\hat{\mu}} = \lambda. \tag{2.41}$$

The choice of $\hat{\mu}$ only changes how the coupling of λ is defined at a particular renormalization scale. However, it does not affect physics. The above condition implies that

$$C = -\frac{3\lambda^2}{32\pi^2}\left(\ln\frac{\lambda\hat{\mu}}{2\Lambda^2} + \frac{11}{3}\right). \tag{2.42}$$

Substituting Eqs. (2.40) and (2.42) into the (2.38), gives the expression for the renormalised effective potential up to one–loop level:

$$V(\phi_c) = \frac{\lambda}{4!}\phi_c^4 + \frac{\lambda^2\phi_c^2}{256\pi^2}\left(\ln\frac{\phi_c^2}{\hat{\mu}^2} - \frac{25}{6}\right). \tag{2.43}$$

For very small values of ϕ_c, $\ln\frac{\phi_c^2}{\hat{\mu}^2}$ becomes large and negative, ϕ_c acquires non–zero VEV and thus the symmetry gets broken by radiative corrections. Clearly, the minimum of this potential is no longer at $\phi_c = 0$ as it was in the classical case, however, we can not use this equation to find a VEV of a field. The reasons will be discussed in the next section.

To see that the renormalization scale is an arbitrary parameter that does not affect physics, we can choose to define the coupling λ at a different scale $\hat{\mu}'$:

$$\lambda' = \left.\frac{d^4V(\phi_c)}{d\phi_c^4}\right|_{\phi_c=\hat{\mu}'} = \lambda + \frac{3\lambda^2}{16\pi^2}\ln\frac{\hat{\mu}'}{\hat{\mu}}. \tag{2.44}$$

Repeating the same steps as above, it is easy to confirm that the potential main-

tains the same functional form:

$$V(\phi_c) = \frac{\lambda'}{4!}\phi_c^4 + \frac{\lambda'^2\phi_c^2}{256\pi^2}\left(\ln\frac{\phi_c^2}{\hat{\mu}'^2} - \frac{25}{6}\right), \tag{2.45}$$

up to $\mathcal{O}(\lambda^3)$, which must be small for the perturbative expansion to be valid.

2.5.2 Renormalization group equations

In this section, we will further explore the validity of the one–loop effective potential expression given by Eqs. (2.43, 2.45). A loop expansion is an expansion in powers of $\alpha \equiv \frac{g^2}{4\pi}$, where in our case $g^2 = \lambda$. In general, n–loop diagrams will have a prefactor of α^{n+1}. However, loop expansions also bring in a factor of $\ln\frac{\phi_c^2}{\hat{\mu}^2}$ for each loop. Therefore, an n–loop expansion will have a prefactor of

$$\alpha^{n+1}\left(\ln\frac{\phi_c^2}{\hat{\mu}^2}\right)^n. \tag{2.46}$$

In order for the perturbative expansion to be valid, the product in the above equation (and not just α^{n+1} alone) has to be less than unity. The renormalization scale can always be chosen in such a way that $\alpha^{n+1}\left(\ln\frac{\phi_c^2}{\hat{\mu}^2}\right)^n \ll 1$, or even zero, but then the expression for the potential will only be valid around a particular scale $\phi_c = \hat{\mu}$. The potential can be improved using renormalization group equations in such a way that it would be valid over a wide range of renormalization scales. In mathematical language, this simply means satisfying the condition $dV/d\ln\hat{\mu} = 0$. Using the chain rule this condition can be expanded as [56]:

$$\left(\hat{\mu}\frac{\partial}{\partial\hat{\mu}} + \beta\frac{\partial}{\partial g} + \gamma\phi_c\frac{\partial}{\partial\phi_c}\right)V(\phi_c) = 0, \tag{2.47}$$

where $\beta = \hat{\mu}\frac{\partial g_i}{\partial \hat{\mu}}$, g_i is a coupling, and γ is an anomalous dimension, parametrising how field normalization changes with $\hat{\mu}$. Further calculations are usually performed by firstly making the following redefinitions [55, 56]:

$$\begin{aligned} \bar{\beta} &\equiv \frac{\beta}{(1+\gamma)}, & \bar{\gamma} &\equiv \frac{\gamma}{(1+\gamma)}, \\ t &\equiv \ln\left(\frac{\phi_c}{\hat{\mu}}\right) \qquad \Rightarrow & \frac{\partial}{\partial t} &= -\hat{\mu}\frac{\partial}{\partial \hat{\mu}}. \end{aligned} \tag{2.48}$$

Noting that the improved potential after renormalization must still be proportional to ϕ^4, we can make the following factorization

$$V(\phi_c) = f(\lambda, t)\frac{\phi_c^4}{4!}. \tag{2.49}$$

Plugging this into Eq. (2.47) and using the redefinitions we have [55, 56]:

$$\left(-\frac{\partial}{\partial t} + \bar{\beta}\frac{\partial}{\partial \lambda} + 4\bar{\gamma}\right) f(\lambda, t) = 0. \tag{2.50}$$

Similarly, as we have a condition for the potential from Eq. (2.47), there is an analogous condition for the wave function renormalization, which reads as [55]:

$$\left(-\frac{\partial}{\partial t} + \bar{\beta}\frac{\partial}{\partial \lambda} + 2\bar{\gamma}\right) Z(\lambda, t) = 0. \tag{2.51}$$

Combining the condition $f(\lambda, 0) = \lambda$ in Eq. (2.50) with the standard condition for wave function renormalization $Z(\lambda, 0) = 1$ in Eq. (2.51), we arrive at expressions for the beta function and the anomalous dimension:

$$\bar{\beta} = \frac{\partial}{\partial t} f(\lambda, t) - 4\bar{\gamma}\lambda, \qquad \text{and} \qquad \bar{\gamma} = \frac{\partial Z(\lambda, 0)}{2\partial t}. \tag{2.52}$$

The solution of Eq. (2.50) has a form of:

$$f(\lambda,t) = g(\lambda'(\lambda,t))\exp\bigg(-4\int\bar{\gamma}(\lambda'(\lambda,t))dt'\bigg). \tag{2.53}$$

Again, using the fact that $f(\lambda,0) = \lambda$ and recalling that $f(\lambda,t)$ is the fourth derivative of an effective potential, we find $g(\lambda'(\lambda,t)) = \lambda'(\lambda,t)$. As the solution of Eq. (2.51) takes the form:

$$Z(\lambda,t) = \exp\bigg(-2\int\bar{\gamma}(\lambda'(\lambda,t))dt'\bigg), \tag{2.54}$$

Eq. (2.53) can now be rewritten in a much more compact form:

$$f(\lambda,t) = \lambda'(\lambda,t)Z^2(\lambda,t). \tag{2.55}$$

This then can be used in Eq. (2.49) to write down the RGE–improved one–loop effective potential.

It can be shown that one–loop corrections to the wave function normalization yields $Z = 1$ [55]. Therefore, since anomalous dimension is proportional to the $\partial Z/\partial t$, we get $\bar{\gamma} = 0$. To find $\lambda'(\lambda,t)$ one first has to calculate the beta function. One way to do this is to use Eqs. (2.52) with $\bar{\gamma} = 0$, $f(\lambda,t) = \frac{dV}{d\phi_c^4}$ and the potential from Eq. (2.45). The other way is to note that $\beta(\lambda)$ was already calculated in the previous section and is given by Eq. (2.44). With a definition of t in mind, the beta function can be rewritten as:

$$\bar{\beta} = \frac{d\lambda'}{dt} = \frac{3\lambda'^2}{16\pi^2}. \tag{2.56}$$

This equation has the solution:

$$\lambda'(\lambda, t) = \frac{\lambda}{1 - \frac{3\lambda t}{16\pi^2}}. \tag{2.57}$$

Therefore, the improved effective potential is:

$$V(\phi_c) = \lambda'(\lambda, t) Z^2(\lambda, t) \frac{\phi_c^4}{4} = \left(\frac{\lambda}{1 - \frac{3\lambda t}{16\pi^2}} \right) \frac{\phi_c^4}{4}. \tag{2.58}$$

This potential is now valid for all t as long as $t \neq \frac{16\pi^2}{3\lambda}$, and can be used to determine VEV of ϕ_c.

2.6 Problems of the Standard Model

2.6.1 Vacuum stability

One of the potential problems in the SM is the vacuum stability. If at some energies, because of it is running, parameter λ develops negative value anywhere below the Planck scale, then this means that the Higgs potential is unbounded from below and that the vacuum of the SM is not stable. The reason for the λ to become negative are the Yukawa couplings of the fermions (and in particular that of the top quark) to the Higgs which give the negative contribution. Within SM, λ's value at any energy scale μ is [13]:

$$\lambda(\mu) \approx \lambda(\Lambda_{EW}) + \left(\frac{1}{16\pi^2} \beta_\lambda^{(1)} + \frac{1}{(16\pi^2)^2} \beta_\lambda^{(2)} \right) \log \left(\frac{\mu}{\Lambda_{EW}} \right). \tag{2.59}$$

One and two loop beta functions of the Higgs self–coupling are functions of

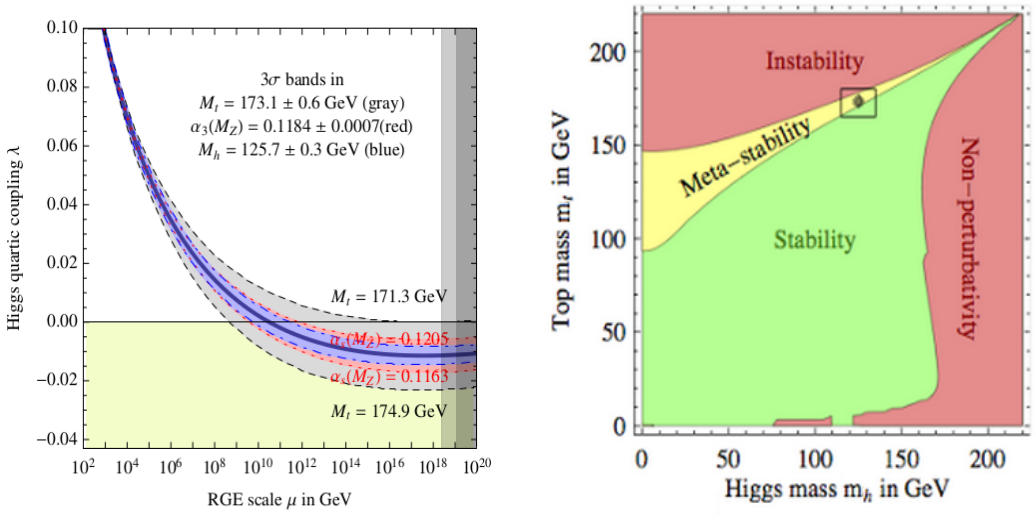

Figure 2.3: Left panel: Evolution of Higgs quartic coupling with varying m_t, m_h and $\alpha_s \equiv \frac{g_3^2}{4\pi}$ [13]. Right: Stability regions of the Standard Model. The box shows latest measurements of m_t, m_h and α_s values.

various (gauge and Yukawa) couplings and most importantly, the top Yukawas [1]. The running of the λ is depicted in Fig. 2.3 left panel. Given the experimental mass of the Higgs, we see, that up to a 3σ level, λ turns negative at around 10^8 GeV. However, it remains very small all the way up to the Planck scale. This in turn implies a large lifetime for tunnelling from false to global vacuum since the probability scales as [59]:

$$P \sim e^{\frac{1}{\lambda}}.$$

It is also interesting to note, that as it can be seen from Fig. 2.3 right panel, we live very close to the stable vacuum of SM, however given all experimental and theoretical errors, the possibility of actually living there is excluded at 98% C.L.

[1] β_g is the function that describes how the strength of the coupling g varies at different energy scales μ and is defined to be $\beta_g \equiv \mu\frac{\partial g}{\partial \mu} = \frac{\partial g}{\partial(\log \mu)}$. In this case, the equations for $\beta_\lambda^{(1)}$ and $\beta_\lambda^{(2)}$ delineate the running of the Higgs quartic coupling λ at one and two loop level. The functional form of them within the SM framework can be found in [61].

[13]. It can be shown, that the Higgs mass bound for the absolute stability up to the Planck scale can be written as [60]:

$$m_h(\text{GeV}) > 129.4 + 1.4\left(\frac{m_t(\text{GeV}) - 173.1}{0.7}\right) - 0.5\left(\frac{\alpha_s(M_z) - 0.1184}{0.0007}\right). \quad (2.60)$$

All this assumes no extra physical ingredients, other than just the SM itself, all the way to the Planck scale.

2.6.2 Hierarchy problem

In the SM the masses of the fermions are protected by the chiral symmetry and the masses of the bosons by the gauge symmetry. However, one of the main motivations for extensions beyond the standard model (BSM) is that the scalars get large radiative corrections that are quadratically divergent and there is no symmetry within SM to stabilize it. For example the correction to the Higgs mass in the SM can be expressed like [62, 63, 64]:

$$\delta m_{\text{h}}^2 = -\frac{|y_t|^2}{8\pi^2}(\Lambda_{\text{UV}}^2 + ...) \quad (2.61)$$

where y_t is top Yukawa coupling. Taking Λ_{UV} up to the scale where the new physics is expected to kick in, i.e. $\Lambda_{\text{UV}} \sim M_{\text{Pl}}^2$, where M_{Pl} is the reduced Planck mass and $M_{\text{Pl}} \equiv \frac{1}{\sqrt{8\pi G}} = 2.44 \times 10^{18}$ GeV, the renormalised Higgs mass m_{h}^2 can be written as:

$$m_{\text{h}}^2 = m_{\text{h tree}}^2 + \delta m_{\text{h 1-loop}}^2 + ... = 10^{36}\ \text{GeV}^2 - 10^{36}\ \text{GeV}^2 \approx (125\ \text{GeV})^2. \quad (2.62)$$

This is an extremely fine tuned scenario, requiring the precision roughly of the order of $\frac{\mathcal{O}(10^2\ \text{GeV})}{\mathcal{O}(10^{18}\ \text{GeV})} \sim \mathcal{O}(10^{-16}\ \text{GeV})$. Ideally, a stabilizing mechanism should be realised in nature in order to explain the Higgs scalar's mass avoiding large cancellations and, as we will show in Chapter 4, SUSY offers an excellent solution by introducing the new d.o.f., which cancel the quadratic corrections, leaving only logarithmic ones.

2.6.3 Dark Matter

Dark Matter is one of the biggest puzzles of modern physics. The presence of large amounts of non–luminous matter initially has been traced by studying the Coma cluster [9], and observing the galaxy rotation curves [10].

If luminous matter would be all what galaxies are made of, then from the Newtonian dynamics the orbital velocity of the stars around the galactic centre should scale down with increasing distance r as:

$$v = \sqrt{\frac{GM(r)}{r}}, \tag{2.63}$$

where $M(r)$ is the mass enclosed within radius r. However, it was found, that up to a leading order, v is independent of r, which could only be explained by the presence of DM [10]. In the case of galaxy (super)clusters, relevant quantity relating amount of the DM in (super)cluster and kinematics of separate galaxies within it is galaxies' velocity dispersion. That is because usually (super)clusters are not relaxed systems and thus can be decomposed into smaller individual subclusters each having its own peculiar rotational velocities [19, 20, 21]. Yet another hint of large amounts of DM comes from the gravitational lensing experiments

[16, 17, 18]. In these experiments the lensing of the light coming from the background source is found to be much larger than one would expect if the massive object, that acts as a lens, would be made up of the luminous matter only.

There is observational evidence, which comes from the bullet cluster, that the DM has a particle–like nature [18]. The bullet cluster consists of the two galaxy clusters colliding at the speed of 4500 km/s [22, 23, 24]. The analysis based on the gravitational lensing techniques enabled to find the spatial offset between the baryonic and remaining matter which, as argued in Ref. [18], could not be explained by modifying the gravity. The X-ray data of the merger revealed a bullet like structures of the interstellar gas exiting the site of the collision, whereas the DM clump lies well ahead of the visible matter and remained largely intact [22, 23, 24]. As it was already mentioned in the introduction, from the analysis of the primordial density fluctuations of the CMB we know that the majority of the DM has to be non–relativistic i.e. $m_{DM} \gtrsim T$ [26, 27, 65]. In fact, at the time when the DM species stopped annihilating in the Early Universe, according to the WIMP (Weakly Interacting Massive Particle) miracle scenario, which is discussed in Section 5.1, the ratio $\frac{m_{DM}}{T}$ was around 20-25 [66]. It should be noted though, that there are three memorable cases: annihilations, coannihilations and thresholds when this calculation is not valid [67]. We will discuss these cases in more detail at the end of Section 5.3.

However, there are no good candidates in the SM: we know that DM particle has to be electrically and colour neutral, it also should be either stable, or has to have lifetime longer than the age of the Universe. The neutrinos, otherwise an excellent candidate, are simply not abundant enough, and all this conclusively rules out all SM particle content.

2.6.4 Baryogenesis in the Standard Model

The fact that our Universe is mainly made of matter and not antimatter is puzzling since one would expect that during the Big Bang equal amounts of both were be produced. In order to generate this asymmetry, three conditions, conceived by Sakharov, have to be met [11]: baryon number (B) violation, charge (C) and charge-parity (CP) violation, and the out-of-equilibrium condition. Even though in the SM these conditions in principle are present, there are still a number of obstacles remaining that point towards the BSM physics. Firstly, the requirement for successful baryogenesis within SM puts an upper bound on the Higgs mass $m_h \leq 40$ GeV [30], which is inconsistent with experimental results [1, 2]. The second problem is related to sphalerons and how they erase baryon asymmetry. Electroweak sphaleron is an unstable static solution of equations of motion for the $\mathrm{SU}(2)_L$ gauge and Higgs fields [1] [68, 69, 70]. Sphalerons mediate transitions between topologically different vacuum states characterised by the winding number with an energy barrier height (also called sphaleron barrier) being ~ 10 TeV [70]. At low temperatures these transitions are exponentially suppressed and proceed via instanton quantum tunnelling whereas at finite temperatures classical thermal fluctuations rather than quantum tunnelling are responsible for the transitions over sphaleron barrier. Because of the chiral anomaly and vacuum structure of $\mathrm{SU}(2)_L$ gauge fields, baryons and leptons are transformed into each other via sphaleron transitions and if they are frequent enough any baryon asymmetry would be wiped out. As a thermal fluctuation triggers a transition of the Higgs VEV to a non–zero value, bubbles of the broken phase grow in the otherwise symmetric Universe. The C and CP violating processes near the bubble

[1] Sphalerons and $B + L$ violation in the SM will be discussed in greater detail in Chapter 8

wall create the asymmetry between LH (and RH) fermions and their respective antiparticles. LH fermions then affect the $B+L$ creation through sphaleron transitions in the symmetric phase, just outside the wall. For the anomalous $B+L$ violating processes to deviate from the equilibrium near the bubble walls, the EW phase transition has to be of first order. Once the asymmetry enters the expanding bubble, $B+L$ violation is suppressed by the sphaleron mass and the asymmetry is preserved. Looking from the SM model perspective, as the Higgs field rolls to its minimum from 0 GeV to 246 GeV, the typical timescale τ for the transition is [71]:

$$\tau \sim \frac{1}{\mathcal{H}} \sim \frac{M_{\mathrm{Pl}}}{T^2} \sim \frac{10^{17}}{T}, \tag{2.64}$$

where $\mathcal{H}$ is the Hubble expansion rate, defined in Section 3.1, and T is the temperature of the Universe in [GeV] units at the time when the phase transition happened. Taking $T \backsimeq 100$ GeV, one gets $\tau \sim 10^{15}$ GeV^{-1}, while typical relaxation timescales in plasma at this temperature is many orders faster – $\tau_{relax.} \sim \mathcal{O}(10^2)$ GeV^{-1} [72, 73, 74]. Finally, the only source of the CP violation in SM are the phases in CKM matrix [33, 34], however, these are not enough and additional contributions are needed.

2.6.5 Strong CP problem

The CP violation can be experimentally studied in a variety of processes including hadron decays, electric dipole moments of neutron, electron and atomic nuclei. CP violating effects in weak interactions were first observed in kaon's hadronic decays to pions. There are two neutral kaon states – CP–even and CP–odd. In order to conserve CP, the CP–odd kaon has to decay into three pions whereas

CP–even kaon has to decay into two pions. However, it was observed that around 1 in 500 CP–odd kaons decay in the CP–even state of two pions, thus violating the CP invariance [75]. The CP symmetry is also violated in the kaon's semileptonic decays – decay rate of the long lived kaon, K^0_{long} ($K^0_{\text{long}} \equiv \frac{d\bar{s}+s\bar{d}}{\sqrt{2}}$), to $\pi^- e^+ \nu_e$ is larger than the decay rate to $\pi^+ e^- \bar{\nu}_e$ [76]. In addition, the CP violation is observed in neutral kaon oscillations, by which K^0 turns into it's antiparticle $\overline{K}^0$ via weak interactions and where the CP violation implies that $\Gamma(K^0 \to \overline{K}^0) \neq \Gamma(\overline{K}^0 \to K^0)$. Similar violations are observed in B mesons, see [77, 78, 79, 80, 81] and references therein.

However, even though there is the term in the SM QCD sector which is allowed by the Lorentz and gauge invariance and which does violate the CP transformation:

$$\mathcal{L}_{\text{QCD}} \supset \bar{\Theta} \frac{g^2}{32\pi^2} G^{a,\mu\nu} \tilde{G}^a_{\mu\nu}, \tag{2.65}$$

where $\tilde{G}_{\mu\nu} = \frac{1}{2}\epsilon_{\mu\nu\rho\sigma} G^{\rho\sigma}$ and the parameter $\bar{\Theta}$ in the range $[0 : 2\pi]$, the CP symmetry in strong interactions is not violated as badly as in the weak sector. If CP would be violated in QCD, neutron would have many orders of magnitude larger electric dipole moment in comparison with experimental observations. In order to comply with experimental bounds on the neutron dipole moment, the parameter $\bar{\Theta}$ is required to be $|\bar{\Theta}| \leq 3 \times 10^{-10}$ [82]. The fact that it is so small is known as the strong CP problem. As we will discuss later in Section 5.2, the attempt to dynamically generate small value of $\bar{\Theta}$ gives rise to a new scalar axion field, which becomes a plausible DM candidate [14].

2.6.6 Origin of neutrino masses

In the SM, neutrinos are treated as massless particles. However, in 1998 Super–Kamiokande collaboration observed the deficit of the muon neutrinos in the atmospheric neutrino flux as compared to the theoretical expectations [3]. The shortage of ν_μ in the experimental data could be explained if one would allow for the flavour mixing, but this could only happen if the neutrinos would be massive. In fact, the data could be explained if the mass splitting between the ν_μ and ν_τ would be $5 \times 10^{-4} < \Delta m^2 < 4 \times 10^{-3}$ eV^2 [3]. Another experiment, called Homestake, was designed to look for solar neutrinos. According to the theoretical models, a large flux of ν_e is produced in the proton–proton chain reactions. However, the Homestake detected only a third of what was expected [4, 5]. The lack of the ν_e can be explained if the electron neutrino changes its flavour and is therefore massive. Actually, the upper bound on the sum over all generations of the neutrino masses is derived from the analysis of photometric redshift catalogue of over 700 000 galaxies combined with the data from WMAP 5 year CMB fluctuations, baryon acoustic oscillations, type Ia supernovae and Hubble space telescope's prior on the Hubble parameter [83]. At 95% confidence level this bound is set to be:

$$\sum_i m_{\nu_i} \leq 0.28 \text{ eV}, \tag{2.66}$$

where $i = e, \mu, \tau$. In order to make neutrinos massive one has to go beyond the SM. The most popular models explaining origin of neutrino masses are type I [84, 85], II [86, 87, 88, 89] and III see–saw [90] mechanisms.

Chapter 3

Standard Model of Cosmology

According to the latest Planck data, assuming the Standard Model of Cosmology, our Universe started from a singularity around 13.813±0.058 (at 68% C.L.) billion years ago [91]. After the Big Bang, the main epochs that the Universe is thought to have undergone are: 1) Inflation – the short period of time when the total energy density of the Universe, ρ, was dominated by the VEV of the inflaton field. 2) Radiation epoch – the period when the radiation energy density was the biggest. 3) Matter domination epoch, which started when the radiation energy density, which as the Universe expands decreases faster than that of the matter, dropped below ρ_{matter}. 4) Λ dominated epoch – the period when the radiation and matter got diluted and the main contribution then comes from the negative pressure of the vacuum which makes the Universe expand at an accelerating rate.

The ΛCDM model is the one that best explains the Universe as we see it, i.e. the primordial perturbations of the CMB formation [26, 65], BBN [92, 93, 94], accelerating expansion that has been detected by observing type Ia supernovae [95, 96, 97]. The model is defined by 6 input parameters: the amplitude of

the primordial perturbations, δ_H, the spectral tilt, n_s, which we will define later in Eqs. (3.46) in (3.48) respectively, baryon density, DM density, dark energy density, and Thomson scattering optical depth due to reionization. According to the Planck data based Monte Carlo simulations, which is run to fit these six parameters as best as it is possible, dark energy constitutes 68.3%, DM 26.8% and baryonic matter 4.9% of the total energy density budget of our Universe [91]. In this chapter we will briefly review the dynamical equations which govern the evolution of the Universe and how they arise from the theory of general relativity (GR) [98]. Later we will review some problems of the Big Bang model and how inflation in the Early Universe could resolve them.

3.1 Dynamics of the Universe

Observational evidence show that our Universe is isotropic and homogeneous on cosmological scales. The FRW metric for the homogeneous and isotropic Universe reads [99, 100, 101]:

$$ds^2 = dt^2 - a^2(t)\left[\frac{dr^2}{1-kr^2} + r^2 d\theta^2 + r^2 \sin^2\theta d\phi^2\right], \tag{3.1}$$

where k is the curvature parameter taking values +1, 0 or -1 depending on whether our Universe is open, flat or closed respectively. Obviously, the entries of the metric tensor are:

$$g_{\mu\nu} = \text{diag}\left(1, -\frac{a^2(t)}{1-kr^2}, -a^2(t)r^2, a^2(t)r^2\sin^2\theta\right). \tag{3.2}$$

Here $\mu, \nu = 0, 1, 2, 3$ are the four vector components. The space–like part of it is usually denoted by Latin letters i and j, and take one of the following values $i, j = 1, 2, 3$. With the help of $g_{\mu\nu}$, one can find that the only non–zero Ricci tensors for the FRW metric are [102]:

$$\begin{aligned} R_{00} &= -3\frac{\ddot{a}}{a}, \\ R_{ij} &= -\left(\frac{\ddot{a}}{a} + 2\frac{k}{a^2} + 2\mathcal{H}^2\right), \end{aligned} \tag{3.3}$$

and the Ricci scalar:

$$R = -6\left(\frac{\ddot{a}}{a} + \frac{k}{a} + \mathcal{H}^2\right). \tag{3.4}$$

$\mathcal{H}$ denotes the Hubble expansion rate and is defined to be $\mathcal{H} \equiv \frac{\dot{a}}{a}$, where the dot indicates differentiation with respect to time. Plugging these into the Einstein field equation:

$$R_{\mu\nu} - \frac{1}{2}g_{\mu\nu}R = 8\pi G T_{\mu\nu} + \Lambda g_{\mu\nu}, \tag{3.5}$$

with $T_{\mu\nu} = \mathrm{diag}(\rho, -p, -p, -p)$, and taking $\mu = \nu = 0$ components one arrives at Friedman equation:

$$\mathcal{H}^2 = \frac{8\pi G\rho}{3} - \frac{k}{a^2} + \frac{\Lambda}{3}. \tag{3.6}$$

The spatial i, j components yields:

$$\frac{\ddot{a}}{a} = \frac{4\pi G}{3}(\rho + 3p) + \frac{\Lambda}{3}. \tag{3.7}$$

Finally, after some manipulations, the continuity equation $\nabla_\mu T^\mu_\nu = 0$ yields:

$$\dot{\rho} + 3\mathcal{H}(\rho + p) = 0. \tag{3.8}$$

The pressure is related to the energy density via $p = \omega\rho$ where ω is the equation of state parameter that is independent of time. $\omega = \frac{1}{3}, 0$ and -1, for radiation, matter and vacuum energy dominated Universe respectively. Inserting equation of state into Eq. (3.8) one finds how the energy density scales with $a(t)$:

$$\begin{aligned} &\text{radiation dominated era:} && \rho = \frac{\rho_0}{a^4}, \\ &\text{matter dominated era:} && \rho = \frac{\rho_0}{a^3}, \\ &\text{vacuum energy dominated era:} && \rho = \rho_0. \end{aligned} \tag{3.9}$$

The subscript "0" denotes the present value. Inserting above in Eq. 3.6, assuming flat Universe (i.e. $k = 0$) and $\Lambda = 0$ it is straightforward to evaluate how the scale parameter and Hubble constant depends on time:

$$\begin{aligned} &\text{radiation dominated era:} && a(t) \propto t^{\frac{1}{2}}, && \mathcal{H} = \frac{1}{2t}, \\ &\text{matter dominated era:} && a(t) \propto t^{\frac{2}{3}}, && \mathcal{H} = \frac{2}{3t}, \\ &\text{vacuum energy dominated era:} && a(t) \propto e^{t\mathcal{H}}, && \mathcal{H} = \mathcal{H}_0. \end{aligned} \tag{3.10}$$

Another important quantity in cosmology is the density parameter:

$$\Omega_i = \frac{\rho_i}{\rho_c}, \tag{3.11}$$

where ρ_c is called the critical density and is defined by setting the curvature parameter, k, and the cosmological constant, Λ, in Eq. (3.6) to zero:

$$\rho_c \equiv \frac{3\mathcal{H}^2}{8\pi G}. \tag{3.12}$$

Therefore, if an actual total energy density of the Universe is equal to the critical, then geometry of the Universe is flat. Given that most recent measurements of

the Hubble constant by Planck satellite combined with the WMAP data yields $\mathcal{H} = (67.3 \pm 1.2)$ (km/s)/Mpc (68% C.L.) [91], the critical density of the Universe is then $\rho_c = (8.51 \pm 0.30) \times 10^{-27}$ kg/m^3.

It is worthwhile mentioning that WMAP–9 satellite observations yielded $\mathcal{H} = (70 \pm 2.2)$ (km/s)/Mpc (68% C.L.) [103] and the Hubble rate derived by observing type Ia supernovas was found to be $\mathcal{H} = (73.8 \pm 2.4)$ (km/s)/Mpc (68% C.L.) [97] – both results above the Planck measured $\mathcal{H}$. While the offset between WMAP–9 and Planck are within the margins of error and could arise due to much higher precision of the latter, the divergence of the Riess's group results is more worrisome and already inspired models on an interaction between DM and dark energy [104, 105].

3.2 Problems with a Big Bang model

The most widely discussed problems with the Big Bang model, which supports the theory of inflation, are following:

•*Horizon problem:* as it was already mentioned, observations suggest, that on large scales, in accordance with the cosmological principle, today our Universe is isotropic and homogeneous [106]. But if two different causally disconnected Hubble patches had never been into contact, how come the CMB looks so homogeneous in all directions? Introducing inflation helps to solve this problem in the following way: the patches that now seem to have been causally disconnected may have been in thermal contact with each other during the very Early Universe stages if the Universe indeed had undergone the phase of inflation.

•*Flatness problem:* is a fine tuning problem that deals with the question why

the observed energy density of the Universe is so close to the critical density. Rearranging Eq. 3.6 with $\Lambda = 0$, it can be shown that:

$$|\Omega - 1| = \frac{|k|}{a^2\mathcal{H}^2}. \tag{3.13}$$

From Eq. 3.10 one can see, that throughout the history of the Universe the $\frac{1}{a^2\mathcal{H}^2}$ on the rhs of Eq. 3.13 always increased, thus any deviation of Ω from the unity in the early times would result in highly curved Universe at a present epoch. The inflation resolves this puzzle in the following way. During inflation the product $\frac{1}{a^2\mathcal{H}^2}$ decreased by many orders of magnitude thus highly suppressing $|\Omega - 1|$ and making the later deviation from 0 completely negligible, no matter what value of Ω the Universe initially started with.

•*Magnetic monopole problem* [107, 108]: grand unified theories (GUT) predict the existence of stable magnetic monopoles, which would be copiously produced at high temperature during the early stages of the Universe. However, none of them have ever been experimentally observed. If inflation really happened, these monopoles would have been diluted so severely that on average only a few of them would have been left within a Hubble horizon and in this way would explain why can't we detect them.

3.2.1 Inflation

Inflation is a period of exponential expansion of the Universe, driven by the potential energy density of the scalar inflaton field. To find the evolution of this field, we will take the generic Lagrangian for a scalar, made of the kinetic term

and yet unspecified inflationary potential $V(\phi)$:

$$\mathcal{L} = \frac{1}{2} g^{\mu\nu} (\partial_\mu \phi)(\partial_\nu \phi) - V(\phi). \tag{3.14}$$

The equation of motion then can be found by using Euler–Lagrange equation:

$$\partial_\mu \left(\frac{\partial \mathcal{L}}{\partial(\partial_\mu \phi)} \right) - \frac{\partial \mathcal{L}}{\partial \phi} = 0. \tag{3.15}$$

Assuming that the field is homogeneous one can eliminate gradient contributions:

$$\ddot{\phi} + 3\mathcal{H}\dot{\phi} + V'(\phi) = 0. \tag{3.16}$$

Under certain assumptions that will be mentioned later the scalar field also gives the desired equation of state with the $\omega = -1$. To see this one has to start with the stress energy tensor of the scalar field that can be expressed as:

$$T_{\mu\nu} = \partial_\mu \phi \partial_\nu \phi - g_{\mu\nu} \left(\frac{1}{2} \partial^\alpha \phi \partial_\alpha \phi - V(\phi) \right). \tag{3.17}$$

Taking $\mu = \nu = 0$ we get:

$$\rho_\phi = \frac{\dot{\phi}^2}{2} + V(\phi), \tag{3.18}$$

and the spatial components gives:

$$p_\phi = \frac{\dot{\phi}^2}{2} - V(\phi). \tag{3.19}$$

It is useful to introduce the slow roll approximation, which neglects certain terms and greatly simplifies calculations. If we define two slow roll parameters:

$$\epsilon \equiv \frac{M_{\rm Pl}^2}{2}\left(\frac{V'}{V}\right)^2 \qquad \text{and} \qquad \eta \equiv M_{\rm Pl}^2\frac{V''}{V}, \tag{3.20}$$

then approximation holds if $\epsilon, |\eta| \ll 1$. First slow roll condition measures the slope of the potential and implies potential energy domination over kinetic term, i.e. $V(\phi) \gg \dot{\phi}^2$. Using this condition in Eqs. 3.19 and 3.18, one arrives at the desired equation of state, i.e. $p \approx -\rho$, with $\omega \approx -1$, for the inflaton vacuum energy density (or cosmological constant) dominated Universe. The Hubble parameter in this case can be calculated using:

$$\mathcal{H}^2 \approx \frac{V(\phi)}{3M_{\rm Pl}^2}. \tag{3.21}$$

Another slow roll condition ensures that $V'(\phi) \gg \ddot{\phi}$ and it greatly ameliorates calculation for the dynamics of scalar field. From Eq. (3.16) we then get:

$$\dot{\phi} \approx -\frac{V'(\phi)}{3\mathcal{H}}, \tag{3.22}$$

or equivalently, using the second slow roll condition:

$$\left|\frac{\ddot{\phi}}{3\mathcal{H}\dot{\phi}}\right| \ll 1. \tag{3.23}$$

Differentiating Eq. (3.21) with respect to time and using Eq. (3.22), one gets

$$2\mathcal{H}\dot{\mathcal{H}} = \frac{\frac{\mathrm{dV}}{\mathrm{d}\phi}\frac{\mathrm{d}\phi}{\mathrm{dt}}}{3M_{\rm Pl}^2} = \frac{V'\dot{\phi}}{3M_{\rm Pl}^2} = -\frac{V'^2}{9\mathcal{H}M_{\rm Pl}^2}. \tag{3.24}$$

Dividing above by $\mathcal{H}^2$, and reusing Eq. (3.22) we get:

$$-\frac{\dot{\mathcal{H}}}{\mathcal{H}^2} = \frac{V'^2}{18\mathcal{H}^4 M_{\rm Pl}^2} = \frac{M_{\rm Pl}^2}{2}\frac{V'^2}{V^2} = \epsilon. \tag{3.25}$$

It is useful to introduce the number of e–foldings, $\mathcal{N}$, by:

$$\mathcal{N} = \int \mathcal{H}\mathrm{d}t = \int \frac{\mathcal{H}}{\dot{\phi}}\mathrm{d}\phi. \tag{3.26}$$

Using above definition of $\mathcal{N}$, the slow roll parameter ϵ can be also expressed as:

$$\epsilon = -\frac{\dot{\mathcal{H}}}{\mathcal{H}^2} = -\frac{\mathrm{d}\mathcal{H}}{\mathcal{H}\mathcal{H}\mathrm{dt}} = -\frac{\mathrm{dln}\mathcal{H}}{\mathrm{d}\mathcal{N}}. \tag{3.27}$$

3.2.2 Density perturbations

In order to quantitatively understand how the density perturbations grow during the inflationary phase we write the inflaton scalar field as the sum of the time dependent background term $\phi(t)$ and the space–time dependent field perturbation $\delta\phi(\mathbf{x}, t)$:

$$\phi = \phi(t) + \delta\phi(\mathbf{x}, t). \tag{3.28}$$

After Fourier transformation the equation of motion for the perturbation can be found to be [109, 110]:

$$\delta\ddot{\phi}_{\mathbf{k}} + 3\mathcal{H}\delta\dot{\phi}_{\mathbf{k}} + \left[\left(\frac{k}{a}\right)^2 + V''\right]\delta\phi_{\mathbf{k}} = 0, \tag{3.29}$$

where $\delta\phi_{\mathbf{k}}$ is:

$$\delta\phi_{\mathbf{k}} = \frac{1}{\sqrt{(2\pi)^3}}\int \delta\phi(\mathbf{x})e^{-i\mathbf{k}\cdot\mathbf{x}}\mathrm{d}^3\mathbf{x}. \tag{3.30}$$

Defining the interval in conformal time $\mathrm{d}\tau$ as $\mathrm{d}\tau \equiv \frac{\mathrm{d}t}{a}$ and $\psi \equiv a\delta\phi$ Eq. (3.29) can be expressed as [109, 110]:

$$\psi_{\mathbf{k}}^{''} + [\mathbf{k}^2 + a^2\mathcal{H}^2(2 - \epsilon - 3\eta)]\psi_{\mathbf{k}} = 0. \tag{3.31}$$

Choosing the conformal time to be 0 at the end of inflation and using the fact that the Hubble expansion rate is constant during the phase of inflation, gives

$$\int_{\tau}^{0} \mathrm{d}\tau = -\tau = \int_{t_i}^{t_f} \frac{\mathrm{d}t}{a} \simeq \frac{1}{\mathcal{H}} \int_{a_i}^{a_f} \frac{\mathrm{d}a}{a^2} = \frac{1}{\mathcal{H}}\bigg(- \frac{1}{a_f} + \frac{1}{a_i}\bigg) \simeq \frac{1}{\mathcal{H}a_i}, \tag{3.32}$$

for $a_f \gg a_i$, where the subscripts i and f denote quantities *during* and *at* the end of inflation, respectively. Inserting $\tau = -\frac{1}{\mathcal{H}a}$ into Eq. (3.31) and requiring that $\epsilon, |\eta| \ll 1$ one finds [109, 110]:

$$\psi_{\mathbf{k}}^{''} + \bigg(\mathbf{k}^2 - \frac{2}{\tau^2}\bigg)\psi_{\mathbf{k}} = 0. \tag{3.33}$$

Expanding $\psi_{\mathbf{k}}$ in terms of the creation and annihilation operators a and $a^{\dagger}$:

$$\psi_{\mathbf{k}} = v_{\mathbf{k}}a_{\mathbf{k}} + v_{-\mathbf{k}}^{*}a_{-\mathbf{k}}^{\dagger}, \tag{3.34}$$

and inserting into the above equation we get the following differential equation [109, 110]:

$$v_{\mathbf{k}}^{''} + \bigg(\mathbf{k}^2 - \frac{2}{\tau^2}\bigg)v_{\mathbf{k}} = 0. \tag{3.35}$$

This has the exact solution:

$$v_{\mathbf{k}} = A\frac{e^{-ik\cdot\tau}}{\sqrt{2k}}\bigg(1 - \frac{i}{k\tau}\bigg) + B\frac{e^{ik\cdot\tau}}{\sqrt{2k}}\bigg(1 + \frac{i}{k\tau}\bigg), \tag{3.36}$$

where $k \cdot \tau = k_\mu \tau^\mu$, k_μ is the four momentum with components $k_\mu = \{E, \mathbf{k}\}$ and $\mathbf{k} = \{k_x, k_y, k_z\}$. At early times, when $t \to 0$ or equivalently $\tau \to -\infty$, cosmological perturbations were in the Bunch–Davies vacuum state [111]. In this state mode functions, $v_\mathbf{k}(\tau)$, are defined by requiring that the expectation value of the Hamiltonian in the vacuum state, i.e. quantity $\langle 0| \mathcal{H} |0\rangle$ is minimised. This translates into a boundary condition [112]:

$$\lim_{\tau \to -\infty} v_\mathbf{k} = \frac{e^{-ik\cdot\tau}}{\sqrt{2k}}, \tag{3.37}$$

which we can use in Eq. (3.36) to find that $A = 1$ and $B = 0$. The final solution in the asymptotic past then becomes:

$$v_\mathbf{k} = \frac{e^{-ik\cdot\tau}}{\sqrt{2k}}. \tag{3.38}$$

The power spectrum of $\psi_\mathbf{k}$ is denoted as $P_\psi(k)$ and can be evaluated by calculating the two point correlation function [109, 110]:

$$\langle 0| \psi_\mathbf{k} \psi^\dagger_\mathbf{p} |0\rangle = (2\pi)^3 P_\psi(k). \tag{3.39}$$

In order to find an expression for $P_\psi(k)$, let us evaluate the left hand side of the above equation. First, we input the expression in Eq. (3.34) into the above equation:

$$\begin{aligned} &\langle 0| \psi_\mathbf{k} \psi^\dagger_\mathbf{p} |0\rangle = \langle 0| (v_\mathbf{k} a_\mathbf{k} + v^*_{-\mathbf{k}} a^\dagger_{-\mathbf{k}})(v_\mathbf{p} a_\mathbf{p} + v^*_{-\mathbf{p}} a^\dagger_{-\mathbf{p}}) |0\rangle \\ &= v_\mathbf{k} v^*_\mathbf{p} \langle 0| a_\mathbf{k} a^\dagger_\mathbf{p} |0\rangle = v_\mathbf{k} v^*_\mathbf{p} \langle 0| [(2\pi)^3 \delta^3(\mathbf{k} - \mathbf{p}) + a^\dagger_\mathbf{p} a_\mathbf{k}] |0\rangle \\ &= (2\pi)^3 |v_\mathbf{k}|^2 \langle 0|0\rangle = (2\pi)^3 |v_\mathbf{k}|^2. \end{aligned} \tag{3.40}$$

In the above calculation many terms vanish due to $a_{\mathbf{k}} |0\rangle = 0 |0\rangle$ and $\langle 0| a^{\dagger}_{\mathbf{k}} = \langle 0| 0$. In the second line we used the commutation relation:

$$[a_{\mathbf{k}}, a^{\dagger}_{\mathbf{p}}] = (2\pi)^3 \delta^3(\mathbf{k} - \mathbf{p}). \tag{3.41}$$

Comparing the derived result with the right hand side of Eq. (3.39), it is easy to see that $P_{\psi}(k) = |v_{\mathbf{k}}|^2$. Finally, recalling the result of Eq. (3.36) with $A = 1$ and $B = 0$ we arrive at the following expression for $P_{\psi}(k)$:

$$P_{\psi}(k) = |v_{\mathbf{k}}|^2 = \frac{1}{2k}\left(1 + \frac{1}{\tau^2 k^2}\right). \tag{3.42}$$

Using the aforementioned definitions for τ and $\delta\phi$ in above equation we get:

$$P_{\delta\phi}(k) = \frac{\mathcal{H}^2}{2k^3}\left[1 + \left(\frac{k}{a\mathcal{H}}\right)^2\right]. \tag{3.43}$$

The length of the perturbation is of the order $1/k$ and the size of the Hubble patch is $1/a\mathcal{H}$. At the time when the wavelength of perturbation exceeds the Hubble patch, or in other words, the condition $a\mathcal{H} \gg k$ is satisfied, the perturbations freeze out and the power spectrum becomes constant [109, 110]:

$$P_{\delta\phi}(k) = \frac{\mathcal{H}^2}{2k^3}. \tag{3.44}$$

The curvature perturbation in spatially flat gauge (i.e. $\psi = 0$) can be expressed as [109, 110]:

$$\zeta = \frac{\mathcal{H}}{\dot{\phi}}\delta\phi, \tag{3.45}$$

and the power spectrum $P_\zeta(k)$ for a mode with momentum $\mathbf{k}$ [109, 110]:

$$P_\zeta(k) = |\delta_H|^2 = \frac{2\pi}{k^3}\frac{\mathcal{H}^2}{\epsilon M_{\rm Pl}^2}. \tag{3.46}$$

δ_H is the amplitude of the density perturbations in the CMB, which we will use extensively in the Chapters 7 and 8 where we will try to encompass MSSM inflation, DM and the baryogenesis within one framework. According to the combined Planck and WMAP data, the best fit value for the curvature perturbation amplitude with an arbitrary reference scale, also known as the pivot scale, chosen at $k_0 = 0.05$ Mpc^{-1} is $P_\zeta(k_0) = 2.196^{+0.051}_{-0.060} \times 10^{-9}$ (68% C.L.) [91]. $P_\zeta(k)$ can also be parametrised by:

$$k^3 P_\zeta(k) = k_0^3 P_\zeta(k_0)\left(\frac{k}{k_0}\right)^{n_s - 1 + \frac{1}{2}\frac{dn_s}{d\ln k}\ln\frac{k}{k_0} + \text{higher order terms.}}, \tag{3.47}$$

where $\frac{dn_s}{d\ln k} = -0.0065 \pm 0.0076$ and is called a running of the spectral tilt n_s. The above expression is often approximated as a power law with $P_\zeta(k) \propto k^{n_s - 1}$, which is equivalent to taking only the first term in a Taylor expansion in $\ln k$ around k_0. A logical definition of a spectral tilt following from Eq. (3.47) is then [113]:

$$n_s - 1 \equiv \frac{\mathrm{d}}{\mathrm{d}\ln k}\ln[k^3 P_\zeta(k)]. \tag{3.48}$$

In other words, from here we see that the spectral index governs the distribution of density fluctuations in the power spectrum with respect to comoving wave number k. A scale–invariant spectrum, also called the Harrison–Zel'dovich spectrum [114, 115], is obtained by setting $n_s = 1$. Power spectrum with $n_s \neq 1$ is called tilted spectrum.

We continue the calculation of the expression for n_s in Eq. (3.48) by using Eqs. (3.26) and (3.46) to write:

$$\frac{\mathrm{d}}{\mathrm{d}\ln k}\ln[k^3 P_\zeta(k)] = \frac{\mathrm{d}}{\mathrm{d}\mathcal{N}}\ln\left[\frac{2\pi\mathcal{H}^2}{\epsilon M_{\rm Pl}}\right] \times \frac{\mathrm{d}\mathcal{N}}{\mathrm{d}\ln k}. \tag{3.49}$$

$\frac{\mathrm{d}\mathcal{N}}{\mathrm{d}\ln k}$ can be evaluated by using the horizon crossing condition $k = a\mathcal{H}$ and Eq. (3.27):

$$\frac{\mathrm{d}\mathcal{N}}{\mathrm{d}\ln k} = \left[\frac{\mathrm{d}\ln k}{\mathrm{d}\mathcal{N}}\right]^{-1} = \left[\frac{\mathrm{d}(\mathcal{N}+\ln\mathcal{H})}{\mathrm{d}\mathcal{N}}\right]^{-1} = \left[1+\frac{\mathrm{d}\ln\mathcal{H}}{\mathrm{d}\mathcal{N}}\right]^{-1} \approx 1+\epsilon. \tag{3.50}$$

The factor $\frac{\mathrm{d}}{\mathrm{d}\mathcal{N}}\ln\left[\frac{2\pi\mathcal{H}^2}{\epsilon M_{\rm Pl}}\right]$ in Eq. (3.48) can be written as:

$$\frac{\mathrm{d}}{\mathrm{d}\mathcal{N}}\ln\left[\frac{2\pi\mathcal{H}^2}{\epsilon M_{\rm Pl}}\right] = 2\frac{\mathrm{dln}\mathcal{H}}{\mathrm{d}\mathcal{N}} - \frac{\mathrm{dln}\epsilon}{\mathrm{d}\mathcal{N}}. \tag{3.51}$$

We know that $\frac{\mathrm{dln}\mathcal{H}}{\mathrm{d}\mathcal{N}} = -\epsilon$ so that all that remains is to compute $\frac{\mathrm{dln}\epsilon}{\mathrm{d}\mathcal{N}}$. This is given by:

$$\begin{aligned}\frac{\mathrm{dln}\epsilon}{\mathrm{d}\mathcal{N}} &= \frac{\mathrm{d}\epsilon}{\epsilon\mathcal{H}\mathrm{dt}} = \frac{M_{\rm Pl}^2}{\mathcal{H}\epsilon}\left(\frac{V'}{V}\right)\frac{\mathrm{d}\phi}{\mathrm{dt}}\frac{\mathrm{d}}{\mathrm{d}\phi}\left(\frac{V'}{V}\right) = \left(\frac{V'}{V}\right)\frac{\dot\phi M_{\rm Pl}^2}{\mathcal{H}\epsilon}\left[\frac{V''}{V}-\left(\frac{V'}{V}\right)^2\right] \\ &= \frac{\dot\phi}{\mathcal{H}\epsilon}\Big[\eta-2\epsilon\Big]\left(\frac{V'}{V}\right) = 4\epsilon-2\eta,\end{aligned} \tag{3.52}$$

where we used the slow roll conditions in Eqs. (3.20). From this, it follows that $\frac{\mathrm{d}}{\mathrm{d}\mathcal{N}}\ln\left[\frac{2\pi\mathcal{H}^2}{\epsilon M_{\rm Pl}}\right] = -6\epsilon+2\eta$. Combining this with $\frac{\mathrm{d}\mathcal{N}}{\mathrm{d}\ln k} \approx 1+\epsilon$ and Eq. (3.48) gives:

$$n_s - 1 \backsimeq -6\epsilon + 2\eta, \tag{3.53}$$

to the first order in slow roll parameters. The spectral tilt value, according

to the measurements made by Planck alone, is $n_s = 0.9616 \pm 0.0094$ at 68% C.L. [91]. n_s is another parameter, along with the δ_H, which is crucial if one seeks to define the parameter space of the MSSM inflation and thus enables us to probe the overlap regions where the DM, inflation and baryogenesis coexist within MSSM with non–Universal Higgs Masses (NUHMII) and NMSSM models. Using a similar approach, i.e. writing the metric for the Universe consisting of the background term and the perturbation, one can calculate the power spectrum of the gravitational waves, which at the time when the mode leaves the Hubble patch is expressed as [109, 110]:

$$P_{\text{grav}}(k) = \frac{2}{M_{\text{Pl}}^2}\left(\frac{\mathcal{H}}{2\pi}\right)^2. \tag{3.54}$$

Using this together with Eq. 3.46, another quantity, called tensor to scalar ratio r, for the single field inflation models is [109, 110]:

$$r \equiv \frac{P_{\text{grav}}(k)}{P_\zeta(k)} = 16\epsilon. \tag{3.55}$$

Chapter 4

Supersymmetry

SUSY is an internal spacetime symmetry between spin–half matter particles and integer spin force carriers. The idea behind SUSY is that in supersymmetric extensions of SM, each fermionic particle of the SM has its bosonic superpartner, and every SM boson has its fermionic superpartner. Particles in SUSY are arranged into supersymmetric multiplets each containing fermionic and bosonic states, regarded as superpartners of each other. SM fermions are placed within chiral or matter supermultiplet which also accommodates their spin 0 superpartners. Gluinos and electroweak gauge bosons are accommodated in gauge or vector supermultiplets with their spin 1/2 superpartners gauginos. Finally, there are up and down type Higgs chiral multiplets with spin 0 up and down type Higgses and their spin 1/2 superpartners Higgsinos. Two Higgs superfields are needed to give masses for leptons, up and down type quarks and to cancel gauge anomalies [37].

There is a fermionic SUSY generator Q, that converts one supersymmetric state into the other:

$$Q\,|\text{Fermion}\rangle = |\text{Boson}\rangle \qquad Q\,|\text{Boson}\rangle = |\text{Fermion}\rangle\,. \tag{4.1}$$

Figure 4.1: Radiative corrections to the Higgs mass due to H coupling to fermions (left) and scalars (right). Figure taken from Ref. [37].

SUSY generators are the left handed Weyl spinors that, without suppressing the indices, should be written as Q_α, and their adjoint denotes the right handed counterpart $Q^\dagger_{\dot{\alpha}}$, where $\alpha, \dot{\alpha} = 1, 2$. Adding the new degrees of freedom to the SM helps to resolve or ameliorate some of the before mentioned fundamental problems. For example in SUSY, the Higgs mass is stabilised against radiative corrections: it receives contributions not only from the coupling of the top quark but also from its scalar partner stop, see Fig. 4.1. This eliminates the quadratic divergences and leaves only logarithmic ones [62, 63, 64]:

$$\delta m_{\mathrm{h}}^2 \sim \frac{m_t^4}{v^2}\left[\ln\left(\frac{\Lambda_{\mathrm{UV}}^2}{m_t^2}\right) + ...\right]. \tag{4.2}$$

Here $\Lambda_{\mathrm{UV}} \sim 10^{19}$ GeV is the cut–off scale, where gravity becomes important and $v = 246$ GeV is the VEV of the Higgs field.

SUSY also provides the possibility of gauge coupling unification at the GUT scale. It should be mentioned though, that the simplest MSSM models with universality conditions at high scale become more and more constrained by the ongoing particle physics and cosmology experiments. However, there are a number of low scale phenomenological SUSY models that do not deal with physics at the GUT scale whatsoever. Another important implication of SUSY is that in or-

der to stabilize the proton against decay, a multiplicatively conserved symmetry, called R parity, should be implemented [37]:

$$P_R = (-1)^{3(B-L)+2s}, \tag{4.3}$$

where B, L and s respectively are the baryon, lepton and spin quantum numbers of a particle. P_R also discriminates particles in the same multiplets. Most notably, this symmetry makes the LSP stable. Whenever it is electric and colour neutral, LSP also becomes an excellent DM candidate. Furthermore, there are two more implications of R parity: 1) in the colliders, where the SM particles with $P_R = 1$ are colliding, an even number of superpartners with $P_R = -1$ must be produced to match $P_R = 1$ before interaction and 2) a sparticle must decay into an odd number of sparticles in the final state.

4.1 SUSY Algebra

The (anti)commutation relations amongst the generators of the SUSY transformations, boosts and spacetime translations form the graded super Poincaré algebra [37, 116, 117]. In this section, we will review these relations and discuss their implications.

• Denoting the rotation generators by J_i, Lorentz boost generators by K_i and defining that $M_{0i} \equiv K_i$ and $M_{ij} \equiv \epsilon_{ijk} J_k$ we get the commutation relations of

Poincaré algebra [118]:

$$\begin{aligned}
[P_\mu, P_\nu] &= 0, \\
[M_{\mu\nu}, M_{\rho\sigma}] &= ig_{\nu\rho}M_{\rho\sigma} - ig_{\mu\rho}M_{\nu\sigma} - ig_{\nu\sigma}M_{\mu\rho} + ig_{\mu\sigma}M_{\nu\rho}, \\
[M_{\mu\nu}, P_\rho] &= -ig_{\rho\mu}P_\nu + ig_{\rho\nu}P_\mu.
\end{aligned} \tag{4.4}$$

These relations ensure the Lorentz invariance of the field theory.

• The commutators between $M_{\mu\nu}$ and Q are the following [37, 119, 120]:

$$\begin{aligned}
[M_{\mu\nu}, Q_\alpha] &= i(\sigma_{\mu\nu})^\beta_\alpha Q_\beta, \\
[M_{\mu\nu}, Q^{\dagger\dot{\alpha}}] &= i(\bar{\sigma}_{\mu\nu})^{\dot{\alpha}}_{\dot{\beta}} Q^{\dagger\dot{\beta}}.
\end{aligned} \tag{4.5}$$

• Denoting the R–symmetry generator as R, two commutation relations can be constructed [37, 119, 120]:

$$\begin{aligned}
[Q_\alpha, R] &= Q_\alpha, \\
[Q^\dagger_{\dot{\alpha}}, R] &= Q^\dagger_{\dot{\alpha}}.
\end{aligned} \tag{4.6}$$

Qualitatively this means that Q_α, acting on the state, increases its R quantum number by one, and turns a SM particle into a sparticle, and likewise $Q^\dagger_{\dot{\alpha}}$ decreases R by unity thus transforming a SUSY particle back to a SM counterpart.

Moving on to the remaining (anti)commutation relations we firstly need to discuss what happens when the SUSY generator Q acts on a vacuum state and what are the consequences. If the vacuum preserves SUSY, then the following equality should hold:

$$|0\rangle = e^{iQ}|0\rangle = (1 + iQ + ...)|0\rangle . \tag{4.7}$$

Therefore, if $Q|0\rangle = 0$, then the vacuum is invariant under SUSY and if $Q|0\rangle \neq 0$

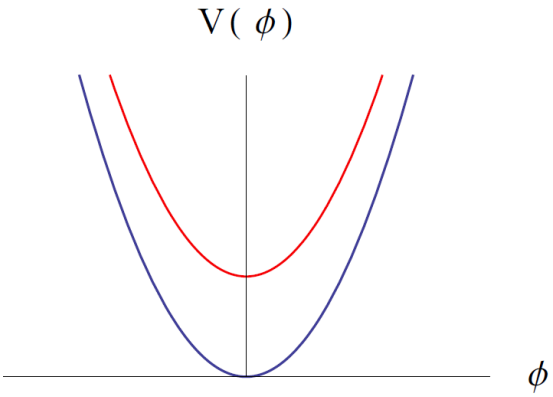

Figure 4.2: Scalar potential for unbroken (blue) and broken (red) potentials.

it is not. This will be important in understanding the physical significance of the anticommutator [37, 119, 120]:

$$\{Q_\alpha, Q^\dagger_{\dot\beta}\} = 2(\sigma^\mu)_{\alpha\dot\beta} P_\mu. \tag{4.8}$$

• Contracting the above expression with $(\bar\sigma^\nu)^{\dot\beta\alpha}$, using $(\bar\sigma^\nu)^{\dot\beta\alpha}(\sigma^\mu)_{\alpha\dot\beta} = 2\eta^{\mu\nu}$ and taking the $\nu = 0$ component one arrives at [37, 119, 120]:

$$\mathscr{H} = \frac{1}{4}(Q_1 Q_1^\dagger + Q_1^\dagger Q_1 + Q_2 Q_1^\dagger + Q_2^\dagger Q_2). \tag{4.9}$$

After taking the expectation value of the vacuum state, i.e. $\langle 0|\,\mathscr{H}\,|0\rangle = \langle 0|\,V\,|0\rangle$, we see that this quantity is always equal to or greater than zero since it is made of the sums of squares. If the vacuum respects SUSY – the expectation value is zero, and otherwise it is positive. Therefore, the implication of the anticommutator is that SUSY will be broken if the expectation value of the scalar potential, or in other words F or/and D terms, does not vanish [37]. The origin of the F and D terms is justified in Sections 4.2.1 and 4.2.4 respectively. This is further graphically illustrated in Fig. 4.2, where the red line depicts the scalar potential

for the broken SUSY because it is positive at the vacuum, i.e. $|\phi\rangle = |0\rangle$ and the blue line demonstrates unbroken SUSY.

$$\{Q_\alpha, Q_\beta\} = \{Q^\dagger_{\dot\alpha}, Q^\dagger_{\dot\beta}\} = 0. \tag{4.10}$$

• These anticommutators simply reflect the fact that acting on a state twice one comes back to the original state.

$$[Q_\alpha, P_\mu] = [Q^\dagger_{\dot\alpha}, P_\mu] = 0. \tag{4.11}$$

• This identity reflects the fact that SUSY is an internal symmetry, i.e. it is independent of spacetime position. Furthermore, this commutator implies that the masses of the fermion and the boson within the same supermultiplet are degenerate. To demonstrate this we start by showing that the square of four momentum and SUSY generator commutes:

$$[P^2, Q_\alpha] = P_\mu[P^\mu, Q_\alpha] + [P_\mu, Q_\alpha]P^\mu = 0. \tag{4.12}$$

The mass of the fermionic state is found by

$$P^2 |\mathrm{F}\rangle = m^2 |\mathrm{F}\rangle , \tag{4.13}$$

where $P^2 = P^\mu P_\mu$. Acting with P^2 on a bosonic state and using Eq. (4.1) gives $P^2 |\mathrm{B}\rangle = P^2 Q_\alpha |\mathrm{F}\rangle$. Remembering that $[P^2, Q_\alpha] = 0$ we get $P^2 Q_\alpha |\mathrm{F}\rangle = Q_\alpha P^2 |\mathrm{F}\rangle$. Now using Eq. (4.13) we find $Q_\alpha P^2 |\mathrm{F}\rangle = m^2 |\mathrm{B}\rangle$, which implies that for every fermionic state there exists bosonic counterpart with the same mass. Obviously, since we have not observed sparticles this implies that SUSY must be

a broken theory [121, 122, 123].

4.2 Supersymmetric Toy Model

4.2.1 Simplest non–interacting theory for chiral supermultiplet

The simplest chiral (or matter) supermultiplet is made of the Weyl fermion, ψ, and it's supersymmetric counterpart scalar particle, ϕ. Below we will briefly review the main steps of how to construct Lagrangian that would be invariant not only under Lorentz and gauge transformations but also under SUSY transformations. The obvious start is to write down the kinetic terms for the fermions and scalars and then try to identify SUSY transformations that would make the variation of the action vanishing. The kinetic part of the Lagrangian is:

$$\begin{aligned} \mathcal{L}_{\text{kinetic}} &= \mathcal{L}_{\text{fermion}} + \mathcal{L}_{\text{scalar}}, \\ &= \bar{\psi} i \bar{\sigma}^{\mu} (\partial_{\mu} \psi) + (\partial^{\mu} \phi^{\dagger})(\partial_{\mu} \phi). \end{aligned} \tag{4.14}$$

As mentioned above, in SUSY the bosonic and fermionic states are treated on an equal basis, i.e. we have a transformation that turns fermionic states into bosonic states and vice versa. Here we define transformation of scalar to Weyl fermion by [37]:

$$\delta\phi = \theta\psi, \qquad \delta\phi^{\dagger} = \bar{\theta}\bar{\psi}. \tag{4.15}$$

We will assume that θ is infinitesimal, anticommuting and, in order to make things simpler, we will consider global symmetry which implies $\partial_{\mu}\theta = 0$. θ and its adjoint are crucial in the superfield formulation and, along with x^{μ}, constitutes

the coordinates of the superspace. To find how the fermion ψ can be transformed into a scalar, we first check how the scalar part of the Lagrangian varies with SUSY transformations defined in Eq. (4.15):

$$\begin{aligned}\delta\mathcal{L}_{\text{scalar}}(\partial^\mu\phi^\dagger, \partial_\mu\phi) &= \frac{\partial\mathcal{L}_{\text{scalar}}}{\partial(\partial^\mu\phi^\dagger)}\partial^\mu(\delta\phi^\dagger) + \frac{\partial\mathcal{L}_{\text{scalar}}}{\partial(\partial_\mu\phi)}\partial_\mu(\delta\phi) \\ &= (\partial_\mu\phi)\bar{\theta}(\partial^\mu\bar{\psi}) + (\partial^\mu\phi^\dagger)\theta(\partial_\mu\psi).\end{aligned} \tag{4.16}$$

To cancel $\delta\mathcal{L}_{\text{scalar}}$ with the $\delta\mathcal{L}_{\text{fermion}}$ the transformation of fermion to scalar can be written as [37]:

$$\delta\psi_\alpha = -i(\sigma^\mu\bar{\theta})_\alpha\partial_\mu\phi, \qquad \delta\bar{\psi}_{\dot{\alpha}} = i(\theta\sigma^\mu)_{\dot{\alpha}}\partial_\mu\phi^\dagger. \tag{4.17}$$

Using these relations one finds that:

$$\begin{aligned}\delta\mathcal{L}_{\text{fermion}} &= -\theta\psi(\partial_\mu\partial^\mu\phi^\dagger) + \bar{\psi}\bar{\theta}(\partial_\mu\partial^\mu\phi) \\ &= -\delta\mathcal{L}_{\text{scalar}} + \partial_\mu[\theta\psi(\partial^\mu\phi^\dagger) + \bar{\psi}\bar{\theta}(\partial^\mu\phi)],\end{aligned} \tag{4.18}$$

and combining Eqs. (4.16) with (4.18) we find that variation of the total kinetic Lagrangian in Eq. (4.14) cancels up to total derivatives:

$$\delta\mathcal{L}_{\text{kinetic}} = \delta\mathcal{L}_{\text{scalar}} + \delta\mathcal{L}_{\text{fermion}} = \partial_\mu[\theta\psi(\partial^\mu\phi^\dagger) + \bar{\psi}\bar{\theta}(\partial^\mu\phi)]. \tag{4.19}$$

The last thing left to show is that SUSY algebra closes, i.e. that the commutator of two successive transformations by a different amount of θ is a symmetry of the

Lagrangian. For a scalar field we have [37]:

$$\begin{aligned}(\delta_{\theta_2}\delta_{\theta_1} - \delta_{\theta_1}\delta_{\theta_2})\phi &= \delta_{\theta_2}\delta_{\theta_1}\phi - \delta_{\theta_1}\delta_{\theta_2}\phi = \theta_1\delta_{\theta_2}\psi - \theta_2\delta_{\theta_1}\psi \\ &= \theta_1(-i)\sigma^\mu\bar{\theta}_2\partial_\mu\phi - \theta_2(-i)\sigma^\mu\bar{\theta}_1\partial_\mu\phi \\ &= -i(\theta_1\sigma^\mu\bar{\theta}_2 - \theta_2\sigma^\mu\bar{\theta}_1)\partial_\mu\phi.\end{aligned} \tag{4.20}$$

Since the four momentum operator, $P_\mu = i\partial_\mu$, is a generator of spacetime translations:

$$e^{-ia^\nu P_\nu}x^\mu \backsimeq (1 + a^\nu\partial_\nu)x^\mu = x^\mu + a^\nu\partial_\nu x^\mu = x^\mu + a^\nu\delta^\mu_\nu = x^\mu + a^\mu, \tag{4.21}$$

we get that the commutator in Eq. (4.20) gives the same field just shifted in a spacetime. Analogous commutator evaluation for the fermions yields:

$$\begin{aligned}(\delta_{\theta_2}\delta_{\theta_1} - \delta_{\theta_1}\delta_{\theta_2})\psi_\alpha = &-i(\theta_1\sigma^\mu\bar{\theta}_2 - \theta_2\sigma^\mu\bar{\theta}_1)\partial_\mu\psi_\alpha - \theta_{2\alpha}\bar{\theta}_1 i\bar{\sigma}^\mu\partial_\mu\psi \\ &+ \theta_{1\alpha}\bar{\theta}_2 i\bar{\sigma}^\mu\partial_\mu\psi,\end{aligned} \tag{4.22}$$

where we used a Fierz identity [37]:

$$(\sigma^\mu\bar{\theta}_1)_\alpha\theta_2\partial_\mu\psi = -\theta_{2\alpha}(\partial_\mu\psi)\sigma^\mu\bar{\theta}_1 - (\partial_\mu\psi)_\alpha\sigma^\mu\bar{\theta}_1\theta_2. \tag{4.23}$$

In Eq. (4.22) the first term reflects the fact that a commutator on a fermion field results in a same field but shifted in spacetime, and other two terms vanish for the massless particles, i.e. in the cases where $i\bar{\sigma}^\mu\partial_\mu\psi = 0$ is valid. Therefore, we showed that the SUSY algebra closes but only for massless on–shell fermions. To make it viable for off–shell cases, the new term $\mathcal{L}_F = FF^*$ needs to be added to Eq. (4.14) where F is the auxiliary field. Auxiliary field has a mass dimension of 2, and doesn't have a kinetic term. The appearance of the new term in Eq.

(4.14) requires the introduction of the transformation rules for the auxiliary field and slight refinement of the ones for the fermionic field [37]:

$$\delta\psi_\alpha = -i(\sigma^\mu\bar{\theta})_\alpha\partial_\mu\phi + \theta_\alpha F, \qquad \delta\bar{\psi}_{\dot{\alpha}} = i(\theta\sigma^\mu)_{\dot{\alpha}}\partial_\mu\phi^\dagger + \bar{\theta}_{\dot{\alpha}}F^*, \tag{4.24}$$

$$\delta F = -i\bar{\theta}\bar{\sigma}^\mu(\partial_\mu\psi), \qquad \delta F^* = -i\theta\sigma^\mu(\partial_\mu\bar{\psi}). \tag{4.25}$$

The transformation for scalar remains unaltered. Repeating the procedure with the new transformation rules we will now show that the theory closes under SUSY transformations:

$$\begin{aligned}
&(\delta_{\theta_2}\delta_{\theta_1} - \delta_{\theta_1}\delta_{\theta_2})\psi_\alpha = \\
&\delta_{\theta_2}[-i(\sigma^\mu\bar{\theta}_1)_\alpha\partial_\mu\phi] + \theta_{1\alpha}\delta_{\theta_2}F - \delta_{\theta_1}[-i(\sigma^\mu\bar{\theta}_2)_\alpha\partial_\mu\phi] - \theta_{2\alpha}\delta_{\theta_1}F = \\
&- i(\sigma^\mu\bar{\theta}_1)_\alpha\theta_2\partial_\mu\psi - i\theta_{1\alpha}\bar{\theta}_2\bar{\sigma}^\mu\partial_\mu\psi + i(\sigma^\mu\bar{\theta}_2)_\alpha\theta_1\partial_\mu\psi + i\theta_{2\alpha}\bar{\theta}_1\bar{\sigma}^\mu\partial_\mu\psi = \\
&- i(\theta_1\sigma^\mu\bar{\theta}_2 - \theta_2\sigma^\mu\bar{\theta}_1)\partial_\mu\psi_\alpha,
\end{aligned} \tag{4.26}$$

where in a third line we again expanded first and third terms using Fierz identity and cancelled equal terms.

Before starting a new section it is worth remembering that putting all the terms in Eq. (4.14) we get a Lagrangian for a free theory per degree of freedom that has the form [37]:

$$\mathcal{L}_{\text{kinetic}} = (\partial^\mu\phi^\dagger)(\partial_\mu\phi) + \bar{\psi}i\bar{\sigma}^\mu(\partial_\mu\psi) + F^{*,i}F_i. \tag{4.27}$$

4.2.2 Interacting supersymmetric field theory

In the non–interacting model the fermionic and bosonic particles were massless. In this section, we will introduce a quantity called the superpotential $W(\phi)$ with

a mass dimension [3], that will be responsible for generating masses. Keeping only renormalizable terms in the Lagrangian one can write it in the form [37]:

$$\mathcal{L}_{\text{interaction}} = -\frac{1}{2}W^{ij}\psi_i\psi_j + W^i F_i - \frac{1}{2}W^{*,ij}\bar{\psi}_i\bar{\psi}_j + F^{*,i}W_i^*, \tag{4.28}$$

where the superpotential takes the following form [37]:

$$W = m^{ij}\phi_i\phi_j + \frac{1}{3!}y^{ijk}\phi_i\phi_j\phi_k, \tag{4.29}$$

and the derivative with respect to the field reduces the mass dimension by one:

$$W^i = \frac{\delta W}{\delta\phi_i}, \qquad W^{ij} = \frac{\delta W}{\delta\phi_i\delta\phi_j}. \tag{4.30}$$

Before proceeding, we could also integrate out the auxiliary field. Taking all the terms containing F from the Eqs. (4.27) and (4.28) it is easy to compute equations of motion for the F:

$$F_i = -W_i^*, \qquad F^{*,i} = -W^i. \tag{4.31}$$

Defining the the scalar potential as $V = W^{*,i}W_i = F^{*,i}F_i = |F_i|^2$ the final Lagrangian for the interacting theory becomes [37]:

$$\mathcal{L}_{\text{chiral}} = (\partial^\mu\phi^\dagger)(\partial_\mu\phi) + \bar{\psi}i\bar{\sigma}^\mu(\partial_\mu\psi) - \frac{1}{2}W^{ij}\psi_i\psi_j - \frac{1}{2}W^{*,ij}\bar{\psi}_i\bar{\psi}_j - V(\phi). \tag{4.32}$$

4.2.3 Lagrangian for a gauge multiplet

A gauge multiplet is made of the gauge bosons, A_μ^a, and their respective fermionic superpartners gauginos, λ^a. The construction of the Lagrangian is based on

writing down the kinetic terms for the gauge boson field and gauginos, and then defining the SUSY transformations in a similar manner as in the previous section. The kinetic terms for the gauge supermultiplet are [37]:

$$\mathcal{L}_{\text{gauge}} = -\frac{1}{4}F^a_{\mu\nu}F^{\mu\nu,a} + i\bar{\lambda}a\bar{\sigma}^\mu\partial_\mu\lambda^a + \frac{1}{2}D^aD^a, \tag{4.33}$$

where D^a is the gauge auxiliary field of mass dimension [2]. Like a chiral auxiliary field F, D^a is introduced to allow for off-shell interactions. This field can also be integrated out using its equation of motion. The Yang-Mills term, just like in the SM, is made of the field strength tensors, $F^a_{\mu\nu}$:

$$F^a_{\mu\nu} = \partial_\mu A^a_\nu - \partial_\nu A^a_\mu + gf^{abc}A^b_\mu A^c_\nu, \tag{4.34}$$

where g is a gauge coupling and f^{abc} is the structure constant for non–Abelian groups. It can be shown that the supersymmetric transformations that leave Eq. (4.33) invariant are [37]:

$$\begin{aligned}
\delta A^a_\mu &= -\frac{1}{\sqrt{2}}(\theta^\dagger\bar{\sigma}_\mu\lambda^a + \lambda^{\dagger a}\bar{\sigma}_\mu\theta), \\
\delta\lambda^a_\alpha &= \frac{i}{2\sqrt{2}}(\sigma^\mu\bar{\sigma}^\nu\theta)_\alpha F^a_{\mu\nu} + \frac{1}{\sqrt{2}}\theta_\alpha D^a, \\
\delta D^a &= \frac{i}{\sqrt{2}}(-\theta^\dagger\bar{\sigma}^\mu\nabla_\mu\lambda^a + \nabla_\mu\lambda^{\dagger a}\bar{\sigma}^\mu\theta).
\end{aligned} \tag{4.35}$$

4.2.4 Supersymmetric gauge interactions

Obviously, the total Lagrangian of the supersymmetric theory not only has to be invariant under SUSY transformations, but also has to respect gauge invariance. To render the Lagrangian gauge invariant, we apply the same technique as in the SM, i.e. promote the ordinary derivatives in Eq. (4.32) to covariant ones, which

then allows for gauge interactions in the matter and vector supermultiplets. The ordinary derivatives for the fermions, sfermions and gauginos then become [37]:

$$\begin{aligned} \nabla_\mu \phi &= \partial_\mu \phi - igA^a_\mu T^a \phi, \\ \nabla_\mu \psi &= \partial_\mu \psi - igA^a_\mu T^a \psi, \\ \nabla_\mu \lambda^a &= \partial_\mu \lambda^a + gf^{abc} A^b_\mu \lambda^c, \end{aligned} \tag{4.36}$$

and corresponding gauge transformations for the vector supermultiplet described in the Lagrangian in Eq. (4.33), are:

$$\begin{aligned} A^a_\mu &\to A^a_\mu + \partial_\mu \Lambda + gf^{abc} A^b_\mu \Lambda^c, \\ \lambda^a &\to \lambda^a + gf^{abc} \lambda^b \Lambda^c. \end{aligned} \tag{4.37}$$

In fact, besides the terms in $\mathcal{L}_{\text{chiral}}$ and $\mathcal{L}_{\text{gauge}}$, there are three more renormalizable terms that respect supersymmetric and gauge interactions [37]:

$$g(\phi^* T^a \psi)\lambda^a, \qquad g\lambda^{\dagger a}(\psi^\dagger T^a \phi), \qquad g(\phi^* T^a \phi) D^a. \tag{4.38}$$

The physical significance of the first two terms is that they appear in the neutralino mass matrix off–diagonal entries and leads to the mixing between gauginos and neutral higgsinos. The last term is used to integrate out the gauge auxiliary field D^a. Actually all these terms arise naturally if the supersymmetric Lagrangian would be build using the superfield formalism. So all in all the full Lagrangian can be expressed as follows [37]:

$$\mathcal{L}_{\text{SUSY}} = \mathcal{L}_{\text{chiral}} + \mathcal{L}_{\text{gauge}} - \sqrt{2} g(\phi^* T^a \psi)\lambda^a - \sqrt{2} g\lambda^{\dagger a}(\psi^\dagger T^a \phi) + g(\phi^* T^a \phi) D^a. \tag{4.39}$$

Using the last term in the gauge Lagrangian Eq. (4.33) and $g(\phi^* T^a \phi) D^a$ term, one finds the equations of motions for D^a to be:

$$D^a = -g(\phi^* T^a \phi). \tag{4.40}$$

Using this the potential can then be written as [37]:

$$V(\phi, \phi^*) = F^{*i} F_i + \frac{D^a D^a}{2}. \tag{4.41}$$

Reiterating the point made in the last section, if SUSY is broken, then $F_i \neq 0$ and/or $D^a \neq 0$ must be satisfied. However, even in the case of broken SUSY, there are certain directions in the field space along which, one or both, of these terms are vanishing. These are called the flat directions and, as we will discuss later, some of them could be a good inflaton candidate.

4.2.5 Soft SUSY breaking

As we discussed in Section 4.1, one of the SUSY graded algebra's implications is that the masses of the particles in chiral and vector supermultiplets are equal. However, since none of the sparticles have ever been observed experimentally it implies that SUSY, if nature respects it at all, must be broken. In this section, we introduce the terms that can be added to $\mathcal{L}_{\text{SUSY}}$ and in the later chapters we will discuss their possible origin in the greater detail. Broadly speaking, soft SUSY breaking means introducing renormalizable terms in a manner that would not lead to UV infinities. General terms allowed in the soft SUSY breaking

Lagrangian, $\mathcal{L}_{\text{soft}}$, are [37]:

$$\mathcal{L}_{\text{soft}} = -(m^2)^i_j \phi^{j*}\phi_i - \left(\frac{1}{2}M_a\lambda^a\lambda^a + \frac{1}{3!}a^{ijk}\phi_i\phi_j\phi_k + \frac{1}{2}b^{ij}\phi_i\phi_j + c^i\phi_i + \text{c.c.}\right). \quad (4.42)$$

So the total Lagrangian for the broken theory becomes:

$$\mathcal{L}_{\cancel{\text{SUSY}}} = \mathcal{L}_{\text{SUSY}} + \mathcal{L}_{\text{soft}}. \quad (4.43)$$

4.3 Superspace and Superfields

The superfield is a function of the superspace. As mentioned above, the superspace is constructed by combining spacetime coordinates x^μ along with a two component spinor (with anticommuting components) and its adjoint:

$$\Phi = \Phi(x^\mu, \theta^\alpha, \bar{\theta}_{\dot{\alpha}}), \quad (4.44)$$

where:

$$\theta^\alpha\theta^\beta = -\theta^\beta\theta^\alpha \qquad \text{and} \qquad \theta^\alpha\theta^\alpha = \theta^\beta\theta^\beta = 0. \quad (4.45)$$

Thus, terms involving more than two components of θ or $\bar{\theta}$ are equal to zero. Therefore, any general function expanded in terms of θ and $\bar{\theta}$ behaves like:

$$g(\theta\bar{\theta}) = g_0 + g_1\theta + g_2\bar{\theta} + g_3\theta\bar{\theta} + \underbrace{\ldots}_{=0} = g_0 + g_1\theta + g_2\bar{\theta} + g_3\theta\bar{\theta}. \quad (4.46)$$

Note, that in this expansion we assumed that θ has only one component. An integration over the θ is then defined as:

$$\int d\theta = 0, \qquad \int d\theta\theta = 1. \quad (4.47)$$

Using this to integrate Eq. (4.46) one gets:

$$\int g(\theta\bar{\theta})d\theta = g_1 + g_3\bar{\theta}. \tag{4.48}$$

In other words, integration simply picks out the terms that contain θ. Similarly, integrating $g(\theta\bar{\theta})$ over $\theta\bar{\theta}$ would give g_3. Coming back to the actual two component θ and $\bar{\theta}$ in terms of which superfields are expanded let us define:

$$d^2\theta \equiv -\frac{1}{4}d\theta^\alpha d\theta^\beta \epsilon_{\alpha\beta}, \qquad d^2\bar{\theta} \equiv -\frac{1}{4}d\bar{\theta}_{\dot{\alpha}} d\bar{\theta}_{\dot{\beta}} \epsilon^{\dot{\alpha}\dot{\beta}}, \tag{4.49}$$

where spinor indices are included for clarity. Any term in a superfield (or a combination of superfields) that is accompanied by a combination of $\theta\theta\bar{\theta}\bar{\theta}$ is called a D term and terms followed by $\theta\theta$ are called F terms. To express them, one simply needs to integrate:

$$\Phi_1...\Phi_n|_D = \int d^2\theta d^2\bar{\theta}(\Phi_1...\Phi_n) \qquad \text{and} \qquad \Phi_1...\Phi_n|_F = \int d^2\theta(\Phi_1...\Phi_n). \tag{4.50}$$

4.3.1 Chiral superfields

A chiral superfield and its conjugate arise from imposing the following constraints on a general superfield expansion in terms of θ and $\bar{\theta}$:

$$\bar{D}_{\dot{\alpha}}\Phi = 0 \qquad \text{and} \qquad D_\alpha\Phi^* = 0, \tag{4.51}$$

where:

$$\bar{\mathcal{D}}_{\dot{\alpha}} = -\frac{\partial}{\partial\bar{\theta}_{\dot{\alpha}}} - i(\theta\sigma^\mu)_{\dot{\alpha}}\frac{\partial}{\partial x^\mu} \qquad \text{and} \qquad \mathcal{D}_\alpha = \frac{\partial}{\partial\theta^\alpha} + i(\sigma^\mu\theta)_\alpha\frac{\partial}{\partial x^\mu}, \tag{4.52}$$

are called chiral covariant derivatives. To find chiral superfields it is convenient to define [37]:

$$\begin{aligned} y^{\mu} &\equiv x^{\mu} + i\bar{\theta}\bar{\sigma}^{\mu}\theta, \\ y^{\mu *} &\equiv x^{\mu} - i\bar{\theta}\bar{\sigma}^{\mu}\theta, \end{aligned} \tag{4.53}$$

which implies that for a field $\Phi(y^{\mu}, \theta, \bar{\theta})$, the first constraint in Eq. (4.51) translates into condition:

$$\begin{aligned} D^{\dagger}_{\dot{\alpha}}\Phi &= -\frac{\partial\Phi}{\partial\bar{\theta}_{\dot{\alpha}}} - \frac{\partial\Phi}{\partial y^{\mu}}\frac{\partial y^{\mu}}{\partial\bar{\theta}_{\dot{\alpha}}} - i(\theta\sigma^{\mu})_{\dot{\alpha}}\frac{\partial\Phi}{\partial y^{\mu}} \\ &= -\frac{\partial\Phi}{\partial\bar{\theta}_{\dot{\alpha}}} - \frac{\partial\Phi}{\partial y^{\mu}} i(-\theta\sigma^{\mu})_{\dot{\alpha}} - i(\theta\sigma^{\mu})_{\dot{\alpha}}\frac{\partial\Phi}{\partial y^{\mu}} \\ &= -\frac{\partial\Phi}{\partial\bar{\theta}_{\dot{\alpha}}} = 0, \end{aligned} \tag{4.54}$$

where in the second line the fact that $\frac{\partial\bar{\theta}^{\dot{\alpha}}}{\partial\bar{\theta}^{\dot{\beta}}} = -\delta^{\dot{\alpha}}_{\dot{\beta}}$ is used. This means that a chiral superfield does not contain any terms involving $\bar{\theta}$, and thus can be expressed as [37]:

$$\begin{aligned} \Phi(y, \theta) &= \phi(y) + \sqrt{2}\theta\psi(y) - \theta\theta F(y), \\ \bar{\Phi}(y^{*}, \bar{\theta}) &= \phi^{*}(y^{*}) + \sqrt{2}\bar{\theta}\bar{\psi}(y^{*}) - \bar{\theta}\bar{\theta}F^{*}(y^{*}). \end{aligned} \tag{4.55}$$

To find the chiral superfield expression in terms of x^{μ}, one has to perform a Taylor expansion:

$$\begin{aligned} \Phi(x, \theta, \bar{\theta}) = \phi(x) + \sqrt{2}\theta\psi(x) + \theta\theta F(x) + i\theta\sigma^{\mu}\bar{\theta}\partial_{\mu}\phi(x) \\ - \frac{i}{\sqrt{2}}(\theta\theta)\partial_{\mu}\psi(x)\sigma^{\mu}\bar{\theta} - \frac{1}{4}(\theta\theta)(\bar{\theta}\bar{\theta})\partial_{\mu}\partial^{\mu}\phi(x). \end{aligned} \tag{4.56}$$

Similarly, its conjugate is:

$$\begin{aligned} \bar{\Phi}(x, \theta, \bar{\theta}) = \phi^{*}(x) + \sqrt{2}\bar{\theta}\bar{\psi}(x) + \bar{\theta}\bar{\theta}\bar{F}(x) - i\theta\sigma^{\mu}\bar{\theta}\partial_{\mu}\phi^{*}(x) \\ + \frac{i}{\sqrt{2}}(\bar{\theta}\bar{\theta})\theta\sigma^{\mu}\partial_{\mu}\bar{\psi}(x) - \frac{1}{4}(\theta\theta)(\bar{\theta}\bar{\theta})\partial_{\mu}\partial^{\mu}\phi^{*}(x). \end{aligned} \tag{4.57}$$

Supersymmetric transformations between the components of the superfield that were explained in Eqs. (4.15), (4.24) and (4.25) can be recovered using:

$$\delta_\theta \Phi = -i(\theta \mathcal{Q} + \bar{\theta}\bar{\mathcal{Q}})\Phi, \tag{4.58}$$

where $\mathcal{Q}$ is an operator responsible for supersymmetry translations:

$$\begin{aligned} \mathcal{Q} &\equiv \frac{\partial}{\partial\theta} - i\sigma^\mu \bar{\theta} \frac{\partial}{\partial x^\mu}, \\ \bar{\mathcal{Q}} &\equiv \frac{\partial}{\partial\bar{\theta}} - i\bar{\sigma}^\mu \theta \frac{\partial}{\partial x^\mu}. \end{aligned} \tag{4.59}$$

Using superfield expressions in Eqs. (4.56) and (4.57), a basic Wess–Zumino model (discussed in previous sections), can be derived from the following Lagrangian:

$$\mathcal{L}_{\mathrm{WZ}} = K(\Phi, \bar{\Phi})|_D + (W(\Phi)|_F + \mathrm{h.c.}), \tag{4.60}$$

where the first term is called Kähler potential and the second is known as the superpotential, defined as [37]:

$$K(\Phi, \bar{\Phi}) = \Phi\bar{\Phi} \qquad \text{and} \qquad W(\Phi) = \frac{m}{2}\Phi^2 + \frac{y}{3}\Phi^3. \tag{4.61}$$

Inserting Eqs. (4.56) and (4.57) into Kähler potential one gets [37]:

$$\begin{aligned} K(\Phi, \bar{\Phi})|_D &= \int d^2\theta d^2\bar{\theta}\Phi\bar{\Phi} \\ &= (\partial^\mu \phi^\dagger)(\partial_\mu \phi) + \bar{\psi} i\bar{\sigma}^\mu (\partial_\mu \psi) + |F|^2 + (\text{total derivatives}). \end{aligned} \tag{4.62}$$

Plugging the superpotential from Eq. (4.61) into $\mathcal{L}_{\text{WZ}}$ one arrives at [37]:

$$\begin{aligned} &W(\Phi)|_F\text{+h.c.} = \int d^2\theta\left(\frac{m}{2}\Phi^2 + \frac{y}{3}\Phi^3\right) + \text{h.c.} = \\ &\left(\frac{m}{2} + \phi y\right)\psi\psi + (m\phi + y\phi^2)F + \text{h.c.} = \frac{\partial^2 W}{\partial\phi^2}\psi\psi + \frac{\partial W}{\partial\phi}F + \text{h.c.}, \end{aligned} \tag{4.63}$$

where $\frac{\partial W}{\partial\Phi}|_{\Phi=\phi} \equiv \frac{\partial W}{\partial\phi}$. Finally, after inserting Eqs. (4.62) and (4.63) into $\mathcal{L}_{\text{WZ}}$ and integrating auxiliary field out, we get exactly the same expression for the Wess–Zumino Lagrangian as we did in Eq. (4.32) of Section 4.2.2.

4.3.2 Vector superfields

Vector superfields must be real, i.e. they must conform to the constraint $V = \bar{V}$. To derive an action for the gauge fields and gauginos, one must make use of a vector superfield, which is defined as [37]:

$$V = \bar{\theta}\bar{\sigma}^\mu\theta A_\mu + \bar{\theta}\bar{\theta}\theta\lambda + \theta\theta\bar{\theta}\bar{\lambda} + \frac{\theta\theta\bar{\theta}\bar{\theta}D}{2}. \tag{4.64}$$

Also, by defining:

$$\mathcal{W}_\alpha \equiv -\frac{1}{4}\bar{\mathcal{D}}\bar{\mathcal{D}}\mathcal{D}_\alpha V, \tag{4.65}$$

where derivatives $\mathcal{D}$ are defined in Eq. (4.52), a Lagrangian for kinetic terms of gauge vector supermultiplet can be calculated by collecting F terms of $\mathcal{W}^\alpha\mathcal{W}_\alpha$ [37], i.e.:

$$\mathcal{L}_{\text{gauge}} = \mathcal{W}^\alpha\mathcal{W}_\alpha|_F\text{+h.c.} = -\frac{1}{4}F_{\mu\nu}F^{\mu\nu} + i\bar{\lambda}\bar{\sigma}^\mu\partial_\mu\lambda + \frac{1}{2}DD, \tag{4.66}$$

just as we had in Eq. (4.33). Finally, to couple fields in gauge supermultiplet to the fields in chiral supermultiplet in a gauge invariant way, the Kähler potential is redefined to [37]:

$$K(\Phi, \bar{\Phi}, V) = \bar{\Phi} e^{2gV} \Phi, \tag{4.67}$$

where g is a gauge coupling. Calculating D terms now gives:

$$\begin{aligned} K(\Phi, \bar{\Phi}, V)|_D = (\partial^\mu \phi^\dagger)(\partial_\mu \phi) + \bar{\psi} i \bar{\sigma}^\mu (\partial_\mu \psi) + |F|^2 + g(\phi^* T^a \psi)\lambda^a \\ + g\lambda^{\dagger a}(\psi^\dagger T^a \phi) + g(\phi^* T^a \phi) D^a, \end{aligned} \tag{4.68}$$

where T^a are the generators of the gauge group. Therefore, superfield formalism grasps the three terms which were included by hand in the previous Section 4.2.4.

In a complete SUSY Lagrangian we will then have two terms that include an auxiliary field D. One comes from $\mathcal{L}_{\text{gauge}}$ in Eq. (4.66) and another, as was just shown, from a modified Kähler potential. From here, as mentioned in Section 4.2.4, equation of motion for the D term is $D^a = -g(\phi^* T^a \phi)$. Substituting this into the total SUSY Lagrangian, we get a D term contribution in the supersymmetric potential.

4.4 Minimal Supersymmetric Standard Model

The particle content of the MSSM and the respective gauge charges are listed in the Table 4.1. The key ingredients to extract the physical content in SUSY models are the superpotential and soft breaking Lagrangian density. Having these the phenomenological consequences can be analysed.

Usually the superpotential is expressed in terms of the chiral superfields, however analysing it in terms of the scalar components allows one to grasp the physics

Superfield	$SU(3)_c \times SU(2)_L \times U(1)_Y$
$\hat{Q}_i = \begin{pmatrix} \hat{u}_L \\ \hat{d}_L \end{pmatrix}_i$	$(\mathbf{3}, \mathbf{2}, \frac{1}{6})$
$\hat{u}^*_{R,i}$	$(\mathbf{3}^*, \mathbf{1}, -\frac{2}{3})$
$\hat{d}^*_{R,i}$	$(\mathbf{3}^*, \mathbf{1}, \frac{1}{3})$
$\hat{L}_i = \begin{pmatrix} \hat{\nu} \\ \hat{e}_L \end{pmatrix}_i$	$(\mathbf{1}, \mathbf{2}, -\frac{1}{2})$
$\hat{e}^*_{R,i}$	$(\mathbf{1}, \mathbf{1}, 1)$
$\hat{H}_u = \begin{pmatrix} \hat{H}^+_u \\ \hat{H}^0_u \end{pmatrix}$	$(\mathbf{1}, \mathbf{2}, \frac{1}{2})$
$\hat{H}_d = \begin{pmatrix} \hat{H}^0_d \\ \hat{H}^-_d \end{pmatrix}$	$(\mathbf{1}, \mathbf{2}^*, -\frac{1}{2})$
$\hat{V}_1$	$(\mathbf{1}, \mathbf{1}, 0)$
$\hat{V}_2$	$(\mathbf{1}, \mathbf{3}, 0)$
$\hat{V}^a_3$	$(\mathbf{8}, \mathbf{1}, 0)$

Table 4.1: The charges of the MSSM particle content. Index i represents the family index and $a = 1, 2...8$. $\hat{V}_1, \hat{V}_2$ and $\hat{V}^a_3$ are the vector superfields.

at the same depth. The superpotential of the MSSM is expressed as[37]:

$$W_{\text{MSSM}} = (\mathbf{y_u})^{ij} \bar{u}_i Q_j H_u - (\mathbf{y_d})^{ij} \bar{u}_i Q_j H_d - (\mathbf{y_e})^{ij} \bar{e}_i L_j H_d + \mu H_d H_u, \qquad (4.69)$$

where i, j are the family indices and the gauge indices are omitted for simplicity. Unlike in the SM, in the MSSM there are two Higgs doublets $H_u = (H^+_u, H^0_u)$ and $H_d = (H^0_d, H^-_d)$ and they are needed for gauge anomaly cancellation and also to give the masses for the up and down type matter fields. The μ is called Higgs mixing parameter and $\mathbf{y}$ are the 3×3 Yukawa matrices. Since Yukawa couplings are relatively large only for top, bottom quarks and the tauon, these matrices can

be greatly simplified in the following manner:

$$\mathbf{y_u} \approx \begin{pmatrix} 0 & 0 & 0 \\ 0 & 0 & 0 \\ 0 & 0 & y_t \end{pmatrix}, \qquad \mathbf{y_d} \approx \begin{pmatrix} 0 & 0 & 0 \\ 0 & 0 & 0 \\ 0 & 0 & y_b \end{pmatrix}, \qquad \mathbf{y_e} \approx \begin{pmatrix} 0 & 0 & 0 \\ 0 & 0 & 0 \\ 0 & 0 & y_\tau \end{pmatrix}. \tag{4.70}$$

As we will discuss later in great detail, choosing Yukawa couplings in this way has further significant phenomenological consequences, i.e. that left/right handed states of the first and second generation squarks and sleptons do not mix and their gauge eigenstates coincide with the mass eigenstates where in the case for stau, sbottom and stop the LH and RH gauge eigenstates mix with each other to produce two, lighter and heavier, mass eigenstates.

4.4.1 F and D–flat directions

Configurations of the fields, satisfying:

$$F_i^* = \frac{\partial W}{\partial X^i} = 0 \qquad \text{and} \qquad D^a = X^\dagger T^a X = 0, \tag{4.71}$$

are respectively called F and D–flat [124, 125, 126, 127]. Here the X can be a condensate of many fields, i.e. $X_m = \Phi_1\Phi_2...\Phi_m$. Gauge invariant monomials from MSSM fields are constructed by contracting colour indices to form $\mathrm{SU}(3)_c$ singlets and then contracting $\mathrm{SU}(2)_L$ isospin indices to form $\mathrm{SU}(3)_c{\times}\mathrm{SU}(2)_L$ singlets. Finally, the fields are combined to form $\mathrm{SU}(3)_c{\times}\mathrm{SU}(2)_L{\times}\mathrm{U}_Y$ zero hypercharge combinations [127]. For example, LH_u monomial, including gauge indices, would take the form $L^a H_u^b \epsilon_{ab}$, where ϵ_{ab} is totally antisymmetric tensor. Using

the superpotential of the MSSM given in Eq. (4.69), one finds:

$$\begin{aligned} F^*_{H_u} &= \mathbf{y_u}\bar{u}Q + \mu H_d, \\ F^*_L &= \mathbf{y_d} H_d \bar{e}. \end{aligned} \tag{4.72}$$

The requirement to satisfy gauge invariance implies that $F^*_{H_u} = F^*_L = 0$ for any ϕ because RH fields, unlike the LH, are the singlets under $SU(2)$. Therefore, the combination $X_2 = LH_u$ is a F–flat. Choosing the isospin components in the following manner:

$$H_u = \frac{1}{\sqrt{2}}\begin{pmatrix} 0 \\ \phi \end{pmatrix} \qquad \text{and} \qquad L = \frac{1}{\sqrt{2}}\begin{pmatrix} \phi \\ 0 \end{pmatrix}, \tag{4.73}$$

we can check that LH_u is also D–flat [124]:

$$\sum_{a=1}^{3} D^a = \sum_{a=1}^{3} (H_u^\dagger \sigma^a H_u + L^\dagger \sigma^a L) = \frac{1}{2}(|\phi|^2 - |\phi|^2) = 0, \tag{4.74}$$

where σ^a are the three Pauli matrices – the generators of the $SU(2)$ gauge group. By using hypercharge values for L and H_u listed in Table 4.1, we can show the $U_Y(1)$ flatness of the LH_u direction:

$$D_Y = -\frac{1}{2}|L|^2 + \frac{1}{2}|H_u|^2 = -\frac{1}{2}|\phi|^2 + \frac{1}{2}|\phi|^2 = 0, \tag{4.75}$$

for any generation of L. In Chapter 7, we will review the inflationary model, where two flat directions – $\widetilde{u}\widetilde{d}\widetilde{d}$ and $\widetilde{L}\widetilde{L}\widetilde{e}$ play the role of the inflaton. Here, tilde emphasises that it is the superpartner of the SM sfermions. Often this is clear in context and, as such, will be omitted in order to reduce clutter. Including gauge indices, these monomials would be expressed as $\widetilde{u}_\alpha \widetilde{d}_\beta \widetilde{d}_\gamma \epsilon^{\alpha\beta\gamma}$ and $\widetilde{L}^a \widetilde{L}^b \epsilon_{ab} \widetilde{e}$,

where indices are written up (down) for the RH (LH) fields. Their $SU(3)_c\times$ $SU(2)_L\times U(1)_Y$ flatness is demonstrated in the Appendix A.

4.4.2 Soft SUSY breaking in the MSSM

The soft SUSY breaking Lagrangian for the MSSM case is given by [37]:

$$\begin{aligned}-\mathcal{L}_{\text{soft}}^{\text{MSSM}} = &\frac{1}{2}(M_1\widetilde{B}\widetilde{B} + M_2\widetilde{W}\widetilde{W} + M_3\widetilde{G}\widetilde{G} + \text{c.c.}) \\ &+ (\tilde{u}\mathbf{a_u}\tilde{Q}H_u + \tilde{\bar{d}}\mathbf{a_d}\tilde{Q}H_d + \tilde{\bar{e}}\mathbf{a_e}\tilde{L}H_d + \text{c.c.}) \\ &+ \tilde{Q}^\dagger\mathbf{m_Q^2}\tilde{Q} + \tilde{L}^\dagger\mathbf{m_L^2}\tilde{L} + \tilde{u}\mathbf{m_{\bar{u}}^2}\tilde{\bar{u}}^\dagger + \tilde{\bar{d}}\mathbf{m_{\bar{d}}^2}\tilde{\bar{d}}^\dagger + \tilde{\bar{e}}\mathbf{m_{\bar{e}}^2}\tilde{\bar{e}}^\dagger \\ &+ m_{H_u}^2 H_u^* H_u + m_{H_d}^2 H_d^* H_d + (B\mu H_u H_d + \text{c.c.}).\end{aligned} \tag{4.76}$$

The first line introduces the masses for gauginos. Massive A-terms appear in the second line. $\mathbf{a_u}$, $\mathbf{a_d}$ and $\mathbf{a_e}$ are the 3×3 matrices in the family space (indices are suppressed). They play a significant role in the flavour violating decays and the LH/RH mixing of third generation sfermions. The value of $(\mathbf{a_u})^3{}_3 = A_t$ is of particular importance for generating sizeable corrections for the Higgs mass. In the third line the soft breaking masses are added. These are also 3×3 matrices in the family space. The presence of the non–zero off–diagonal elements would also contribute to flavour changing interactions. Finally, in the forth line, soft breaking parameters for the up and down type Higgs fields appear which play an essential role in EW symmetry breaking. Fig. 4.3 depicts the Feynman diagrams where the soft breaking terms contribute to the $\mu \to e\gamma$ decay. In the first diagram the off–diagonal elements $(m_{\tilde{e}}^2)_{12}$ + c.c. are non–zero. Similarly, in the b diagram the left handed slepton matrix has non–vanishing off–diagonal elements. In the c diagram the trilinear term $\mathbf{a_e}$ contributes after the H_d acquires a VEV

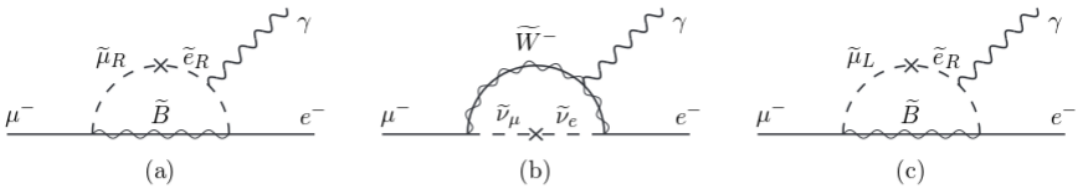

Figure 4.3: Lepton number violating diagrams for $\mu \to e\gamma$ process. The figure is from Ref. [37].

[37].

The origin of the soft breaking terms are subject to intense research, but in general they emerge via similar mechanisms: hidden sector, that does not couple directly to the MSSM particle content, and the messenger field, that interacts with visible and hidden sectors, are introduced. SUSY is broken in the hidden sector and this is mediated by the messenger field to the MSSM. The most widely discussed mechanisms for explaining the origin of the terms in Eq. (4.76) are the following:

• *Gravity mediated breaking* [120, 128, 129, 130]. In this scenario, SUSY is broken in the hidden sector by very heavy scalars. However, particles in the hidden sector do not interact directly with ordinary SM particles and their superpartners. A graviton and its superpartner, the gravitino, then act as messenger fields between observable and hidden sectors. Therefore the supergravity coupling is responsible for the SUSY breaking. To show how SUSY breaking in the hidden sector can induce soft breaking terms in an observable sector, let us consider a superpotential, Kähler potential and gauge kinetic function expanded in terms of

$M_{\rm Pl}$ [37]:

$$\begin{aligned} W &= W_{\rm MSSM} - \frac{1}{M_{\rm Pl}}\left(\frac{1}{3!}yX\Phi^3 + \frac{1}{2}\mu X\Phi^2\right) + ..., \\ K &= \bar{\Phi}\Phi + \frac{1}{M_{\rm Pl}}(nX + \bar{n}\bar{X})\bar{\Phi}\Phi - \frac{1}{M_{\rm Pl}^2}k^2\bar{X}X\bar{\Phi}\Phi + ..., \\ f_{ab} &= \frac{\delta_{ab}}{g_a^2}\left(1 - \frac{2}{M_{\rm Pl}}f_a X + ...\right), \end{aligned} \tag{4.77}$$

where y, k, n, μ and f_a are couplings between fields that they precede. X is the chiral superfield residing in the hidden sector. SUSY is broken once the field X develops $\langle V_F(X)\rangle = |F_X|^2 = \left|\frac{\partial W}{\partial X}\right|^2 \neq 0$ and the effective soft SUSY breaking Lagrangian then reads [37]:

$$\begin{aligned} -\mathcal{L}_{\rm soft} = &\frac{F}{2M_{\rm Pl}}f_a\lambda^a\lambda^a + \frac{F}{6M_{\rm Pl}}y\phi^3 + \frac{F}{2M_{\rm Pl}}\mu\phi^2 + \\ &\frac{|F|^2}{M_{\rm Pl}}(k + |n|^2)\phi^2 + \frac{F}{M_{\rm Pl}}n\phi W_{\rm MSSM} + \text{c.c.}. \end{aligned} \tag{4.78}$$

From this equation it is obvious that induced soft breaking terms are of the order:

$$m_{\rm soft} \sim m_0 \sim m_{1/2} \sim A_0 \sim B_0 \sim \frac{\langle F_X\rangle}{M_{\rm Pl}}, \tag{4.79}$$

where m_0, $m_{1/2}$, A_0 and B_0 are expressed as a functions of couplings defined in Eq. (4.77), and masses of scalars, gauginos, trilinear couplings and B parameter all converge to m_0, $m_{1/2}$, A_0 and B_0 at the GUT scale.

• *Gauge mediated SUSY breaking (GMSB)* [131, 132, 133]. In this model, the soft breaking terms arise due to gauge interactions between the hidden and visible sectors. As a result, the gaugino masses arise at one–loop and scalar masses at two loops. The LSP in the GMSB is always the gravitino and the NLSP is usually the lightest neutralino $\widetilde{\chi}_1^0$. The gauginos have the same mass hierarchy as in Eq. (4.80).

•*Anomaly mediated breaking (AMSB)* [134, 135]. This scenario is similar to gravity mediated SUSY breaking but here there are no tree level interactions between observable and the hidden sectors. The relation for gaugino masses at any energy scale holds as [136]:

$$M_1 : M_2 : M_3 \approx 2.8 : 1 : 8.3. \tag{4.80}$$

One deficiency of this type of SUSY breaking is that it induces negative squared masses for the fermions and therefore some universal scalar parameter has to be added or another contribution of SUSY breaking must be present to make the masses positive. The crucial thing though is that in this type of SUSY breaking, the upper bound on the Higgs mass is 121 GeV [137], and this is very likely to be ruled out in the nearest future as more data comes from the LHC.

These scenarios are the top–bottom approach where the theories, due to imposed universality conditions are defined by a relatively few input parameters and the running of RGE relates GUT physics with the low energy scale. Since SUSY is yet to be found the reverse method of the bottom-up approach is attracting more attention because it provides more freedom as the theories generally have more free parameters at the EW scale.

4.4.3 Electroweak symmetry breaking

Though the idea behind the EW symmetry breaking in the MSSM is the same as in SM, i.e. calculating the VEV of the Higgs field at which its potential is minimum, but the presence of the Higgs doublets renders the theory of EW symmetry breaking within MSSM more complicated. In order to write down the

Higgs scalar potential we have to collect the relevant terms. First, we have the soft breaking terms for the up and down Higgs doublets, see the last line in Lagrangian in Eq. (4.76). The $b = B\mu$ term adds $\mathcal{L}_{\text{soft}} \supset (b(H_u^+ H_d^- - H_u^0 H_d^0) + \text{c.c.})$. Another contribution arises from the F–term in the scalar potential applied on the $\mu H_u H_d$ in the superpotential Eq. (4.69). The last contribution is from the D–term in Eq. (4.40). Collecting all these the have [37]:

$$\begin{aligned} V &= (|\mu|^2 + m_{H_u}^2)(|H_u^0|^2 + |H_u^+|^2) + (|\mu|^2 + m_{H_d}^2)(|H_d^0|^2 + |H_d^-|^2) \\ &+ (b(H_u^+ H_d^- - H_u^0 H_d^0) + \text{c.c.}) + \frac{1}{8}(g_1^2 + g_2^2)(|H_u^0|^2 + |H_u^+|^2 - |H_d^0|^2 - |H_d^-|^2)^2 \\ &+ \frac{1}{2} g_2^2 |H_u^+ H_d^{0*} + H_u^0 H_d^{-*}|^2. \end{aligned} \tag{4.81}$$

In order to have electromagnetic theory unbroken, the charged Higgs components can not develop a VEV and thus have to be equal to zero. This reduces the above potential to [37]:

$$\begin{aligned} V &= (|\mu|^2 + m_{H_u}^2)|H_u^0|^2 + (|\mu|^2 + m_{H_d}^2)|H_d^0|^2 - (bH_u^0 H_d^0 + \text{c.c.}) \\ &+ \frac{1}{8}(g_1^2 + g_2^2)(|H_u^0|^2 - |H_d^0|^2)^2. \end{aligned} \tag{4.82}$$

Choosing

$$\langle H_u^0 \rangle = v_u = v \sin\beta \qquad \text{and} \qquad \langle H_d^0 \rangle = v_d = v \cos\beta, \tag{4.83}$$

the minimization conditions

$$\frac{\partial V}{\partial H_u^0} = \frac{\partial V}{\partial H_d^0} = 0, \tag{4.84}$$

are satisfied if

$$\frac{1}{2} m_Z^2 = \frac{m_{H_d}^2 - m_{H_u}^2 \tan^2\beta}{\tan^2\beta - 1} - \mu^2, \tag{4.85}$$

along with

$$\sin 2\beta = \frac{2b}{m_{H_d}^2 + m_{H_u}^2 + 2\mu^2}, \tag{4.86}$$

are satisfied as well [37]. Note that from Eq. (4.85) it can be seen that for moderate to large $\tan\beta$, the mass of m_Z is insensitive to m_{H_d}:

$$\frac{1}{2}m_Z^2 \simeq -m_{H_u}^2 - \mu^2. \tag{4.87}$$

4.4.4 Parametrizing the fine tuning

The SUSY naturalness issue is closely related to Eq. (4.85). If the soft breaking masses m_{H_u} and m_{H_d} get pushed high, then a delicate cancellation between the first term on the right hand side in Eq. (4.85) and μ^2 is required to yield m_Z^2. Therefore, this equation is used to parametrize the fine tuning. The fine tuning measure is quantified to show the input parameters' sensitivity to the Z mass [138, 139]:

$$\Delta p_i = \left| \frac{\partial \ln M_Z^2(p_i)}{\partial \ln p_i} \right| = \left| \frac{p_i}{M_Z^2} \frac{\partial M_Z^2}{\partial p_i} \right| \tag{4.88}$$

with $p_i = \{\mu^2, b, m_{H_u}, m_{H_d}\}$. Using Eqs. (4.85) and (4.86) in the above equation for each p_i one can find:

$$\Delta\mu^2 = 4\frac{\mu^2}{m_Z^2}\left(1 + \frac{m_A^2 + m_Z^2}{m_A^2}\tan^2 2\beta\right), \tag{4.89}$$

$$\Delta b = \left(1 + \frac{m_A^2}{m_Z^2}\right)\tan^2 2\beta, \tag{4.90}$$

$$\Delta m_{H_u}^2 = \left|\frac{1}{2}\cos 2\beta + \frac{m_A^2}{m_Z^2}\cos^2\beta - \frac{\mu^2}{m_Z^2}\right|\left(1 - \frac{1}{\cos 2\beta} + \frac{m_A^2 + m_Z^2}{m_A^2}\tan^2 2\beta\right), \tag{4.91}$$

$$\Delta m_{H_d}^2 = \left|-\frac{1}{2}\cos 2\beta + \frac{m_A^2}{m_Z^2}\sin^2\beta - \frac{\mu^2}{m_Z^2}\right|\left(1 + \frac{1}{\cos 2\beta} + \frac{m_A^2 + m_Z^2}{m_A^2}\tan^2 2\beta\right). \tag{4.92}$$

The total fine tuning is then defined as:

$$\Delta_{\rm tot} = \sqrt{(\Delta\mu^2)^2 + (\Delta b)^2 + (\Delta m^2_{H_u})^2 + (\Delta m^2_{H_d})^2}. \tag{4.93}$$

Large $\Delta_{\rm tot}$ indicates that a theory is highly fine tuned.

4.4.5 Focus point: natural multi-TeV scalars in CMSSM

In a top–down class of supersymmetric models that respect universality conditions, like for example mSUGRA or CMSSM [1], scalar particles have equal masses, usually denoted m_0 at the GUT scale. Naively one would expect that the larger universal scalar mass parameter m_0 is the larger m_{H_u} would be at $Q_{\rm weak}$. That would require large cancellations between μ and m_{H_u} as can be seen from Eqs. (4.85) and (4.87), and the theory would be unnatural. Analysis of the RGEs for the scalar m_0, trilinear A and gaugino breaking terms $m_{1/2}$, revealed that some RG trajectories of up type Higgs breaking mass m_{H_u} have a focus point at the weak scale irrespective of the m_0 value at the UV [140, 141]. More precisely the Eqs. (4.85) and (4.87) can be written as:

$$\frac{1}{2}m_Z^2 \approx -0.04 m_0^2 + 1.4 m_{1/2}^2 - \mu^2, \tag{4.94}$$

therefore even very heavy scalars, at the focus point, are natural!

4.4.6 Higgs sector

As already mentioned, there are two complex Higgs doublets in the MSSM which amounts to eight degrees of freedom. After the EW symmetry breaking, three

[1] More discussion on mSUGRA and CMSSM can be found in Section 4.5.1.

of them become longitudinal modes for the massive Z and $W^{\pm}$ bosons and the remaining five Higgses are the CP–even light h^0 and heavy H^0 states, electrically neutral pseudoscalar, thus CP–odd A^0 and finally the charged states $H^{\pm}$ [37]. The neutral components can be expanded as [37]:

$$\begin{pmatrix} H_u^0 \\ H_d^0 \end{pmatrix} = \begin{pmatrix} v_u \\ v_d \end{pmatrix} + \frac{R_\alpha}{\sqrt{2}} \begin{pmatrix} h^0 \\ H^0 \end{pmatrix} + \frac{iR_{\beta_0}}{\sqrt{2}} \begin{pmatrix} G^0 \\ A^0 \end{pmatrix}, \tag{4.95}$$

where:

$$R_\alpha = \begin{pmatrix} \cos\alpha & \sin\alpha \\ -\sin\alpha & \cos\alpha \end{pmatrix}, \qquad R_{\beta_0} = \begin{pmatrix} \sin\beta_0 & \cos\beta_0 \\ -\cos\beta_0 & \sin\beta_0 \end{pmatrix}, \tag{4.96}$$

are the rotation matrices that are introduced to make transformations from the gauge to mass eigenstates. Similarly, the charged components are [37]:

$$\begin{pmatrix} H_u^+ \\ H_d^{-*} \end{pmatrix} = R_{\beta_\pm} \begin{pmatrix} G^+ \\ H^+ \end{pmatrix} \qquad \text{with} \qquad R_{\beta_\pm} = \begin{pmatrix} \sin\beta_\pm & \cos\beta_\pm \\ -\cos\beta_\pm & \sin\beta_\pm \end{pmatrix}. \tag{4.97}$$

In the case where v_u and v_d minimize the Higgs potential at the tree level the equality $\beta = \beta_0 = \beta_\pm$ holds and using Eq. (4.83) $\beta = \arctan(v_u/v_d)$. The β can be slightly different if one chooses to minimize the Higgs potential including the contributions from the loops [37]. After diagonalization the quadratic part of the Higgs potential looks like:

$$\begin{aligned} V = &\frac{1}{2} m_{h^0}^2 (h^0)^2 + \frac{1}{2} m_{H^0}^2 (H^0)^2 + \frac{1}{2} m_{G^0}^2 (G^0)^2 + \frac{1}{2} m_{A^0}^2 (A^0)^2 + \\ &\frac{1}{2} m_{G^\pm}^2 |G^+|^2 + \frac{1}{2} m_{H^\pm}^2 |H^+|^2 + ... \end{aligned} \tag{4.98}$$

with the mass eigenstates [37]:

$$m_{A^0}^2 = \frac{2b}{\sin 2\beta} = 2|\mu|^2 + m_{H_u}^2 + m_{H_d}^2, \tag{4.99}$$

$$m_{h^0,H^0}^2 = \frac{1}{2}\left(m_{A^0}^2 + m_Z^2 \mp \sqrt{(m_{A^0}^2 - m_Z^2)^2 + 4m_{A^0}^2 m_Z^2 \sin^2 2\beta}\right), \tag{4.100}$$

$$m_{H^\pm}^2 = m_{A^0}^2 + m_W^2. \tag{4.101}$$

The mixing angle α in the R_α matrix can be calculated using [37]:

$$\frac{\sin 2\alpha}{\sin 2\beta} = -\left(\frac{m_{H^0}^2 + m_{h^0}^2}{m_{H^0}^2 - m_{h^0}^2}\right), \qquad \frac{\tan 2\alpha}{\tan 2\beta} = \left(\frac{m_{A^0}^2 + m_Z^2}{m_{A^0}^2 - m_Z^2}\right). \tag{4.102}$$

Note that only m_A and $\tan\beta$ are needed to describe the Higgs sector spectrum at the tree level. Since the mass of m_{A^0} increases as the ratio $\frac{b}{\sin 2\beta}$ increases, this also increases the masses of H^0 and $H^\pm$, which virtually are bounded from below. However, as we will show now, the h^0 mass is bounded from above. Ignoring the $\mathcal{O}\left(\frac{m_Z^4}{m_{A^0}^4}\right)$ terms and taking the experimentally justified limit $m_{A^0} \gg m_Z$, Eq. (4.100) can be expanded as:

$$\begin{aligned} m_{h^0}^2 \leq & \frac{1}{2}\left(m_{A^0}^2 + m_Z^2 - m_{A^0}^2\sqrt{1 - \frac{2m_Z^2}{m_{A^0}^2}\left[1 - 2\sin^2 2\beta\right]}\right) \approx \\ & \frac{1}{2}\left(m_{A^0}^2 + m_Z^2 - m_{A^0}^2\left\{1 - \frac{m_Z^2}{m_{A^0}^2}\left[1 - 2\sin^2 2\beta\right]\right\}\right) = \\ & \frac{1}{2}(m_Z^2 + m_Z^2[1 - 2\sin^2 2\beta]) = m_Z^2\cos^2 2\beta, \end{aligned} \tag{4.103}$$

which, taking the positive values for the cosine function, implies the upper bound on m_{h^0}:

$$m_{h^0} \leq m_Z|\cos 2\beta|, \tag{4.104}$$

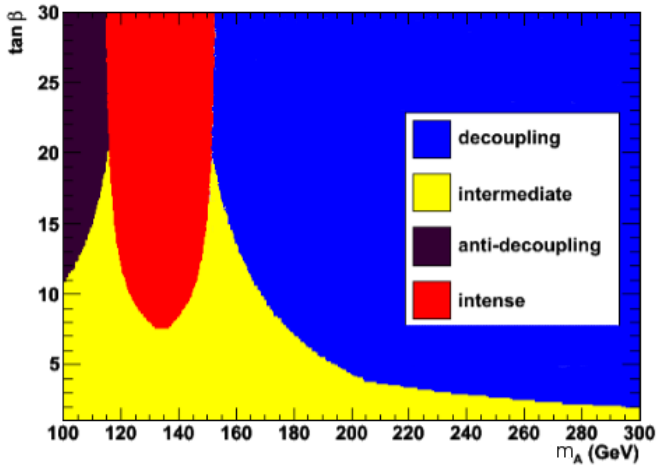

Figure 4.4: M_A–$\tan\beta$ plane depicting decoupling (blue), intermediate (yellow), antidecoupling (pink) and intense (red) regimes of the Higgs sector [143]. The low $\tan\beta - m_{A^0}$ region is ruled out by the LHC in the context of the CMSSM.

at tree level. This implies that large quantum corrections, due to coupling mainly to (s)tops, have to be present in order for h^0 to be a viable SM Higgs candidate. Specific values of $m_{A^0} - \tan\beta$ forces particular behaviour of the MSSM Higgses that can be split into various regimes [142, 143]:

•*Decoupling regime* [144]: In this limit, a hierarchy $m_A \gg m_Z$ is assumed and Eqs. (4.99), (4.100) and (4.101) become:

$$m_{h^0} \simeq m_Z^2 |\cos^2 2\beta|, \qquad m_{H^0} \simeq m_{A^0}^2 + m_Z^2 \sin^2 2\beta, \qquad m_{H^\pm}^2 = m_{A^0}^2 + m_W^2. \quad (4.105)$$

In the decoupling regime the light CP–even h^0 plays the role of the SM model Higgs and the pseudoscalar A^0 becomes mass degenerate with the heavy CP–even H and charged $H^\pm$ Higgses. The decoupling regime is shown in blue in Fig. 4.4.

•*Antidecoupling regime* [145]: as the name suggests, this regime is opposite to the decoupling regime and occurs at $m_{A^0} \leq m_{h_{\rm SM}}$. The values of $\tan\beta$ have to be in the range such that the last term in Eq. (4.100) would contribute enough for

the mass of 125 GeV. In this case, the heavy Higgs H^0 appears indistinguishable from the SM Higgs, and the light h, in particular for the low $\tan\beta$, is degenerate with the pseudoscalar A^0. The antidecoupling regime is coloured in black in Fig. 4.4.

•*Intense coupling regime* is where the pseudoscalar mass is comparable to 125 GeV. In this case, all of the Higgses have masses comparable to that of the SM within 10–20 GeV, where the precise value depends on the $\tan\beta$ [143]. In Fig. 4.4 the parameter space for this regime is shown in red.

•*Intermediate coupling regime* occurs for low $\tan\beta$ and a pseudoscalar lighter than 500 GeV [142]. This differs from the decoupling regime by the manner in which the CP–even Higgses couple to the gauge bosons and fermions. This regime is shown in yellow in Fig. 4.4.

4.4.7 Masses of squarks and sleptons

In this section, we will describe how the squark and slepton spectrum changes after EW symmetry breaking. Here we consider the terms of the stop mass matrix, but the discussion can be generalised for any MSSM matter content degree of freedom. The complication arises because, after the EW symmetry breaking, the two neutral components of the Higgs doublets develop vacuum expectation value and terms, that constituted to the trilinear or quartic couplings of Higgses to the sleptons, now contribute to the sparticles masses. To uncover the precise pattern we have to collect the relevant terms. The first contribution is the LH and RH masses which, in models without universality conditions (like the NMSSM or pMSSM), are just free input parameters. Another important contribution is $m_{\tilde{t}} = y_{\tilde{t}}^2 v^2$, which comes from the F–terms $y_{\tilde{t}}^2 H_u^{0*} H_u^0 \tilde{t}_L^* \tilde{t}_L$ and $y_{\tilde{t}}^2 H_d^{0*} H_d^0 \tilde{t}_R^* \tilde{t}_R$

in superpotential (see Eq. (4.69)), after H_u and H_d develops the VEV. These terms constitute the diagonal part of the stop mass matrix. The off–diagonal contribution has the same origin as the $m_{\tilde{t}}^2$ term but it is due to the last term in the MSSM superpotential and has the form $-\mu y_{\tilde{t}} v \cos\beta \tilde{t}_R^* \tilde{t}_L$, where v_d is the VEV of H_d^0 and, as previously defined, $v_d = v\cos\beta$. Finally the last contribution comes from the trilinear terms and has the form $a_{\tilde{t}} v \sin\beta \tilde{t}_L \tilde{t}_R^* + \text{c.c.}$ after H_u^0 acquires a VEV. After collecting all the terms, the mass matrix for the top squark can be written as [37]:

$$\mathcal{L}_{\mathbf{m}_{\tilde{\mathbf{t}}}} = -(\widetilde{t}_L^* \quad \widetilde{t}_R^*)\mathbf{m}_{\tilde{\mathbf{t}}}^{\mathbf{2}} \begin{pmatrix} \widetilde{t}_L \\ \widetilde{t}_R \end{pmatrix}, \tag{4.106}$$

where

$$\mathbf{m}_{\tilde{\mathbf{t}}} = \begin{pmatrix} m_{Q_3}^2 + m_{\tilde{t}}^2 + \Delta_{\widetilde{u}_L} & v(a_{\tilde{t}}^* \cos\beta - \mu y_{\tilde{t}} \sin\beta) \\ v(a_{\tilde{t}} \cos\beta - \mu^* y_{\tilde{t}} \sin\beta) & m_{\widetilde{u}_3}^2 + m_{\tilde{t}}^2 + \Delta_{\widetilde{u}_R} \end{pmatrix}, \tag{4.107}$$

and Δs are the quantum corrections. The off–diagonal terms are often simplified using the so called left/right mixing parameter, which is defined to be $X_{\tilde{t}} = a_{\tilde{t}} - \mu y_{\tilde{t}} \cot\beta$. It often appears in the radiative corrections to the Higgs mass squared due to the coupling of the Higgs to the (s)top. This matrix can be diagonalised by the unitary matrix to give the two mass eigenstates [37]:

$$\begin{pmatrix} \widetilde{t}_1 \\ \widetilde{t}_2 \end{pmatrix} = \begin{pmatrix} c_{\tilde{t}} & -s_{\tilde{t}}^* \\ s_{\tilde{t}} & c_{\tilde{t}} \end{pmatrix} \begin{pmatrix} \widetilde{t}_L \\ \widetilde{t}_R \end{pmatrix}, \tag{4.108}$$

where $m_{\tilde{t}_1} < m_{\tilde{t}_2}$ by definition. In exactly the same manner the terms that constitutes the mass matrices $\mathbf{m}_{\tilde{\mathbf{b}}}^{\mathbf{2}}$ and $\mathbf{m}_{\tilde{\tau}}^{\mathbf{2}}$ can be collected and after diagonalization one finds the two mass eigenstates for the sbottom and stau that are mixtures of the left and right handed gauge eigenstates. The off diagonal elements in mass

matrices determine the mass splitting between the light and the heavy state. Note that the major effect comes through the Yukawa couplings as the trilinear terms are multiplied by $\cos\beta$, which is modest or even negligible in most of the parameter space. Therefore, only the particles with large Yukawas have significant mixing. This has direct implications for the first and second generation sparticles because all the terms containing Yukawa couplings can be ignored and since the off-diagonal entries in their respective mass matrices vanish, their gauge eigenstates are the same as the mass eigenstates.

4.4.8 Dark Matter in MSSM

The most widely studied DM candidate within SUSY is the neutralino $\widetilde{\chi}_1^0$. Nevertheless we will review other possible candidates later in the Section 5.2. The neutralino mass matrix in the MSSM in gauge eigenstate $(\widetilde{B}, \widetilde{W}^0, \widetilde{H}_d^0, \widetilde{H}_u^0)$ is given by [37]:

$$M_{\widetilde{\chi}^0} = \begin{pmatrix} M_1 & 0 & -\frac{g_1 v_d}{\sqrt{2}} & \frac{g_1 v_u}{\sqrt{2}} \\ 0 & M_2 & \frac{g_2 v_d}{\sqrt{2}} & -\frac{g_2 v_u}{\sqrt{2}} \\ -\frac{g_1 v_d}{\sqrt{2}} & \frac{g_2 v_d}{\sqrt{2}} & 0 & -\mu \\ \frac{g_1 v_u}{\sqrt{2}} & -\frac{g_2 v_u}{\sqrt{2}} & -\mu & 0 \end{pmatrix}.$$

M_1 and M_2 in the diagonal entries arise due to the soft breaking terms in Eq. (4.76). The contribution to the off–diagonal entries comes from the following: 1) $-\mu$ is the Higgsino mass term, 2) the rest are the terms due to Higgs-Higgsino-gaugino interactions, where after the EW symmetry breaking the Higgs field acquired a VEV v. One can find the mass eigenstates by diagonalizing $M_{\widetilde{\chi}^0}$ with the help of unitary matrix $\mathbf{N}$. After diagonalization one finds the mass eigenstates

being [37, 146]:

$$\begin{aligned}
m_{\widetilde{\chi}_1^0} &= M_1 - \frac{m_Z^2 s_W^2 (M_1 + \mu \sin 2\beta)}{\mu^2 - M_1^2} + ..., \\
m_{\widetilde{\chi}_2^0} &= M_2 - \frac{m_W^2 (M_1 + \mu \sin 2\beta)}{\mu^2 - M_2^2} + ..., \\
m_{\widetilde{\chi}_3^0} &= |\mu| + \frac{m_Z^2 (I - \sin 2\beta)(\mu + M_1 c_W^2 + M_2 s_W^2)}{2(\mu + M_1)(\mu + M_2)} + ..., \\
m_{\widetilde{\chi}_4^0} &= |\mu| + \frac{m_Z^2 (I + \sin 2\beta)(\mu - M_1 c_W^2 - M_2 s_W^2)}{2(\mu - M_1)(\mu - M_2)} + ...
\end{aligned} \tag{4.109}$$

The convention is that $m_{\widetilde{\chi}_1^0} < m_{\widetilde{\chi}_2^0} < m_{\widetilde{\chi}_3^0} < m_{\widetilde{\chi}_4^0}$. If, for example, it happens to be that $M_2 < M_1$ then the lightest neutralino is wino. In the limits where $m_Z \ll |M_1 \pm \mu|$ and $|M_2 \pm \mu|$, the neutralino eigenstates are almost pure gaugino and higgsino eigenstates. It is worthwhile mentioning, that in the same limit, the chargino $\widetilde{\chi}_1^\pm$, which is the mixture of electrically charged winos and higgsinos, up to corrections, has degenerate mass eigenstates with the neutralino:

$$m_{\widetilde{\chi}_1^\pm} = M_2 + ..., \qquad\qquad m_{\widetilde{\chi}_2^\pm} = |\mu| + ... \tag{4.110}$$

Since the generic experimental bound on the mass of the chargino is $m_{\widetilde{\chi}_1^\pm} > 103.5$ GeV [147] it implies that a lighter than 103.5 GeV neutralino would have to have a sizeable fraction of bino. In fact, as we will demonstrate later, the very lightest neutralino in the MSSM has to be dominantly bino. In a spirit of being complete, it should be added that the chargino mass limit is not the only reason for the lightest neutralino to be bino. Another issue is the invisible Z decay, which we discuss in greater detail in Section 6.1. The major difficulty in having a bino neutralino is that it produces too large relic abundance $\Omega_{\widetilde{B}} h^2$. One of the modes that the bino annihilates in the Early Universe is through the t–channel exchange

of light squark or slepton, which are the subject of intense investigation at LHC and LEP.

4.5 Extensions of the MSSM

4.5.1 mSUGRA and CMSSM

mSUGRA [128, 129, 130] and CMSSM [148, 149, 150, 151] are terms often used interchangeably for a class of gravity mediated SUSY breaking models. However, there is a difference between the two: mSUGRA has an additional constraint between the parameters, which CMSSM leaves unrelated. Therefore, in a sense, mSUGRA is an even more constrained version of CMSSM.

Free input parameters of CMSSM are those that enter into soft SUSY breaking Lagrangian given by Eq. (4.76). These include gaugino masses with $M_1 = M_2 = M_3 = m_{1/2}$ at the GUT scale; likewise, all trilinear breaking parameters converge to A_0; and finally, all scalar masses converge to m_0 at the GUT scale. Besides this, we also require $\tan\beta$, which is the ratio of the up and down Higgses' expectation values, and the sign of μ, since it is the magnitude, and not the sign, which is fixed by EWSB. Therefore, to explore a parameter space of CMSSM, one has to come up with values of:

$$m_0, m_{1/2}, A_0, \tan\beta, \text{sign}(\mu). \tag{4.111}$$

mSUGRA has an additional constraint [152]:

$$B_0 = A_0 - m_0, \tag{4.112}$$

where B_0 dependent terms are the last two in Eq. (4.76). This constraint implies that $\tan\beta$ parameter is now also determined by EWSB conditions [152] and the input parameters for mSUGRA is then:

$$m_0, m_{1/2}, A_0, \text{sign}(\mu). \tag{4.113}$$

For more discussion on supergravity please see Section 4.4.2.

4.5.2 MSSM with non–universal Higgs masses

The NUHMII is a variant of the MSSM with non–universal soft breaking masses for the up and down type Higgs doublets which we denote m_1 and m_2 respectively. [153, 154, 155]. The universality of scalar masses m_0 at the unification scale, i.e. the GUT scale, is still assumed, but in the NUHMII model, they are different from m_1 and m_2. It is well known that the Higgs masses can be written as, see [154, 155]:

$$\begin{aligned} m_1^2(1+\tan^2\beta) &= m_{A^0}^2\tan^2\beta - \mu^2(\tan^2\beta + 1 - \Delta_\mu^{(2)}) \\ &- (c+2c_\mu)\tan^2\beta - \Delta_A\tan^2\beta - \frac{1}{2}m_Z^2(1-\tan^2\beta) - \Delta_\mu^{(1)}, \end{aligned} \tag{4.114}$$

and

$$\begin{aligned} m_2^2(1+\tan^2\beta) &= m_{A^0}^2 - \mu^2(\tan^2\beta + 1 + \Delta_\mu^{(2)}) \\ &- (c+2c_\mu) - \Delta_{A^0} + \frac{1}{2}m_Z^2(1-\tan^2\beta) + \Delta_\mu^{(1)}, \end{aligned} \tag{4.115}$$

where c, c_μ, $\Delta_\mu^{(1,2)}$, Δ_{A^0} are radiative corrections and m_{A^0} is the mass of the CP–odd pseudoscalar Higgs. In fact these equations are just the EW symmetry breaking conditions which are now solved for m_1 and m_2. So from the above, we

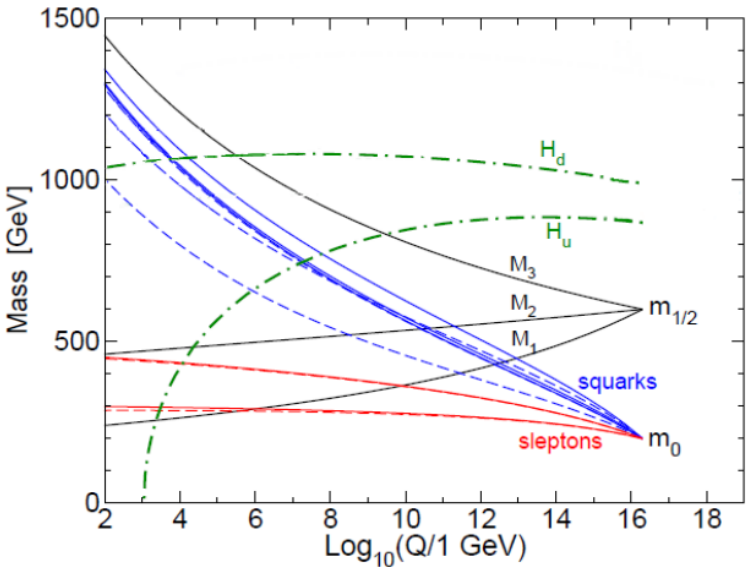

Figure 4.5: Evolution of masses in the NUHMII model [37].

see that m_1 and m_2 can now be expressed in terms of μ and m_{A^0}, which tells us that NUHMII has the following free parameters:

$$m_0,\ m_{1/2},\ A_0,\ \tan\beta,\ \mu,\ m_{A^0}, \tag{4.116}$$

where the trilinear soft breaking term is A_0. The DM sector of NUHMII is the same as that of MSSM. In Section 7.3 it will be shown how inflation and DM can be encompassed within NUHMII.

4.5.3 Next–to–the–minimal MSSM

In the NMSSM model, the μ term is generated dynamically and this enables the EW fine tuning of the MSSM to be ameliorated. This is done by introducing an additional scalar singlet S and replacing the Higgs mass parameter in the MSSM

superpotential in Eq. (4.69), by a product λS [156]:

$$W_{\text{NMSSM}} = W_{\text{MSSM}}^{\mu=0} + \lambda S H_u H_d + \frac{1}{3}\kappa S^3 \tag{4.117}$$

In this setup, S acquires an expectation value and the size of the $\mu = \lambda S$ term depends on the VEV of the S field and the size of the coupling λ. In order to treat the theory in a perturbative manner, the ranges for λ and κ are typically assumed to be within $0 \leq \lambda \leq 0.75$ and $0 \leq \kappa \leq 0.65$. As $\lambda, \kappa \to 0$, there is the decoupling limit in which the NMSSM becomes the MSSM.

At the point where $\kappa = 0$, the NMSSM superpotential has a global U(1) Peccei–Quinn (PQ) symmetry [37, 156]:

$$\begin{gathered} H_u^{'} \to H_u e^{i\phi_{\text{PQ}}}, \qquad H_d^{'} \to H_d e^{i\phi_{\text{PQ}}}, \qquad S^{'} \to S e^{-2i\phi_{\text{PQ}}}, \\ Q^{'} \to Q e^{-i\phi_{\text{PQ}}}, \qquad L^{'} \to L e^{-i\phi_{\text{PQ}}}, \end{gathered} \tag{4.118}$$

where $\bar{u}$, $\bar{d}$, $\bar{e}$ have zero PQ charge. This symmetry is broken when H_u, H_d and S acquire a non–zero VEV, and as a result, a pseudo–Goldstone boson – a light pseudoscalar PQ axion – appears. Within NMSSM, it plays the role of the lightest CP–odd Higgs, helps to resolve the strong CP problem and is a good DM candidate. Breaking PQ symmetry by including the singlet self–coupling term with non–zero κ helps to avoid phenomenological, cosmological and astrophysical constraints, see for eg. [157, 158, 159, 160, 161].

Further note that NMSSM, at the renormalizable level, possesses a discrete $\mathbb{Z}_3$ symmetry, under which all terms in the superpotential remain invariant if the fields are rotated by $e^{i\frac{2\pi}{3}}$. This discrete symmetry is broken during the phase transition associated with the EW symmetry breaking in the Early Universe and

cosmologically dangerous domain walls can then be produced [156, 162, 163]. However, it has been shown that this cosmological problem is eliminated after imposing a $\mathbb{Z}_2$ R–symmetry on the non–renormalizable sector of the NMSSM [164].

The appearance of these new terms has great implications for the DM sector. In the NMSSM the DM has 5×5 matrix and the additional ingredient in the neutralino is that it can get an admixture of singlino. In particular, the large singlino component is needed for the case of light DM candidate with a large $\widetilde{\chi}^0 - p$ interaction cross section – as is claimed in a number of DD experiments. The neutralino mass matrix in NMSSM is then given by [37, 156]:

$$M_{\widetilde{\chi}^0} = \begin{pmatrix} M_1 & 0 & -\frac{1}{\sqrt{2}}g_1 v_d & \frac{1}{\sqrt{2}}g_1 v_u & 0 \\ 0 & M_2 & \frac{1}{\sqrt{2}}g_2 v_d & -\frac{1}{\sqrt{2}}g_2 v_u & 0 \\ -\frac{1}{\sqrt{2}}g_1 v_d & \frac{1}{\sqrt{2}}g_2 v_d & 0 & -v_s\lambda & -v_u\lambda \\ \frac{1}{\sqrt{2}}g_1 v_u & -\frac{1}{\sqrt{2}}g_2 v_u & -v_s\lambda & 0 & -v_d\lambda \\ 0 & 0 & -v_u\lambda & -v_d\lambda & 2v_s\kappa \end{pmatrix}.$$

The mass of the lightest neutralino can then be written as:

$$\widetilde{\chi}_1^0 = N_{11}\widetilde{B} + N_{12}\widetilde{W}^0 + N_{13}\widetilde{H}_d^0 + N_{14}\widetilde{H}_u^0 + N_{15}\widetilde{S}. \tag{4.119}$$

A phenomenologically interesting limit is where the neutralino is dominated by the singlino component. Its mass can then be expressed via the following equation [165]:

$$m_{\widetilde{\chi}_1^0} = \lambda^2 \frac{v^2}{\mu} \sin 2\beta + 2\frac{\kappa}{\lambda}\mu. \tag{4.120}$$

As we will show latter, the singlino neutralino has a large $\widetilde{\chi}_1^0$–nucleon spin independent cross section and therefore is a plausible candidate to explain potential

signals from direct DM detection experiments.

Chapter 5

Frontier of the Dark Matter

Cosmological observations made by the Planck satellite suggest, that DM accounts for as much as 26.8% of the total energy budget of the Universe [91]. The existence of DM was first inferred from its gravitational interactions by observing the velocity dispersion of galaxies in the Coma cluster [9]. Evidence of DM also comes from the study of galaxy rotation curves [10]. The left panel of Fig. 5.1 shows expected (lower curve) and actual (upper curve) rotational velocities of the stars in the galactic disk, as a function of the distance from the galaxy centre. If the matter that emits light would be all what the galaxies are made of, from the Newtonian mechanics one would expect, that the orbital velocity of for eg. star would decrease as the distance from the centre increases, just like it is shown by the lower curve in the same figure. However, the observations suggest, that to a leading order, the rotational velocity does not depend on the distance as it is depicted by the upper curve. In the case of the Sun in the Milky Way (MW), one would expect the Sun to rotate at $\sim$ 160 km/s around the MW centre while it actually has an orbital velocity of about 220 km/s. This can only be explained by

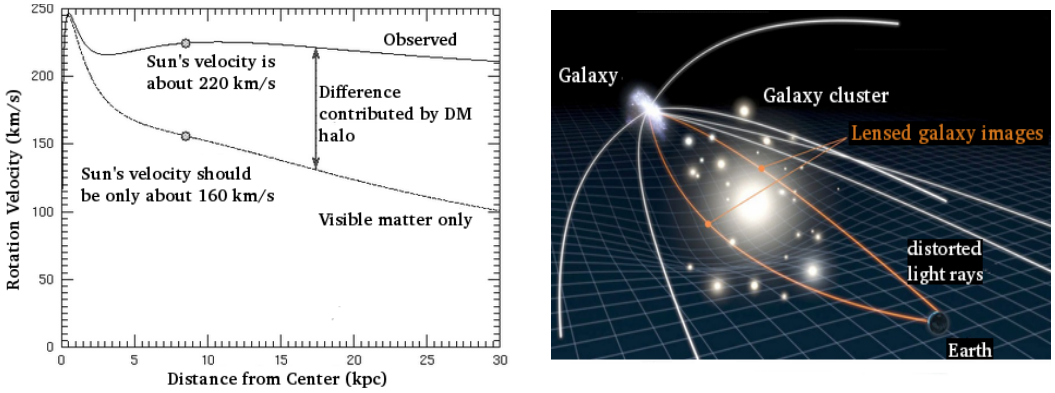

Figure 5.1: Left panel: rotational velocity around Galactic centre vs. the distance from Galactic centre for the cases with and without a presence of DM halo. Right panel schematically depicts the setup for gravitational lensing effect. Figures taken from Ref. [166] (left) and NASA/ESA (right).

the existence of some form of matter that we can not see directly. DM presence can also be inferred by measuring velocity dispersions of the galaxies in galaxy clusters and superclusters [19, 20]. Another classical example that proves the presence of the DM is the gravitational lensing [16, 17, 18]. It is common array in nature when a massive object, which acts as a gravitational lens, lies in between observer (the Earth) and the source of light (the galaxy). This setup is graphically depicted in the right panel of Fig. 5.1. As the light from the source travels towards the observer, it gets bent by the massive object that curves the space around it. The amount of the effect largely depends on the mass of the object that acts as a gravitational lens and is easily calculable. It also turns out to be the case, that the bending is much larger compared to what one could expect if the lens would be made of the visible matter only.

In Ref. [18] authors argue that compelling piece of the evidence that DM is of a particle like nature, comes from the bullet cluster, which consists of two colliding galaxy clusters [22, 23, 24]. In the Picture 5.2, one can see the blue

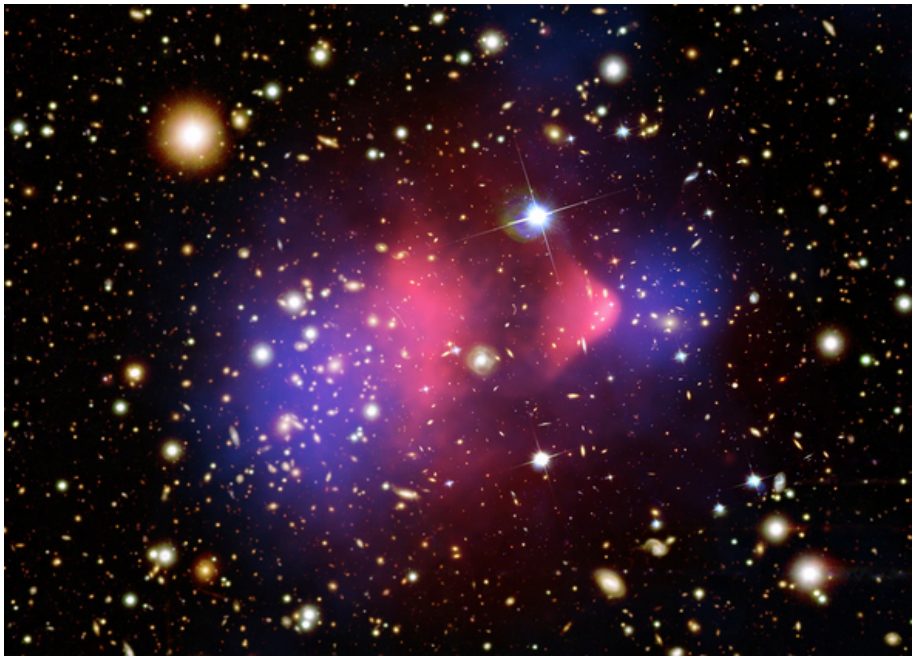

Figure 5.2: The bullet cluster – an evidence for a particle–like origin of the DM. The figure is taken from Ref. [167].

and the red regions: blue is the gravitational potential due to the presence of the DM, and was located by the gravitational lensing effects, and the red is a visible baryonic matter that emits X-rays due to the shock waves of the collision. Note that the blue regions, unlike the red ones that represent hot X–ray emitting gas, seem to be unaffected by the collision.

There were a number of attempts to explain the DM phenomena by trying to modify gravity. And indeed, the lensing maps of the bullet cluster can also be explained in modified gravity theories by scaling the gravitational constant with an interpolation function and adding ordinary SM neutrinos of 2 eV mass as a hot DM [25].

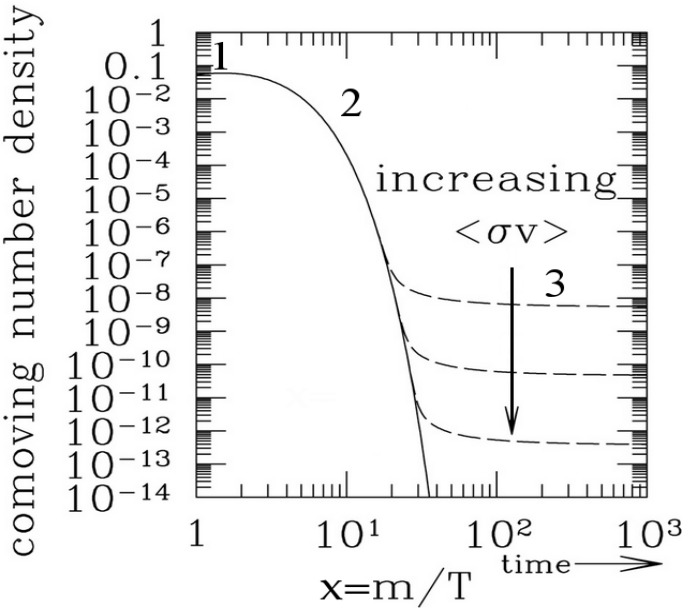

Figure 5.3: Evolution of comoving DM number density as the function of m/T or time equivalently. Arrow denote increase in DM annihilation cross section [169].

5.1 Relic density

The most popular mechanism explaining how the relic density of the DM abundance could have settled to the level that we observe today is called the freeze out mechanism [168]. It is depicted in the Fig. 5.3. In the freeze out scenario, the heavier DM species initially are assumed to be in thermal equilibrium with the lighter ones of the thermal bath. During this phase, that is labelled by 1 in the figure, the Universe is hot enough, so that the processes of the DM particles annihilating into SM degrees of freedom and backwards, i.e. $DM+DM \leftrightarrow X+X$ is ongoing at the same rate, and the relic density remains unaltered. However, as the Universe cools down and its temperature drops below the m_{DM}, the DM particles still annihilates into lighter species that the thermal bath is made of, but these lighter particles are not energetic enough anymore to produce DM, i.e.

$DM + DM \rightarrow X + X$ – and, as shown in phase 2 in the figure, the relic density starts dropping, simply because the number density of DM, n_{DM}, decreases. Once the Hubble expansion rate exceeds the rate of the annihilation of DM particles into SM ones, the relic abundance freezes out, as shown in the phase 3. This is also called *chemical decoupling*. The downwards pointing arrow demonstrates, how the change in the annihilation cross section of DM affects their final number density – the larger the rate the more effective the annihilation of DM, which in turn implies fewer particles left and therefore a smaller abundance $\Omega_{DM}h^2$. However, since the DM particles are not relativistic at this stage anymore, their number density n_{DM} scales roughly as $n \sim T^3$. For the case of relativistic SM species, their number density is exponentially suppressed and can be written as $n_{SM} \sim (mT)^{3/2} \exp(-\frac{m}{T})$ [170]. Therefore $n_{SM} \gg n_{DM}$ which means that the DM still scatters of the SM particles in the thermal bath and remains in thermal equilibrium with it. Once the Hubble rate $\mathcal{H}$ exceeds the scattering rate Γ, the DM completely decouples and this is called *kinetic decoupling*. The temperature at which the kinetic decoupling occurs, can be calculated by equating the elastic scattering rate with the Hubble expansion rate [171, 172]:

$$T_{\text{kin. dec.}} \sim 1 \text{ MeV} \left(\frac{m_{DM}}{\text{GeV}} \right)^{\frac{2}{3}}. \tag{5.1}$$

The value of the $T_{\text{kin. dec.}}$ is very important in determining the sizes of the proto-halos. See for eg. [173, 174] and references therein.

5.2 Dark Matter candidates

As it was already mentioned, one of the motivations to go beyond the SM is that it does not have any viable DM candidate. To some extent, in Chapter 4, we have already discussed the most popular DM candidate in SUSY – the lightest neutralino $\widetilde{\chi}_1^0$. We will start this section by elaborating on further properties of the neutralino and then continue by reviewing some other DM candidates, in and out of the scope of SUSY.

- Lightest neutralino – $\widetilde{\chi}_1^0$. Despite being the most widely studied candidate, the neutralino has some drawbacks. In the standard WIMP miracle calculation, the thermal relic abundance for a bino like neutralino is given by [175]:

$$\Omega_{\widetilde{B}}h^2 = 1.3 \times 10^{-2} \left(\frac{m_{\tilde{l}_R}}{100\text{GeV}}\right)^2 \frac{(1+r)^4}{r(1+r^2)} \left(1 + 0.07 \log \frac{\sqrt{r}100\text{GeV}}{m_{\tilde{l}_R}}\right), \tag{5.2}$$

  where $r \equiv \frac{M_1^2}{m_{\tilde{l}_R}^2}$. From here it is easy to see that in order to satisfy the upper Planck bound on DM relic density [176] by the presence of the very light neutralino species, just as recent DD experiments suggest [177, 178, 179, 180, 181], light right handed sleptons are required. However, the scale of the sparticles is constantly being pushed up by the collider experiments and thus leads to the overproduction of light, bino dominated neutralino. Yet, for the wino and higgsino like neutralinos the relic density respectively can be expressed as [175]:

$$\Omega_{\widetilde{W}}h^2 \simeq 0.1\left(\frac{M_2}{2.2\text{ TeV}}\right)^2, \qquad \Omega_{\widetilde{H}}h^2 \simeq 0.1\left(\frac{\mu}{1\text{ TeV}}\right)^2, \tag{5.3}$$

which leads to the underproduction for the wino (higgsino) like neutralino that is lighter than 2.2 TeV (1 TeV), and overproduction for the neutralinos that are heavier than the quoted values. In order for the neutralino to account for the full DM content of the Universe, for a given mass, $\widetilde{\chi}_1^0$ has to have a very specific admixture of gauginos and higgsinos, or get depleted via special (co)annihilation channels and/or resonances, which in either case is a somewhat fine tuned scenario.

- SM neutrino. Ever since in Super–Kamiokande it was found that the neutrinos have masses [3], it became clear, that in principle, they contribute to the relic density of the Universe. However, the first problem is that the N-body simulations of the structure formation show that DM is non–relativistic, i.e. cold [26, 27], and neutrino could only account for the hot DM. The classification of DM candidates into hot or cold depends on their thermal velocity in the Early Universe. When galaxy–sized masses are first encompassed within the horizon, hot DM particles, like the SM neutrino, are still relativistic. As a result, fluctuations on galaxy scales are wiped out by the free streaming of such particles. Yet another reason is that the relic density of neutrinos can be expressed as:

$$\Omega_\nu h^2 \simeq \frac{\sum_i m_{\nu,i}}{93.14 \text{ eV}}. \tag{5.4}$$

The upper bound on the sum over all generations of neutrino masses is found to be [83]:

$$\sum_i m_{\nu,i} \leq 0.28 \text{ eV} \tag{5.5}$$

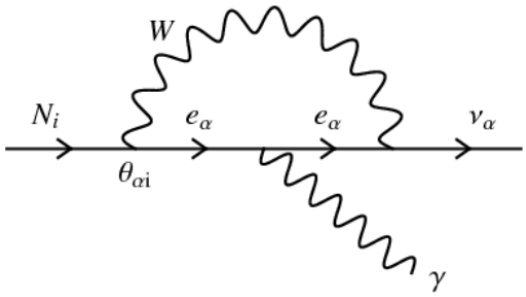

Figure 5.4: γ production by the decay of the sterile neutrino $N_i \to \gamma\nu_\alpha$, where $\alpha = e, \mu, \tau$ [187].

at 95% C.L., with a very clear implication that neutrino contribution towards the total relic abundance is minute.

- Sterile neutrinos (N). The disappearance of SM neutrinos as they propagate from their source is an experimentally well established fact [182, 183, 184]. One way to explain this anomaly is to introduce the sterile neutrino [185, 186]. Sterile neutrinos are the neutrinos which mainly interact via gravitational interaction. The interaction rate between the sterile neutrino itself and its SM counterparts is parametrised by some mixing angle $\theta_{\alpha,i}$. By changing this mixing angle and the mass, one can make its lifetime longer than the age of the Universe, as required for a DM candidate. The mixing angle is responsible for both the production of N in the early Universe as well as its decay. A possible decay channel is shown in Fig. 5.4. So the photons would be a smoking gun signature of the decay of N. Sterile neutrinos that are heavier than 50 keV are excluded, since the γ flux they would produce would be too large [188]. The lower bound is of the order of few keV, which comes from the large scale structure formation. Interestingly, as we will discuss in Section 5.4.3, an unidentified monochromatic line of

$E_\gamma \approx 3.5$ keV was recently observed by two groups in galaxies and galaxy clusters [189, 190], that could possibly be due to the decay of N.

- Sneutrinos. In supersymmetric extensions of SM, sneutrinos are the scalar partners of neutrinos. One of the problems with the LH sneutrinos being the DM candidate is its large scattering cross section from the nuclei in the DD experiments exceeding the experimental bounds by several orders of magnitude [191]. Furthermore, the LH sneutrino's annihilation rate is usually too rapid to provide enough DM and multicomponent scenarios have to be invoked [191]. The observation of neutrino oscillations gives a natural motivation for adding the RH neutrino to the SM, whose supersymmetric partner – RH sneutrino becomes a viable DM candidate. However, the RH sneutrino, being sterile under SM gauge interactions, cannot be brought into thermal equilibrium, yet extending gauge symmetries, allows to accommodate RH sneutrinos that avoid all current constraints [192, 193].

- Gravitino is the spin 3/2 supersymmetric partner of the graviton. In the Early Universe, it can be produced either thermally or in the late decays of an NLSP. In gravity mediated SUSY breaking models, its mass is related to the SUSY breaking scale via [37]:

$$m_{3/2} \sim \frac{\langle F \rangle}{M_{Pl}}. \tag{5.6}$$

Since the scale of $\langle F \rangle$ is not known, there is a large parameter space where the gravitino indeed could be the LSP. In an unbroken SUSY (i.e. $\langle F \rangle = 0$) the gravitino is massless. One of the problems is that since gravitino

interactions are Planck scale suppressed, there is no hope of finding it in the direct detection experiments or producing at colliders. Gravitinos is also subject to the astrophysical constraints. When it is not the LSP, its decay width can be written as [194, 195]:

$$\Gamma_{3/2} = \frac{c}{2\pi}\frac{m_{3/2}^3}{M_{pl}^2}, \tag{5.7}$$

where $c \sim \mathcal{O}(1)$. The decay temperature can be calculated by equating the decay rate to the Hubble expansion rate and is found to be [194, 195]:

$$T_{\text{decay}} \simeq (5\text{ MeV})\sqrt{c}\left(\frac{m_{3/2}}{100\text{ TeV}}\right) \tag{5.8}$$

In order for the gravitino to decay before BBN, it has to have a lifetime shorter than 0.1 s, which corresponds to $T_{\text{decay}} \geq 3$ MeV or equally to a lower bound of $m_{3/2} \geq \mathcal{O}(40)$ TeV. In Ref. [194] it is argued, that if the soft SUSY breaking terms arise due to the combination of modulus and anomaly mediation, respecting the lower bound on the mass of gravitino $\mathcal{O}(40)$ GeV leads to the lightest neutralino, in the range of < 1 TeV, being dominantly higgsino. As mentioned before, due to the efficient annihilation of higgsinos through Z boson and SM-like Higgs, pseudoscalar and/or heavy Higgses (when kinematically allowed) leads to the underabundance of < 1 TeV neutralino DM in the Universe, see Eq. (5.3). In this case, additional DM production mechanisms have to be invoked, if $\widetilde{\chi}_1^0$ is to account for a total DM budget.

- Axion is the scalar particle that is invoked in the PQ mechanism to dynam-

ically resolve the strong CP problem in the QCD [14]. It is known, that CP in strong sector is not violated as easily as in the weak interactions, however in the SM there is the term that violates CP symmetry:

$$\mathcal{L}_{\mathrm{QCD}} \supset \bar{\Theta}\frac{g^2}{32\pi^2}G^{a,\mu\nu}\tilde{G}^a_{\mu\nu}. \tag{5.9}$$

Here, $G^{a,\mu\nu}$ is a $\mathrm{SU}(3)_c$ field strength tensor, its dual is defined as $\tilde{G}_{\mu\nu} \equiv \frac{1}{2}\epsilon_{\mu\nu\rho\sigma}G^{\rho\sigma}$ and the parameter Θ can be in the range $[0 : 2\pi]$. To comply with the experimental limits on neutron dipole model requires $\Theta \leq 10^{-10}$. To explain the smallness of this term, the axion scalar field is added [14]:

$$\mathcal{L} \supset \frac{g^2}{32\pi^2}\left(\bar{\Theta} + \frac{a}{f_{\mathrm{PQ}}}\right)G^{a,\mu\nu}\tilde{G}^a_{\mu\nu}, \tag{5.10}$$

whose breaking allows to generate dynamically the term in the brackets of the desirable smallness. Taking the PQ breaking scale f_{PQ} anywhere in the range of 100–10^{19} GeV, gives a mass of the axion in between 1 MeV and 10^{-12} eV [102].

- Axino. If nature realizes SUSY, then the axion should have its supersymmetric spin 1/2, R parity odd superpartner axino. Axino masses typically are in the mass range of keV–MeV [196]. It is possible, that in the Early Universe the neutralino could be the NLSP and would decay to the LSP – axino. In such case, the relic density of axinos could be extracted via:

$$\Omega_{\tilde{a}}h^2 = \left(\frac{m_{\tilde{a}}}{m_{\tilde{\chi}^0_1}}\right)\Omega_{\tilde{\chi}^0_1}h^2. \tag{5.11}$$

- Kaluza–Klein lightest state (LKP) arises in a generic class of models in

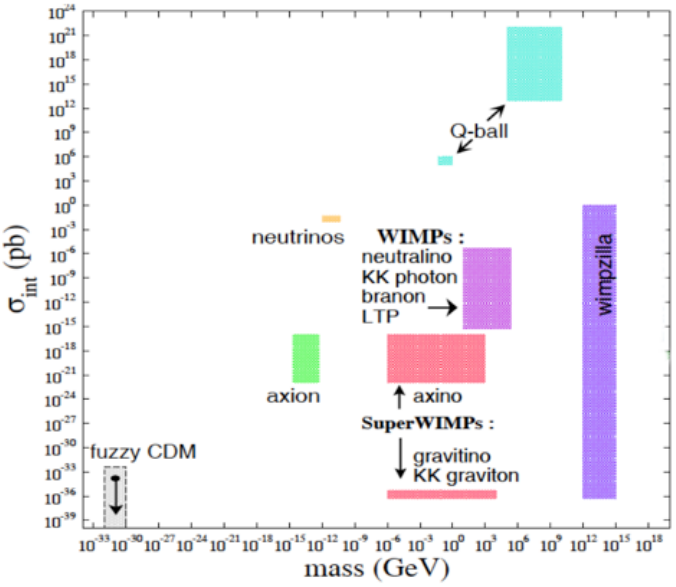

Figure 5.5: Favoured mass and interaction ranges of various DM candidates [216].

which all the fields (including the fermions) propagate in compact extra dimensions. The compactification scale in these models comes from EW precision measurements and is limited to be $1/R \gtrsim 300$ GeV [197]. LKP is coupled to the SM degrees of freedom and the symmetry, called Kaluza–Klein parity, prevents its decay to the lighter SM particles. In Ref. [198] it is shown, that for the LKP to account for the total observed relic abundance, its mass should lie in the range 400–1200 GeV, though any lighter mass in a range below 400 GeV would be subject to subdominant component of DM.

- Other candidates include fuzzy CDM [199], scalar particles [200], mirror DM [201, 202], massive graviton [203, 204], very heavy WIMPS – wimpzillas [205, 206], Q–balls [207, 208, 209], self interacting DM [210], cryptons [211, 212], primordial black holes [213, 214, 215].

The preferred regions of mass and interaction ranges for various DM candidates

are summarised graphically in Fig. 5.5.

5.3 Boltzmann equation

The analytical expression for the relic density calculation was firstly derived in Ref. [66]. Let $f = f(\vec{p}, \vec{x}, t)$ be the phase space distribution function which obeys Fermi–Dirac or Bose–Einstein statistics, depending on whether the particles are fermionic or bosonic. Its evolution is governed by the Boltzmann transportation equation, which schematically can be written as:

$$\hat{\mathbf{L}}[f] = \hat{\mathbf{C}}[f], \tag{5.12}$$

where $\hat{\mathbf{L}}$ is Liouville operator that takes into account the external force $\vec{F}$ acting upon the particles in the thermal bath and the diffusion processes. On the right hand side is the collision term $\hat{\mathbf{C}}$, which accounts for forces between particles as they interact amongst themselves. In the non–relativistic regime the Liouville operator takes the form [102, 170]:

$$\hat{\mathbf{L}} = \frac{d}{dt} + \frac{d\vec{x}}{dt} \cdot \vec{\nabla}_x + \frac{d\vec{v}}{dt} \cdot \vec{\nabla}_v = \frac{d}{dt} + \vec{v} \cdot \vec{\nabla}_x + \frac{\vec{F}}{m} \cdot \vec{\nabla}_v \tag{5.13}$$

and the relativistic generalization is:

$$\hat{\mathbf{L}} = p^\alpha \frac{\partial}{\partial x^\alpha} - \Gamma^\alpha_{\beta\gamma} p^\beta p^\gamma \frac{\partial}{\partial p^\alpha}. \tag{5.14}$$

For the Friedman–Robertson–Walker Universe, the phase space distribution function can be approximated to:

$$f(\vec{x},\vec{p},t) \to f(|\vec{p}|,t) \qquad \text{or} \qquad f(E,t). \tag{5.15}$$

In this case, the operator $\hat{\mathbf{L}}$ is:

$$\hat{\mathbf{L}}[f(E,t)] = E\frac{\partial f}{\partial t} - \frac{\dot{a}}{a}|\vec{p}|^2\frac{\partial f}{\partial E} \tag{5.16}$$

where $\mathcal{H} = \frac{\dot{a}}{a}$ being the expansion rate of the Universe and $E^2 = |\vec{p}|^2 + m^2$. The number density can be expressed as:

$$n(t) = \frac{g}{(2\pi)^3}\int f(E,t)d^3p, \tag{5.17}$$

where g is the number of spin states. To calculate the evolution of the number density, we will firstly evaluate the operator $\hat{\mathbf{L}}/E$, where $\hat{\mathbf{L}}$ is defined in Eq. (5.16):

$$\begin{aligned}\frac{\hat{\mathbf{L}}[n(t)]}{E} &= \frac{g}{(2\pi)^3}\int \frac{\hat{\mathbf{L}}[f(E,t)]}{E}d^3\vec{p} \\ &= \frac{g}{(2\pi)^3}\int \frac{\partial f(E,t)}{\partial t}d^3\vec{p} - \frac{gH}{(2\pi)^3}\int \frac{|\vec{p}|^2}{E}\frac{\partial f}{\partial E}d^3\vec{p} \\ &= \dot{n} + 3Hn = \frac{1}{a^3}\frac{d(na^3)}{dt}.\end{aligned} \tag{5.18}$$

This is equal to the change in number density because of the collisional interactions between the particles:

$$\dot{n} + 3Hn = \frac{g}{(2\pi)^3}\int \frac{\hat{\mathbf{C}}[f(E,t)]}{E}d^3\vec{p}. \tag{5.19}$$

Denoting $d\Pi_i \equiv \frac{g_i}{(2\pi)^3 2E_1} d^3\vec{p_1}$ the collisional term for the $i + j \longleftrightarrow k + l$ process can be expressed as:

$$\frac{g}{(2\pi)^3}\int \frac{\hat{\mathbf{C}}[f(E,t)]}{E} d^3\vec{p} = -\int d\Pi_l d\Pi_k d\Pi_j d\Pi_i (2\pi)^4 \delta^4(p_i + p_j - p_k - p_l) \times [|\mathcal{M}|^2_{i+j\to k+l} f_i f_j (f_k \pm 1)(f_l \pm 1) - |\mathcal{M}|^2_{k+l\to i+j} f_k f_l (f_i \pm 1)(f_j \pm 1)] \tag{5.20}$$

This expression can be significantly simplified under the following assumptions [102, 217]:

- assume CP (or T) invariance, which implies that $|\mathcal{M}|^2_{i+j\to k+l} = |\mathcal{M}|^2_{k+l\to i+j} = |\mathcal{M}|^2$.
- since we are dealing with CDM, we have that $E \gg T$, in fact more precisely $E/T \approx 20$, and this implies that we can neglect quantum mechanical effects in the phase space distribution function and approximate it by the classical Maxwell–Boltzmann distribution, also, in the above equation, we can substitute $f_i \pm 1 \simeq 1$.

Under these assumptions Eq. (5.20) becomes:

$$\dot{n} + 3Hn = -\int d\Pi_l d\Pi_k d\Pi_j d\Pi_i (2\pi)^4 \delta^4(p_i + p_j - p_k - p_l) \times |\mathcal{M}|^2 [f_i f_j - f_k f_l]. \tag{5.21}$$

From now on we will assume that i and j are the annihilating DM particles and k and l are the products X, i.e. we have the process $\overline{DM} + DM \leftrightarrow \bar{X} + X$ which is extensively discussed in Section 5.1. We will not make assumptions for now on whether the DM and X particles are Majorana or not. The next step is to deal with the $f_{\overline{DM}} f_{DM} - f_{\bar{X}} f_X$ term of Eq. (5.21). The delta function takes care of energy conservation and imposes the condition that $E_{\overline{DM}} + E_{DM} = E_{\bar{X}} + E_X$.

Using the Maxwell–Boltzmann distribution with the zero chemical potential we have that:

$$f_X f_{\bar{X}} = e^{-(E_X+E_{\bar{X}})/T} = e^{-(E_{DM}+E_{\overline{DM}})/T} = f^{eq}_{DM} f^{eq}_{\overline{DM}}. \tag{5.22}$$

This assumes that DM particles are in kinetic equilibrium before the freeze out, which is the case as elaborated in Section 5.1. So we have that:

$$[f_{\overline{DM}} f_{DM} - f_{\bar{X}} f_X] = [f_{\overline{DM}} f_{DM} - f^{eq}_{DM} f^{eq}_{\overline{DM}}]. \tag{5.23}$$

Assuming that $n_{DM} = n_{\overline{DM}} = n$, which does not necessarily have to be the case like, for example, in scenarios with asymmetric DM, the Boltzmann transfer equation becomes [102, 217]:

$$\dot{n} + 3Hn = -\langle \sigma v \rangle (n^2 - n^2_{eq}) \tag{5.24}$$

with the thermally averaged annihilation cross section times the velocity expressed as:

$$\langle \sigma v \rangle \equiv -\frac{(2\pi)^4}{n^2_{eq}} \int d\Pi_{\overline{DM}} d\Pi_{DM} d\Pi_X d\Pi_{\overline{X}} \delta^4(p_{DM} + p_{\overline{DM}} - p_X - p_{\overline{X}}) \times |\mathcal{M}|^2 e^{-(E_{DM}+E_{\overline{DM}})/T}. \tag{5.25}$$

Introducing another variable Y such that:

$$Y \equiv \frac{n}{s}, \tag{5.26}$$

where n and s are the particle number and entropy densities respectably, the Eq. (5.24) can be rewritten as:

$$\frac{dY}{dx} = -\frac{xs\,\langle\sigma v\rangle}{H}(Y^2 - Y_{eq}^2). \tag{5.27}$$

where at the time of freeze–out $x \equiv m/T \sim 25$ [66]. When the annihilation rate of the DM particles drops below the expansion rate of the Universe, the number density of DM freezes out. Then the parameter Y at the present epoch for the DM yields:

$$Y_0 \approx 0.145\frac{g}{g_{*S}}x^{\frac{3}{2}}e^{-x}. \tag{5.28}$$

Using Eqs. (3.11), (3.12) and (5.26) the relic density can be related to the parameter Y in the simple way:

$$\Omega_{DM}h^2 = \frac{\rho_{DM}}{\rho_c}h^2 = \frac{m_{DM}n_{DM}}{\rho_c}h^2 = \frac{m_{DM}s_0Y_0}{\rho_c}h^2, \tag{5.29}$$

which finally can be written as [66]:

$$\Omega_{DM}h^2 = \frac{3\times10^{-27}\mathrm{cm}^3\mathrm{s}^{-1}}{\langle\sigma v\rangle}. \tag{5.30}$$

To get $\Omega_{DM}h^2 \sim 0.1$ one has to have $\langle\sigma v\rangle \sim 10^{-26}\mathrm{cm}^3\mathrm{s}^{-1}$, which is common for the weak interactions. This coincidence is called the WIMP miracle.

However, this calculation is not applicable in certain fine–tuned scenarios like resonances, coannihilations and thresholds [67].

• *Resonances:* an example of resonance is the funnel region in the CMSSM, where in the particular cases where $m_{DM} = 2m_{A^0}$ the annihilation rate of the DM is very high, which results in the underabundance of the DM in the Universe,

as can be seen from Eq. (5.30).

• *Coannihilations:* the same effect on $\langle\sigma v\rangle$ happens in the case of coannihilations, where the certain level of degeneracy is required between the mass of LSP and NLSP. In the common case, where the NLSP is $\widetilde{\tau}_1$ the mass splitting has to be very small, however, less fine–tuning of masses is required if the NLSP is a strongly interacting particle, like $\widetilde{t}_1$. We will meet both cases in Chapter 7, in the context of NUHMII model.

• *Thresholds:* Eq. (5.30) is also not applicable in certain threshold regions where the mass of DM in annihilation process is slightly smaller than it is in the resonance regions. That is the condition $2m_{DM} < m_X + m_{\bar{X}}$ is satisfied and the process $DM + DM \to X + \bar{X}$ is kinematically suppressed.

Analytical expressions for the relic abundance calculations in these cases can be found in Ref. [67].

5.4 Dark Matter detection

There are three main methods of how DM particles could be detected. The Feynman diagrams of all them are shown schematically in the Fig. 5.6. Labelled arrows denote the direction of time for each method and the blue circle represents unspecified physics, which will vary within different extensions of SM. Below we will review each method in more detail.

5.4.1 Collider production

One of the possibilities is that the DM can be created in colliders. In this case, if the colliding SM particles are energetic enough, they could possibly excite super-

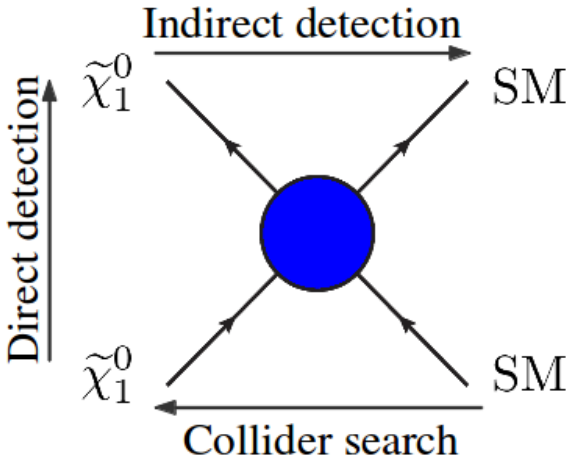

Figure 5.6: Schematic representation of the Feynman rules for the collider search, direct and indirect detection (DD/ID) of DM.

symmetric particles (for eg. $\widetilde{qg}, \widetilde{qq}, \widetilde{gg}$ in LHC) that would cascade decay through the heavier neutralinos and charginos with the final states containing $\widetilde{\chi}_1^0$ [218]. The sign of the presence of neutralinos would be an excess of missing transverse energy. In most cases the collider searches are complementary to the direct and indirect detection experiments. Collider search results also come in a model dependent fashion, where the CMSSM is the most widely studied possibility.

Fig. 5.7 summarizes the exclusion limits in the $m_{\widetilde{\chi}_1^0} - m_{\widetilde{t}_1}$ plane, from the search for stop quark production. Final states containing one or two leptons, large missing transverse momentum and b-jets are used to reconstruct the top squark mass [219, 221]. As can be seen from the figure, no excess over SM expectations was found. In this analysis, besides the constraints on the $\widetilde{\chi}_1^0$–stop masses, it is also assumed that the stop decays exclusively into sbottom and chargino ($\widetilde{t}_1 \to \widetilde{\chi}_1^{\pm} b$), and the chargino decays to the DM candidate neutralino ($\widetilde{\chi}_1^{\pm} \to W\widetilde{\chi}_1^0$). All other masses are assumed to be above TeV scale.

Fig. 5.8 shows the 95% C.L. exclusion regions in the $m_{\widetilde{\chi}_1^{\pm}} - m_{\widetilde{\chi}_1^0}$ plane, under

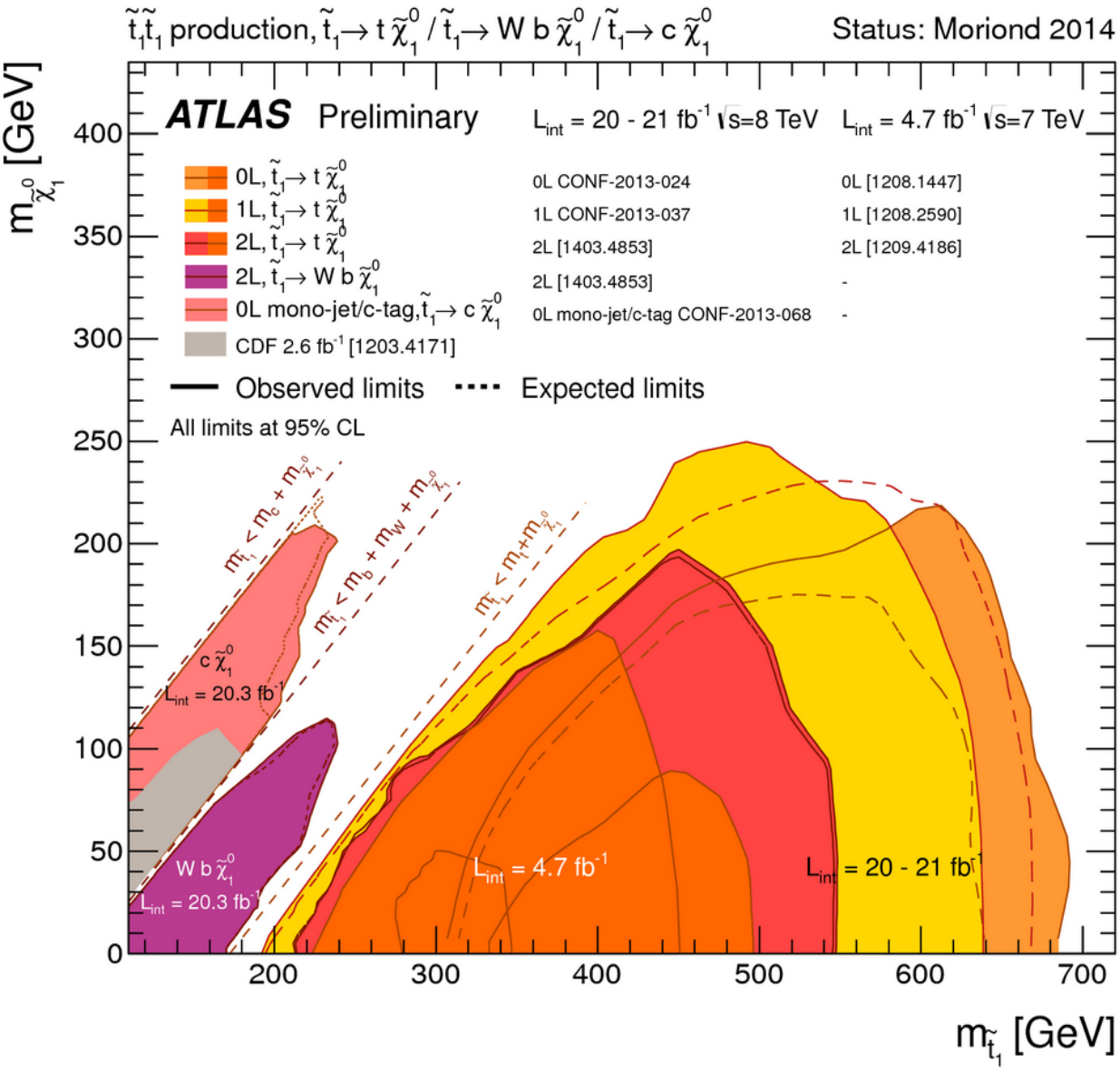

Figure 5.7: Exclusion limit in the $m_{\tilde{\chi}_1^0} - m_{\tilde{t}_1}$ plane assuming various stop quark production possibilities [219].

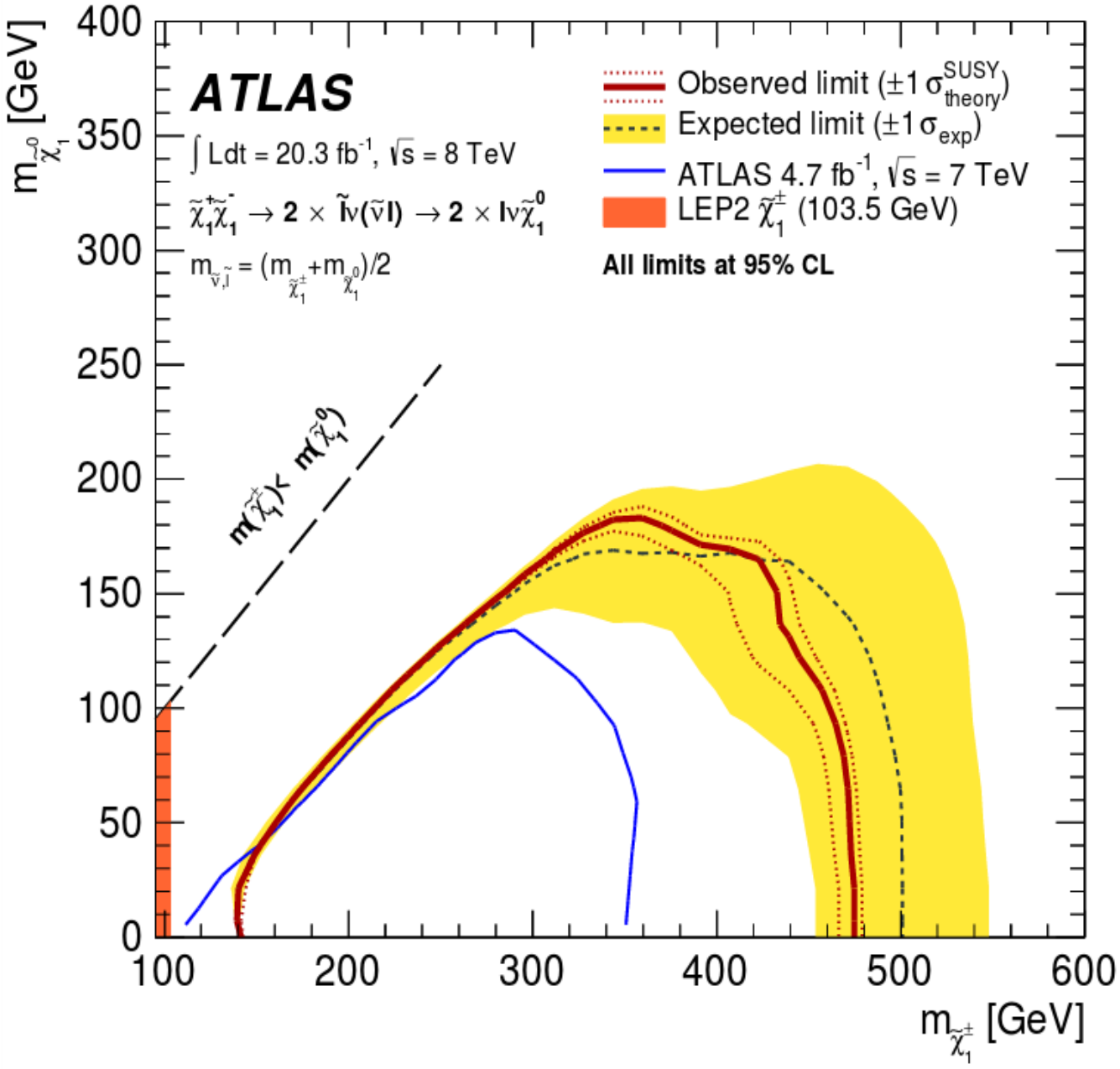

Figure 5.8: 95% C.L. exclusion regions in the $m_{\tilde{\chi}_1^\pm} - m_{\tilde{\chi}_1^0}$ plane for the simplified model with $m_{\tilde{l}} = m_{\tilde{\nu}} = (m_{\tilde{\chi}_1^\pm} + m_{\tilde{\chi}_1^0})/2$. Figure from Ref. [220].

these special assumptions about the sparticle spectrum, with the significance of the lines' explained in the plot itself. Despite all the efforts even using 20.3 fb^{-1} of data at $\sqrt{s} = 8$ TeV no significant excess beyond SM expectations were observed [220].

5.4.2 Direct detection

There are many experiments already built trying to directly detect suspersymmetric DM particle, i.e. register a recoil between the nucleons of the detector and the DM particles passing us all the time. Since the Milky Way's halo is made of DM particles, there should be a good chance that, even though interacting weakly, sensitive detectors could register the recoil. The Feynman diagram on which DD experiments rely on, can be seen in Fig. 5.6 with the time arrow pointing upwards. The typical expected recoil energies in such experiments are very low – of the order of 10 keV. It is desirable to have large volumes of target material in the detector, to increase the probability of the interaction because only a few tens of scatterings are expected per kilogram per year. One of the challenges in DD is how to take into account the background, as the neutrons from the cosmogenic or radioactive processes can produce nuclear recoils that are indistinguishable from those of an incident WIMP [222]. The results obtained so far are quite contradictory since there are four: DAMA/LIBRA [177, 178], CoGeNT [179], CRESST–II (1^{st} phase run) [180], and CDMS [181, 222] experiments that announced hints for the DM – all in the region of low mass region, while some other experiments, most notably XENON100 [223] and LUX [224] are ruling out all the parameter space favoured by former ones. Recent 2^{nd} phase aggregation of CRESST–II results also disfavours light DM – collaboration announced no excess

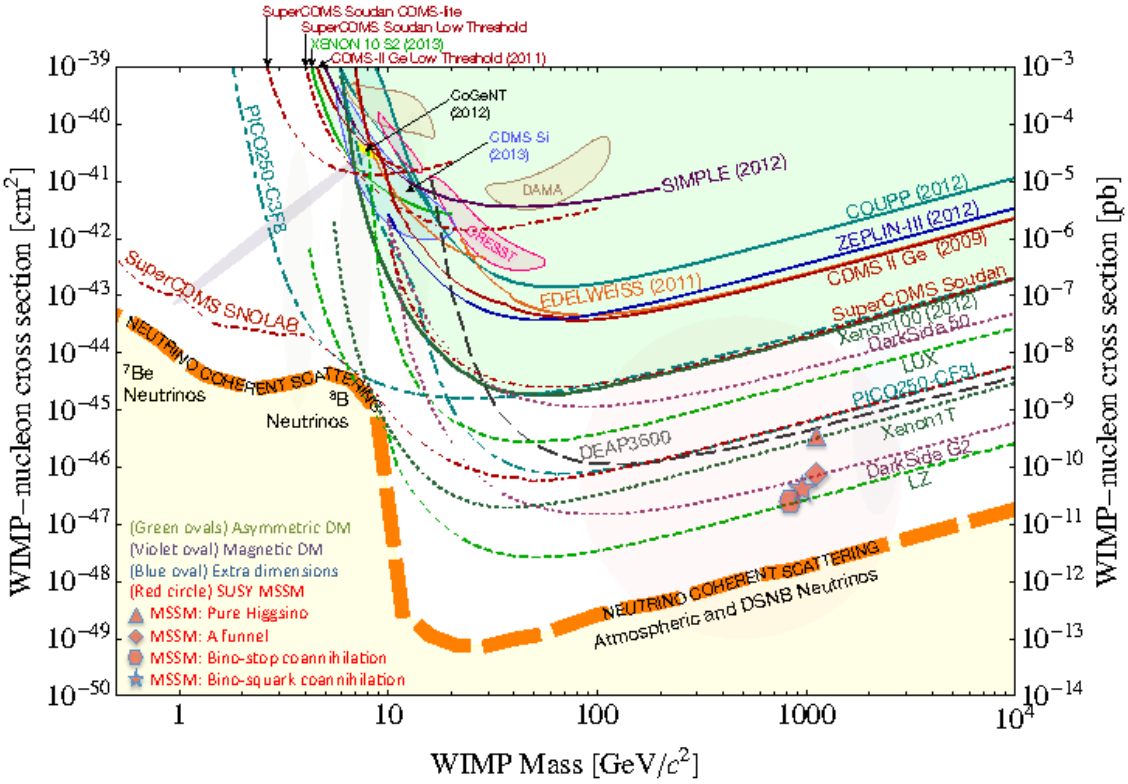

Figure 5.9: The parameter space of spin independent DM–nucleon scattering versus WIMP mass from various DM DD experiments. The figure is taken from Ref. [225].

signal over the expected background [226]. Therefore, as it stands, there is no conclusive evidence that rule in or out light DM.

However, in principle, it is possible to reconcile these results if one assumes isospin violating DM [227]. As already mentioned, spin independent nucleon–$\widetilde{\chi}_1^0$ scattering cross section can be schematically written as $\sigma^{SI} \propto [f_p Z + f_n(A-Z)]^2$, where Z is atomic number of the active material in detector, A is number of nucleons and $f_{p(n)}$ is the relative coupling strength of DM to the protons (neutrons). Therefore, with some fine–tuning of the $\widetilde{\chi}_1^0$ coupling to the proton and neutron in the detector, consistent results across variety of seemingly contradictory ex-

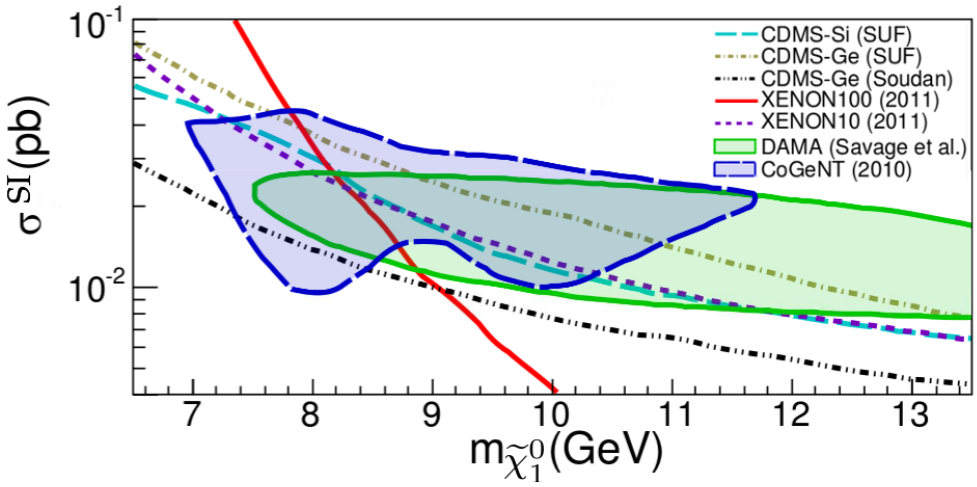

Figure 5.10: Favoured regions and exclusion bounds assuming isospin violating DM in the case of $f_n = -0.7 f_p$. Favoured regions of DAMA at 3σ C.L., assuming scattering from Na only [177] and CoGeNT at 90% C.L. [179]; exclusion limits of XENON100 [223] and XENON10 at 90% C.L. [228], and 90% CDMS Ge and Si bounds [229, 230] are shown. The figure is taken from Ref. [227].

periments can be obtained. In the Ref. [227] authors show that in the range $-0.72 \lesssim f_n/f_p \lesssim -0.66$ DAMA and CoGeNT regions overlap and sensitivity of XENON10 and XENON100 is reduced enough to keep the data from all of these in agreement. Fig. 5.10 graphically demonstrates the case where $f_n = -0.7 f_p$, with colour coding explained in the caption.

In the rest of the section, an overview of results from a few leading collaborations is given. All bounds are evaluated using standard assumptions, i.e. DM density in the Galactic halo $\rho_{\tilde{\chi}_1^0} = 0.3$ GeV/cm^3, the circular velocity $v = 220$ km/s and the Galactic escape velocity $v_{\rm esc} = 544$ km/s [231].

• DAMA/LIBRA experiment tries to verify the presence of the DM particles in the halo by utilizing the annual modulation signal [232]. The expectation is that as the Earth goes through the halo on June, Earth's orbital velocity around the Sun and the Sun's rotational velocity around the Galaxy centre add construc-

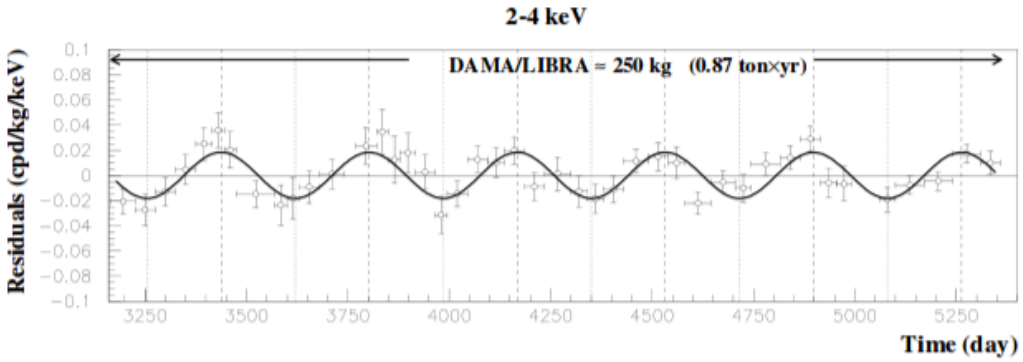

Figure 5.11: Annual modulation signal observed by DAMA/LIBRA in 2–4 keV energy intervals as the function of time. The figure is taken from Ref. [178]

tively, but after precisely half year the two add destructively. The resulting effect is the different flux of DM particles crossing the Earth and therefore yearly varying interaction rate between DM and the nuclei of the detector throughout the year. Fig. 5.11 shows the residual interaction counts observed by DAMA/LIBRA. The highest rate was registered on 2^{nd} of June and lowest on 2^{nd} of December – a half year later. More precisely, the period in the plot is equal to (0.999± 0.002) years, well in agreement with the expectation. The modulation is observed only in a single hit events (where only one detector of many register scattering) and that is also in line with the expectations because DM, which interacts weakly, is unlikely to scatter off more than once. The statistical significance claimed by DAMA for such modulation is measured to be 8.9 σ [177, 178].

• CoGeNT is the Germanium detector operated in Minnesota, US. The best fit is for $m_{\widetilde{\chi}_1^0} \sim 7-11$ GeV and the spin independent cross section $\sigma^{SI} \approx 6.7 \times 10^{-41}$ cm^2. CoGeNT also observed an annual modulation effect.

• CRESST–II is a cryogenic DM search facility operating at temperatures as low as 15 mK. In this experiment, DM is expected to scatter off $CaWO_4$

crystal nuclei. At such low temperatures all excitations in the crystal stands still and even least energetic scatterings can be registered. In Ref. [180] collaboration

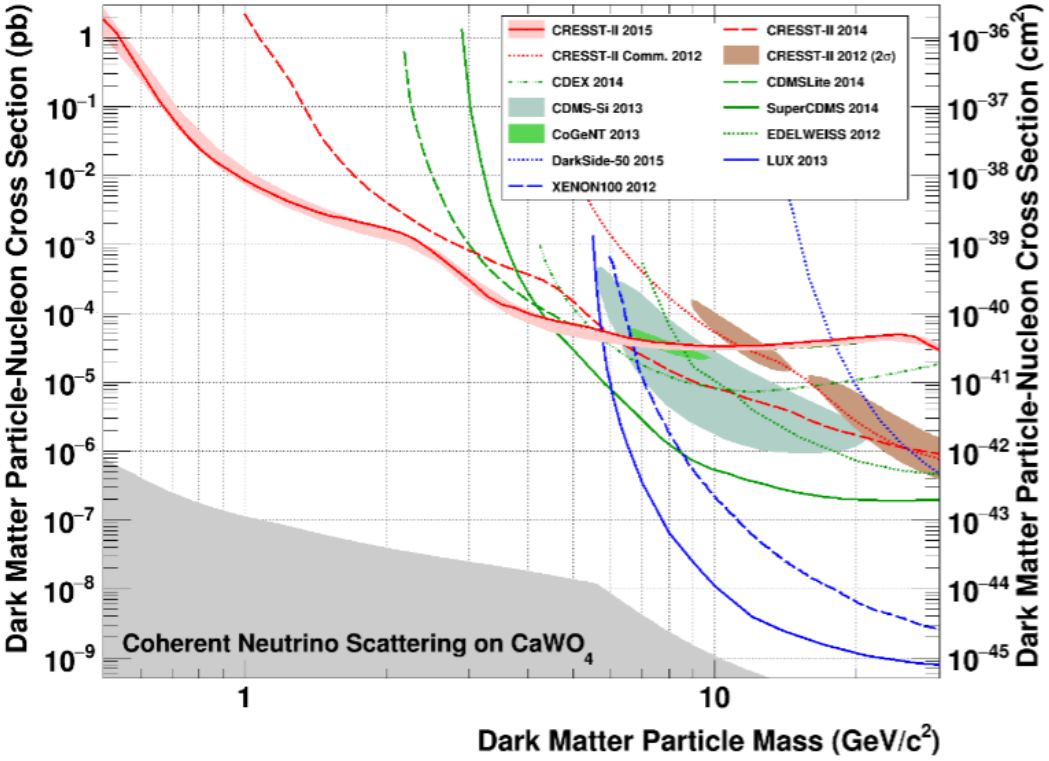

Figure 5.12: Parameter space of the DM–nucleon scattering from the phase 2 data taking campaign. Grey area denotes irreducible background of supernovae and solar neutrino scatterings from detector's target material. The figure is taken from [226].

announced results of the phase I data taking campaign where maximum likelihood analysis of WIMP related interactions yielded two best fits for the mass of DM: $m_{\tilde{\chi}_1^0} = 25.3$ GeV and $m_{\tilde{\chi}_1^0} = 11.6$ GeV with spin independent cross sections $\sigma^{SI} = 1.6 \times 10^{-6}$ pb and $\sigma^{SI} = 3.7 \times 10^{-5}$ pb respectively. The possibility of two different solutions arises because of the different nuclei present in detector's target material and for a given WIMP mass scatterings of different nuclei in $CaWO_4$ crystal are dominant.

In the phase II aggregation of two years data, collaboration did not observe any excess over the expected background and instead announced an exclusion limit for the WIMP–nucleon scattering. This is denoted by the solid red line of the Fig. 5.12 together with 1σ C.L. by the light red [226].

• CDMS II collaboration seeks to register interactions using detectors operating at $\sim$ 40 mK. It is made of 30 detectors: 19 Ge and 11 Si, for a total of $\sim$ 4.6 kg of Ge and $\sim$ 1.2 kg of Si. In the data collected between July 2007 and September 2008, there have been observed 3 event candidates for a recoil energy range 7–100 keV. Likelihood analysis yielded best fit for a WIMP mass $m_{\widetilde{\chi}_1^0} = 8.6$ GeV and WIMP–nucleon cross section $\sigma^{SI} \approx 1.9 \times 10^{-41}$ cm^2.

Positive results obtained are summarised in Fig. 5.9 with a different colour coding for different experiments. However, these results are challenged by the competitive results released most notably by XENON100 and LUX. As it can be seen from the plot, the bounds put on a parameter space by them are ruling out all the before mentioned potential positive signals.

5.4.3 Indirect detection

Indirect detection relies on the processes where the DM particles annihilate or decays into other lighter SM species like leptons or photons. Therefore, observing an excess of these particles in the cosmic rays potentially could be a clear signal for the existence of dark matter. The analysis of the indirect detection experiments is subject to astrophysical backgrounds and therefore inherits a lot of uncertainty and is hard to deal with.

If the DM annihilation or decay products are charged particles, astrophysics gets a lot more complicated. One reason is that the internal properties and

behaviour of some of the cosmic bodies are not conclusively understood, and this makes it hard to quantify fluxes of particles emitted into the outer space. It is also very hard to track down the region of the source of the excess particles, since they are under Lorentz force influence due to the Galactic and Solar magnetic fields before they reach the Earth. In general, propagation of the charged products in the Galaxy is modelled by [233, 234, 235]:

$$K\nabla^2\psi + \frac{\partial(b\psi)}{\partial E} + q = \frac{\partial\psi}{\partial t}, \tag{5.31}$$

where $\psi \equiv \psi(\vec{x}, E, t)$ is the particle number density per unit energy (dn/dE), at location $\vec{x}$ and time t. $b(\vec{x}, E)$ is the total energy loss of the particle by synchrotron radiation and inverse Compton scattering and $q \equiv q(\vec{x}, E, t)$ is the source term. K is the diffusion coefficient. The loss term can be written as [170]:

$$b_e(\vec{x}, E) \simeq b^0_{\rm IC}\left(\frac{u_{\rm ph}}{1\ {\rm eV/cm^3}}\right)E^2 + b^0_{\rm sync}\left(\frac{B}{1\ \mu{\rm G}}\right)E^2, \tag{5.32}$$

where $u_{\rm ph}$ together with constants $b^0_{\rm IC} \simeq 0.76 \times 10^{-16}$ GeV/s and $b^0_{\rm sync} \simeq 0.025 \times 10^{-16}$ GeV/s correspond to the background radiation energy density and B to the ambient magnetic field.

• PAMELA (Payload for Antimatter Matter Exploration and Light–Nuclei Astrophysics) and ATIC (Advanced Thin Ionization Calorimeter). One of the experiments, PAMELA, announced that they have observed an excess of the positrons in the cosmic ray radiation in the range of 10 GeV $\lesssim E_{e^\pm} \lesssim$ 100 GeV [236]. The positrons are created by a cosmic ray nuclei (mainly protons and helium nuclei) interaction with the interstellar matter (mainly hydrogen and he-

lium) for eg [237]:

$$p + H \rightarrow p + n + \pi^+$$
$$\pi^+ \rightarrow e^+ + \nu_e$$

and so the positron fraction should decrease with the increasing energy as it becomes energetically harder to produce them. Moreover, energetic positrons effectively loose energy due to the inverse Compton scattering and synchrotron radiation. However, contrary to theoretical prediction, PAMELA's observation shows an increase of the positron flux, see Fig. 5.13. To justify observed positron excess by DM species, the annihilation cross section should be of the order $\mathcal{O}(10^{-23})$ cm^3/s i.e., thousand times larger than that expected for the thermal DM. This could be achieved either by having DM overdensities in the Galactic halo [238, 239, 240], producing DM non–thermally [241] or via resonant annihilation [242], when the resonance mass differs by less than 1% from twice of DM mass [243]. Furthermore, DM has to be leptophilic and annihilate mostly into leptons because otherwise quarks would hadronize and antiproton measurements would be exceeded [243]. This, for example, can be achieved by assuming that DM shares a quantum number with leptons [244, 245]. However, as already mentioned above, an astrophysical treatment might play a key role in the analysis. One source of electrons are pulsars – fast rotating neutron stars with a very strong magnetic field that extracts $e^{\pm}$ from the star into the outer space [246]. In Ref. [247, 248] authors claim, that the excess of the positrons measured by PAMELA and also by ATIC [249] can be naturally explained by the presence of a few nearby pulsars. From the PAMELA data, it is also possible to make a naive first order estimation about the lifetime of the pulsar. Assuming a burst–like injection of

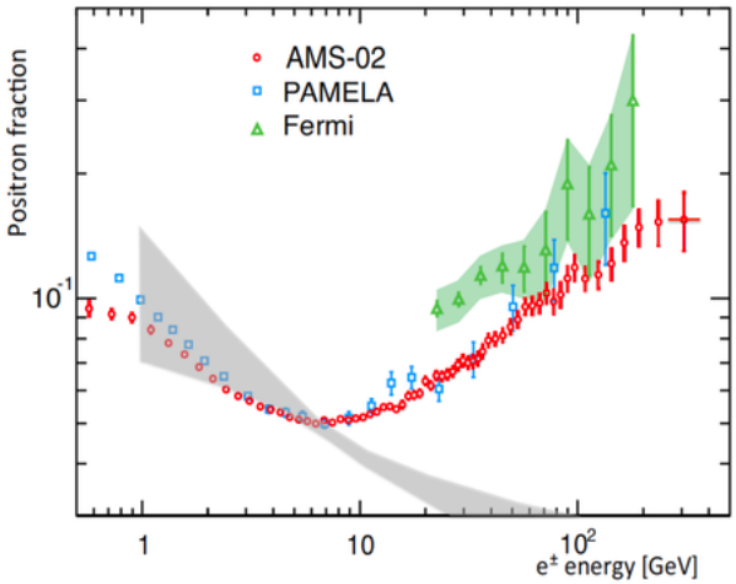

Figure 5.13: The excesses of positrons in the cosmic rays as measured by AMS–02 [251], PAMELA [236] and Fermi–LAT [252]. Grey shaded area denotes theoretically predicted secondary positron fraction [253, 254, 255].

positrons and inverse Compton scattering and synchrotron losses only, the time required to cool them from an injection energy $E_{e^\pm}$ to the rest energy $E_{e^\pm} = m_e$ can be expressed as

$$t \sim 5 \times 10^5 \left(\frac{\text{TeV}}{E_{e^\pm}} \right) \text{yr}, \tag{5.33}$$

therefore, if the injected positrons have energies of about 1 TeV [248], then in order to still have these particles around us energetic enough, injection should have happened in the last 5×10^5 years.

• Fermi–LAT (Fermi Large Area Telescope) and AMS–02 (Alpha Magnetic Spectrometer). More recently two collaborations – Fermi–LAT [250, 252] performed a refined analysis in between 20 and 200 GeV and AMS–02 [251] released the data in the range of 0.5 – 350 GeV, with an observed excess in the 10 to 250 GeV window – both in agreement with the PAMELA data. The results from

AMS–02, PAMELA and Fermi–LAT are summarised in Fig. 5.13. Grey shaded area denotes theoretically predicted secondary positron fraction [253, 254, 255]. In the latest improved update from the AMS–02 collaboration [256] the positron excess in the range of 0.5–500 GeV is presented showing monotonically increasing positron fraction as a function of their energy above $\sim$ 10 GeV. This behaviour can still be explained by the presence of the nearby pulsars [257].

However, if decay products are the photons or neutrinos, these could be used to pin down the original source of them. If there would be observed the sharp spectral features in the γ ray spectrum, it would allow to discriminate this signal from astrophysical backgrounds and would be a smoking gun evidence for the DM annihilation or decay. The above–mentioned Fermi–LAT telescope also has an instrument enabling to register γ rays. The search based on an excess of 50 photon signal of monochromatic rays in the Fermi–LAT data revealed, that in the regions close to the Galactic centre, there is an indication for the $E_\gamma = 130$ GeV line at $\sigma = 4.6$ confidence level [258, 259]. Assuming DM annihilation to two photons, the best fit for the mass was found to be $m_{\tilde{\chi}_1^0} = 129.8$ GeV. Independent analysis yielding the same line with the similar statistical significance can be found at [260, 261, 262, 263]. It's worthwhile mentioning that there are number of alternative ongoing attempts to explain the origin of this line: one possibility is that this could be due to Fermi bubbles – a very powerful sources of γ rays originating from the centre of our Galaxy [264]; depending on the angle at which photons from the Earth limb fall into detector, they can also produce a $\sim$ 130 GeV feature with more than 3σ significance [265, 266, 267]; another possibility is that these photons are actually coming from the Sun [267]. Besides, a speculation about 130 GeV line, another emission line at 111 GeV is also found in [268].

Recently two groups independently announced that they observed $E_\gamma \sim 3.5$ KeV X–ray line in the Andromeda galaxy and 73 galaxy clusters [189, 190]. This line is found to be stronger towards the centre of these objects and completely absent in the "blank sky" dataset. Moreover, authors argue that this line is absent in any kind of the atomic transitions that could take place in interstellar gas. However, in ref. [269], different group carried out an independent study and found no evidence of ~ 3.5 KeV X–ray line. In any case, there already have been a number of attempts to explain the observation by the axions [270], axinos [271], string moduli [272], augmenting neutrino sector [190], or trying to explain it minimally by adding SM with the non–renormalizable operators with pseudo(scalar) or fermion coupling to the photons, through the operators of the kind [273]:

$$\frac{\phi}{f} F_{\mu\nu} F^{\mu\nu}, \tag{5.34}$$

where f is a massive coupling constant.

Chapter 6

Light neutralino Dark Matter in p19MSSM and NMSSM

In this chapter, we explore the possibility of light neutralino DM in two popular SUSY models:

• Phenomenological MSSM (p19MSSM): an unconstrained MSSM has 105 free parameters in addition to 19 that come from the SM [37]. The majority of them appear in the complex matrices of sfermions and trilinear couplings in the soft breaking Lagrangian, $\mathcal{L}_{\rm soft}^{\rm MSSM}$, given in Eq. (4.76). However, there exist well–motivated assumptions, which allow us to reduce the number of free inputs [274, 275, 276]:

1) CP violating phases in the SUSY sector vanish, based on the electron and neutron electric dipole moments and from results on K-meson experiments.

2) As already discussed in Section 4.4.2, in order to suppress flavour changing neutral currents, all off–diagonal elements in the matrices of sfermions and trilinear couplings can be set to zero.

3) The mixing rate of $K^0 - \bar{K}^0$ and other kaon physics experiments suggest the universality of the first and second generation sfermions [277].

4) Since trilinear couplings are proportional to the corresponding Yukawa coupling matrix, only third generation couplings, A_τ, A_b and A_t, can have significant phenomenological consequences.

Taking the above assumptions into account, the number of free parameters in the theory boils down to 19, making phenomenological studies far more practical.

• NMSSM: a motivation and DM sector of the NMSSM has already been discussed in Section 4.5.3.

Since SUSY is yet to be found, we also addressed the issue of naturalness within the p19MSSM. However, within NMSSM, the EW fine tuning is highly ameliorated since the Higgs mass parameter, μ, is generated by the VEV of a singlet.

We start this chapter by discussing methods that we used to probe a parameter space of SUSY models and the constraints that we applied on various observables. The same techniques are used later in Chapter 7 to investigate the link between DM and inflation within MSSM with non–universal Higgs masses (NUHMII).

6.1 Method and constraints

To explore the parameter space that is consistent with the experiments we used `micrOMEGAs2.4` software package [278]. `micrOMEGAs` is widely used in evaluating DM relic abundance, fluxes of photons, antiprotons, and positrons; cross sections of DM interactions with nuclei and energy distribution of recoil nuclei; neutrino and the corresponding muon flux from DM particles captured by the Sun; collider

cross sections and particles' decay widths within a BSM models that provide a viable WIMP DM candidate. It also calculates muon anomalous magnetic moment $(g-2)_\mu$, branching ratios of various decay channels, including those that are particularly sensitive to the BSM physics, like $b \to s\gamma$ and $B_s \to \mu^+\mu^-$ [279].

The `micrOMEGAs` can provide these estimates for a desired particle physics model once the key files, called model or `CalcHEP` files, are generated, see Fig. 6.1. Model files contain model specific information about the properties of all particles, parameters and interactions' vertices. Most popular packages used to generate these files are `LanHEP` [280], `FEYNRULES` [281] and `SARAH` [282, 283]. The user has to solely define either the Lagrangian or the superpotential and desired files are produced. Subsequently, they are used by `CalcHEP` for identifying the DM particle and for the automatic calculation of elementary particle (co)annihilation and decay rates. Finally, the `micrOMEGAs` uses `CalcHEP` output to calculate previously mentioned quantities. To extract observables of the NMSSM model, `micrOMEGAs` is coupled to NMSSMTools [284].

In order to thoroughly probe a very complex region of the light neutralino DM, we performed MCMC likelihood analysis. We also used MCMC to analyse NUHMII model. The main advantage of the MCMC over MC is that it is more efficient and less time consuming. The first step in the MCMC is to randomly generate a point, say $M \in [x_1, x_2, ...x_i]$, where x_i is the input parameter of a specific model. For example, in the constrained MSSM (CMSSM) $i = 5$, in NUHMII $i = 6$, in p19MSSM $i = 19$. Once the points are generated `micrOMEGAs2.4` can calculate the values of the observable z. Once every observable of interest is calculated we evaluate the likelihood function for each of them and calculate the

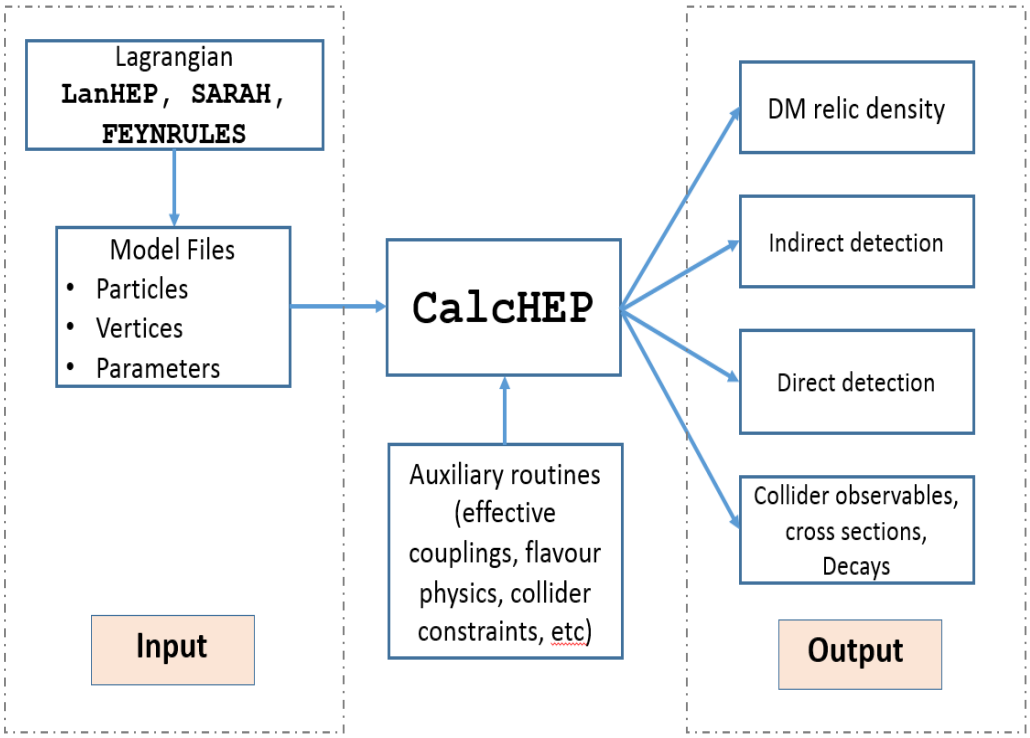

Figure 6.1: `micrOMEGAs` flow chart [279].

total product:

$$\mathscr{L}^{\mathrm{M}}_{\mathrm{total}} = \prod_i e^{-\frac{(z_j-\mu)^2}{2\sigma^2}}, \tag{6.1}$$

where j runs over the observables that are itemised below. If, for a particular set of input values $\mathscr{L}^{\mathrm{M}}_{\mathrm{total}}$ is smaller than some certain numerical estimate, then the new set of input parameters $M \in [x_1, x_2, ...x_i]$ are generated, which are completely independent of the previous ones. However, if $\mathscr{L}^{\mathrm{M}}_{\mathrm{total}}$ is large, then the values of the input parameters are varied infinitesimally, i.e. $x' = x \pm \delta_x$ with an expectation that the new set will also have high $\mathscr{L}^{\mathrm{M}'}_{\mathrm{total}}$ and thus the values of the observables within desired ranges. The whole process is graphically shown in Fig. 6.2 and an example code of the MCMC routine used to scan p19MSSM parameter space is given in the Appendix B.

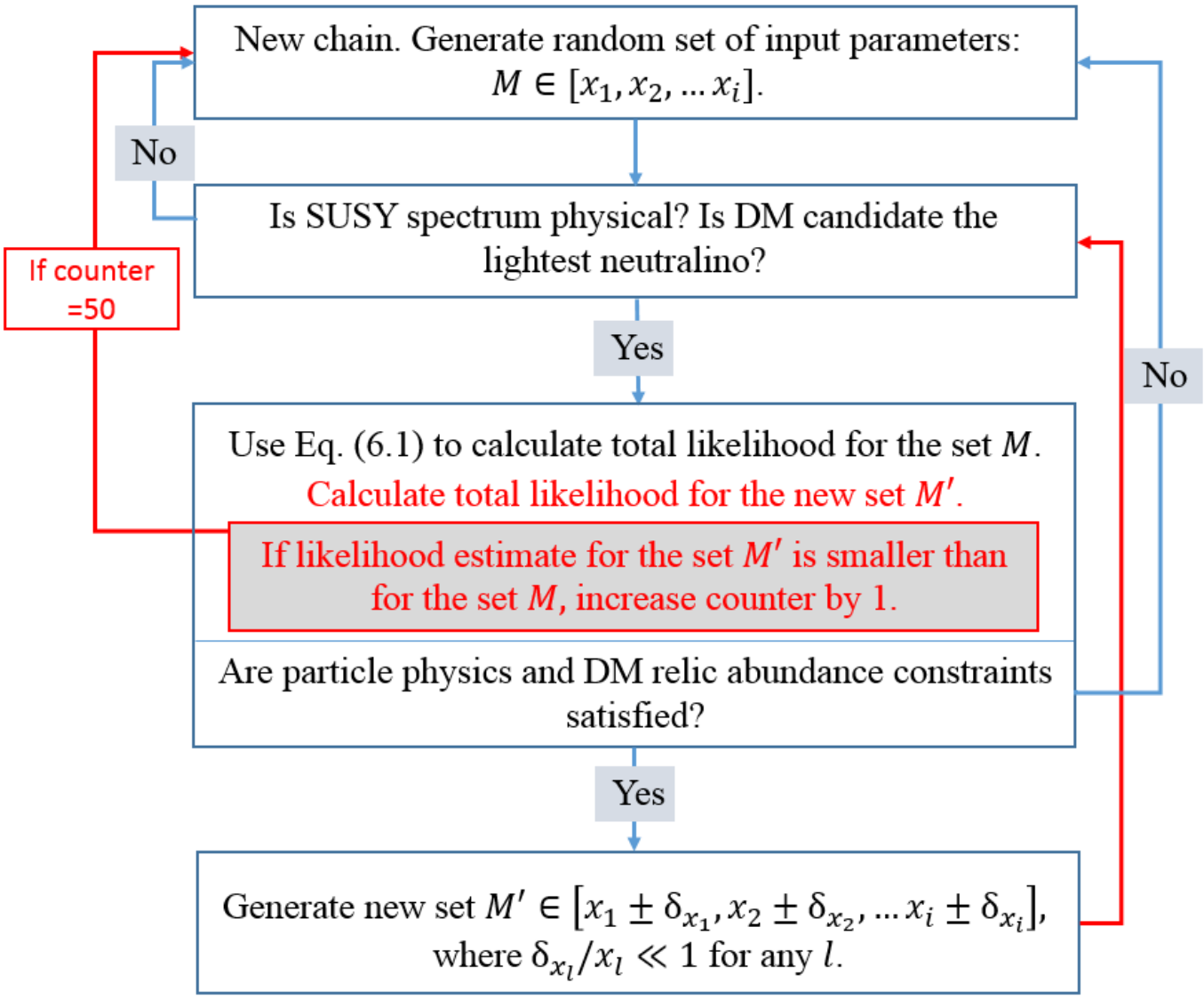

Figure 6.2: Markov Chain Monte Carlo scan strategy [285].

The limits from the various experiments, that we imposed in scans, are as follows:

- *Relic abundance*: We require that all model points satisfy the upper limit on DM relic abundance found by the Planck satellite, i.e. $\Omega_{\tilde{\chi}_1^0} h^2 < 0.128$ [91]. In a large part of the parameter space of SUSY models the abundance

of neutralinos is not enough to account for the total Planck measured value, and additional DM candidates should be considered.

- *Higgs mass*: We impose the LHC bound on the Higgs boson mass by taking the combined theoretical and experimental uncertainties within the following range, i.e. $121.5 < m_h < 129.5$ GeV.

- *Direct DM detection*: We take into account various bounds on the neutralino–nucleon interaction cross–section. We often consider the projected bound of the XENON1T [286] as well. As already mentioned in Section 5.4.2, these bounds are derived using standard assumptions, i.e. DM relic density in the Galactic halo $\rho_{\widetilde{\chi}_1^0} = 0.3$ GeV/cm^3, the circular velocity $v = 220$ km/s and the Galactic escape velocity $v_{\rm esc} = 544$ km/s [231].

- *Flavour physics*: We enforce the limits on the branching ratios of the flavour violating decays, $\mathcal{B}(B_s \to \mu^+\mu^-) = \left(3.2^{+1.5}_{-1.2}\right) \times 10^{-9}$ [287] and $\mathcal{B}(b \to s\gamma) = (3.43 \pm 0.22) \times 10^{-4}$ at 3σ confidence level [288]. We found that most of the scenarios in the study of light neutralino and baryogenesis within the NMSSM are not affected by these constraints, because the light neutralinos and the requirement for the first order phase transition in the NMSSM have a preference for a moderate to low $\tan\beta$ values, whereas both branching ratios are enhanced for large $\tan\beta$. The parameter space of the p19MSSM and NUHMII is also largely unconstrained by these processes.

- *Chargino mass*: We take the lower LEP bound on the mass of the chargino to be $m_{\widetilde{\chi}_1^+} > 103.5$ GeV [147] [1]. A null result in LEP searches on a process

[1] We used a general limit on the chargino mass, however for possible caveats, see Ref. [290].

$e^+e^- \to \widetilde{\chi}_1\widetilde{\chi}_j$ with $j > 1$, sets an upper bound on the neutralino production cross–section $\sigma(e^+e^- \to \widetilde{\chi}_1\widetilde{\chi}_j) \lesssim 10^{-2}$pb [156], which can be translated into $(m_{\widetilde{\chi}_1^0} + m_{\widetilde{\chi}_2^0}) > 209$ GeV [289] which we apply only in the Chapter 8.

- *Invisible Z boson decay width*: In the light neutralino regions where $m_{\widetilde{\chi}_1^0} < M_Z/2$, one has to take into account the invisible decay width of Z boson into neutralinos. An analytical expression for the rate of this process is given by [156]:

$$\Gamma_{Z\to\widetilde{\chi}_1^0\widetilde{\chi}_1^0} = \frac{M_Z^3 G_F}{12\sqrt{2}\pi}(|N_{13}|^2 + |N_{14}|^2)^2\left(1 - \frac{4m_{\widetilde{\chi}_1^0}^2}{M_Z^2}\right)^{3/2}$$

In the mass basis, the total composition of the lightest neutralino in p19MSSM and NUHMII can be expressed as:

$$\widetilde{\chi}_1^0 = N_{11}\widetilde{B} + N_{12}\widetilde{W}^0 + N_{13}\widetilde{H}_d^0 + N_{14}\widetilde{H}_u^0,$$

and in the case of NMSSM:

$$\widetilde{\chi}_1^0 = N_{11}\widetilde{B} + N_{12}\widetilde{W}^0 + N_{13}\widetilde{H}_d^0 + N_{14}\widetilde{H}_u^0 + N_{15}\widetilde{S}$$

where $|N_{11}|^2$ gives the bino, $|N_{12}|^2$ the wino, $|N_{13}|^2 + |N_{14}|^2$ the higgsino and $|N_{15}|^2$ the singlino fraction of the LSP. Alternatively, a small M_1 entry can render the lightest neutralino to acquire mostly bino admixture. This relationship is derived assuming three massless neutrinos. In order to satisfy this constraint the lightest neutralino must mostly be bino in the case of p19MSSM (a fact which we will confirm at the end of this chapter) and either bino or a singlino, with minimal or no admixture from higgsinos,

within NMSSM.

Our constraints are summarised in Table. 6.1.

Quantity	Value	Source
m_h	125.5 ± 4 GeV	[1, 2]
$\Omega_{\widetilde{\chi}_1^0} h^2$	< 0.128	[91]
$m_{\widetilde{\chi}_1^+}$	> 103.5 GeV	[147]
$\mathcal{B}(B_s \to \mu^+\mu^-)$	$\left(3.2^{+1.5}_{-1.2}\right) \times 10^{-9}$	[287]
$\mathcal{B}(b \to s\gamma)$	$[2.77 : 4.09] \times 10^{-4}$	[288]
$(m_{\widetilde{\chi}_1^0} + m_{\widetilde{\chi}_2^0})$	> 209 GeV	[156] [289]
$\Gamma_{Z \to \widetilde{\chi}_1^0 \widetilde{\chi}_1^0}$	< 3MeV	[291]

Table 6.1: The list of the experimental constraints which we imposed in the p19MSSM, NUHMII and NMSSM scans. The $(m_{\widetilde{\chi}_1^0} + m_{\widetilde{\chi}_2^0}) > 209$ GeV constraint is only used in the Chapter 8, and not elsewhere.

6.2 Light neutralino in p19MSSM

The recent hints of positive signals in three DM direct detection experiments, namely, DAMA [177, 178], CoGeNT [179], CRESST-II [180] and more recently by CDMS [222], have generated a lot of interest in light WIMP candidates. This interpretation is however challenged by the null results from various other direct detection experiments, most notably XENON100 [223] and LUX [224], which provide the most stringent upper limits on the spin independent WIMP-nucleon scattering cross section for $m_{\widetilde{\chi}_1^0} > 7$ GeV. Nonetheless, due to the relatively poor sensitivity of the XENON100 experiment in the very low WIMP mass regime, it is believed that an agreement between the positive and null sets of experimental results could be possible, if at all, only in this low mass region. Hence, it might be worthwhile examining the allowed MSSM parameter space to see if there exists

a lower bound on the lightest neutralino mass irrespective of the direct detection results.

As already mentioned in Section 4.4.8, the neutralino mass eigenstates in the MSSM result from the mixing of the neutral bino ($\widetilde{B}$), wino ($\widetilde{W}^0$) and higgsinos ($\widetilde{H}_d^0, \widetilde{H}_u^0$). This mixing is determined by the $\tan\beta$ parameter and the bino, wino and higgsino mass parameters M_1, M_2 and μ, respectively. In the SUSY models with gaugino mass unification at the GUT scale, a relation between the bino and wino mass follows at the EW scale: $M_1 = \frac{5}{3}\tan^2\theta_W M_2 \approx 0.5 M_2$ (see Section 4.4.2) which, after mixing, translates into a chargino–neutralino mass relation. Therefore, a lower limit on the lightest neutralino $\widetilde{\chi}_1^0$ mass of about 46 GeV, can be derived for these models from the LEP chargino mass limit [290], whereas in the constrained CMSSM with both gaugino and sfermion mass unification, this limit increases to well above 100 GeV from the strong constraints set by the recent LHC data [292].

On the other hand, in a generic MSSM scenario without the assumption of gaugino mass unification, there is no general lower limit on the lightest neutralino mass [293]. The LEP limit on the invisible decay width of the SM Z boson applies to light neutralinos with a mass below $m_Z/2 = 45.6$ GeV, but it depends on the $Z\widetilde{\chi}_1^0\widetilde{\chi}_1^0$ coupling which could be small or even zero, depending on the higgsino component of the neutralino. In such a case, light neutralinos are mainly constrained by the DM relic density measurement as well as by the collider and flavour constraints on the SUSY parameter space. Assuming that the lightest neutralino is non-relativistic and provides the entire CDM content of the Universe, while satisfying the LEP bounds on chargino and $\widetilde{\tau}$ masses, Ref. [294] obtained a lower bound of $m_{\widetilde{\chi}_1^0} \gtrsim 18$ GeV. This was relaxed to about 6 GeV without

violating the LEP bounds and flavour sector constraints in SUSY models with a pseudo-scalar Higgs boson (A) mass $m_A < 200$ GeV and a large $\tan\beta$ [295, 296]. This was even further lowered to about 3 GeV by allowing explicit CP violation in the MSSM Higgs sector [297]. Ever since these estimates the new scalar Higgs–like particle has been discovered at the LHC with a mass of $m_h = 125$ GeV [298, 299], also the updates on the B–physics and cosmological observables have been released.

Another important issue to be addressed in the light of the recent LHC results is the apparent "little supersymmetric hierarchy problem", i.e., how does a multi-TeV SUSY particle spectrum conspire to give a weak-scale Z-boson mass and also the measured value of the Higgs boson? One way of analysing this issue quantitatively is already described in detail in Section 4.4.4. It is well-known that radiative corrections play a crucial role in determining the allowed SUSY parameter space necessary to generate a 125 GeV Higgs boson mass, depending on $\tan\beta$, comparable or even much larger than its tree-level prediction of $m_h \leq m_Z$. This, in general, can lead to a large fine-tuning. In addition to this, the requirement of a light neutralino DM will pose a challenge for any MSSM scenario, the severity of which is however strongly model dependent. The naturalness of various SUSY models with a neutralino LSP has been analysed in the literature (for an incomplete list, see [300, 301, 302, 303, 304, 305, 306, 307, 308, 309, 310, 311, 312, 313], and references therein).

In this section, we perform a dedicated study focusing on the naturalness of a light neutralino also examining how light the neutralino could be, after taking into account all the existing theoretical and experimental constraints listed in 6.1. Most of the earlier studies on SUSY focused on the CMSSM having only

5 parameters, assuming universality conditions at the GUT scale. However, in view of the latest null results from SUSY searches at the $\sqrt{s} = 8$ TeV LHC, the CMSSM seems too restrictive for low–scale SUSY phenomenology as the allowed CMSSM parameter space accessible to the $\sqrt{s} = 14$ TeV LHC is rapidly shrinking. Therefore, here we do not make any assumptions at the high scale and focus only on the low–scale MSSM parameter space from a phenomenological point of view with 19 free parameters at the EW scale. We also study the level of fine-tuning for the light neutralino scenario in this context.

In order to efficiently explore the p19MSSM parameter space, we perform a MCMC likelihood analysis discussed in Section 6.1, with the priors chosen to focus on a light neutralino scenario with mass below the conservative LEP lower limit of 46 GeV. An actual code used to get results in this section can be found in the Appendix B. All the latest experimental bounds on particle physics and cosmology are included. We show that the neutralino as light as 10 GeV is still allowed. However, as it can be seen from Eq. (5.2) such neutralinos, which are required to be mostly bino-like, are severely fine-tuned and require the existence of light right handed sleptons below 100 GeV in order to provide an efficient annihilation channel to reduce the bino relic density to be consistent with the observed limit.

To explore the 19D parameter space we adopt the scan ranges as shown in Table 6.2. Note that besides imposing the constraints listed in Section 6.1 we also apply the cuts listed in Table 6.3

We emphasize here that for light neutralino DM with $m_{\widetilde{\chi}_1^0} < m_Z/2$ as considered in our case, the dominant annihilation channels will be the t-channel

Parameter	Description	Prior Range
$\tan\beta$	Ratio of the scalar doublet VEVs	[1, 60]
μ	Higgs-Higgsino mass parameter	[−3, 3] TeV
M_A	Pseudo-scalar Higgs mass	[0.3, 3] TeV
M_1	Bino mass	[−0.5, 0.5] TeV
M_2	Wino mass	[−1, 1] TeV
M_3	Gluino mass	[0.8, 3] TeV
$m_{\widetilde{q}_L}$	First/second generation Q_L squark	[0, 3] TeV
$m_{\widetilde{u}_R}$	First/second generation U_R squark	[0, 3] TeV
$m_{\widetilde{d}_R}$	First/second generation D_R squark	[0, 3] TeV
$m_{\widetilde{\ell}_L}$	First/second generation L_L slepton	[0, 3] TeV
$m_{\widetilde{e}_R}$	First/second generation E_R slepton	[0, 3] TeV
$m_{\widetilde{Q}_{3L}}$	Third generation Q_L squark	[0, 3] TeV
$m_{\widetilde{t}_R}$	Third generation U_R squark	[0, 3] TeV
$m_{\widetilde{b}_R}$	Third generation D_R squark	[0, 3] TeV
$m_{\widetilde{L}_{3L}}$	Third generation L_L slepton	[0, 3] TeV
$m_{\widetilde{\tau}_R}$	Third generation E_R slepton	[0, 3] TeV
A_t	Trilinear coupling for top quark	[−10, 10] TeV
A_b	Trilinear coupling for bottom quark	[−10, 10] TeV
A_τ	Trilinear coupling for τ-lepton	[−10, 10] TeV

Table 6.2: The p19MSSM parameters and their range of values used in our MCMC numerical analysis.

processes mediated by light sfermions unless the s-channel Z-resonance or coannihilation are effective. Hence, the lower limits on the chargino and sfermion masses as given in Table 6.3 are crucial ingredients in our numerical analysis.

6.2.1 The parameter space for a light neutralino

Since the parameter space of the light neutralino region is highly constrained, we implement Markov Chain Monte Carlo likelihood scan into `micrOMEGAs2.4`.

First we discuss our MCMC scan results for the relic density of a light neutralino DM candidate as shown in Fig. 6.3. We require the allowed points to

Particle	Mass limit (GeV)	Validity Condition
$\widetilde{\chi}_1^{\pm}$	103.5	$m_{\widetilde{\chi}_1^+} - m_{\widetilde{\chi}_1^0} > 3$ GeV, $m_{\widetilde{f}} > m_{\widetilde{\chi}^{\pm}}$
	70	$m_{\widetilde{\nu}} > 300$ GeV, $\lvert\mu\rvert \geq \lvert M_2\rvert$
	45	generic LEP bound
$\widetilde{\mu}_R$	88	$m_{\widetilde{\mu}_R} - m_{\widetilde{\chi}_1^0} > 15$ GeV, BR$(\widetilde{\mu} \to \mu\widetilde{\chi}_1^0) = 1$
$\widetilde{\tau}_1$	76	$m_{\widetilde{\tau}_1} - m_{\widetilde{\chi}_1^0} > 15$ GeV, BR$(\widetilde{\tau}_1 \to \tau\widetilde{\chi}_1^0) = 1$
$\widetilde{e}_R$	95	$m_{\widetilde{e}_R} - m_{\widetilde{\chi}_1^0} > 15$ GeV, BR$(\widetilde{e} \to e\widetilde{\chi}_1^0) = 1$, $\mu = -200$ GeV, $\tan\beta = 2$
$\widetilde{\ell}_{R\ (L)}$	40 (41)	generic LEP bound
$\widetilde{\nu}$	43.7	generic LEP bound
$\widetilde{g}$	800	
$\widetilde{q}$	500	
$\widetilde{t}_1$	400	
$\widetilde{b}_1$	300	

Table 6.3: The lower limits on the sparticle masses used in our numerical analysis. The chargino and slepton mass limits are derived from the LEP data [290] while the squark and gluino mass limits are derived from the LHC data [31, 32] which now supersede the LEP as well as the Tevatron [43, 44] limits.

satisfy the experimental constraints given in Section 6.1, along with the LEP limits on sparticle masses given in Table 6.3. The latest LHC results put much tighter bounds on the strongly interacting squarks and gluinos and further eliminate some of otherwise allowed parameter space, as shown by the starred points in Fig. 6.3. The WMAP-9 2σ band is shown in grey, whereas the latest Planck result is shown as dark shaded region. We find that light neutralinos with mass as low as 10 GeV are still allowed, though severely fine-tuned with the EW fine-tuning measure defined by Eq. 4.93: $\Delta_{\rm tot} \gg 1$.

The bino, wino and higgsino fractions of the lightest neutralino for all the allowed points in our p19MSSM parameter space are shown in Fig. 6.4. We reproduce the well-known result that the lightest neutralino is mostly bino-like for the masses below $m_Z/2$, primarily due to the 103.5 GeV bound on the mass

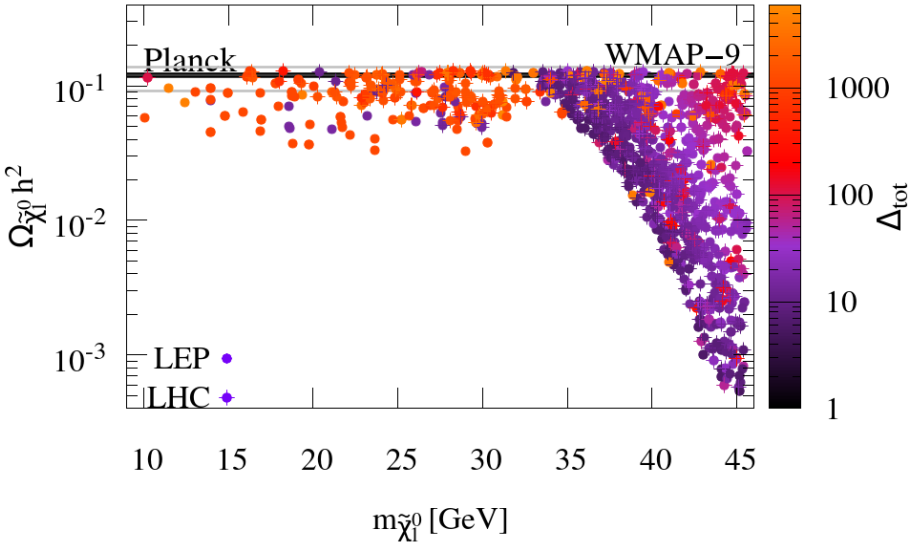

Figure 6.3: The relic density of light neutralino DM in p19MSSM satisfying all the experimental constraints discussed in Section 6.1. The colour-coding denotes the fine-tuning measure defined by Eq. 4.93. The points denoted by circles satisfy all the experimental constraints, except that the squark masses are only required to satisfy the LEP lower limits. For the starred points (a subset of the circled points), the corresponding squark masses satisfy the latest LHC constraints. The top (bottom) grey horizontal line shows the 2σ upper (lower) limit of the CDM relic density from WMAP-9 data, whereas the black (shaded) region shows the 1σ allowed range from the recent Planck data.

of lightest chargino and secondarily due to the invisible Z-decay width constraint in Eq. 6.1. Unless purely bino neutralino has an efficient enough annihilation channel that has the thermal WIMP annihilation rate of at least 3×10^{-26} cm$^3 \cdot$ s^{-1}, relic bino DM abundance, $\Omega_{\widetilde{B}} h^2$, would normally exceed the bound set by Planck. One possibility is to consider a "well-tempered" neutralino [175], which corresponds to the boundary between a pure bino and a pure higgsino or wino. Another possibility to reduce the bino relic abundance is by annihilation via the t-channel slepton exchange (the so-called "bulk region") which is efficient for light sleptons, or by using coannihilation with a light slepton, squark, chargino or second-lightest neutralino in configurations, where such light sparticles are

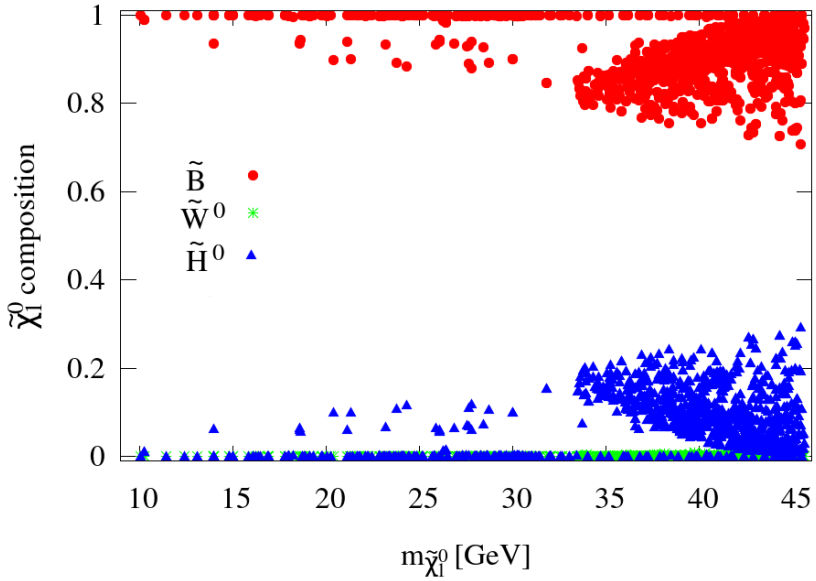

Figure 6.4: The gaugino ($\widetilde{B}$, $\widetilde{W}^0$) and higgsino ($\widetilde{H}_d^0$, $\widetilde{H}_u^0$) components of the lightest neutralino in our p19MSSM parameter scan.

not yet excluded by the experimental searches. We find that most of the points with $m_{\widetilde{\chi}_1^0}$ close to 45 GeV can have either slepton coannihilation or a resonant Z-annihilation due to a non–negligible higgsino component, and hence, can easily satisfy the WMAP and Planck upper limit on the relic density. These points are also less fine-tuned. On the other hand, the light neutralino DM points in the 10 - 30 GeV range, as shown in Fig. 6.4, have to be mostly bino-like and lie in the bulk region, thus leading to significant fine-tuning. Note that in the latter case, the NLSP masses are much higher than the LSP mass, thus eliminating the possibility of a coannihilation.

The dominant annihilation channels are shown in Fig. 6.5. For bino dominated neutralinos that are lighter than 35 GeV the relic density is reduced by the $\widetilde{\chi}_1^0$ annihilation via sfermion exchange. Since the sleptons are usually lighter than the squarks the former is responsible for the annihilation. It also requires a

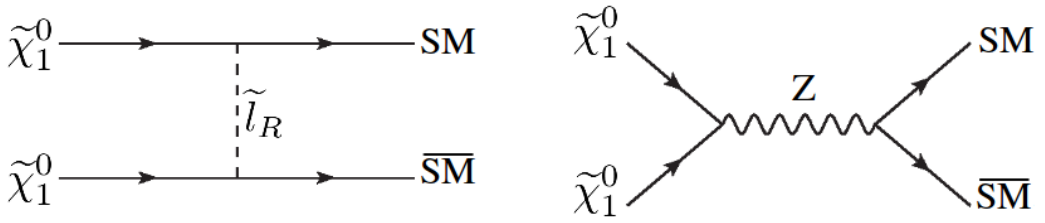

Figure 6.5: The dominant annihilation channels for reducing the relic density shown in Fig. 6.3. The first diagram is via right handed selectron exchange into two SM particles that are kinematically allowed and takes place for neutralinos with masses lower than 35 GeV. The second diagram is the resonance via Z boson.

right handed particle since the modulus of the hypercharge is larger than those of the left handed counterparts [175]. The second diagram is for the heavier and less fine tuned DM particles (see also Fig. 6.3) which annihilate by s-channel resonance via Z boson.

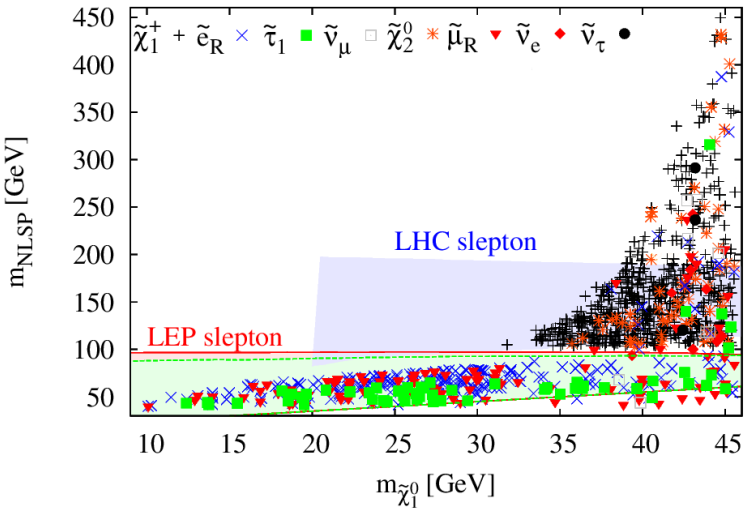

Figure 6.6: The various NLSP masses as a function of the LSP mass for the allowed points. The LEP exclusion regions strictly applicable for $\widetilde{\mu}_R$ (red shaded) and $\widetilde{\tau}_1$ (green shaded) and the LHC exclusion region for $\widetilde{\ell}$ ($l = e, \mu$) (blue shaded) are also shown.

Fig. 6.6 shows the various NLSPs and their masses as a function of the lightest neutralino mass. It can be seen that all the allowed points with $m_{\widetilde{\chi}_1^0} < 35$

GeV have a charged slepton NLSP with a mass below 100 GeV. Especially the points with a light stau are severely fine-tuned since they usually require a mass suppression by the off-diagonal elements in the slepton mass matrix, or a large μ-term. We also show in Fig. 6.6 the LEP exclusion regions in the charged slepton-neutralino mass plane, derived under the assumption of gaugino mass unification [290]. The limits for light smuons and staus are still applicable to the p19MSSM case as long as $\Delta m_\ell > 15$ GeV, but not directly to light selectrons if we assume non–universal gaugino masses, and hence, can still allow the low neutralino mass regime. The latest 95% C.L. ATLAS exclusion limits [314] are also shown in Fig. 6.6 which were derived from searches for direct slepton (selectron and smuon) pair production and interpreted in the pMSSM. A similar dedicated analysis of the LEP data is required in order to completely rule out the light selectrons, and hence, the lightest neutralino DM mass below 30–35 GeV for the p19MSSM scenario.

Fig. 6.7 shows the spin independent nucleon–$\widetilde{\chi}_1^0$ cross section as a function of LSP mass. Bino dominated neutralinos that are lighter than 35 GeV are yet to be probed by the XENON1T and LUX experiments, whereas the heavier and less fine tuned scenarios mostly fall in the exclusion regions of LUX. These have higher cross section mainly due to the higher fraction of higgsino in the neutralino, as can be seen from Fig. 6.4. No points fall within the 2σ region of CRESST–II, but as we will see in the next section, a neutralino with a large fraction of singlino within NMSSM framework, have some points in the regions of DAMA, CoGeNT, CRESST and CDMS.

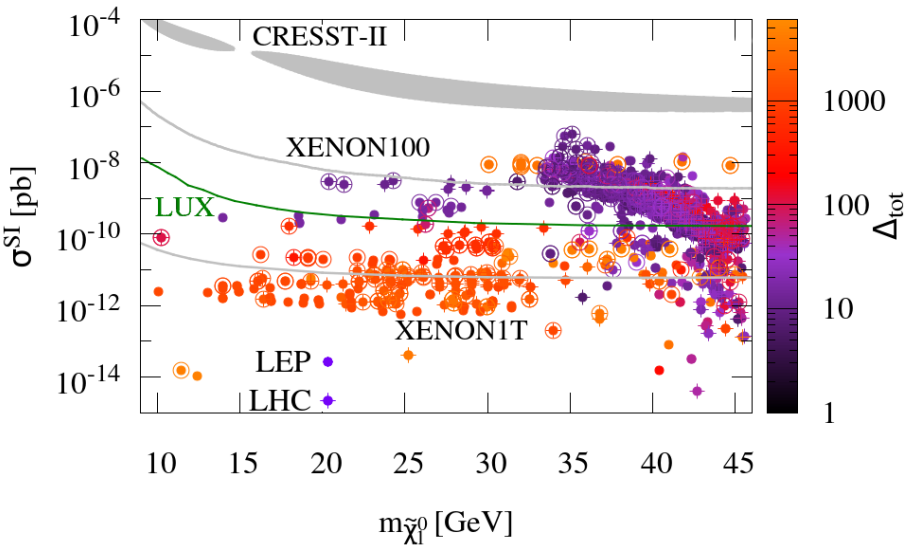

Figure 6.7: The spin independent direct detection cross section values for the allowed points in our p19MSSM scan. The colour-coding and labelling of the points are the same as in Fig. 6.3. The circled points correspond to those within the WMAP allowed band in Fig. 6.3. The current upper limits from the XENON100 and LUX and the projected XENON1T limit are shown as solid lines. The 2σ-preferred range of CRESST-II is shown as the shaded region.

6.3 Light neutralino in NMSSM

Since the most simple and popular SUSY model, CMSSM, is getting more constrained and posses severe shortages in trying to explain potential positive signals of a very light neutralino claimed to have been observed by DAMA, CoGeNT, CRESST–II and CDMS, we try to analyse this issue in NMSSM, which gives somewhat more freedom by manipulating various parameters, to satisfy current bounds, most importantly for the light neutralino case – the cosmological bound on the DM relic density set by WMAP and more recently by Planck.

As already mentioned in Section 4.5.3, the NMSSM is conceived to give a natural explanation for the dynamic origin of μ term via the symmetry breaking during which the singlino field acquires a VEV. This method also ameliorates

the little supersymmetric hierarchy problem. In the spirit of being complete, we remind that the mass eigenstates of the neutralino in NMSSM are the mixtures of bino, singlino and neutral wino and higgsino components. The mass matrix for $\widetilde{\chi}_1^0$ in NMSSM is given by the matrix in Eq. (4.5.3). The very lightest neutralino, that can evade all of the existing constraints, has to have a significant singlino admixture. As it can be seen from Eq. (4.120), the lightest singlino dominated neutralino favours small κ and $\tan\beta$.

Parameter	Description	Range
λ	λ coupling	$[0 : 0.7]$
A_λ	Trilinear λ term	[-3000:5000] GeV
κ	κ coupling	$[0 : 0.5]$ GeV
A_κ	Trilinear κ term	$[-3000 : 3000]$ GeV
$\tan\beta$	$\tan\beta$ parameter	[0.1:40]
μ	Higgs mixing term	$[-500 : 500]$ GeV
M_1	Bino Mass	[1:300] GeV
M_2	Wino Mass	[1:1000] GeV
M_3	Gluino Mass	[800:3000] GeV
$m_{\widetilde{e}_L} = m_{\widetilde{\mu}_L} = m_{\widetilde{\tau}_L}$	LH sleptons	[100:3000] GeV
$m_{\widetilde{e}_R} = m_{\widetilde{\mu}_R} = m_{\widetilde{\tau}_R}$	RH sleptons	[100:3000] GeV
$m_{\widetilde{Q}_{1L}} = m_{\widetilde{Q}_{2L}}$	1st and 2nd generation LH squarks	[1000:4000] GeV
$m_{\widetilde{Q}_{3L}}$	LH stop quark	[1000:4000] GeV
$m_{\widetilde{u}_R} = m_{\widetilde{c}_R}$	1st and 2nd generation RH squarks	[1000:4000] GeV
$m_{\widetilde{t}_R}$	RH stop quarks	[1000:4000] GeV
$m_{\widetilde{d}_R} = m_{\widetilde{s}_R} = m_{\widetilde{b}_R}$	RH down type quark	[1000:4000] GeV
A_t	Trilinear top coupling	[-10000:10000] GeV
A_τ	Trilinear τ coupling	-2500 GeV
A_b	Trilinear bottom coupling	-2500 GeV

Table 6.4: Scan ranges of the NMSSM parameters. We adopted narrowed κ and $\tan\beta$ intervals in order to better grasp the light dark matter regions.

In order to explore the parameter space of the light neutralino, just like in the previous case, we adopted the MCMC algorithm explained in Section 6.1. The

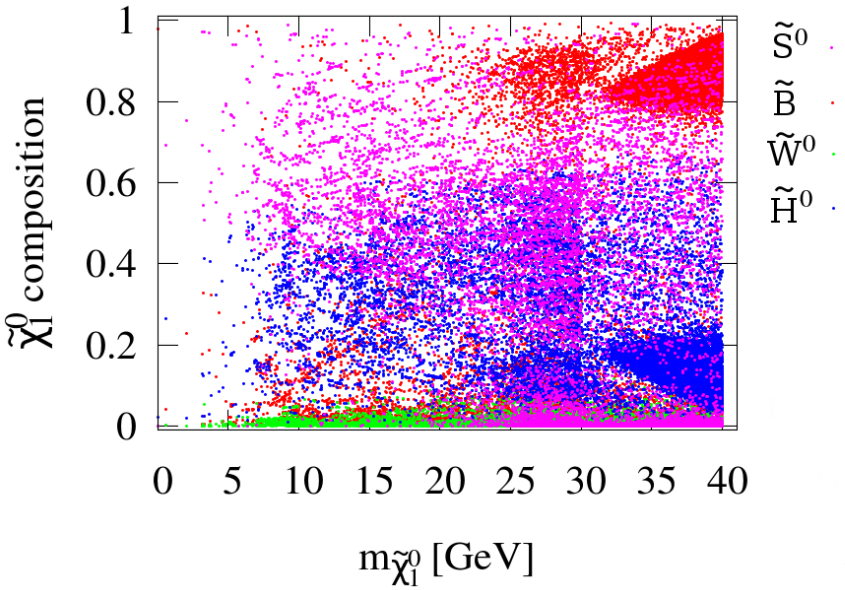

Figure 6.8: Lightest neutralino composition dependence on the mass of DM. Pink points represents singlino, red– bino, green– wino and blue–higgsino admixture in LSP. All points satisfy the constraints listed in Table 6.1 apart from the $(m_{\tilde{\chi}_1^0} + m_{\tilde{\chi}_2^0}) > 209$ GeV bound.

MCMC scan ranges of NMSSM model are shown in the Table 8.1. To target the light neutralino we narrowed κ and $\tan\beta$ intervals. All points with $m_{\tilde{\chi}_1^0} > 40$ GeV were dismissed.

Fig. 6.8 shows the composition of the LSP within NMSSM. The lightest neutralino has to have a sizeable amount of singlino and bino components because of the bound on the invisible Z–decay and the mass of the lightest chargino. The singlino fraction in neutralino increases as the combination of $\kappa\frac{\mu}{\lambda}$ decreases.

Fig. 6.9 shows the relic density constraint, with the most recent value measured by the Planck satellite. The blue lines mark the 3σ range, however most of the points fall well below the upper bound and therefore other DM components have to be introduced to account for the total relic abundance in the Universe, required by the Standard model of Cosmology. The relic density constraint is one

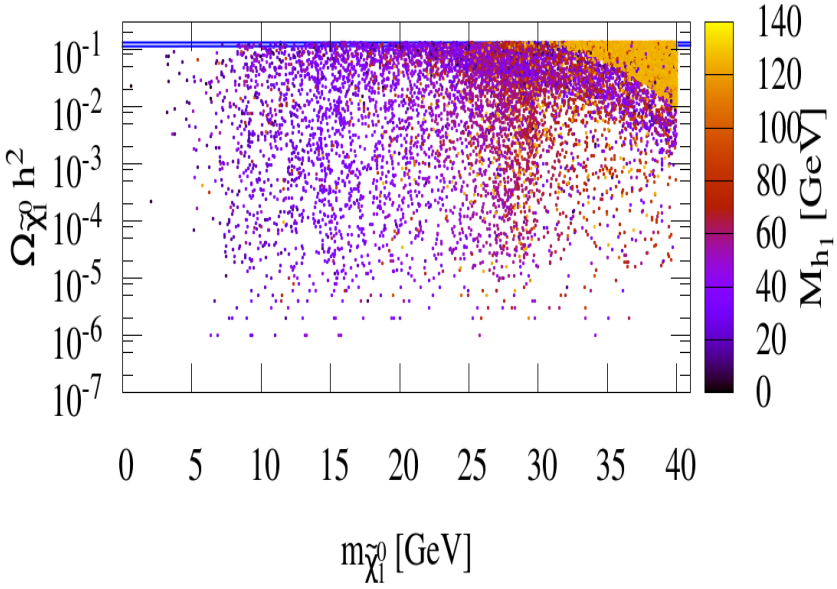

Figure 6.9: The relic density constraint. All points satisfy constraints listed in Table 6.1 apart from the $(m_{\widetilde{\chi}_1^0} + m_{\widetilde{\chi}_2^0}) > 209$ GeV bound.

of the most important, that rules out all LSPs with a masses lower than 10 GeV within p19MSSM [315]. As elaborated in the previous section, this is due to the fact that for the bino dominated neutralino, Ωh^2 is brought down by the exchange of light slepton, and the lower bound on these is set by LEP to be around ~ 100 GeV, with some extra assumptions for selectrons. However, it is very easy to satisfy the relic density bound for the light $\widetilde{\chi}_1^0$ within NMSSM. This is achieved by having light CP–even (h_1) and/or CP–odd (a_1) pseudoscalar Higgses. The role of the SM $m_h = 125$ GeV Higgs usually goes to the h_2.

Fig. 6.10 shows the spin independent DM–nucleon interaction versus the mass of the LSP. The blue region is a favoured region of CRESST–II (1^{st} phase run results), brown is of DAMA, green depicts the latest LUX results and the upper and lower grey lines are XENON100 and projected XENON1T bounds

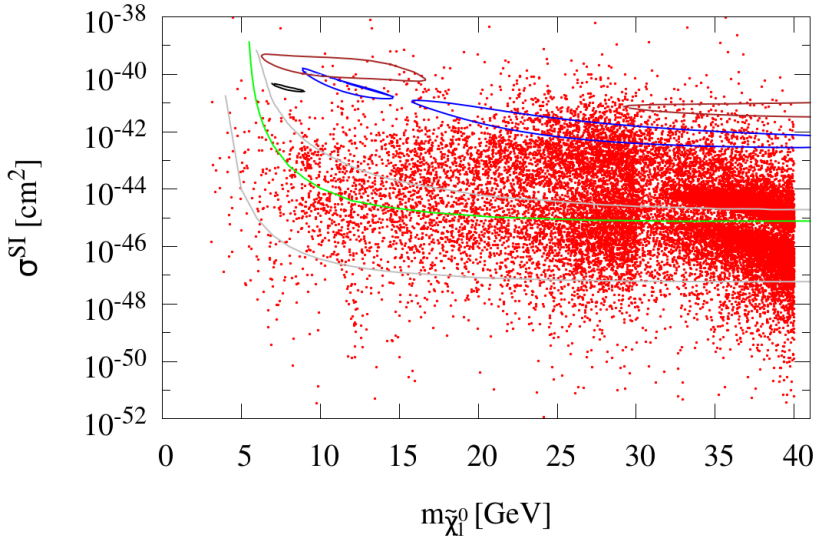

Figure 6.10: Spin independent cross sections vs mass of the DM. The blue region is a bound of CRESST–II, brown regions denote DAMA, green shows the latest LUX results and upper and lower grey lines are XENON100 and projected XENON1T bounds respectively. All points satisfy constraints listed in Table 6.1 apart from the $(m_{\widetilde{\chi}_1^0} + m_{\widetilde{\chi}_2^0}) > 209$ GeV bound.

respectively. DAMA, CoGeNT, CRESST–II and CDMS collaborations found that the light DM particle has high σ^{SI}. NMSSM has been the leading and most thoroughly studied theory candidate to explain the positive signals by these experiments. It is the presence of a large singlino fraction in the neutralino that increases $\widetilde{\chi}_1^0 - p$ spin independent cross section. However, even though the XENON100 and more recently LUX experiments rule out all the positive results, there is still a possibility for the light LSP, that would satisfy LUX and even projected XENONT1T results. There is a well–motivated case of the isospin violating DM, where, with some fine–tuning of the $\widetilde{\chi}_1^0$ coupling to the proton and neutron in the detector, all results can be made compatible [227].

6.4 Summary

A possibility of a light neutralino DM candidate in the p19MSSM and NMSSM models was motivated by the discovery of the Higgs–like particle and a number of direct detection experiments. Also, within the context of p19MSSM, the issue of naturalness is addressed. In order to efficiently scan over the multidimensional parameter space of both models, a MCMC likelihood analysis, optimised for a light neutralino, is performed, which is particularly important in the case of p19MSSM, as it is far more constrained than NMSSM.

Studies showed that a light neutralino DM with mass as low as 10 GeV is still allowed in the p19MSSM, while satisfying all the existing experimental constraints. However, neutralinos of this, which are required to be mostly bino-like, are severely fine-tuned. In order to have an efficient annihilation channel to reduce the light neutralino relic density below the observed upper limit, the existence of light sleptons is required. Such light sleptons are excluded from LEP searches if one assumes gaugino mass unification. A dedicated analysis of the LEP data in the context of a p19MSSM scenario could completely eliminate the possibility of a light neutralino in the mass range of 10 – 30 GeV. In [316, 317] authors found that a light sbottom ($\sim$10 GeV) would be sufficient to validate light neutralino solutions in p19MSSM, however, we set $m_{\tilde{b}_1} > 300$ GeV which is valid when $m_{\tilde{b}_1} - m_{\tilde{\chi}_1^0} > m_b$ is satisfied, which turns out to be always the case for the light neutralino solutions. Low fine–tuning regions can be obtained around $m_{\tilde{\chi}_1^0} = 45$ GeV where the resonant annihilation via the s-channel Z-exchange is possible for a bino–higgsino mixture of neutralino LSP. However, such regions also predict much lower spin–independent DM–nucleon scattering cross section, compared

to the favoured regions announced by DAMA/LIBRA, CoGeNT, CDMS–II and CRESST–II (1^{st} phase run). Besides that, most of the scenarios with $m_{\widetilde{\chi}_1^0} < 46$ GeV are excluded by the XENON100 limits and the remaining such points are within the reach of the XENON1T projected limits.

Latest experimental results from collider, flavour, dark matter and astrophysical/cosmological sectors can be far more easily satisfied within NMSSM. In this case, spin independent neutralino–nucleon scattering cross section tends to be significantly larger than in p19MSSM – often falling within preferred regions, compared to the DD experiments that claim an existence of light DM. Also, within p19MSSM, the key obstacle in satisfying relic abundance limits set by WMAP–9 and Planck, can be easily overcome in NMSSM. This is achieved by χ_1^0 with a sizeable singlino fraction, which doesn't necessarily need a light slepton but annihilates via lightest CP–even or CP–odd Higgses instead.

Chapter 7

Unifying Inflation and Dark Matter within MSSM with non–universal Higgs masses

7.1 Gauge invariant inflation

Inflation is consistent with the current temperature anisotropy in the CMB radiation measured by the Planck satellite. Since inflation dilutes matter, the end of inflation must excite all the relevant SM degrees of freedom without any excess of dark matter and dark radiation, along with the seed initial perturbations for structure formation. This can be achieved by embedding inflation within a visible sector of BSM, such as the MSSM [28, 29, 318].

Inflation is driven by the vacuum energy density of the inflaton field ϕ which implies that it has to have non–vanishing F, D or both components which in turn implies that SUSY is broken during inflation for the field ϕ was explained in Section 4.1.

There are two D–flat directions, $\widetilde{u}\widetilde{d}\widetilde{d}$ and $\widetilde{L}\widetilde{L}\widetilde{e}$, that can be inflaton candidates [28, 29, 319, 320]. To have canonically normalised inflaton field ϕ, the representation for the flat directions, up to a phase factor, are given by:

$$\begin{aligned} \widetilde{u}_i^{\alpha} &= \frac{\phi}{\sqrt{3}}, \qquad & \widetilde{d}_j^{\beta} &= \frac{\phi}{\sqrt{3}}, \qquad & \widetilde{d}_k^{\gamma} &= \frac{\phi}{\sqrt{3}}, \\ \widetilde{L}_i^{a} &= \frac{1}{\sqrt{3}}\begin{pmatrix}\phi\\0\end{pmatrix}, \qquad & \widetilde{L}_j^{b} &= \frac{1}{\sqrt{3}}\begin{pmatrix}0\\\phi\end{pmatrix}, \qquad & \widetilde{e}_k &= \frac{\phi}{\sqrt{3}}, \end{aligned} \tag{7.1}$$

which implies that inflaton field then can be expressed as:

$$\phi = \frac{\widetilde{u}_i^{\alpha} + \widetilde{d}_j^{\beta} + \widetilde{d}_k^{\gamma}}{\sqrt{3}}, \qquad \phi = \frac{\widetilde{L}_i^{a} + \widetilde{L}_j^{b} + \widetilde{e}_k}{\sqrt{3}}, \tag{7.2}$$

for the $\widetilde{u}\widetilde{d}\widetilde{d}$ and $\widetilde{L}\widetilde{L}\widetilde{e}$ flat directions respectively, where $\widetilde{u}$, $\widetilde{d}$ and $\widetilde{e}$ represent RH squarks and sleptons, and $\widetilde{L}$ stands for the LH isospin slepton doublets. Flatness requires generation indices to satisfy $i \neq j \neq k$ for $\widetilde{L}\widetilde{L}\widetilde{e}$ and $j \neq k$ for $\widetilde{u}\widetilde{d}\widetilde{d}$ inflaton candidates. The constraint on colour indices for $\widetilde{u}\widetilde{d}\widetilde{d}$ is $\alpha \neq \beta \neq \gamma$ and $a \neq b$ on isospin components for LH doublets.

An inflationary potential with an inflection point can be constructed in the following way: firstly we have a contribution from the soft breaking mass of the inflaton $\frac{m_\phi}{2}\phi^2$, that already has been motivated in Chapter 4. Then, there can be self couplings of the flat direction, that would give rise to the non–renormalizable A_y term [125]. Finally, there could be other Planck scale suppressed terms, which can be expanded in inverse powers of $M_{\rm Pl}$ in the following fashion [127]:

$$W = \sum_{n>3} \frac{\lambda}{n M_{\rm Pl}^{n-3}} \Phi^n, \tag{7.3}$$

which gives a contribution to the inflationary potential of the form:

$$V = \left|\frac{\partial W}{\partial \phi}\right|^2 = \frac{\lambda^2}{M_{\rm Pl}^{2n-6}}\phi^{2n-2}. \tag{7.4}$$

$\widetilde{u}\widetilde{d}\widetilde{d}$ and $\widetilde{L}\widetilde{L}\widetilde{e}$ flat directions are lifted by the $n = 6$ term [127], therefore the inflationary potential can be written as [28, 29]:

$$V(\phi) = \frac{1}{2}m_\phi^2\,\phi^2 + A_y\cos(n\theta + \theta_{A_y})\frac{\lambda\phi^6}{6\,M_{\rm Pl}^3} + \lambda^2\frac{\phi^{10}}{M_{\rm Pl}^6}. \tag{7.5}$$

As already mentioned, here m_ϕ and A_y are the soft breaking mass and the A term respectively. ϕ and θ denote the radial and angular parts of the scalar superfield $\Phi = \frac{\phi e^{i\theta}}{\sqrt{2}}$, while θ_{A_y} is the phase of the A_y term. Note that A_y is not related to MSSM A term couplings. Since the first and last terms are positive, an inflection point in the potential can be achieved by adjusting the phases of the ϕ and A_y terms in such way that $\cos(n\theta + \theta_{A_y}) < 0$. Thus we can rewrite Eq. (7.5) as:

$$V(\phi) = \frac{1}{2}m_\phi^2\,\phi^2 - A_y\frac{\lambda\phi^6}{6\,M_{\rm Pl}^3} + \lambda^2\frac{\phi^{10}}{M_{\rm Pl}^6}, \tag{7.6}$$

where the precise numerical value of the cosine function can be restored from the fine tuning parameter that will be introduced shortly in Eq. (7.8).

The masses for $\widetilde{L}\widetilde{L}\widetilde{e}$ and $\widetilde{u}\widetilde{d}\widetilde{d}$ inflaton condensates are given by [28, 29]:

$$m_\phi^2 = \frac{m_{\widetilde{L}}^2 + m_{\widetilde{L}}^2 + m_{\widetilde{e}}^2}{3}\,, \qquad m_\phi^2 = \frac{m_{\widetilde{u}}^2 + m_{\widetilde{d}}^2 + m_{\widetilde{d}}^2}{3}\,. \tag{7.7}$$

The inflationary perturbations will be able to constrain the inflaton mass only at the scale of inflation, i.e. ϕ_0, while LHC will constrain the masses at the LHC scale. However, both the physical quantities are related to each other via RGEs,

as we will discuss below in Section 7.2. We will use these equations to show that MSSM inflation is consistent with the particle physics models which we analysed. For further convenience it is useful to make the following definition [321]:

$$\frac{A_y^2}{40m_\phi^2} \equiv 1 - 4\alpha^2\,, \tag{7.8}$$

where α is a fine tuning parameter. If $\alpha^2 \ll 1$, there exists a point of inflection ($V^{''}(\phi) = 0$) at ϕ_0, where [28, 29]:

$$\phi_0^4 = \frac{m_\phi M_{\rm Pl}^3}{\lambda\sqrt{10}} + \mathcal{O}(\alpha^2)\,, \tag{7.9}$$

at which:

$$V(\phi_0) = \frac{4}{15}m_\phi^2\phi_0^2 + \mathcal{O}(\alpha^2)\,, \tag{7.10}$$

$$V'(\phi_0) = 4\alpha^2 m_\phi^2\phi_0 \, + \mathcal{O}(\alpha^4)\,, \tag{7.11}$$

$$V'''(\phi_0) = 32\frac{m_\phi^2}{\phi_0} + \mathcal{O}(\alpha^2)\,. \tag{7.12}$$

Relation in Eq. 7.8 is realistic in theories where supersymmetry breaking is mediated by gravity i.e. where $A_y \sim m_\phi$. The renormalization scale $\hat{\mu}$, introduced in Section 2.5.1, can be chosen in a such way, that loop corrections to the renormalised parameters are very small. Therefore, it can be achieved, that at some scale $\hat{\mu}$, quantum corrections to the inflaton mass have negligible effect on this relation and model in general. Including the essentially would imply multiplying m_ϕ by $(1+u)$ where $|u| \ll 1$ [322, 323]. In ref. [322] authors studied the degree of fine tuning for the ratio m_ϕ^2/A_y^2. By exploring parameter space where the spectral tilt and curvature perturbation values satisfy experimental bounds, and varying

λ, m_ϕ and α they found that MSSM inflation requires high degree of fine tuning i.e. $|\alpha| < 10^{-10}$ [322].

Note that inflation occurs within an interval:

$$|\phi - \phi_0| \sim \frac{\phi_0^3}{60 M_{\rm Pl}^2}, \tag{7.13}$$

in the vicinity of the point of inflection ϕ_0, within which the slow roll parameters ϵ and η, defined in Eq. (3.20) of the Chapter 3, are smaller than 1. The Hubble expansion rate during inflation is given by:

$$\mathcal{H}_{\rm inf} \simeq \frac{1}{\sqrt{45}} \frac{m_\phi \phi_0}{M_{\rm Pl}}\,. \tag{7.14}$$

The amplitude of the density perturbations δ_H, defined in Eq. (3.46), and the scalar spectral index n_s are given by [322]:

$$\delta_H = \frac{8}{\sqrt{5}\pi} \frac{m_\phi M_{\rm Pl}}{\phi_0^2} \frac{1}{\Delta^2}\, \sin^2[\mathcal{N}\sqrt{\Delta^2}]\,, \tag{7.15}$$

and

$$n_s = 1 - 4\sqrt{\Delta^2}\, \cot[\mathcal{N}\sqrt{\Delta^2}], \tag{7.16}$$

respectively, where

$$\Delta^2 \equiv 900\alpha^2 \mathcal{N}^{-2} \Big(\frac{M_{\rm Pl}}{\phi_0}\Big)^4. \tag{7.17}$$

In the above, $\mathcal{N}$ is the number of e-foldings between the time when the observationally relevant perturbations are generated till the end of inflation and follows: $\mathcal{N} \simeq 66.9 + (1/4)\ln(V(\phi_0)/M_{\rm P}^4) \sim 50$ [29]. The parameter space for gauge invariant inflation is shown in Fig. 7.1. The blue region denotes a parameter space

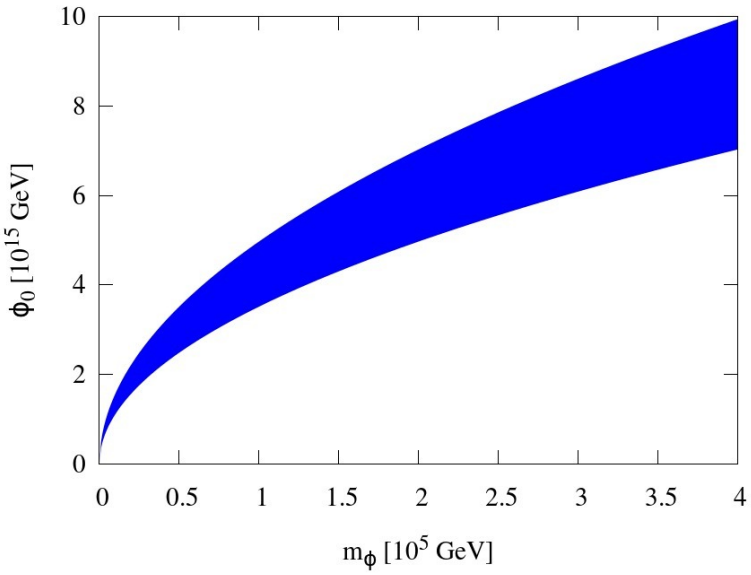

Figure 7.1: (ϕ_0, m_ϕ) plane in which inflation is in agreement with the cosmological observations of the anisotropies in the CMB. The blue region shows inflation energy scale and inflaton mass which are compatible with the central value of the amplitude of the primordial perturbations, $\delta_H = 4.68 \times 10^{-5}$, and the 2σ allowed range of the spectral tilt $0.9457 \leq n_s \leq 0.9749$ [91]. Note that we restricted ourselves to inflaton VEVs ϕ_0 below the GUT scale.

of MSSM inflation, where the amplitude of the density perturbations and the 2σ range for the spectral index n_s take values as measured by Planck and the y and x axes label the scale of inflation and the mass of the inflaton respectively. A study of how the matter d.o.f. can be produced after MSSM inflation can be found in Ref. [324].

As mentioned above, to relate the high scale physics at the scale of inflation with the observables at the low scale, which is accessible with modern colliders, we need to use the renormalization group equations. In this particular case, we take ϕ_0 up to the GUT scale since the new physics may appear at higher energies and significantly modify the behaviour of RGEs for the mass of the inflaton and A_y term. In the next section, we review the RGEs for the soft breaking terms of

the inflationary potential and their solutions.

7.2 Renormalization group equations

For the $\widetilde{u}\widetilde{d}\widetilde{d}$ flat direction the renormalization group flow can be written as [29, 319]:

$$\begin{aligned}\hat{\mu}\frac{dm_{\phi}^{2}}{d\hat{\mu}} &= -\frac{1}{6\pi^{2}}\left(4M_{3}^{2}g_{3}^{2}+\frac{2}{5}M_{1}^{2}g_{1}^{2}\right),\\ \hat{\mu}\frac{dA_{y}}{d\hat{\mu}} &= -\frac{1}{4\pi^{2}}\left(\frac{16}{3}M_{3}g_{3}^{2}+\frac{8}{5}M_{1}g_{1}^{2}\right),\end{aligned} \tag{7.18}$$

where $\hat{\mu}=\hat{\mu}_{0}=\phi_{0}$ is the VEV at which inflation occurs and should not be confused with the Higgs mass parameter. For the $\widetilde{L}\widetilde{L}\widetilde{e}$ condensate inflaton candidate:

$$\begin{aligned}\hat{\mu}\frac{dm_{\phi}^{2}}{d\hat{\mu}} &= -\frac{1}{6\pi^{2}}\left(\frac{3}{2}M_{2}^{2}g_{2}^{2}+\frac{9}{10}M_{1}^{2}g_{1}^{2}\right),\\ \hat{\mu}\frac{dA_{y}}{d\hat{\mu}} &= -\frac{1}{4\pi^{2}}\left(\frac{3}{2}M_{2}g_{2}^{2}+\frac{9}{5}M_{1}g_{1}^{2}\right),\end{aligned} \tag{7.19}$$

where M_1, M_2, M_3 are $U(1)$, $SU(2)$ and $SU(3)$ gaugino masses, which all equate to $m_{1/2}$ at the unification scale, and g_1, g_2 and g_3 are the associated couplings. To solve these equations, one needs to take into account the running of the gaugino masses and coupling constants, which are given by, see Ref. [120]:

$$\beta(g_{i})=\alpha_{i}g_{i}^{3} \qquad\qquad \beta\left(\frac{M_{i}}{g_{i}^{2}}\right)=0, \tag{7.20}$$

with $\alpha_1=\frac{11}{16\pi^2}$, $\alpha_2=\frac{1}{16\pi^2}$ and $\alpha_3=-\frac{3}{16\pi^2}$. Since:

$$\left(\frac{g_{i}(\hat{\mu})}{g_{i}(\Lambda)}\right)^{2}=\frac{1}{1+2\alpha_{i}g_{i}^{2}(\Lambda)\ln\left(\frac{\hat{\mu}}{\Lambda}\right)}. \tag{7.21}$$

The solutions for the $\widetilde{u}\widetilde{d}\widetilde{d}$ flat direction can be written as:

$$m_\phi^2(\hat{\mu}) = m_\phi^2(\Lambda) - \frac{8}{9}M_3^2(\Lambda)\left(1 - \left[\frac{g_3(\hat{\mu})}{g_3(\Lambda)}\right]^4\right) + \frac{4}{165}M_1^2(\Lambda)\left(1 - \left[\frac{g_1(\hat{\mu})}{g_1(\Lambda)}\right]^4\right), \quad (7.22)$$

$$A_y(\hat{\mu}) = A_y(\Lambda) - \frac{32}{9}M_3(\Lambda)\left(1 - \left[\frac{g_3(\hat{\mu})}{g_3(\Lambda)}\right]^2\right) + \frac{16}{55}M_1(\Lambda)\left(1 - \left[\frac{g_1(\hat{\mu})}{g_1(\Lambda)}\right]^2\right). \quad (7.23)$$

While the solutions for the $\widetilde{L}\widetilde{L}\widetilde{e}$ flat direction can be written as:

$$m_\phi^2(\hat{\mu}) = m_\phi^2(\Lambda) + M_2^2(\Lambda)\left(1 - \left[\frac{g_2(\hat{\mu})}{g_2(\Lambda)}\right]^4\right) + \frac{3}{55}M_1^2(\Lambda)\left(1 - \left[\frac{g_1(\hat{\mu})}{g_1(\Lambda)}\right]^4\right), \quad (7.24)$$

$$A_y(\hat{\mu}) = A_y(\Lambda) + 3M_2(\Lambda)\left(1 - \left[\frac{g_2(\hat{\mu})}{g_2(\Lambda)}\right]^2\right) + \frac{18}{55}M_1(\Lambda)\left(1 - \left[\frac{g_1(\hat{\mu})}{g_1(\Lambda)}\right]^2\right). \quad (7.25)$$

We will use these analytical expressions in the next section where we will demonstrate a correlation between masses of the two inflaton candidates, lightest stop and stau quarks. We also use these equations to show that MSSM inflation is compatible with NUHMII and NMSSM models.

7.3 Unifying inflation and dark matter

7.3.1 Identifying benchmark points for the dark matter and Higgs

In this section, we will try to find a parameter space within NUHMII model, where the right DM abundance and MSSM inflation coexist. NUHMII is a variant of the MSSM with universality conditions imposed at the GUT scale. The main difference between NUHMII and the CMSSM is that the soft breaking masses of the Higgs doublets differ from the masses of sleptons and squarks at the GUT. A

more detailed description of NUHMII is in Section 4.5.2.

We start the study by performing a 2D scan of the 6D space of NUHMII, varying the scalar and gaugino masses at the GUT scale and keeping the rest of the input parameters fixed. The first task is to find the allowed points in the $(m_0 : m_{1/2})$ plane, where all the constraints listed in Section 6.1 are satisfied [1]. These would enable us then to solve the RGEs for the $\widetilde{u}\widetilde{d}\widetilde{d}$ and $\widetilde{L}\widetilde{L}\widetilde{e}$ inflaton candidates given in Eqs. (7.22) and (7.24) and relate the high energy physics of inflation with low energy physics that is currently being tested at LHC.

Our first results are summarised in Fig. 7.2a. In this figure, the regions of the parameter space, where the neutralino relic density is in agreement with the Planck observations are represented by a red strips. The regions where the LSP is not a neutralino but an electrically charged stau, are coloured in green and the region excluded by the LEP2 limits on the chargino mass is represented in blue. The grey region corresponds either to where the stop is the LSP or unphysical configurations with tachyonic particle(s) are present.

Since we are looking for points which satisfy both the Higgs and the DM constraints, we define benchmark scenarios as the points which lie at the intersection between the red line representing the $\widetilde{\chi}_1^0$ relic density and the three black lines corresponding respectively to a Higgs mass of $m_h = 124.5$, $m_h = 125$ and $m_h = 125.5$ GeV. Even though theoretical plus experimental bound on the Higgs mass is in the range of [121.5:129.5] we chose the central region for simplicity, but this can be easily generalised for any m_h. There are two mechanisms that explain how the relic density is reduced in this figure. In the parallel red lines, extending

[1] We ignore the bound on $(m_{\widetilde{\chi}_1^0} + m_{\widetilde{\chi}_2^0}) > 209$ GeV which is not applicable in the case of the NUHMII model.

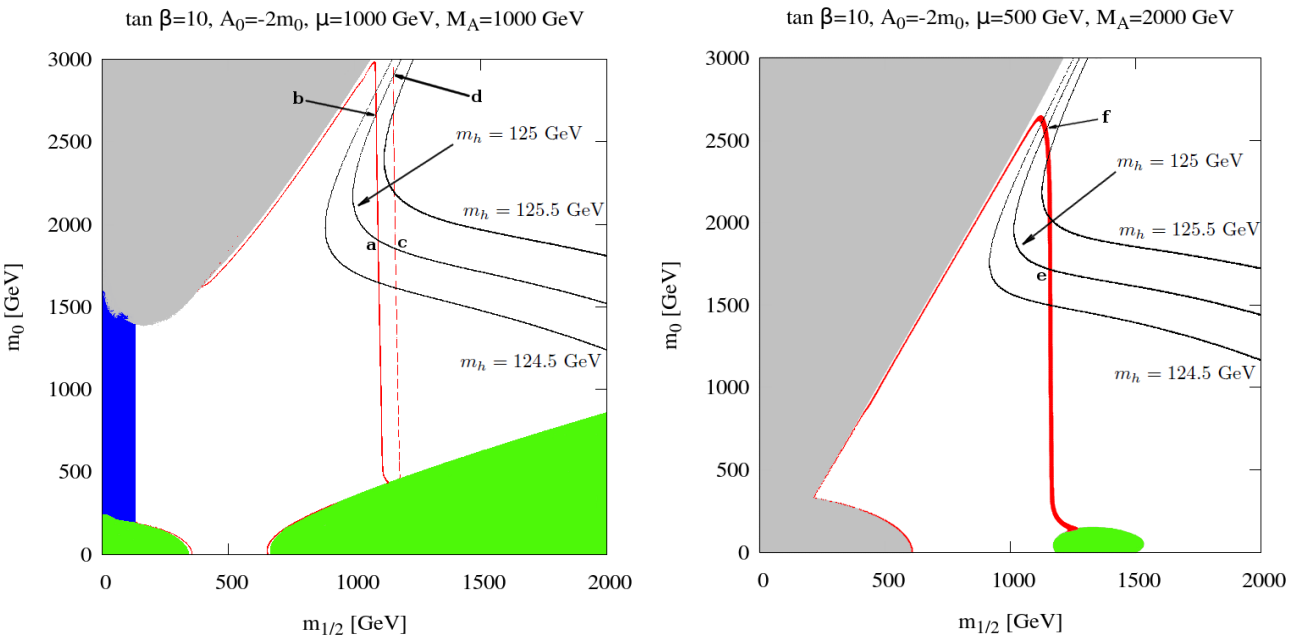

Figure 7.2: 2D scan of $(m_0 : m_{1/2})$ for NUHMII model. Left panel has the following input parameters: $\tan\beta = 10$, $A_0 = -2m_0$, $\mu = 1000$ GeV, $m_{A^0} = 1000$ GeV and the right panel: $\tan\beta = 10$, $A_0 = -2m_0$, $\mu = 500$ GeV, $m_{A^0} = 2000$ GeV. The red region denotes the relic density within 2σ range given by Planck [91], black curves shows the respective values of the Higgs mass, grey and green regions are the exclusion limits where the LSP is not a neutralino and the blue denotes the exclusion bound on chargino.

over a large range of m_0, the correct LSP abundance is achieved through CP-odd Higgs A^0 s-channel self-annihilations. To explain the observed abundance, the neutralino mass must be close to (but not exactly on) the resonance region. This leads to the relation $m_{\chi_1^0} \approx m_{A^0}/2$ and thus implies that the neutralino mass is about $m_{\chi_1^0} \approx 500$ GeV for the chosen value of $M_{A^0} = 1000$ GeV. This region is referred to as the funnel region. Between the two red strips, the relic density falls below the observed DM abundance, because the annihilation process becomes resonant and reduces the relic density too much. This region is of interest in the

case of multi–component DM scenarios. It is worth noting that since we have $\mu = 1000$ GeV we have a bino dominated neutralino. Another two strips with the correct relic abundance are bordering the green and grey regions where the stau and stop are the LSP respectively and it is the coannihilation between $\widetilde{\chi}_1^0$ and $\widetilde{\tau}$ (in the green area) or $\widetilde{t}$ (in the grey area) that depletes $\Omega_{\widetilde{\chi}_1^0}h^2$ in the early Universe. The $(m_0 : m_{1/2})$ points where the 125 GeV Higgs intersects the right relic density strips we denote as the benchmark points 'a', 'b', 'c' and 'd'. The relatively large value of μ has also an effect on neutralino and forces it to be more gaugino like. Note that, as discussed at the end of Section 5.3, the right relic density, in this case, is achieved by coannihilation and annihilation processes i.e. the ones for which the WIMP miracle approximation is not valid.

The situation is a bit different in Fig. 7.2b. Here we have a larger mass of the pseudoscalar A^0 and smaller μ. The mass of the bino at any RG scale can be found using the relation $M_1 \approx 0.42 m_{1/2}$. Since from the plots $m_{1/2} \approx 1150$ GeV, we find $M_1 = 483$ GeV which is a bit lower than the value of the μ parameter and this forces a fraction of bino in the neutralino to be a bit larger than that of higgsino. This also has an impact on $\widetilde{\chi}_1^0$ (co)annihilation Feynman diagrams. Such composition favours annihilation channels such as $\chi_1^0\chi_1^0 \to W^+W^-,\ ZZ,\ Zh$ as well as neutralino-chargino co-annihilation and thus explains the vertical red strip in the Fig. 7.2b. Since $M_1 \lesssim \mu$ our neutralino should also have a similar mass. More precisely we find $m_{\widetilde{\chi}_1^0} = 460$ GeV. We label two benchmark points 'e' and 'f' where the right $\Omega_{\widetilde{\chi}_1^0}h^2$ and $m_h = 125$ GeV coexists.

Fig./ Label	$(m_0 : m_{1/2})$ (GeV)	$\Omega_{\widetilde{\chi}_1^0}h^2$	Dominant component(s)	$m_{\widetilde{\chi}_1^0}$ (GeV)	Channel	$m_{\phi_{\widetilde{u}\widetilde{d}\widetilde{d}}}$ (GeV)	$m_{\phi_{\widetilde{L}\widetilde{L}\widetilde{e}}}$ (GeV)
7.2a 'a'	(1897:1093)	0.112	$\widetilde{B}$	473	A^0	2249	1955
7.2a 'b'	(2668:1085)	0.111	$\widetilde{B}$	473	A^0	2925	2709
7.2a 'c'	(1847:1161)	0.113	$\widetilde{B}$	503	A^0	2249	1914
7.2a 'd'	(2897:1152)	0.112	$\widetilde{B}$	503	A^0	3165	2939
7.2b 'e'	(1715:1158)	0.111	$0.69\widetilde{B}+0.31\widetilde{H}$	465	$\widetilde{\chi}^{+,0}$	2140	1787
7.2b 'f'	(2556:1140)	0.110	$0.71\widetilde{B}+0.29\widetilde{H}$	462	$\widetilde{\chi}^{+,0}$	2850	2603

Table 7.1: Benchmark points considered in this study and associated predictions for important observables. The figures which they are associated to and the dominant mechanism ($\tilde{\tau}, \tilde{t}$ coannihilations, $\chi^{+,0}$ exchange, A-pole) for the relic density calculations are specified in the last two columns of the table. The mass of the inflaton is at low scale. All points have $m_h = 125$ GeV.

7.3.2 Inflaton mass for the benchmark points

Using the RGEs for the inflaton mass and normalization that at the GUT scale it is equal m_0, one can map each point in the $(m_0 : m_{1/2})$ plane of Fig. 7.2 onto the $(\phi_0 : m_\phi)$ plane. This is shown in Fig. 7.3, where grey region shows inflation energy scale and inflaton mass which are compatible with the central value of the amplitude of the primordial perturbations, $\delta_H = 4.68 \times 10^{-5}$, and the 2σ allowed range of the spectral tilt $0.9457 \leq n_s \leq 0.9749$ [91]. In the left panel we map according to $\widetilde{L}\widetilde{L}\widetilde{e}$ and in the right according to $\widetilde{u}\widetilde{d}\widetilde{d}$ inflaton candidate behaviour. Black, red and pink lines depict the running of the points where $m_h = 124.5$, 125 and 125.5 GeV strip intersects red lines depicting right DM relic abundance in Fig. 7.2a. From here one immediately can read off the mass of the inflaton, which implicitly is constrained by the mass of the Higgs scalar and other particle physics observables. This figure also shows the allowed range of the VEV of inflation ϕ_0 on y axis. In table 7.1 we show the characteristics of the benchmark

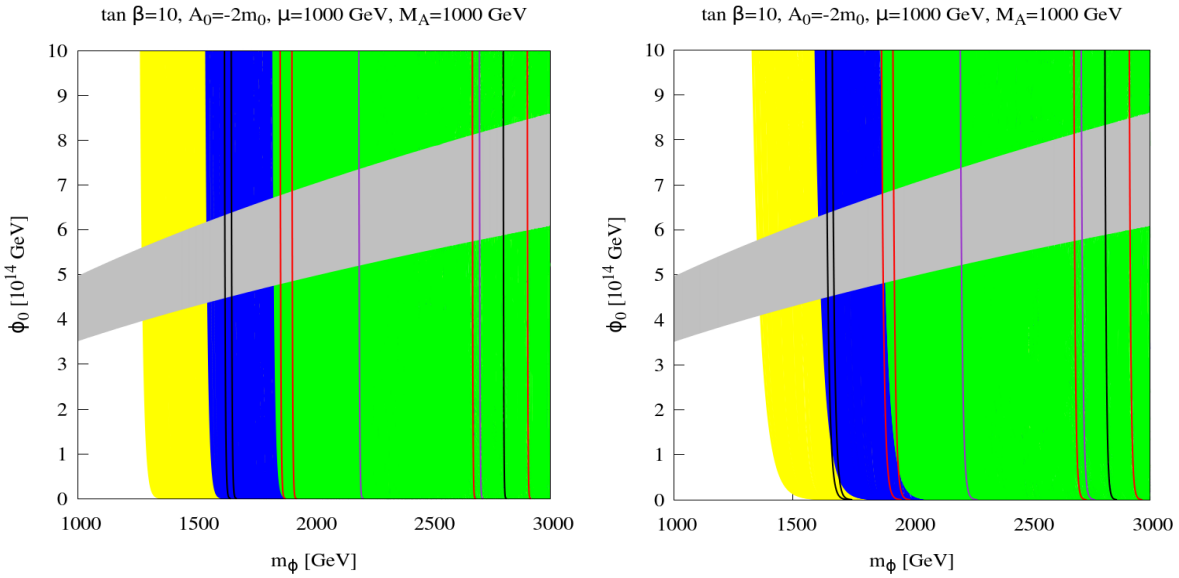

Figure 7.3: Projections of the $(m_0 : m_{1/2})$ plane in the Fig. 7.2a to $(\phi_0 : m_\phi)$ plane for $\widetilde{L}\widetilde{L}\widetilde{e}$ inflaton candidate (a panel) and $\widetilde{u}\widetilde{d}\widetilde{d}$ (b panel) for $\tan\beta = 10$, $A_0 = -2m_0$, $\mu = 1000$ GeV, and $m_{A^0} = 1000$ GeV. Yellow, blue and green regions represent parameter space for $m_h = 124.5$, 125 and 125.5 GeV respectively. Black, red and pink lines depict where the $m_h = 124.5$, 125 and 125.5 GeV strip intersects the red lines of the right relic density in Fig. 7.2a. Grey region shows inflation energy scale and inflaton mass which are compatible with the central value of the amplitude of the primordial perturbations, $\delta_H = 4.68 \times 10^{-5}$, and the 2σ allowed range of the spectral tilt $0.9457 \leq n_s \leq 0.9749$ [91].

points denoted by letters in Figs. 7.2a and 7.2b. For simplicity, we collected only the points with the $m_h = 125$ GeV Higgs. The information in the second column is essential in solving the RGE equations for the inflaton and we use it to calculate the mass of the inflaton condensates at the low scale – shown in last two columns.

7.3.3 6D scan of the NUHMII parameter space

In this section, we present the results of the full scan where we varied all the input parameters of the NUHMII model. To make the scan more efficient we employed

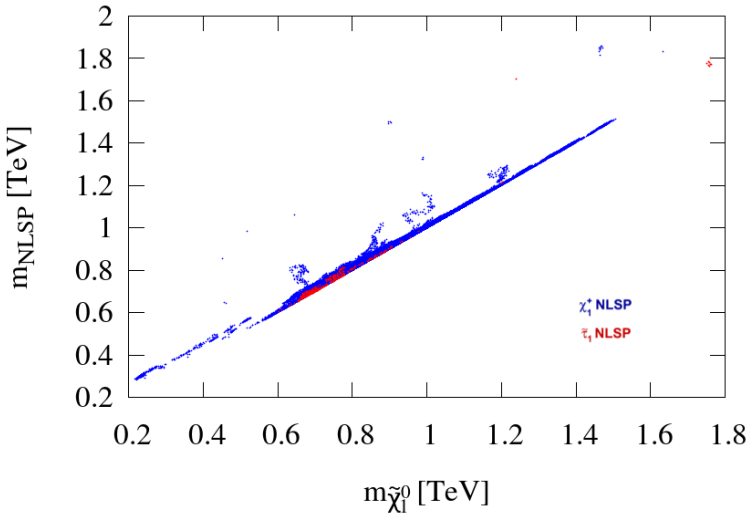

Figure 7.4: Mass of the LSP vs the mass of the NLSP, depending on the nature of the NLSP: blue and red denote scenarios where NLSP is lightest chargino and stau respectively.

MCMC strategy discussed in Section 6.1. Our scan parameter ranges are shown in Table 7.2. We start our analysis with a Fig. 7.4, by showing that there is

Parameter	Range
m_0	]0, 4] TeV
$m_{1/2}$	]0, 4] TeV
A_0	[-6, 6] TeV
$\tan\beta$	[2, 60]
μ	]0, 3] TeV
m_{A^0}	]0, 4] TeV

Table 7.2: Range chosen for the free parameters in the NUHMII model.

a very strong correlation between the mass of the LSP and that of the NLSP, suggesting that the neutralino relic density either relies on the co-annihilation mechanism or a t-channel exchange of the NLSP (or both). The NLSP is found to be mostly chargino and stau, along with very few scenarios were NLSP is the second lightest neutralino $\widetilde{\chi}_2^0$ as it was found for the benchmark points 'e' and 'f'

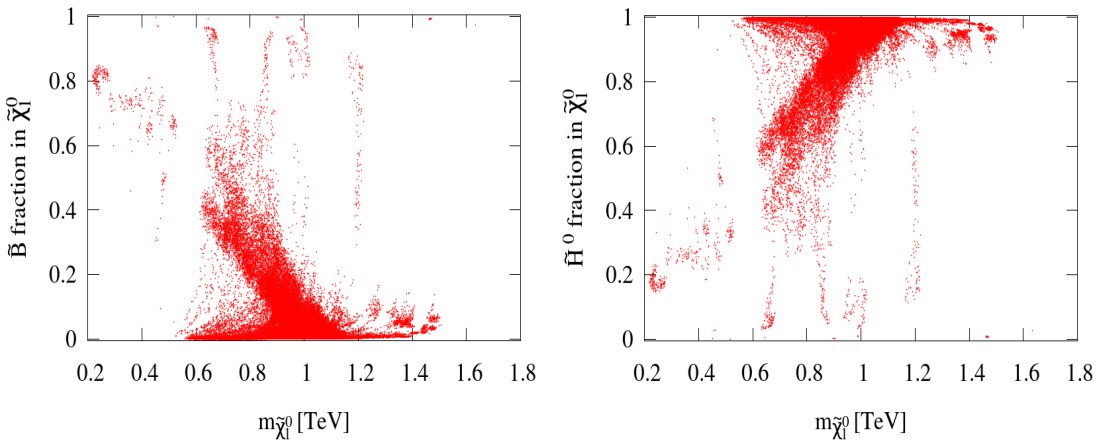

Figure 7.5: Neutralino composition dependence on its mass. Left panel shows the bino content vs the neutralino mass while the bottom panel shows the Higgsino fraction.

(see Table 7.1). The A^0-pole resonance corresponding to the benchmark points 'a','b','c','d' however requires a certain amount of fine tuning i.e. $m_{\chi_1^0} \simeq m_{A^0}/2$ has to be satisfied.

The exchange of a pseudoscalar Higgs is actually significant when $m_{\tilde{\chi}_1^0} \sim m_{A^0}/2$ but neutralino-chargino coannihilation or chargino t-channel exchange are dominant when the Higgsino fraction is very large. In fact, among the configurations with a non–negligible Higgsino fraction, the larger the bino fraction, the more favoured the A^0-pole since small neutralino couplings to the Higgs can be compensated by having $m_{\tilde{\chi}_1^0}$ closer to m_{A^0}. Finally, we see from Fig. 7.5, that heavy neutralinos with a mass $m_{\tilde{\chi}_1^0} \geq 0.6$ TeV have a large Higgsino fraction, thus suggesting even more dominant coannihilations with charginos (or annihilations through chargino exchange) and resonant annihilations via the pseudoscalar Higgs A^0, when the neutralino becomes fairly heavy.

To have a chance of identifying the inflaton condensate candidate at the LHC,

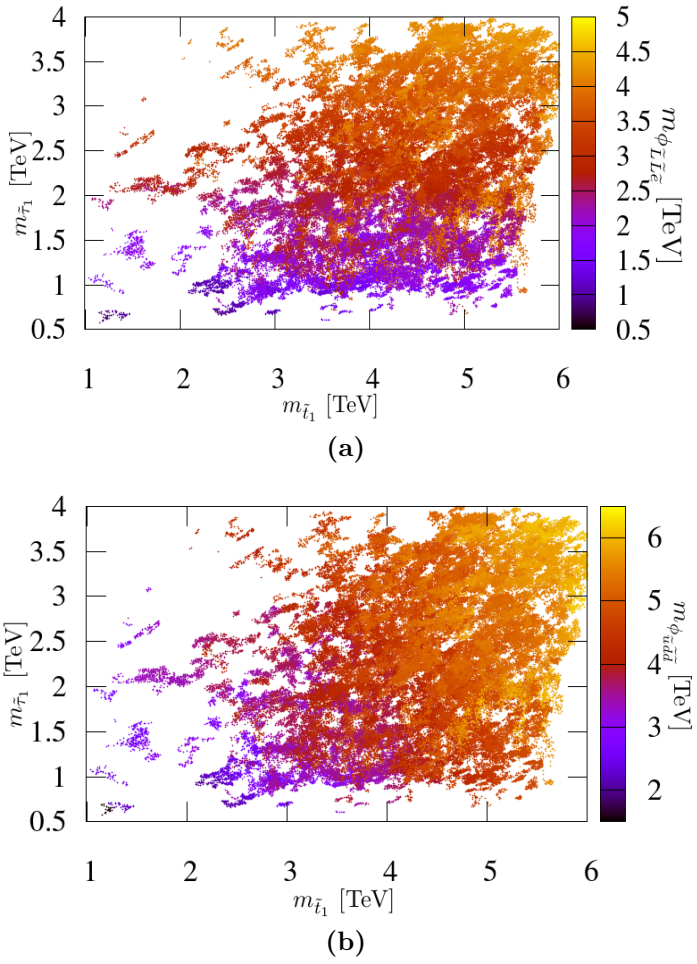

Figure 7.6: The correlation between stau mass, $m_{\tilde{\tau}_1}$ [TeV], and the lightest stop mass, $m_{\tilde{t}_1}$ [TeV]. The colour coding corresponds to the inflaton masses for $\widetilde{L}\widetilde{L}\widetilde{e}$ and $\widetilde{u}\widetilde{d}\widetilde{d}$ flat directions. The mass of the inflaton is evaluated at the low scale.

if it exists at all, its mass measurements should be supported with other observables, such as the $\widetilde{\tau}_1$ and the $\widetilde{t}_1$ mass as it is shown in Figs. 7.6. Obviously, the prediction differs depending on whether the inflaton corresponds to the $\widetilde{u}\widetilde{d}\widetilde{d}$ or $\widetilde{L}\widetilde{L}\widetilde{e}$ flat direction. For the $\widetilde{L}\widetilde{L}\widetilde{e}$ case, one finds that scenarios with the inflaton with a mass lower than 2 TeV, correspond to staus lighter than 2 TeV and stops lighter than 2-3 TeV. More generally there is a one–to–one correspondence between the values of inflaton, stau and the stop masses. This correlation between

the stau and the $\widetilde{L}\widetilde{L}\widetilde{e}$ inflaton mass can be understood because the inflaton is of leptonic origin. Similarly, for the $\widetilde{u}\widetilde{d}\widetilde{d}$ case, the inflaton mass is related to the stop mass but the constraint on the stau is somewhat more obscure. Although such a feature can be easily understood given the nature of the inflaton, using LHC observables and searches for sparticles could provide a way to distinguish between the $\widetilde{u}\widetilde{d}\widetilde{d}$ and $\widetilde{L}\widetilde{L}\widetilde{e}$ scenarios. In addition, we find that the staus in both scenarios can be lighter than 1 TeV, thus offering another possible window for probing this model at LHC. Discovering a relatively light stau at LHC together with a specific stop mass would provide a determination of the inflaton condensate mass and VEV of inflation.

7.3.4 Summary

In this section, we investigated regions of the NUHMII parameter space which are compatible with the particle physics constraints discussed in Section 6.1 and the constraints set on the inflationary potential via the amplitude of primordial perturbations of the CMB and the spectral index of its power spectrum. Two inflaton candidates were considered, $\widetilde{u}\widetilde{d}\widetilde{d}$ and $\widetilde{L}\widetilde{L}\widetilde{e}$, for which a high scale of inflation, ϕ_0, is tied up via RGEs to the low scale physics that is currently being tested at the LHC.

Several methods have been used to explore the NUHMII. One was a simple 2–dimensional MC routine in $(m_0 : m_{1/2})$ space which helped to find benchmark points, satisfying known particle physics constraints and explore what a particular realisation of NUHMII input parameters would imply to MSSM inflation. The other method was a complete 6–dimensional scan, by using an efficient MCMC algorithm explained, in Section 6.1.

The key finding is that, for most configurations, the $\widetilde{u}\widetilde{d}\widetilde{d}$ inflaton appears to be heavier than 1.5 TeV, while the $\widetilde{L}\widetilde{L}\widetilde{e}$ inflaton can be as light as 500 GeV. In both cases, however, it is possible to find configurations in which both staus and stops are within the reach of the LHC, thus indicating that sparticle searches at LHC could actually provide a means of constraining the inflaton mass for some subset of the NUHMII parameter space. Such constraints would have to be cross correlated with the measurements of $\mathcal{B}(B_s \to \mu^+\mu^-)$ and $\mathcal{B}(b \to s\gamma)$ since all scenarios found in this section have predicted values for these two branching ratios close to the present experimental limits.

We also showed that MSSM inflation can be easily accommodated within the NUHMII model. By identifying benchmark points, we demonstrated how particle physics and cosmological constraints, in particular the mass of the Higgs and DM relic abundance, can be used to find a mass and field strength of the inflaton condensate candidates. It should be noted though, that the requirement of successful MSSM inflation does not lead to any predictions about particle physics that can be tested at the LHC.

Analogous analysis can be performed where the inflaton is the SUSY Higgs, i.e. H_uH_d [325], and when the inflaton is NH_uL in the case of $MSSM \times U(1)_{B-L}$ (in which case, the inflaton is gauged under both MSSM and $U(1)_{B-L}$ [326]). Moreover, if claims of light DM species made by DAMA, CoGeNT, CRESST–II (1^{st} phase run) and CDMS collaborations turn out to be correct, it will be necessary to perform a complementary study with MCMC likelihood function priors chosen in such a way that the light neutralino state would be targeted. This would be a challenging task since most of the light neutralinos appear to have a dominant bino component.

Chapter 8

Baryogenesis

Baryogenesis seeks to explain the observed matter antimatter disparity in the Universe. In fact, there is negligible a amount of antimatter in the Solar system and Milky Way. For example, antiprotons are observed. However, this abundance is consistent with their production in the cosmic rays via $p + p \rightarrow 3p + \bar{p}$ interactions [57, 327]. Furthermore, antimatter seems to be very scarce in the whole Universe, as the matter antimatter collisions would produce a γ ray background which has not been detected. An important parameter parametrising this asymmetry is defined as:

$$\eta \equiv \frac{n_b - n_{\bar{b}}}{n_\gamma}, \tag{8.1}$$

and has never changed since the BBN. η serves as the only input parameter in the very successful theory of BBN, and in order to match the theoretical predictions to the observations, η has to be of the order $\mathcal{O}(10^{-10})$. This asymmetry can be achieved if the three Sakharov conditions are satisfied [11, 327]:

• Baryon number (B) violation: This is the most intuitive condition as the B violating process is a prerequisite in order to generate non–zero η from a baryon

symmetric universe.

• Charge (C) and charge–parity (CP) violation: Let us assume that we have a heavy particle X decaying into a lighter particle Y which has B=0 and another particle q which carries non–zero baryon number. Branching ratios, r, of the particle X and its antiparticle $\bar{X}$ can then be expressed as:

$$r_1 = \frac{\Gamma(X \to Y + q)}{\Gamma_X} \qquad \text{and} \qquad r_2 = \frac{\Gamma(\bar{X} \to \bar{Y} + \bar{q})}{\Gamma_{\bar{X}}}. \tag{8.2}$$

The rate of the net baryon number production is then proportional to the difference between r_1 and r_2. In addition, from the CPT theorem [328, 329], we have that lifetimes of any particle and its antiparticle are the same, thus we set $\Gamma_X = \Gamma_{\bar{X}}$ to get [330]:

$$\frac{\delta \mathrm{B}}{\delta t} \propto r_2 - r_1 = \frac{\Gamma(\bar{X} \to \bar{Y} + \bar{q}) - \Gamma(X \to Y + q)}{\Gamma_X}. \tag{8.3}$$

The conservation of charge implies:

$$\Gamma(X \to Y + q) = \Gamma(\bar{X} \to \bar{Y} + \bar{q}), \tag{8.4}$$

thus we have that $r_1 = r_2$ which implies $\frac{\delta \mathrm{B}}{\delta t} = 0$ and therefore the C violation is a necessary condition to create the baryon asymmetry. However, this is not enough. Let us assume X decays to two LH or two RH particles with a baryon number. Thus, we would have [330]:

$$\begin{aligned} \Gamma(X \to q + q) &= \Gamma(X \to q_L + q_L) + \Gamma(X \to q_R + q_R), \\ \Gamma(\bar{X} \to \bar{q} + \bar{q}) &= \Gamma(\bar{X} \to \bar{q}_L + \bar{q}_L) + \Gamma(\bar{X} \to \bar{q}_R + \bar{q}_R), \end{aligned} \tag{8.5}$$

for a particle and antiparticle. The net baryon asymmetry would then be proportional to:

$$\frac{\delta \mathrm{B}}{\delta t} \propto \frac{\Gamma(X \to q_L + q_L) + \Gamma(X \to q_R + q_R) - \Gamma(\bar{X} \to \bar{q}_L + \bar{q}_L) - \Gamma(\bar{X} \to \bar{q}_R + \bar{q}_R)}{\Gamma_X},$$

and having the C violation would not imply that δB>0, because even though:

$$\begin{aligned} \Gamma(X \to q_L + q_L) &\neq \Gamma(\bar{X} \to \bar{q}_L + \bar{q}_L), \\ \Gamma(X \to q_R + q_R) &\neq \Gamma(\bar{X} \to \bar{q}_R + \bar{q}_R), \end{aligned} \tag{8.6}$$

as a result of the CP symmetry, we would still have:

$$\Gamma(X \to q_L + q_L) + \Gamma(X \to q_R + q_R) = \Gamma(\bar{X} \to \bar{q}_L + \bar{q}_L) + \Gamma(\bar{X} \to \bar{q}_R + \bar{q}_R),$$

and there would be no net baryon asymmetry generated in the Universe. Therefore CP symmetry should also be violated.

• Out of the equilibrium condition: Considering again the process $X \to Y + q$, the equilibrium condition guarantees that:

$$\Gamma(X \to Y + q) = \Gamma(Y + q \to X), \tag{8.7}$$

and η remains zero. An example of the departure from thermal equilibrium is the expansion of the Universe. Initially, when the Universe was so hot that $T_{\mathrm{Universe}} > M_X$, because of the decay of the X, the rate at which baryons were produced was the same as the rate at which Y and q annihilated back to X. Once the temperature of the thermal bath fell below M_X, Y and q were not energetic enough to annihilate to X and baryon asymmetry was created. Other examples

of out of the equilibrium condition include the phase transition or dynamics of topological defects [331, 332, 333]. The phase transition is of the particular interest in the EW baryogenesis. Interactions outside the equilibrium happen during the EW phase transition when bubbles with a broken phases expand into an otherwise symmetrical Universe. We will discuss bubble nucleation in detail in Section 8.2.

All these ingredients are present within the SM but, as already mentioned in Section 2.6.4, with the 126 GeV Higgs, the model lacks sufficiently strong first order phase transition to keep the baryon asymmetry intact and the sources of the CP violation are not sufficient. Although MSSM provides all three ingredients the EW baryogenesis in this model is increasingly constrained by the LHC data. In the simplest MSSM EW baryogenesis scenario it is hard, if not impossible, to generate enough asymmetry with a 126 GeV Higgs boson in a natural manner [334]. So we turn our attention to the EW baryogenesis in the NMSSM model. The NMSSM has more flexibility as it introduces a new SM gauge singlet, which helps to achieve the strongly first order EW phase transition, since an order parameter is now determined by the singlet sector and becomes independent of the Standard Model–like Higgs mass.

8.1 B and L violation in the SM

Classically baryon and lepton number currents are conserved in the SM, however at a quantum level j^{μ}_{B} and j^{μ}_{L} can be violated in a non–perturbative manner by the chiral anomaly. The Feynman diagram of a process in which violation occurs is depicted in Fig. 8.1, where a chiral fermion running in a loop is connected to

external gauge fields. Calculating this one–loop divergent diagram yields [335]:

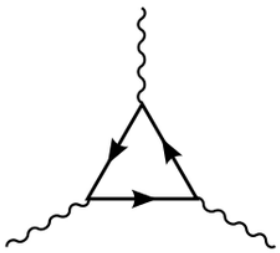

Figure 8.1: The Feynman diagram responsible for violating baryon and lepton number. In a loop there is a chiral fermion with external gauge fields at vertices. Figure from Ref. [336].

$$\partial_\mu j^\mu_{\mathrm{B}} = \partial_\mu j^\mu_{\mathrm{L}} = \frac{N_g}{32\pi^2}(g_2^2 W^a_{\mu\nu}\widetilde{W}^{\mu\nu,a} - g_1^2 Y_{\mu\nu}\widetilde{Y}^{\mu\nu}), \tag{8.8}$$

where $N_g = 3$ is the number of generations, $\widetilde{W}_{\mu\nu}$ and $\widetilde{Y}_{\mu\nu}$ are duals the of $\mathrm{SU}(2)_L$ and $\mathrm{U}(1)_Y$ field strength tensors respectively. From here it is obvious that B+L is anomalous and B-L is conserved:

$$\begin{aligned} &\partial_\mu j^\mu_{\mathrm{B+L}} = \partial_\mu j^\mu_{\mathrm{B}} + \partial_\mu j^\mu_{\mathrm{L}} = \frac{N_g}{16\pi^2}(g_2^2 W^a_{\mu\nu}\widetilde{W}^{\mu\nu,a} - g_1^2 Y_{\mu\nu}\widetilde{Y}^{\mu\nu}), \\ &\text{and likewise} \qquad \partial_\mu j^\mu_{\mathrm{B\text{-}L}} = \partial_\mu j^\mu_{\mathrm{B}} - \partial_\mu j^\mu_{\mathrm{L}} = 0. \end{aligned} \tag{8.9}$$

This anomaly is induced by topological fluctuations between adjacent vacua states of non–Abelian SU(2) gauge fields. In the vacuum state, the field strength tensor $W_{\mu\nu}$ vanishes and a condition $W_{\mu\nu} = 0$ is only satisfied if[1]:

$$W_\mu = -\frac{i}{g_2}[\partial_\mu U(x)]U^{-1} = \frac{i}{g_2}U(x)\partial_\mu U^{-1}(x), \tag{8.10}$$

is true, with $W_\mu = \frac{\sigma^{(a)}}{2}W^{(a)}_\mu$ and $U(x) \in \mathrm{SU}(2)_L$. Therefore, vacua can then be cast as a collection of infinitely many pure gauge field configurations all separated

[1]This equality follows directly from the gauge field transformation for non–Abelian fields.

by an energy barrier. The field configuration with the highest energy is called a sphaleron. The sphaleron is a saddle point solution of the $\mathrm{SU}(2)_L$ gauge and Higgs fields equation of motion and, as such, it is a static but unstable. Each of the vacuum states separated by a barrier is topologically inequivalent (homotopically distinct) and characterised by the specific Chern–Simons number N_{CS} defined as [57]:

$$N_{CS} = \frac{g_2^2}{32\pi^2} \int d^3x \epsilon^{ijk} \left(W_{ij}^a W_k^a - \frac{g_2}{3} \epsilon_{abc} W_i^a W_j^b W_k^c \right), \tag{8.11}$$

which is not a gauge invariant quantity but ΔN_{CS} is. The fact that the baryon and lepton number violations are closely related to the Chern–Simons number can be seen by rewriting the $W\widetilde{W}$ term on a right hand side of Eq. (8.8) as $W\widetilde{W} = \partial_\mu k_W^\mu$ with[1] [57]:

$$k_W^\mu = \epsilon^{\mu\nu\alpha\beta} \left(W_{\nu\alpha}^a W_\beta^a - \frac{g_2}{3} \epsilon_{abc} W_\nu^a W_\alpha^b W_\beta^c \right). \tag{8.12}$$

The expected number of baryons and leptons produced by field fluctuations between vacuum states during t_i to t_f period can then be easily calculated by using Eqs. (8.8), (8.11) and (8.12) [337]:

$$\begin{aligned} &\langle \mathrm{B}(t_f) - \mathrm{B}(t_i) \rangle = \langle \mathrm{L}(t_f) - \mathrm{L}(t_i) \rangle \\ &= \frac{1}{t_f - t_i} \int_{t_i}^{t_f} \int_{\forall x} dt d^3x \, \langle \partial_\mu j_{\mathrm{B(L)}}^\mu \rangle = N_g \langle N_{CS}(t_f) - N_{CS}(t_i) \rangle \, . \end{aligned} \tag{8.13}$$

In general terms, sphalerons mediate transitions between topologically different but physically equivalent adjacent vacuum states with $|\Delta N_{CS}| = 1$ and in each transition $\Delta\mathrm{B}{=}\Delta\mathrm{L}{=}N_g \Delta N_{CS}$ is produced i.e. 9 quarks (3 colour states for each

[1] Contribution of B and L violation from $Y\widetilde{Y}$ term is not observable. For a detailed discussion see [57].

generation) and 3 leptons so that net B-L remains conserved. At zero temperatures, the transitions between the vacuum states are exponentially suppressed and unobservable because they happen via quantum tunnelling of the instanton. However, at higher temperatures, because of the classical thermal fluctuations, the rate at which the sphaleron barrier separating different vacuum states are crossed increases. At finite temperature T, below the EW phase transition, the sphaleron transition rate can be expressed as [335, 338, 339]:

$$\Gamma = T^4 f(T/m_W) \sim e^{-E_{\text{sph.}}/T}, \tag{8.14}$$

where $E_{\text{sph.}} \sim \frac{m_W}{g_2}$ is the energy barrier height, and from this it follows that the transition rate in a broken phase is large when the temperature of a thermal bath is close to the mass of W boson and then quickly drops as the Universe cools down. In the symmetric phase, where $m_W = 0$ GeV, the transition rate inducing the B and L violations is approximated by [57, 340]:

$$\Gamma = k\left(\frac{g_2^2 T}{4\pi}\right)^4, \tag{8.15}$$

where k is a numerically evaluated coefficient in the range $0.1 \lesssim k \lesssim 1$ [57, 341]. This implies that in the Early Universe, when T were large, the transitions through sphaleron configurations and anomalous violations of baryon and lepton numbers were significant.

If initially there were baryon and lepton charge created with B-L=0, the fact that sphaleron processes were abundant in the primordial Universe implies that any B and L would be wiped out during sphaleron transitions because Δ(B-L)=0 directly implies ΔB=ΔL. On the other hand, if one starts with a Universe with

B-L$\neq$ 0, baryon and lepton numbers will be preserved and of the order of original B-L. Therefore, to explain the baryon asymmetry one has to have non–vanishing net B-L in the Early Universe or the other possibility is to generate a baryon number during EW phase transition.

8.2 Bubble nucleation and the baryon asymmetry

At very high temperatures, EW symmetry is restored [342]. As the Universe cools, the EW symmetry is broken during the phase transition. If the phase transition is of the first order, the EW symmetry is broken through tunnelling processes. In such case, the bubbles of the broken phase, where Higgs developed a VEV and $W^{\pm}$ and Z bosons are massive, growing in the otherwise symmetric Universe until the phase transition is complete and symmetry is broken everywhere in the Universe. This process is known as bubble nucleation and is depicted in Fig. 8.2. The C and CP violating processes near the bubble wall create the asymmetry between LH (and RH) fermions and their respective antiparticles. LH fermions then affect the B+L creation through sphaleron transitions in the symmetric phase just outside the wall. As the bubble expands, the baryons created outside the wall are swept into the area with a broken phase. If EW phase transition is of the first order, anomalous B+L violating processes will deviate from the equilibrium near the bubble walls [344]. Subsequently, baryons that were created outside the bubble and got swept into it by an expanding wall will not be washed out because transitions over sphaleron configurations are exponentially dampened within the broken phase. The requirement that sphaleron transitions would cease also puts

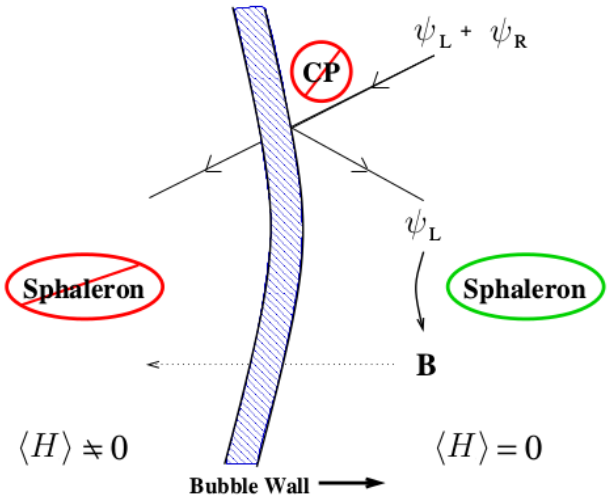

Figure 8.2: Baryon asymmetry production during bubble nucleation. Figure from Ref. [343].

constraint on a VEV of a Higgs field (and equivalently Higgs mass) which has to be large since the sphaleron barrier height is proportional to $E_{\text{sph.}} \sim m_W \sim \langle H \rangle$ and is directly related to the transition rate between distinct vacuum states, see Eq. (8.14).

The condition for the first order phase transition translates into requiring that [345, 346, 347, 348]:

$$\frac{T_c}{\varphi_c} \equiv \gamma \lesssim 1, \tag{8.16}$$

where T_c is the critical temperature at which the temperature dependent effective potential obtains degenerate minima and ϕ_c is the VEV of the Higgs field at T_c. This is known as the baryon washout condition. If it is not satisfied, the baryons created will be washed out. In the next section we will further investigate the effective potential and the conditions required for the phase transition to be of the first order.

8.3 The scalar potential at high temperature

The one–loop temperature corrections to the effective potential are given by[1] [102]:

$$V_1^\beta(\phi) = \pm\frac{g_\pm}{2\pi^2\beta^4}\int_0^\infty dx x^2 \log\left(1 \mp e^{-\sqrt{x^2+m(\phi)^2\beta^2}}\right), \tag{8.17}$$

where in this case g is the number of fermionic or bosonic degrees of freedom and $\beta \equiv 1/T$. In this expression, $-$ is for fermions and $+$ for bosons. Therefore, the full effective potential up to one–loop is:

$$V_{\text{eff.}}^\beta(\phi) = V_{\text{tree}}(\phi) + V_1(\phi) + V_1^\beta(\phi), \tag{8.18}$$

where $V_{\text{tree}}(\phi), V_1(\phi), V_1^\beta(\phi)$ are the tree level, one–loop correction at $T = 0$ and one–loop correction at finite temperature respectively. Using the high temperature approximation given in Eq. (C.15) we can write above as:

$$V_{\text{eff.}}^\beta(\phi) = D(T^2 - T_0^2)\phi^2 - ET\phi^3 + \frac{\lambda^\beta\phi^4}{4}, \tag{8.19}$$

where D, T_0 and E are temperature independent coefficients, and $\lambda^\beta = \lambda(T)$ is a slowly varying function of T [57]. Now we will take a closer look at two cases, one with $E = 0$ and another with $E \neq 0$.

- $E = 0$: using $\frac{dV_{\text{eff.}}^\beta(\phi)}{d\phi} = 0$ it is easy to calculate two solutions satisfying this extremum condition:

$$\phi(T) = 0 \text{ GeV} \qquad \text{and} \qquad \phi(T) = \sqrt{\frac{2D(T_0^2 - T^2)}{\lambda(T)}}. \tag{8.20}$$

[1] The finite temperature effective potential is the free energy of the field. The minimum of the potential gives the average value of the field in thermal equilibrium. The proof of the one–loop effective potential at finite temperature is given in the Appendix C.

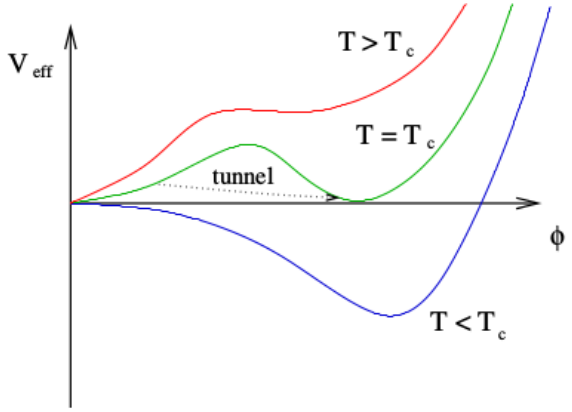

Figure 8.3: The one–loop effective potential above (red), below (blue) and at (green) the critical temperature when $E \neq 0$. Fig. from Ref. [343].

At $T = T_0$ the two minima converge to one and, as it can be seen from Eq. (8.19), the mass of the scalar field vanishes and the minimum of the effective potential is at $\phi(T_0) = 0$ GeV. At temperatures above T_0, the mass of the field is positive and the minimum remains at $\phi(T > T_0) = 0$ GeV. However, as a temperature drops below T_0 the mass squared term in the finite temperature effective potential becomes negative. In this regime, $V^{\beta}_{\text{eff.}}(\phi)$ at $\phi(T < T_0) = 0$ GeV acquires a local maximum and at the same moment a global minimum develops at $\phi(T < T_0)$ as given by the second expression in Eq. (8.20). This kind of transition is of the second order because there is no barrier between the symmetric and broken phases [57].

- $E = 0$: from Eq. (8.18) it is obvious that at a very large T the effective potential has the only minimum at $\phi(T) = 0$ GeV. However, as the temperature drops further to T_1, because of the $ET\phi^3$ term, an inflection point in the effective potential appears at [57]:

$$\phi(T_1) = \frac{3ET_1}{2\lambda(T_1)}. \tag{8.21}$$

As the temperature drops below T_1 a local minimum at $\phi(T < T_1) \neq 0$ GeV starts developing which is separated by a barrier of an increasing height. This situation is shown by the red line in a Fig. 8.3. When the temperature falls to $T = T_c$ (green line), the effective potential has two degenerate minima separated by a barrier, and a phase transition now proceeds by tunnelling. Such a transition is of the first order. T_c is called a critical temperature and is given by:

$$T_c = T_0 \sqrt{\frac{\lambda(T_c)D}{\lambda(T_c)D - E^2}}. \tag{8.22}$$

Just below T_c, a minimum at $\phi(T < T_c) = 0$ GeV becomes metastable and, finally, as the Universe cools further down a barrier disappears, as depicted by the blue line in the same figure.

8.3.1 The toy model

Previous analysis of the EW phase transition within the NMSSM near the PQ limit (i.e. $\kappa = 0$, see Section 4.5.3) found that the parameter space that satisfies the baryon washout condition is heavily constrained [349]. In a this analysis, Wagner *et al.* considered a toy model which included the tree level effective potential of the NMSSM at the PQ limit with the largest temperature corrections. In this chapter, we derive a semi-analytic solution to the toy model from Ref. [349] and consider higher order temperature corrections, loop corrections and small deviations from the so called PQ limit as perturbations to the toy model solution.

The high temperature expansion of Eq. (8.17) is, up to an overall temperature

dependent constant, [350]

$$\begin{aligned} V_1^\beta(\phi) &\sim \frac{g_+ m^2(\phi) T^2}{24} - \frac{g_+ [m(\phi)^2]^{3/2}(\phi) T}{12\pi} - \frac{g_+ m(\phi)^4}{64\pi^2} \log\left(\frac{m(\phi)^2}{a_b T^2}\right) \\ &\equiv \frac{g_+ m^2(\phi) T^2}{24} - \frac{g_+ [m(\phi)^2]^{3/2}(\phi) T}{12\pi} + \Delta V_T \,, \end{aligned} \tag{8.23}$$

for bosons, and

$$\begin{aligned} V_1^\beta(\phi) &\sim \frac{g_- m^2(\phi) T^2}{48} + \frac{g_- m(\phi)^4}{64\pi^2} \log\left(\frac{m(\phi)^2}{a_f T^2}\right) \\ &\equiv \frac{g_- m^2(\phi) T^2}{48} + \Delta V_T \,, \end{aligned} \tag{8.24}$$

for fermions. Here $a_b = (4\pi e^{-\gamma_E})^2$ and $a_f = (\pi e^{-\gamma_E})^2$. $\gamma_E \approx 0.57721...$ is the Euler–Mascheroni constant [351]. We have also identified the log term as ΔV_T to highlight that these terms will be treated as a perturbation. To keep the notation compact, all small temperature corrections that are not included in our toy model (i.e. the ones that we treat as a perturbation) and their sum we denote as ΔV_T. The temperature dependent effective potential is a function of the Higgs field and the singlet field which we denote φ_S. (We also use the short hand that $\varphi \equiv \sqrt{H_u^2 + H_d^2}$.) Within one–loop accuracy under the high temperature expansion, it is given by

$$V(\varphi, \varphi_s, T) = V^{\mathrm{T}} + \Delta V_S + \Delta V_{\mathrm{loop}} + \Delta V_T \,. \tag{8.25}$$

Here we have defined ΔV_{loop} as the loop corrections, ΔV_S as the terms that violate the PQ limit (which is approximately $\kappa A_\kappa \varphi_s^3/3$). The term V^{T} is the toy model

effective potential, which is given by [165]

$$V^{\mathrm{T}} = M^2\varphi^2 + cT^2\varphi^2 - ET\varphi^3 + m_s^2\varphi_s^2 + \lambda^2\varphi_s^2\varphi^2 - 2\tilde{a}\varphi^2\varphi_s + \frac{\tilde{\lambda}}{2}\varphi^4 \ , \quad (8.26)$$

where E, as discussed in previous section, is a dimensionless constant needed to have first order phase transition and:

$$\begin{aligned} M^2 &= m_{H_u}^2 \cos^2\beta + m_{H_d}^2 \sin^2\beta, \\ \tilde{a} &= \lambda A_\lambda \sin\beta\cos\beta, \\ \frac{\tilde{\lambda}}{2} &= \frac{g_1^2+g_2^2}{8}\left(\cos^2\beta - \sin^2\beta\right)^2 + \lambda^2\sin^2\beta\cos^2\beta + \frac{\delta\tilde{\lambda}}{2}. \end{aligned} \quad (8.27)$$

In the last equation the parameter $\delta\tilde{\lambda}$ acquires large loop corrections from the stop mass. We recall that at the critical temperature the effective potential obtains degenerate minima with one minima at $\varphi = 0$. It is easy to see that $V(0,0,T) = V^{\mathrm{T}}(0,0,T) = 0$. As mentioned before, let the critical temperature and the non–zero VEV at this temperature for our toy model be denoted by T_c and φ_c, respectively. It is also useful to define $\tilde{\gamma} = T/\varphi$ for $T \neq T_c$. Note that V can be written as a function of φ, φ_S and $\tilde{\gamma}$. We will denote the fields, φ_x, away from the respective minima as $\tilde{\varphi}_x$. Let us assume that V is continuous in its three arguments near the critical temperature. It is then apparent that $V(\varphi_c+\delta\varphi_c, \tilde{\varphi}_s+\delta\varphi_s, \gamma+\delta\gamma) = 0$, where the non–trivial VEV of the full temperature dependent potential at the critical temperature is a small perturbation to the tree level critical VEV, $\varphi_c+\delta\varphi_c$. Similarly, the singlet VEV at the critical temperature and the inverse order parameter both obtain small corrections, $\delta\varphi_s, \delta\gamma$, respectively.

From the small change formula in three variables, we can write:

$$\begin{aligned} & V(\varphi_c + \delta\varphi_c, \tilde{\varphi}_s + \delta\tilde{\varphi}_s, \gamma + \delta\gamma) \\ \approx\ & V^{\mathrm{T}}(\varphi_c, \tilde{\varphi}_s, \gamma) + (\Delta V_T + \Delta V_{\mathrm{loop}} + \Delta V_S)|_{\varphi_c, \tilde{\varphi}_s, \gamma} \\ & + \left.\frac{\partial V^{\mathrm{T}}}{\partial \tilde{\varphi}}\right|_{\varphi_c,\varphi_s,\gamma} \delta\varphi_c + \left.\frac{\partial V^{\mathrm{T}}}{\partial \tilde{\varphi}_s}\right|_{\varphi_c,\varphi_s,\gamma} \delta\varphi_s + \left.\frac{\partial V^{\mathrm{T}}}{\partial \tilde{\gamma}}\right|_{\varphi_c,\varphi_s,\gamma} \delta\gamma \ . \end{aligned} \tag{8.28}$$

The first term on the right hand side of the above equation is identical to zero for the reasons discussed above. Furthermore, the derivative of our toy model effective Lagrangian with respect to either φ or φ_c is also zero by definition when the derivative is evaluated at its minimum. Setting the left hand side of the above equation to zero and defining $\Delta V \equiv \Delta V_T + \Delta V_S + \Delta V_{\mathrm{loop}}$, we can then write:

$$\delta\gamma = -\Delta V \Big/ \left.\frac{\partial V^T}{\partial \tilde{\gamma}}\right|_{\varphi_c,\varphi_s,\gamma} . \tag{8.29}$$

Noting that $\partial\varphi/\partial\tilde{\gamma} = -\varphi/\tilde{\gamma}$, we can write

$$\frac{\partial V}{\partial \tilde{\gamma}} = \frac{2G\varphi^2}{\tilde{\gamma}} - 2c\tilde{\gamma}\varphi^4 - \frac{2\tilde{\lambda}\varphi^4}{\tilde{\gamma}} + 3E\varphi^4 + \frac{\tilde{a}^2\varphi^4(4m_s^2 + 2\lambda^2\varphi^2)}{\tilde{\gamma}(m_s^2 + \lambda^2\varphi^2)^2}. \tag{8.30}$$

Finally, we solve our toy model. We begin this calculation by insisting that the zero temperature VEV is $v = 174$ GeV. This gives us the relation:

$$-M^2 = v^2\left(\tilde{\lambda} - \frac{\tilde{a}^2(2m_s^2 + \lambda^2 v^2)}{(m_s^2 + \lambda^2 v^2)^2}\right) \equiv G \ . \tag{8.31}$$

Using the condition of degenerate minima occurring at a critical temperature, it

is easy to derive the following equation

$$0 = -\frac{\tilde{\lambda}}{2} + \gamma E - c\gamma^2 + \frac{\sqrt{\tilde{a}^2(\tilde{\lambda} - \gamma E)}}{\sqrt{2}m_s} + \frac{\lambda^2 G}{-m_s^2 + \sqrt{\frac{2\tilde{a}^2 m_s^2}{\tilde{\lambda} - \gamma E}}} \equiv F(\gamma) \ . \qquad (8.32)$$

Note that, apart from γ, this equation is a function of only four parameters: $\{m_s, \lambda, A_\lambda, \tan\beta\}$. We therefore calculate $\delta\gamma$ for values of $\{m_s, \lambda, A_\lambda, \tan\beta\}$ such that $F(\gamma + \delta\gamma)$ is significantly smaller than any of its five components. We ensure that all components of ΔV are small compared to the derivative of V^{T} with respect to gamma evaluated at the VEV at the critical temperature. Finally, we insist that perturbation $\delta\gamma \lesssim 0.4$ and the baryon washout condition are satisfied for $\gamma + \delta\gamma \lesssim 1$.

8.4 NMSSM parameter space for DM and the first order phase transition

In Table 8.1 the parameter ranges of NMSSM scan are shown. We fixed the first and second generation sfermionic masses to high values in order to avoid large potential suspersymmetric contributions to electron and nuclear electric dipole moments [352]. The masses of left and right handed stops are adjusted to yield the measured value of the Higgs boson mass. In order to probe the DM phenomenology, it is essential to vary the EW gaugino masses in a wide range. Varying the gluino mass is important to determine the running of the $\widetilde{u}\widetilde{d}\widetilde{d}$ inflaton candidate. High selected ranges also guarantee that our spectrum does not conflict with the LEP [42], ATLAS [31] and CMS [32] bounds on squarks and sleptons.

Parameter	Description	Range
λ	λ coupling	$[0:0.7]$
A_λ	Trilinear λ term	[0:10000] GeV
$\tan\beta$	$\tan\beta$ parameter	[1:65]
$A_\kappa \cdot \kappa$	$A_\kappa \cdot \kappa$	[0:0.01] GeV
μ	Higgs mixing term	$[0 : A_\lambda \cos\beta \sin\beta]$ GeV
M_1	Bino Mass	[10:3000] GeV
M_2	Wino Mass	[10:4000] GeV
M_3	Gluino Mass	[800:6000] GeV
$m_{\tilde{e}_{L,R}} = m_{\tilde{\mu}_{L,R}} = m_{\tilde{\tau}_{L,R}}$	LH/RH sleptons	6000 GeV
$m_{\tilde{Q}_{1L}} = m_{\tilde{Q}_{2L}}$	1st and 2nd generation LH squarks	6000 GeV
$m_{\tilde{Q}_{3L}}$	3rd generation LH squarks	3300 GeV
$m_{\tilde{u}_R} = m_{\tilde{c}_R}$	1st and 2nd generation RH squarks	6000 GeV
$m_{\tilde{t}_R}$	3rd generation RH squark	4000 GeV
$m_{\tilde{d}_R} = m_{\tilde{s}_R} = m_{\tilde{b}_R}$	RH squarks	6000 GeV
A_t	Trilinear top coupling	-5000 GeV
$A_\tau = A_b$	Trilinear τ and bottom coupling	-2500 GeV

Table 8.1: Scan ranges of the NMSSM parameters in the MC scan. The upper bound on the parameter μ comes from the requirement of the 1st order phase transition and controls the Higgsino fraction in the neutralino.

Fig. 8.4 shows the bino (green dots), wino (red stars), higgsino (blue squares), and singlino (pink diamonds) fractions of the lightest neutralino. We restrict the relic density of the lightest neutralino below $\Omega_{\tilde{\chi}_1^0} h^2 < 0.128$ which is the upper value on the DM abundance set by Planck at 3σ confidence level. As mentioned above, neutralinos with masses $m_{\tilde{\chi}_1^0} < m_Z/2$ have to have small higgsino fraction due to strict limits on the invisible Z boson decay (from Eq. (6.1)). The mass bound on the lightest chargino imposes further restrictions on the wino and higgsino fractions of light neutralinos. Also, as it has been thoroughly discussed in Sections 6.2 and 6.3 the light DM regions are very fine tuned and require separate detailed analysis and more sophisticated scanning techniques such as the MCMC scan. The heavier neutralinos can have the larger higgsino fraction. This

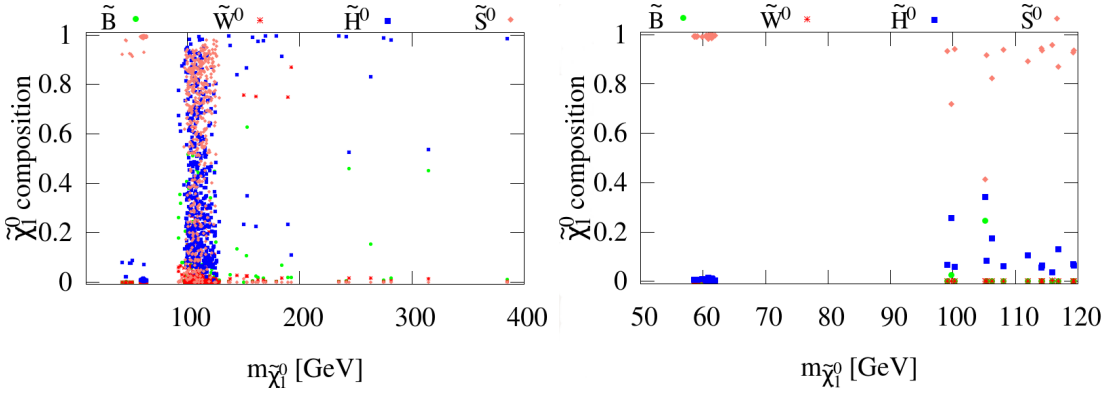

Figure 8.4: Bino (green dots), wino (red stars), higgsino (blue squares), and singlino (pink diamonds) components of the lightest neutralino for the scanned model points. All points shown satisfy the condition of the strongly first order EW phase transition and pass all constraints listed in Section 6.1. On the right hand panel we only show the points that fall within 3σ of the Planck central value for the relic abundance of DM: $0.1118 < \Omega_{\tilde{\chi}_1^0} h^2 < 0.128$ [91].

is also connected to the fact that the positivity of m_s^2 sets an upper bound on the parameter $\mu < A_\lambda \cos\beta \sin\beta$, which allows larger higgsino fraction in the lightest neutralino. As we shall argue in the next paragraph, this opens up more annihilation channels to satisfy the relic density constraint.

In Fig. 8.5, we show the DM relic density dependence on $m_{\tilde{\chi}_1^0}$. We only show points for which the DM relic density falls below the upper limit from Planck, that is to satisfy $\Omega_{\tilde{\chi}_1^0} h^2 < 0.128$ at 3σ confidence level [91]. The points clustering at around $m_{\tilde{\chi}_1^0} \approx 63$ GeV is due to neutralino annihilation through the 126 GeV Higgs. This resonant annihilation depletes the neutralino abundance making it possible to satisfy the Planck bound. The second, a larger group of points originate from the lightest neutralino with an enhanced higgsino component coupling to the Z boson. As this, and the previous, figure shows our model points also have the potential to explain the origin of the 130 GeV γ-ray line observed from the Galactic Centre in terms of the annihilation of a 130 GeV neutralino [258, 259].

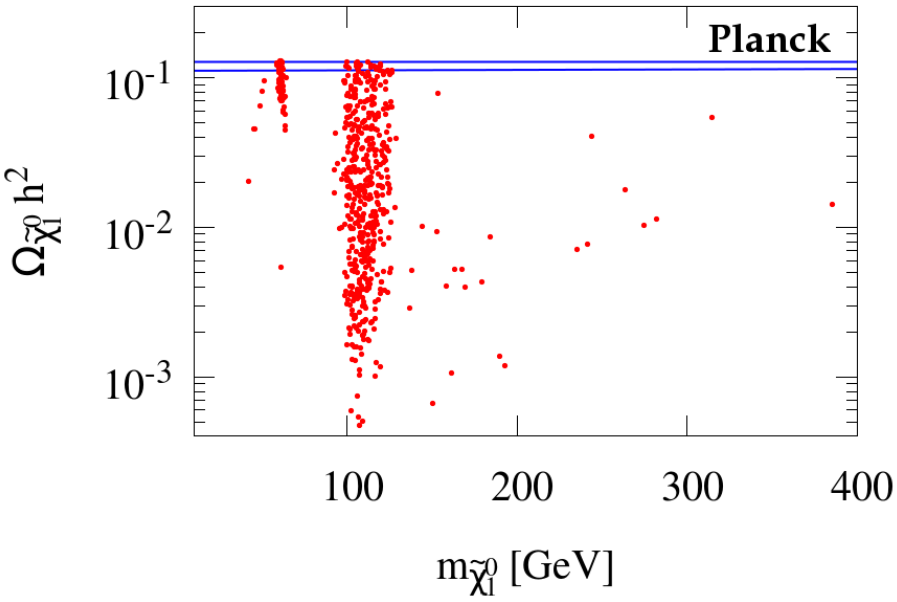

Figure 8.5: Relic abundance versus the mass of the DM particle for our scan. The blue lines indicate the bounds on DM density implied by the Planck satellite: $0.1118 < \Omega_{\tilde{\chi}_1^0} h^2 < 0.128$. All the points satisfy the condition for a first order EW phase transition, as indicated by Eq. (8.32). They also pass all the cosmological and particle physics constraints listed in Section 6.1.

In Fig. 8.6, we show how spin independent DM–nucleon scattering experiments probe the scenarios with the constraints listed in Section 6.1 and $F(\gamma) = 0$, see Eq. (8.32). The points that are circled in black fall within the range $0.1118 < \Omega_{\tilde{\chi}_1^0} h^2 < 0.128$ set by Planck. It is interesting to note that quite a few points lie in the regions where the LSP is relatively light within the ranges where DAMA/LIBRA [178], CRESST–II (1^{st} phase run) [180], CoGeNT [179] and CDMS [222] detected excess interactions over expected background. All the points with the smallest $m_{\tilde{\chi}_1^0}$ have a large singlino fraction, and are ruled out by the XENON100 experiment. We also show the current LUX and projected bound from the XENON1T. These bounds are based on the assumptions already mentioned in the 6.1 Section.

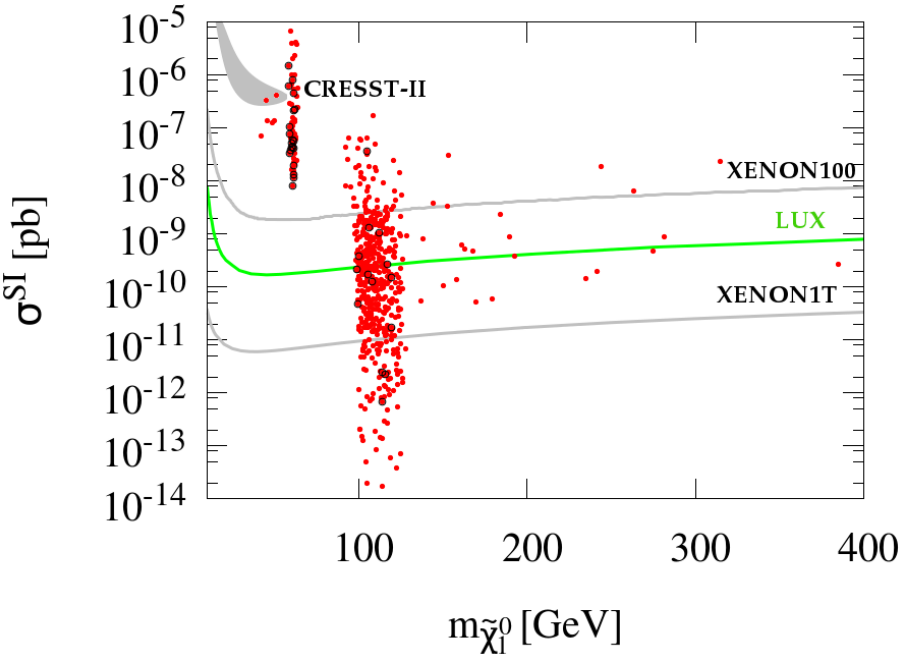

Figure 8.6: Spin independent direct detection cross section vs. mass of the neutralino in our scan. The current bounds from XENON100, LUX and the 2σ signal region from CRESST–II (1^{st} phase run) are shown. We also show projected bound for XENON1T. The points where neutralino relic abundance accounts for the full dark matter content of the Universe measured by Planck within 3σ, i.e. $0.1118 < \Omega_{\tilde{\chi}_1^0} h^2 < 0.128$, are highlighted in black circles.

Exclusion limits from DD experiments are drawn under assumption that neutralino accounts for a total DM content of the Universe whereas in most cases that we have found a relic abundance is significantly lower than the Planck measured value. Therefore, before considering which points avoid DD constraints and which do not, we need to lower the cross section $\sigma^{\rm SI}$ by a factor $(\Omega_{\tilde{\chi}_1^0}/\Omega_{\rm observed})$ in cases where neutralino constitute only a fraction of the whole DM. Here we take the Planck central value $\Omega_{\rm observed} = 0.1199$. As we see, most of the points that fall below XENON100 will be tested very soon by LUX and XENON1T experiments.

In Fig. 8.7, we show how the relevant parameters that enter Eq. (8.32) are distributed in the scans. In the top left panel we can see that $\tan\beta$ tends to

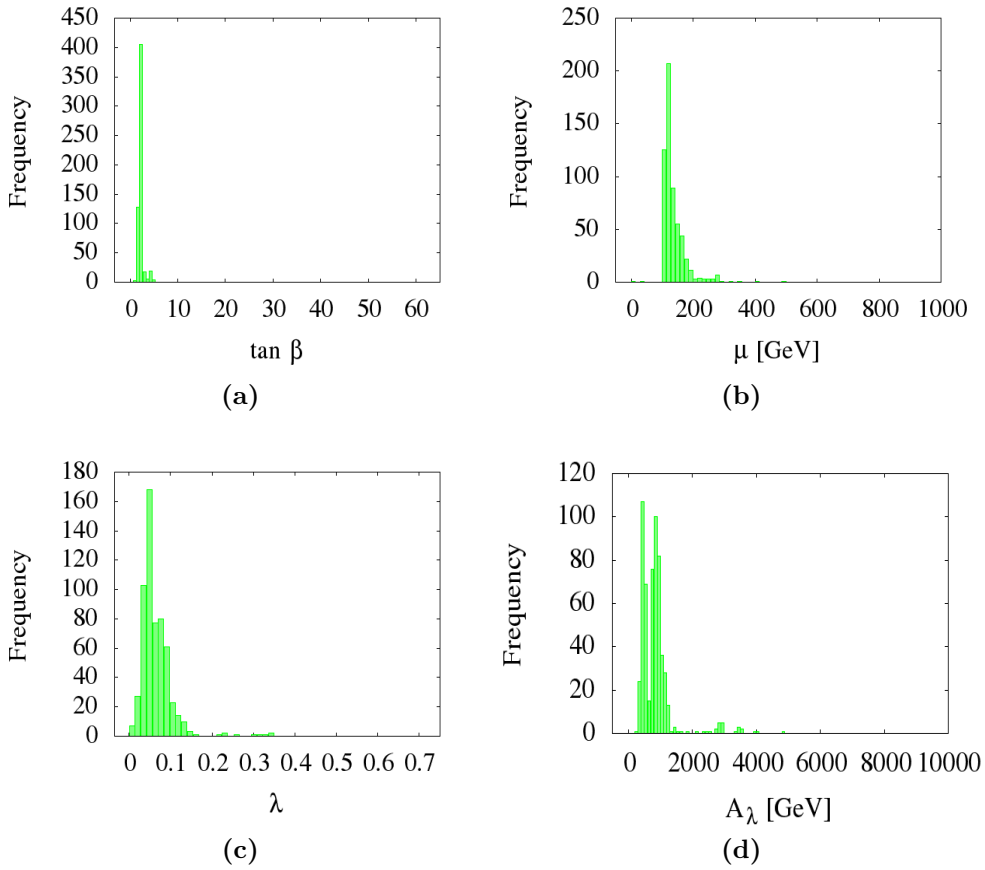

Figure 8.7: Distribution of the parameters which are relevant for baryogenesis in our scan.

cluster around lower values. This is not because a higher $\tan\beta$ is inconsistent with the baryon washout condition, just that our approximations break down for the large $\tan\beta$ so we avoided scanning those. The breakdown is due to terms in ΔV that are $\tan\beta$ dependent and for large $\tan\beta$ can make ΔV too large so that our assumption of ΔV being small is violated. Similarly the upper bound on A_λ and λ is a relic of our approximations rather than any real difficulty in satisfying the baryon washout condition in that parameter range. The lower bound on λ, however, originates from baryogenesis since the low κ and low λ region is the

Parameter	a	b	c	d	Constrained by
λ	0.06405	0.06520	0.10418	0.02906	1^{st} order phase transition
A_λ(GeV)	1127	524	772	796	1^{st} order phase transition
$\tan\beta$	2.659	2.042	2.276	2.123	1^{st} order phase transition
$\mu_{\rm eff}$(GeV)	165.214	142.985	176.515	137.963	1^{st} order phase transition
$\Omega_{\widetilde{\chi}_1^0}h^2$	0.119	0.112	0.124	0.112	DM abundance
$m_{\widetilde{\chi}_1^0}$(GeV)	61.17	119.2	59.8	126.3	DM abundance
M_1(GeV)	2151	2006	1375	1084	Inflaton RGE
M_3(GeV)	5269	4986	4281	861	Inflaton RGE
$\phi_0[\times 10^{14}]$(GeV)	$3.5-3.8$	$4.2-4.6$	$5.3-5.7$	$6.6-7.3$	CMB temperature anisotropy
m_ϕ(GeV)	1425	2120	3279	5349	CMB temperature anisotropy

Table 8.2: We show the benchmark points that are depicted in Fig. 8.8. The gaugino masses which enter in the RG equations are mainly sensitive to M_1 and M_3. The parameters $\lambda, A_\lambda, \tan\beta, \mu_{\rm eff}$ are constrained from baryogenesis point of view, and this in turn uniquely determine the mass of the lightest stop which sets the mass for $\widetilde{u}_3\widetilde{d}_i\widetilde{d}_j$ inflaton candidate ($i \neq j$). Once again we reiterate that without our approximation scheme, constraints on baryogenesis would be significantly less strict. The mass of the inflaton is given at the inflationary scale ϕ_0.

MSSM limit and it is difficult to satisfy the baryon washout condition in the MSSM for a Higgs mass of 125 GeV [334]. We kept $A_t = -5000$ GeV fixed to be able to satisfy the Higgs mass bound more easily. Values of μ are mainly within a 100–200 GeV range because, as mentioned above, large values are constrained by the requirement of m_s^2 being positive. This translates into an upper bound, lower than $A_\lambda \cos\beta \sin\beta$, for a particular $\tan\beta$. Lower μ values are constrained because of the invisible Z decay and the chargino mass, which set bounds on the higgsino component of the neutralino which is directly related to low μ. Since A_λ enters Eq. (8.32) through $\widetilde{a}$, in order to satisfy condition $F(\gamma) = 0$ there needs to be some tuning between the fourth and fifth terms. This fine tuning increases with increasing A_λ, and so condition 8.32 is much easier met at low values.

8.5 Parameter space for inflation, dark matter and baryogenesis

Since the requirement for a successful baryogenesis implicitly constraints the right handed squark, i.e. $\widetilde{u}_3$, we can assign the flat direction combination to be: $\widetilde{u}_i\widetilde{d}_j\widetilde{d}_k$, where $i = 3$ and $j \neq k$.

In order to relate the low energy physics that we can probe at the LHC with the high energy inflation, which is constrained by the Planck data, we use the RGEs for the $\widetilde{u}\widetilde{d}\widetilde{d}$ flat direction, already stated in Eq. (7.18). As mentioned before, the mass of the inflaton made of $\widetilde{u}_i\widetilde{d}_j\widetilde{d}_k$ condensate can be written as:

$$m_\phi^2 = \frac{m_{\widetilde{u}}^2 + m_{\widetilde{d}}^2 + m_{\widetilde{d}}^2}{3}. \tag{8.33}$$

This then allows us to evaluate the mass of the inflaton at the EW scale and by using the RGEs we are able to evolve it to the high scale ϕ_0, where inflation can happen, and check if there is an overlap within NMSSM where DM, baryogenesis and inflation coexist. This can be seen in Fig. 8.8. The blue region shows the parameter of $\widetilde{u}_3\widetilde{d}_j\widetilde{d}_k$ as an inflaton for $j \neq k$. It shows the central value of density perturbations together with $\pm 1\sigma$ variation in spectral tilt n_s. The brown lines show the mass of the inflaton at a particular scale and its running from high scale to low scale is determined by the RGEs, which is mostly sensitive to bino and gluino masses and the energy scale.

In Fig. 8.8, we show the four benchmark points, $a,\ b,\ c,\ d$, which satisfy the condition for a successful baryogenesis, Eq. (8.32), and also accommodate neutralino as a DM which satisfies the relic abundance constraint $0.1118 < \Omega_{\widetilde{\chi}_1^0} h^2 <$

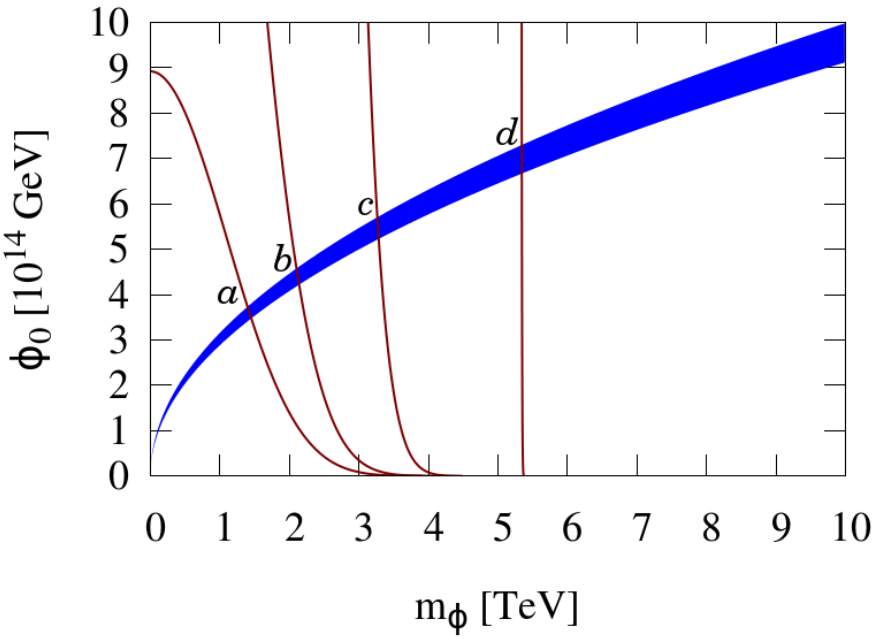

Figure 8.8: Blue region depicts the parameter space for inflation where it yields the right amplitude of density perturbations in the CMB, i.e. $P_\zeta = 2.196 \times 10^{-9}$ and the $\pm 1\sigma$ variance of the spectral tilt, $n_s = 0.9603 \pm 0.0073$, where both quantities based on combined Planck and WMAP data [91]. Brown lines show the running of the inflaton mass, where they intersect with the blue region depict the correct relic abundance, $0.1118 < \Omega_{\tilde{\chi}_1^0} h^2 < 0.128$ [91], and strongly first order phase transition. From these intersections, a, b, c, d we can determine the masses of the inflaton at the inflationary scale ϕ_0. The running of the inflaton mass is mainly determined by the bino and gluino masses, see Table 8.2.

0.128. In Table 8.2, we summarize the relevant parameters for NMSSM required to explain the Universe beyond the Standard Model.

8.6 Summary

In this chapter, we examined inflation, baryogenesis and DM in the context of NMSSM. We have found that all of them can be simultaneously accommodated by the theory. In particular, we derived a semi-analytic solution to the toy model analysed in Ref. [349] and considered higher order temperature corrections, loop

corrections to the effective potential and small deviations from the PQ limit as perturbations to the toy model solution. We have shown that a strongly first order phase transition can be easily achieved even with recent LHC constrains applied. We investigated this by utilizing a simple MC routine to explore the parameter space of NMSSM. Even using much less efficient scanning strategy than MCMC, we were able to find a number of points that satisfy constraints imposed by a requirement to have a strongly first order phase transition, particle physics constraints – most notably a mass of ~ 125 GeV Higgs, bounds from the ID/DD experiments and the relic abundance measurements by Planck.

We also demonstrated that an abundance of the lightest neutralinos can be generated thermally, which satisfies the present DM density limits set by the Planck satellite. Part of these model points also pass the most stringent dark matter direct detection constraints and potentially could explain $\sim$130 GeV γ–ray line from the Fermi–LAT, if it is confirmed. Finally, we have shown that the presented scenario is fully consistent with inflation, where the inflaton is a D–flat direction made up of right handed squarks.

A key step in validating the presented picture is subject to positive experimental data: the discovery of SUSY at the LHC and unambiguous claims from DD experiments, especially with a high neutralino–nucleon spin independent cross section, would provide the means to consider more critically the proposed BSM framework.

Chapter 9

Conclusion

We have performed a detailed study of how various supersymmetric extensions of the SM can explain inflation, DM and the first order phase transition during EW symmetry breaking. Since SUSY is yet to be found in the present or future colliders, we have also addressed the naturalness issue in one of the most general particle physics models – p19MSSM. In the light of the potential positive results announced by the direct DM detection experiments and the discovery of the ~ 125 GeV Higgs–like scalar particle we also have looked at how light $\widetilde{\chi}_1^0$ can be in the p19MSSM and NMSSM.

By utilizing the efficient MCMC scanning technique, we found that a neutralino as light as 10 GeV is still in principle viable in p19MSSM, though scenarios in a range of 10 GeV $< m_{\widetilde{\chi}_1^0} <$ 30 GeV have a large EW fine tuning, $\Delta_{\rm tot} \sim \mathcal{O}(10^3)$. Most of these points have quite a low spin independent nucleon–$\widetilde{\chi}_1^0$ cross section, $\sigma^{SI}_{\widetilde{\chi}_1^0-p}$, and escape bounds set by XENON100 and more recently by LUX. However, $\sigma^{SI}_{\widetilde{\chi}_1^0-p}$ is not large enough to explain the potential positive signals released by DAMA, CoGeNT, CRESST–II (1^{st} phase run) and CDMS. In

order to deplete the relic density in the Early Universe, these points also require light sleptons, which are excluded from LEP searches if one assumes gaugino mass unification at the GUT scale. A dedicated analysis of the LEP data in the context of a p19MSSM scenario could completely eliminate the possibility of a light neutralino in the mass range of $10 - 30$ GeV. In [316, 317] authors claimed that a light sbottom ($\sim$10 GeV) would be sufficient to validate very light neutralino ($\sim$1 GeV) solutions in p19MSSM. However, we set $m_{\widetilde{b}_1} > 300$ GeV which is valid when $m_{\widetilde{b}_1} - m_{\widetilde{\chi}_1^0} > m_b$ is satisfied and that turns out always to be the case for light neutralino solutions. The second group of points with $m_{\widetilde{\chi}_1^0} > 30$ GeV are where the annihilation via the s-channel Z-exchange is possible for a bino–higgsino mixture of neutralino LSP. These scenarios are much less fine–tunned, but many of them are ruled out by XENON100 and LUX, and the remaining scenarios will soon be tested by XENON1T. It should be noted though, that these DD exclusion limits can be avoided by making a realistic assumption that neutralino DM does not interact equally with protons and neutrons. However, if it does, then these results strongly hint that, if claims of light DM are correct and the nature indeed realizes SUSY, then one should endeavour to probe the particle physics models with additional ingredients.

One such possibility is the NMSSM. Here the DM can be as light as 1 GeV, and because of the large fraction of singlino, it has a high spin independent cross–section for a $\widetilde{\chi}_1^0 - p$ scattering, which is claimed to be observed by the formerly mentioned experiments. In case of further experimental evidence for a light neutralino with large spin independent nucleon–$\widetilde{\chi}_1^0$ cross section from DD searches, NMSSM potentially would become a leading BSM theory. It is also appealing that the fine–tuning issue is of little importance because of the additional singlet

field. When a singlet develops a VEV, it dynamically generates the μ term and large cancellations between the Higgs soft breaking masses and the μ term can easily be avoided to yield the right mass for the Z boson.

After demonstrating that there is ample parameter space where the DM relic abundance together with particle physics constraints are satisfied, we tried to explore the regions of the NUHMII model, where DM and inflation can coexist. We studied how the particle physics constraints, most notably the relic abundance and the latest bound on a mass of the Higgs scalar, could pinpoint the mass of the inflaton and the scale of inflation within the gauge invariant MSSM inflation model. In the study, two inflaton candidates were considered, $\widetilde{u}\widetilde{d}\widetilde{d}$ and $\widetilde{L}\widetilde{L}\widetilde{e}$, for which the high scale of inflation, ϕ_0, is tied up via the RGE to the low scale physics that is currently being tested at the LHC. Two methods have been used to explore the NUHMII. One was a simple 2 dimensional MC routine in $(m_0 : m_{1/2})$ space, which helped to find benchmark points satisfying known particle physics constraints and explore what a particular realisation of NUHMII input parameters would mean to MSSM inflation. The other method was a complete 6 dimensional scan by using an efficient MCMC algorithm explained in Section 6.1.

The key finding is that for most configurations, the $\widetilde{u}\widetilde{d}\widetilde{d}$ inflaton appears to be heavier than 1.5 TeV, while the $\widetilde{L}\widetilde{L}\widetilde{e}$ inflaton can be as light as 500 GeV. In both cases, however, it is possible to find configurations in which both staus and stops are within the reach of the LHC, thus indicating that sparticle searches at LHC could actually provide a means of constraining the inflaton mass for some subset of the NUHMII parameter space. Such constraints would have to be cross correlated with the measurements of $\mathcal{B}(B_s \to \mu^+\mu^-)$ and $\mathcal{B}(b \to s\gamma)$, since all the scenarios found in this section have predicted values for these two branching

ratios close to the present experimental limits.

Analogous analysis can be performed where the inflaton is the SUSY Higgs, and when the inflaton is NH_uL, in the case of $MSSM \times U(1)_{B-L}$, in which case, the inflaton is gauged under both MSSM and $U(1)_{B-L}$. Moreover, if claims of light DM species made by DAMA, CoGeNT, CRESST–II (1^{st} phase run) and CDMS collaborations turn out to be correct, it will be necessary to perform a complementary study with MCMC likelihood function priors chosen in a way that would target light neutralino solutions. This would be a challenging task since most of the light neutralinos appear to have a dominant bino component. This requires light sleptons to satisfy DM abundance constraints.

While we demonstrated how particle physics and cosmological constraints, in particular the mass of the Higgs and DM relic abundance, can be used to find a mass and field strength of the inflaton condensate candidates, it is important to note that the requirement of successful MSSM inflation does not lead to any predictions about particle physics that can be tested at the LHC.

In the last part of the thesis we discussed the highly efficient mechanism for determining the parameter space of the NMSSM, where the first order phase transition can happen, together satisfying constraints on the relic abundance and particle physics. Previous analysis of the EW phase transition within the NMSSM near the PQ limit found that the parameter space that satisfies the baryon washout condition is heavily constrained. In a prior analysis [349], the authors considered a toy model which included the tree level effective potential of the NMSSM at the PQ limit with the largest temperature corrections. In the last chapter we derived a semi-analytic solution to the toy model analysed in ref. [349] and considered higher order temperature corrections, loop corrections to the

effective potential and small deviations from the PQ limit as perturbations to the toy model solution. In particular, we have shown that a strongly first order phase transition can be easily achieved in the PQ limit even with recent LHC constrains applied. We scanned over the variety of input parameters of NMSSM and the algorithm for the 1^{st} order phase transition constrained the set of $(\mu, \tan\beta, \lambda, A_\lambda)$, with the preference for low $\tan\beta$ and λ, 200 GeV$\lesssim \mu \lesssim$ 300 GeV and 0 GeV$< A_\lambda \lesssim$ 3000 GeV. This then has phenomenological implications, most notably on the composition of the DM and mass of the Higgs scalar. We demonstrated that an abundance of lightest neutralinos can be generated thermally, which satisfies the present DM density limits set up by Planck satellite. A fraction of these model points also pass the most stringent DM DD constraints and fall within parameter space regions were potential positive signals for the light DM were announced. Moreover, many of them could potentially explain ∼130 GeV γ–ray line from the Fermi–LAT, if it is confirmed. Finally, by choosing a few validated benchmark points we calculated the mass of the inflaton and the VEV of inflation, thus covering a large part of a complete picture of the BSM physics.

A key step in validating the presented picture is subject to positive experimental data: the discovery of SUSY at the LHC and unambiguous claims from DD experiments, especially with a high neutralino–nucleon spin independent cross section, would provide the means to consider more critically the proposed BSM framework.

Appendix A

$\widetilde{L}\widetilde{L}\widetilde{e}$ and $\widetilde{u}\widetilde{d}\widetilde{d}$ flatness

Here, we demonstrate the $\mathrm{SU}(3)_c\times$ $\mathrm{SU}(2)_L\times\mathrm{U}(1)_Y$ D–flatness of the $\widetilde{L}_i\widetilde{L}_j\widetilde{e}_k$ and $\widetilde{u}_i\widetilde{d}_j\widetilde{d}_k$ flat directions using the second condition in Eq. (4.71).

- $\widetilde{L}_i\widetilde{L}_j\widetilde{e}_k$ case: to show the $\mathrm{U}(1)_Y$ D–flatness, we employ the hypercharges provided by Table 4.1. Thus, $Y_L=-\frac{1}{2}$ and $Y_e=1$, therefore:

$$D_Y=-\frac{1}{2}|\widetilde{L}_i|^2-\frac{1}{2}|\widetilde{L}_j|^2+|\widetilde{e}_k|^2=-|\phi|^2+|\phi|^2=0. \tag{A.1}$$

The $\mathrm{SU}(2)_L$ D–flatness calculation is analogous as for $\widetilde{L}\widetilde{H}_u$ case, showed in Section 4.4.1. For the choice of:

$$\widetilde{L}_i=\frac{1}{\sqrt{3}}\begin{pmatrix}0\\ \phi\end{pmatrix} \qquad \text{and} \qquad \widetilde{L}_j=\frac{1}{\sqrt{3}}\begin{pmatrix}\phi\\ 0\end{pmatrix}, \tag{A.2}$$

we have:

$$\sum_{a=1}^{3}D^{(a)}=\widetilde{L}_i^{\dagger}\sigma^{(3)}\widetilde{L}_i+\widetilde{L}_j^{\dagger}\sigma^{(3)}\widetilde{L}_j=\frac{1}{3}(|\phi|^2-|\phi|^2)=0, \tag{A.3}$$

where superscripts in brackets denote the component and not the power.

- $\widetilde{u}_i\widetilde{d}_j\widetilde{d}_k$ case: from Table 4.1, we have that $Y_u = -\frac{2}{3}$ and $Y_d = \frac{1}{3}$ thus:

$$D_Y = -\frac{2}{3}|\widetilde{u}_i|^2 + \frac{1}{3}|\widetilde{d}_j|^2 + \frac{1}{3}|\widetilde{d}_k|^2 = -\frac{2}{3}|\phi|^2 + \frac{2}{3}|\phi|^2 = 0. \tag{A.4}$$

To demonstrate the $\mathrm{SU}(3)_c$ D–flatness, we choose the following representation of the fields in the colour space:

$$\widetilde{u}_i = \frac{1}{\sqrt{3}}\begin{pmatrix}\phi\\0\\0\end{pmatrix}, \qquad \widetilde{d}_j = \frac{1}{\sqrt{3}}\begin{pmatrix}0\\\phi\\0\end{pmatrix}, \qquad \widetilde{d}_k = \frac{1}{\sqrt{3}}\begin{pmatrix}0\\0\\\phi\end{pmatrix}. \tag{A.5}$$

Using this, we get:

$$\begin{aligned}\sum_{a=1}^{8} D^{(a)} &= \widetilde{u}_i^\dagger\lambda^{(3)}\widetilde{u}_i + \widetilde{u}_i^\dagger\lambda^{(8)}\widetilde{u}_i + \widetilde{d}_j^\dagger\lambda^{(3)}\widetilde{d}_j + \widetilde{d}_j^\dagger\lambda^{(8)}\widetilde{d}_j + \widetilde{d}_k^\dagger\lambda^{(8)}\widetilde{d}_k \\ &= \frac{1}{3}\left(|\phi|^2 + \frac{|\phi|^2}{\sqrt{3}} - |\phi|^2 + \frac{|\phi|^2}{\sqrt{3}} - \frac{2|\phi|^2}{\sqrt{3}}\right) = 0,\end{aligned} \tag{A.6}$$

where λ are the Gell-Mann matrices – generators of $\mathrm{SU}(3)_c$.

Appendix B

MCMC routine implementation in micrOMEGAs

Below is the MCMC code used to explore light neutralino in p19MSSM as discussed in Section 6.2. All micrOMEGAs built-in functions are defined in [278].

```
#include"../sources/micromegas.h"
#include"../sources/micromegas_aux.h"
#include"lib/pmodel.h"
#include <stdio.h>
#include <math.h>
#include <time.h>  //seeds random number related to the time

#define SUGRAMODEL_(A) A ## SUGRA
#define SUGRAMODEL(A) SUGRAMODEL_(A)

#define AMSBMODEL_(A) A ## AMSB
#define AMSBMODEL(A) AMSBMODEL_(A)

#define EWSBMODEL_(A) A ## EwsbMSSM
#define EWSBMODEL(A) EWSBMODEL_(A)

#define PRINTRGE_(A) printf(" Spectrum calculator is %s\n", #A)
#define PRINTRGE(A)  PRINTRGE_(A)
```

```
int main(int argc,char** argv)
{  int err;
   char cdmName[10];
   int spin2, charge3,cdim;
 delFiles=0; /* switch to save/delete RGE input/output */
 ForceUG=0;  /* to Force Unitary Gauge assign 1 */
// sysTimeLim=1000;

//Open a file for writing
FILE *f1 = fopen("1.dat","w");
fprintf(f1,"1h 2k 3massbino 4masswino 5massgluino 6mu 7MA 8Mh 9NLSP 10MNLSP 11tanbeta
12mchi1 13Omega 14amu 15bsgamma 16bsmumu 17SIsigmap 18SIsigman 19Zn11 20Zn12 21Zn13 22Zn14 23heavyHiggs
24mscl 25mssl 26msne 27msel 28msmr 29msur 30mser 31mcha1 32mchi2 33mchi3 34mstop1 35mchi4 36mcha2 37mstau1
38msb1 39mstop2 40msnm 41msml 42msdr 43msg 44msb2 45msul 46msdl 47mssr 48msul 49mstau2 50mscr 51Atop
52Abottom 53Atau 54Amu 55LOm 56Lmh 57Lmchi1 58LTOT 59Photonflux 60Positronflux 61Antiprotonflux 62deltatotal
63Zv11 64Zv12 65Zu11 66Zu12 67msnl\n");

#elif defined(EWSB)
{
   printf("\n========= EWSB scale input =========\n");
   PRINTRGE(RGE);

   printf("Initial file  \"%s\"\n",argv[1]);

   err=readVarMSSM(argv[1]);

   if(err==-1)     { printf("Can not open the file\n"); exit(2);}
   else if(err>0)  { printf("Wrong file contents at line %d\n",err);exit(3);}

   double mchi1, mchi2, LHslepton1, LHslepton2, LHslepton3, RHselectron, RHsmuon, RHstau, LHsquark1, LHsquark2,
   LHsquark3, RHupsquark, RHdownsquark,    RHstrangesquark, RHcharmsquark, RHbottomsquark, RHtopsquark, Atop,
   Abottom, Atau, Amu, mcha1, mcha2, Mh, Omega, Xf, SMbsg, amu, bsgamma, bmumu, taunu, Zn11, Zn12, Zn13, Zn14,
   mstop1, mstop2, mstau1, mstau2, SIsigmap, SIsigman, SCcoeff, MNLSP, mscr, msg, msdr, msne, msnl, msel, mser,
   msb1, msb2, msnm, msur, mssr, msml, msul, msdl, heavyHiggs, LOm, Lmh, LTOT, LTOTP, LTmax, Lgmu, Lbsg, Lbmu,
   Lbnu, Lmchi1, massbino, masswino, massgluino, tanbeta, muparameter, MA, mscl, mssl, mchi3, mchi4, msmr, beta,
   pi, cosb, deltamiusquared, deltab, deltaHUsquared, deltaHDsquared, deltatotal, OijL, OijR, Zinv;
   double massbinoP, masswinoP, massgluinoP, muparameterP, tanbetaP, MAP, LHslepton1P, LHslepton2P, LHslepton3P,
   RHselectronP, RHsmuonP, RHstauP, LHsquark1P, LHsquark2P, LHsquark3P, RHupsquarkP, RHcharmsquarkP, RHtopsquarkP,
   RHdownsquarkP, RHstrangesquarkP, RHbottomsquarkP, AtopP, AbottomP, AtauP, AmuP, rdvar, Lrho, Zv11, Zv12,
   Zu11, Zu12;
   int h, k=0, nw, warning=0, stuck=0, NLSP, p, rdsgn;
```

```
   int err,i;

   double Emin=1,SMmev=320;/*Energy cut in GeV and solar potential in MV*/
   double  sigmaV,vcs_gz,vcs_gg,SpA[NZ],SpE[NZ],SpP[NZ],FluxA[NZ],FluxE[NZ],FluxP[NZ],SpNe[NZ],SpNm[NZ],SpNl[NZ];
   char txt[100];
   double Etest=Mcdm/2, fi=0.,dfi=M_PI/180, lowest=9.9*pow(10,-99);

   int fast=1;
   double Beps=1.E-5, cut=0.01;  //needed for relic density calculation
   double pA0[2],pA5[2],nA0[2],nA5[2];   //for Calculation of CDM-nucleons amplitudes
   double Nmass=0.939; /*nucleon mass*/   //for Calculation of CDM-nucleons amplitudes
   srand(time(NULL));
   LTmax=lowest;LTOTP=lowest;

//randomly generating p19MSSM parameters
assignValW("MG1",rand()%501); assignValW("MG2",rand()%1001);assignValW("MG3",rand()%2200+800);
assignValW("mu",(rand()%600001)*pow(10,-2)-3000); assignValW("tb",((rand()%5900)*pow(10,-2))+1);
assignValW("MH3",rand()%2700+300); assignValW("Ml1",rand()%3001); assignValW("Ml3",rand()%3001);
assignValW("Mr1",rand()%3001); assignValW("Mr3",rand()%3001); assignValW("Mq1",rand()%3001);
assignValW("Mq3",rand()%3001); assignValW("Mu1",rand()%3001); assignValW("Mu3",rand()%3001);
assignValW("Md1",rand()%3001); assignValW("Md3",rand()%3001);
assignValW("At",rand()%20001-10000); assignValW("Ab",rand()%20001-10000);
assignValW("Al",rand()%20001-10000); assignValW("Am",0);

massbino=findValW("MG1"); masswino=findValW("MG2"); massgluino=findValW("MG3");
muparameter=findValW("mu");
if(muparameter<0 && massbino>=masswino)
massbino=-1*massbino;
if(muparameter<0 && masswino>=massbino)
masswino=-1*masswino; tanbeta=findValW("tb"); MA=findValW("MH3");
LHslepton1=findValW("Ml1"); LHslepton2=LHslepton1; LHslepton3=findValW("Ml3");
RHselectron=findValW("Mr1"); RHsmuon=RHselectron; RHstau=findValW("Mr3");
LHsquark1=findValW("Mq1"); LHsquark2=LHsquark1; LHsquark3=findValW("Mq3");
RHupsquark=findValW("Mu1"); RHcharmsquark=RHupsquark; RHtopsquark=findValW("Mu3");
RHdownsquark=findValW("Md1"); RHstrangesquark=RHdownsquark; RHbottomsquark=findValW("Md3");
Atop=findValW("At"); Abottom=findValW("Ab"); Atau=findValW("Al"); Amu=findValW("Am");

//Starting MCMC loop
for(h=1;h<=200000000;h++){
//Cheking if p19MSSM parameters do not fall out of chosen ranges in MCMC. If they do, then generate new
//set of input.
```

```
if ((massbino>500 || massbino<-500) || (masswino>1000 || masswino<-1000) || (massgluino>3000 ||
massgluino<800) || (muparameter>3000 || muparameter<-3000) || (tanbeta>60 || tanbeta<1) || (MA>3000
|| MA<300) || (LHslepton1>3000 || LHslepton1<0) || (LHslepton2>3000 || LHslepton2<0) ||
(LHslepton3>3000 || LHslepton3<0) || (RHselectron>3000 || RHselectron<0) || (RHsmuon>3000 || RHsmuon<0)
|| (RHstau>3000 || RHstau<0) || (LHsquark1>3000 || LHsquark1<0) || (LHsquark2>3000 || LHsquark2<0)
|| (LHsquark3>3000 || LHsquark3<0) || (RHupsquark>3000 || RHupsquark<0) || (RHcharmsquark>3000 ||
RHcharmsquark<0) || (RHtopsquark>3000 || RHtopsquark<0) || (RHdownsquark>3000 || RHdownsquark<0) ||
(RHstrangesquark>3000 || RHstrangesquark<0) || (RHbottomsquark>3000 || RHbottomsquark<0) || (Atop>10000
|| Atop<-10000) || (Abottom>10000 || Abottom<-10000) || (Amu>1 || Amu<-1) || (Atau>10000 ||
Atau<-10000)){printf("out of the box");

assignValW("MG1",rand()%501);assignValW("MG2",rand()%1001);assignValW("MG3",rand()%2200+800);
assignValW("mu",(rand()%600001)*pow(10,-2)-3000);assignValW("tb",((rand()%5900)*pow(10,-2))+1);
assignValW("MH3",rand()%2700+300);assignValW("Ml1",rand()%3001);assignValW("Ml3",rand()%3001);
assignValW("Mr1",rand()%3001);assignValW("Mr3",rand()%3001);assignValW("Mq1",rand()%3001);
assignValW("Mq3",rand()%3001);assignValW("Mu1",rand()%3001);assignValW("Mu3",rand()%3001);
assignValW("Md1",rand()%3001);assignValW("Md3",rand()%3001);assignValW("At",rand()%20001-10000);
assignValW("Ab",rand()%20001-10000);assignValW("Al",rand()%20001-10000);assignValW("Am",0);

massbino=findValW("MG1");masswino=findValW("MG2");massgluino=findValW("MG3");muparameter=findValW("mu");
if(muparameter<0 && massbino>=masswino)
masswino=-1*masswino;
if(muparameter<0 && masswino>=massbino)
massbino=-1*massbino;
tanbeta=findValW("tb");MA=findValW("MH3");LHslepton1=findValW("Ml1");LHslepton2=LHslepton1;
LHslepton3=findValW("Ml3");RHselectron=findValW("Mr1");RHsmuon=RHselectron;RHstau=findValW("Mr3");
LHsquark1=findValW("Mq1");LHsquark2=LHsquark1;LHsquark3=findValW("Mq3");RHupsquark=findValW("Mu1");
RHcharmsquark=RHupsquark;RHtopsquark=findValW("Mu3");RHdownsquark=findValW("Md1");
RHstrangesquark=RHdownsquark;RHbottomsquark=findValW("Md3");Atop=findValW("At");
Abottom=findValW("Ab");Atau=findValW("Al");Amu=findValW("Am");}

err=EWSBMODEL(RGE)(); //calculates particle spectrum

Mh=findValW("Mh");
qNumbers(cdmName,&spin2, &charge3, &cdim);

err=sortOddParticles(cdmName);
Omega=darkOmega(&Xf,fast,Beps);

if(strcmp(cdmName,"~o1"))
{warning++;printf("=========~o1 is not CDM=======...warning=%d\n\n\n\n",warning);}
```

```
nw=slhaWarnings(stdout);
if(nw==0) printf("==no spectrum problems===\n\n\n");
if(err) warning++;
printf("warning=%d\n",warning);

//check if observables satisfies experimental bounds.
if(warning==0){

if(Omega>0.13) LOm=exp(-pow((Omega-0.1158),2.)/(2*pow(0.0035,2.)));
else LOm=1.;

if(Mh<124.96) Lmh=exp(-pow((Mh-124.96),2.)/(2*pow(0.54,2.)));
else if(Mh>126.04) Lmh=exp(-pow((Mh-126.04),2.)/(2*pow(0.54,2.)));
else Lmh=1.;

if(gmuon()>0.) Lgmu=1/( 1+ exp( -(gmuon()-25.5*pow(10,-10))/
(-sqrt(pow(6.3*pow(10,-10),2.) + pow(4.9*pow(10,-10),2.))) ));
else Lgmu=0.;

Lbsg=exp(-pow((bsgnlo(&SMbsg)-3.55*pow(10,-4)),2.)/(2*(pow(0.24*pow(10,-4),2.) +
pow(0.09*pow(10,-4),2.) + pow(0.23*pow(10,-4),2.))));

if(bsmumu()>4.7*pow(10,-9))
Lbmu=1/( 1+ exp( -(bsmumu()-4.7*pow(10,-9))/(-4.5*pow(10,-11)) ));
else Lbmu=1;

Lbnu=1/( 1+ exp( -(btaunu()-2.219)/(-0.5) ));

mchi1=fabs(findValW("MNE1"));
if (mchi1>30)
Lmchi1=exp(-pow((mchi1-30),2.)/(1*pow(2,2.)));
else Lmchi1=1;

Etest=Mcdm/2;
if(Mcdm>2.001){
sigmaV=calcSpectrum( 1+2+4,SpA,SpE,SpP,SpNe,SpNm,SpNl ,&err);
gammaFluxTab(fi,dfi, sigmaV, SpA, FluxA);
posiFluxTab(Emin, sigmaV, SpE, FluxE);
pbarFluxTab(Emin, sigmaV, SpP,  FluxP);}

amu=gmuon();
```

```
taunu=btaunu();

//calculation of gaugino fractions in neutralino
Zn11=pow(findValW("Zn11"),2);
Zn12=pow(findValW("Zn12"),2);
Zn13=pow(findValW("Zn13"),2);
Zn14=pow(findValW("Zn14"),2);

Zv11=pow(findValW("Zv11"),2);
Zv12=pow(findValW("Zv12"),2);
Zu11=pow(findValW("Zu11"),2);
Zu12=pow(findValW("Zu12"),2);

//Calculation of invisible Z decay width
OijL=-0.5*Zn13+0.5*Zn14;
OijR=-OijL;
Zinv=2*sqrt(1-4*pow(mchi1,2)/pow(91.1876,2))*((1-pow(mchi1,2)/pow(91.1876,2))*
(OijL*OijL+OijR*OijR)+6*pow(mchi1,2)/pow(91.1876,2)*OijL*OijR)*0.50162;
printf("Zinv=%lf\n",Zinv);

//finding NLSP
mcha1=findValW("MC1");MNLSP=mcha1;NLSP=1;
mchi2=fabs(findValW("MNE2"));if(mchi2<=MNLSP){MNLSP=mchi2;NLSP=2;}
mstau1=findValW("MSl1");if(mstau1<=MNLSP){MNLSP=mstau1;NLSP=3;}
mstop1=findValW("MSt1");if(mstop1<=MNLSP){MNLSP=mstop1;NLSP=4;}
mscr=findValW("MScR");if(mscr<=MNLSP){MNLSP=mscr;NLSP=5;}
msg=findValW("MSG");if(msg<=MNLSP){MNLSP=msg;NLSP=6;}
msdr=findValW("MSdR");if(msdr<=MNLSP){MNLSP=msdr;NLSP=7;}
msne=findValW("MSne");if(msne<=MNLSP){MNLSP=msne;NLSP=8;}
msnl=findValW("MSnl");if(msnl<=MNLSP){MNLSP=msnl;NLSP=9;}
msel=findValW("MSeL");if(msel<=MNLSP){MNLSP=msel;NLSP=10;}
mser=findValW("MSeR");if(mser<=MNLSP){MNLSP=mser;NLSP=11;}
msb1=findValW("MSb1");if(msb1<=MNLSP){MNLSP=msb1;NLSP=12;}
msnm=findValW("MSnm");if(msnm<=MNLSP){MNLSP=msnm;NLSP=13;}
msur=findValW("MSuR");if(msur<=MNLSP){MNLSP=msur;NLSP=14;}
mssr=findValW("MSsR");if(mssr<=MNLSP){MNLSP=mssr;NLSP=15;}
msml=findValW("MSmL");if(msml<=MNLSP){MNLSP=msml;NLSP=16;}
msul=findValW("MSuL");if(msul<=MNLSP){MNLSP=msul;NLSP=17;}
msdl=findValW("MSdL");if(msdl<=MNLSP){MNLSP=msdl;NLSP=18;}
mscl=findValW("MScL");if(mscl<=MNLSP){MNLSP=mscl;NLSP=19;}
mssl=findValW("MSsL");if(mssl<=MNLSP){MNLSP=mssl;NLSP=20;}
```

```
msmr=findValW("MSmR");if(msmr<=MNLSP){MNLSP=msmr;NLSP=21;}

mstau2=findValW("MSl2");
mstop2=findValW("MSt2");
msb2=findValW("MSb2");
mchi3=fabs(findValW("MNE3"));
mchi4=fabs(findValW("MNE4"));
msmr=findValW("MSmR");
mcha2=findValW("MC2");
heavyHiggs=findValW("MHH");

nucleonAmplitudes(FeScLoop, pA0,pA5,nA0,nA5);
SCcoeff=4/M_PI*3.8937966E8*pow(Nmass*Mcdm/(Nmass+ Mcdm),2.);
SIsigmap=SCcoeff*pA0[0]*pA0[0];
SIsigman=SCcoeff*nA0[0]*nA0[0];

LTOT=Lmchi1*Lmh*Lbnu*Lrho*Lbmu*LOm;

/************************FINE TUNNING**********************/
pi = 4.0 * atan(1.0);
beta=atan(tanbeta);
deltamiusquared=4*pow(muparameter,2)/pow(91.1876,2)*(1+(MA*MA+pow(91.1876,2))/(MA*MA)*pow(tan(2*beta),2));

deltab=(1+MA*MA/pow(91.1876,2))*pow(tan(2*beta),2);

deltaHUsquared=abs(0.5*cos(2*beta)+MA*MA/pow(91.1876,2)*pow(cos(beta),2)-pow((muparameter/91.1876),2))*
(1-1/cos(2*beta)+(MA*MA+pow(91.1876,2))/(MA*MA)*pow(tan(2*beta),2));

deltaHDsquared=abs(-0.5*cos(2*beta)+MA*MA/pow(91.1876,2)*pow(sin(beta),2)-pow((muparameter/91.1876),2))*
(1+1/cos(2*beta)+(MA*MA+pow(91.1876,2))/(MA*MA)*pow(tan(2*beta),2));

deltatotal=sqrt(pow(deltamiusquared,2)+pow(deltab,2)+pow(deltaHUsquared,2)+pow(deltaHDsquared,2));
/************************************************************/
}

if(LTOT>=lowest && warning==0 && stuck<50){
if(LTOT>=LTOTP){massbinoP=massbino, masswinoP=masswino, massgluinoP=massgluino, muparameterP=muparameter,
tanbetaP=tanbeta, MAP=MA, LHslepton1P=LHslepton1, LHslepton2P=LHslepton2, LHslepton3P=LHslepton3,
RHselectronP=RHselectron, RHsmuonP=RHsmuon, RHstauP=RHstau, LHsquark1P=LHsquark1, LHsquark2P=LHsquark2,
LHsquark3P=LHsquark3, RHupsquarkP=RHupsquark, RHcharmsquarkP=RHcharmsquark, RHtopsquarkP=RHtopsquark,
RHdownsquarkP=RHdownsquark, RHstrangesquarkP=RHstrangesquark, RHbottomsquarkP=RHbottomsquark, AtopP=Atop,
```

```
AbottomP=Abottom, AtauP=Atau, AmuP=Amu, LTOTP=LTOT, k++;
if (LTOTP>LTmax) {LTmax=LTOT;stuck=0;}
else stuck++;
if (h>0 && h<200000000 && nw==0 && (Mh>123) && (Mh<127) && (Omega<0.13) && (bsmumu()<4.7*pow(10,-9)) &&
(bsmumu()>2*pow(10,-9)) && (bsgnlo(&SMbsg)>3.29*pow(10,-4)) && (bsgnlo(&SMbsg)<3.81*pow(10,-4)) && (Zinv<0.003) &&
(mcha1>103.5))
 fprintf(f1,"%d %d %lf %lf %lf %lf %lf %lf %d %lf %lf %lf %lf
 %.5E %lf %.31E %.3E %.3E %.5e %.5e %.5e %.5e %lf %lf %lf %lf %lf
 %lf %lf %lf %lf %lf %lf %lf %lf %lf %lf %lf %lf %lf %lf %lf
 %lf %lf %lf %lf %lf %lf %lf %lf %lf %lf %lf %lf %lf %lf %.3e
 %.3e %.3e %.3e %.2E %.2E %.2E %lf %lf %lf %lf %lf %lf\n",h, k, massbino,
 masswino,massgluino,muparameter,MA,Mh,NLSP,MNLSP, tanbeta,mchi1,Omega,amu,bsgnlo(&SMbsg),bsmumu(),
 SCcoeff*pA0[0]*pA0[0],SCcoeff*nA0[0]*nA0[0], Zn11, Zn12, Zn13, Zn14, heavyHiggs, mscl, mssl, msne, msel, msmr,
 msur, mser, mcha1, mchi2, mchi3, mstop1, mchi4, mcha2, mstau1, msb1, mstop2, msnm, msml, msdr, msg, msb2, msul,
 msdl, mssr, msul, mstau2, mscr, Atop, Abottom, Atau, Amu, LOm, Lmh, Lmchi1, LTOT, SpectdNdE(Etest, FluxA),
 SpectdNdE(Etest, FluxE), SpectdNdE(Etest, FluxP), deltatotal, Zv11, Zv12, Zu11, Zu12, msnl);
 else if (h>200000000 && h<400000000 && nw==0 && (Mh>123) && (Mh<127) && (Omega<0.13) &&
 (bsmumu()<4.7*pow(10,-9)) && (bsmumu()>2*pow(10,-9))  && (bsgnlo(&SMbsg)>3.29*pow(10,-4)) &&
 (bsgnlo(&SMbsg)<3.81*pow(10,-4)) && (Zinv<0.003) && (mcha1>103.5))

 else
 { p=floor(-100*log(LTOTP));
   rdvar=(rand() % p)*pow(10,-2)  + 1;

 if(LTOTP/rdvar<LTOT){massbinoP=massbino, masswinoP=masswino, massgluinoP=massgluino, muparameterP=muparameter,
 tanbetaP=tanbeta, MAP=MA, LHslepton1P=LHslepton1, LHslepton2P=LHslepton2, LHslepton3P=LHslepton3,
 RHselectronP=RHselectron, RHsmuonP=RHsmuon, RHstauP=RHstau, LHsquark1P=LHsquark1, LHsquark2P=LHsquark2,
 LHsquark3P=LHsquark3, RHupsquarkP=RHupsquark, RHcharmsquarkP=RHcharmsquark, RHtopsquarkP=RHtopsquark,
 RHdownsquarkP=RHdownsquark, RHstrangesquarkP=RHstrangesquark, RHbottomsquarkP=RHbottomsquark, AtopP=Atop,
 AbottomP=Abottom, AtauP=Atau, AmuP=Amu, LTOTP=LTOT,k++;
 if (LTOTP>LTmax) {LTmax=LTOTP;stuck=0;}
 else {stuck++;}
 if (h>0 && h<200000000 && nw==0 && (Mh>123) && (Mh<127) && (Omega<0.13) && (bsmumu()<4.7*pow(10,-9)) &&
 (bsmumu()>2*pow(10,-9))  && (bsgnlo(&SMbsg)>3.29*pow(10,-4)) && (bsgnlo(&SMbsg)<3.81*pow(10,-4)) &&
 (Zinv<0.003) && (mcha1>103.5))
 fprintf(f1,"%d %d %lf %lf %lf %lf %lf %lf %d %lf %lf %lf %lf
 %.5E %lf %.31E %.3E %.3E %.5e %.5e %.5e %.5e %lf %lf %lf %lf %lf
 %lf %lf %lf %lf %lf %lf %lf %lf %lf %lf %lf %lf %lf %lf %lf
 %lf %lf %lf %lf %lf %lf %lf %lf %lf %lf %lf %lf %lf %lf %.3e
  %.3e %.3e %.3e %.2E %.2E %.2E %lf %lf %lf %lf %lf %lf\n",h, k, massbino,
  masswino,massgluino,muparameter,MA,Mh,NLSP,MNLSP, tanbeta,mchi1,Omega,amu,bsgnlo(&SMbsg),bsmumu(),
```

```
 SCcoeff*pA0[0]*pA0[0],SCcoeff*nA0[0]*nA0[0], Zn11, Zn12, Zn13, Zn14, heavyHiggs, mscl, mssl, msne, msel, msmr,
 msur, mser, mcha1, mchi2, mchi3, mstop1, mchi4, mcha2, mstau1, msb1, mstop2, msnm, msml, msdr, msg, msb2, msul,
 msdl, mssr, msul, mstau2, mscr, Atop, Abottom, Atau, Amu, LOm, Lmh, Lmchi1, LTOT, SpectdNdE(Etest, FluxA),
 SpectdNdE(Etest, FluxE), SpectdNdE(Etest, FluxP), deltatotal, Zv11, Zv12, Zu11, Zu12,msnl);
else if (h>200000000 && h<400000000 && nw==0 && (Mh>123) && (Mh<127) && (Omega<0.13) && (bsmumu()<4.7*pow(10,-9))
&& (bsmumu()>2*pow(10,-9))  && (bsgnlo(&SMbsg)>3.29*pow(10,-4)) && (bsgnlo(&SMbsg)<3.81*pow(10,-4)) &&
(Zinv<0.003) && (mcha1>103.5))

}
else {stuck++;}//if likelihood was falling for every new set add stuck.
}
}

else if (LTOT<=lowest || warning==11 || warning==10 || stuck>=50){
assignValW("MG1",rand()%501);assignValW("MG2",rand()%1001);assignValW("MG3",rand()%2200+800);
assignValW("mu",(rand()%600001)*pow(10,-2)-3000);assignValW("tb",((rand()%5900)*pow(10,-2))+1);
assignValW("MH3",rand()%2700+300);assignValW("Ml1",rand()%3001);assignValW("Ml3",rand()%3001);
assignValW("Mr1",rand()%3001);assignValW("Mr3",rand()%3001);assignValW("Mq1",rand()%3001);
assignValW("Mq3",rand()%3001);assignValW("Mu1",rand()%3001);assignValW("Mu3",rand()%3001);
assignValW("Md1",rand()%3001);assignValW("Md3",rand()%3001);assignValW("At",rand()%20001-10000);
assignValW("Ab",rand()%20001-10000);assignValW("Al",rand()%20001-10000);assignValW("Am",0);

massbino=findValW("MG1");masswino=findValW("MG2");massgluino=findValW("MG3");muparameter=findValW("mu");
if(muparameter<0 && massbino>=masswino)
masswino=-1*masswino;
if(muparameter<0 && masswino>=massbino)
massbino=-1*massbino;
tanbeta=findValW("tb");MA=findValW("MH3");LHslepton1=findValW("Ml1");LHslepton2=LHslepton1;
LHslepton3=findValW("Ml3");RHselectron=findValW("Mr1");RHsmuon=RHselectron;RHstau=findValW("Mr3");
LHsquark1=findValW("Mq1");LHsquark2=LHsquark1;LHsquark3=findValW("Mq3");RHupsquark=findValW("Mu1");
RHcharmsquark=RHupsquark;RHtopsquark=findValW("Mu3");RHdownsquark=findValW("Md1");
RHstrangesquark=RHdownsquark;RHbottomsquark=findValW("Md3");Atop=findValW("At");Abottom=findValW("Ab");
Atau=findValW("Al");Amu=findValW("Am");

massbinoP=massbino; masswinoP=masswino; massgluinoP=massgluino; muparameterP=muparameter; tanbetaP=tanbeta;
MAP=MA; LHslepton1P=LHslepton1; LHslepton2P=LHslepton2; LHslepton3P=LHslepton3; RHselectronP=RHselectron;
RHsmuonP=RHsmuon; RHstauP=RHstau; LHsquark1P=LHsquark1; LHsquark2P=LHsquark2; LHsquark3P=LHsquark3;
RHupsquarkP=RHupsquark; RHcharmsquarkP=RHcharmsquark; RHtopsquarkP=RHtopsquark; RHdownsquarkP=RHdownsquark;
RHstrangesquarkP=RHstrangesquark; RHbottomsquarkP=RHbottomsquark; AtopP=Atop; AbottomP=Abottom; AtauP=Atau;
AmuP=Amu;stuck=0;warning=0;LTmax=lowest;LTOTP=lowest;continue;}
```

```
LTOT=lowest;

printf("LTOTP=%.8e\n",LTOTP);
printf("LTOTmax=%.8e\n",LTmax);
printf("stuck=%d\n",stuck);

//if point satisfied all constraints, change p19MSSM input parameters infinitesimally.
printf("==================================PROBING====================================");
while (rdsgn==0)
{rdsgn=(rand() % 3) - 1;}
massbino=massbinoP + rdsgn*(rand() % 10);rdsgn=0;

while (rdsgn==0)
{rdsgn=(rand() % 3) - 1;}
masswino=masswinoP + rdsgn*(rand() % 10);rdsgn=0;

while (rdsgn==0)
{rdsgn=(rand() % 3) - 1;}
massgluino=massgluinoP + rdsgn*(rand() % 10);rdsgn=0;

while (rdsgn==0)
{rdsgn=(rand() % 3) - 1;}
muparameter=muparameterP + rdsgn*(rand() % 10);rdsgn=0;

while (rdsgn==0)
{rdsgn=(rand() % 3) - 1;}
tanbeta=tanbetaP + rdsgn*(rand() % 3);rdsgn=0;

while (rdsgn==0)
{rdsgn=(rand() % 3) - 1;}
MA=MAP + rdsgn*(rand() % 10);rdsgn=0;

while (rdsgn==0)
{rdsgn=(rand() % 3) - 1;}
LHslepton1=LHslepton1P + rdsgn*(rand() % 10);rdsgn=0;

LHslepton2=LHslepton1;

while (rdsgn==0)
{rdsgn=(rand() % 3) - 1;}
LHslepton3=LHslepton3P + rdsgn*(rand() % 10);rdsgn=0;
```

```
while (rdsgn==0)
{rdsgn=(rand() % 3) - 1;}
RHselectron=RHselectronP + rdsgn*(rand() % 10);rdsgn=0;

RHsmuon=RHselectron;

while (rdsgn==0)
{rdsgn=(rand() % 3) - 1;}
RHstau=RHstauP + rdsgn*(rand() % 10);rdsgn=0;

while (rdsgn==0)
{rdsgn=(rand() % 3) - 1;}
LHsquark1=LHsquark1P + rdsgn*(rand() % 10);rdsgn=0;

LHsquark2=LHsquark1;

while (rdsgn==0)
{rdsgn=(rand() % 3) - 1;}
LHsquark3=LHsquark3P + rdsgn*(rand() % 10);rdsgn=0;

while (rdsgn==0)
{rdsgn=(rand() % 3) - 1;}
RHupsquark=RHupsquarkP + rdsgn*(rand() % 10);rdsgn=0;

RHcharmsquark=RHupsquark;

while (rdsgn==0)
{rdsgn=(rand() % 3) - 1;}
RHtopsquark=RHtopsquarkP + rdsgn*(rand() % 10);rdsgn=0;

while (rdsgn==0)
{rdsgn=(rand() % 3) - 1;}
RHdownsquark=RHdownsquarkP + rdsgn*(rand() % 10);rdsgn=0;

RHstrangesquark=RHdownsquark;

while (rdsgn==0)
{rdsgn=(rand() % 3) - 1;}
RHbottomsquark=RHbottomsquarkP + rdsgn*(rand() % 10);rdsgn=0;
```

```
while (rdsgn==0)
{rdsgn=(rand() % 3) - 1;}
Atop=AtopP + rdsgn*(rand() % 10);rdsgn=0;

while (rdsgn==0)
{rdsgn=(rand() % 3) - 1;}
Abottom=AbottomP + rdsgn*(rand() % 10);rdsgn=0;

while (rdsgn==0)
{rdsgn=(rand() % 3) - 1;}
Atau=AtauP + rdsgn*(rand() % 10)*pow(10,-1);rdsgn=0;

Amu=0;

assignValW("MG1",massbino);assignValW("MG2",masswino);assignValW("MG3",massgluino);assignValW("mu",muparameter);
assignValW("tb",tanbeta);assignValW("MH3",MA);assignValW("Ml1",LHsquark1);assignValW("Ml2",LHsquark2);
assignValW("Ml3",LHsquark3);assignValW("Mr1",RHselectron);assignValW("Mr2",RHsmuon);assignValW("Mr3",RHstau);
assignValW("Mq1",LHsquark1);assignValW("Mq2",LHsquark2);assignValW("Mq3",LHsquark3);assignValW("Mu1",RHupsquark);
assignValW("Mu2",RHcharmsquark);assignValW("Mu3",RHtopsquark);assignValW("Md1",RHdownsquark);
assignValW("Md2",RHstrangesquark);assignValW("Md3",RHbottomsquark);assignValW("At",Atop);
assignValW("Ab",Abottom);assignValW("Al",Atau);assignValW("Am",Amu);
   }
}
```

Appendix C

Derivation and interpretation of the one–loop effective potential at finite temperature

A derivation of the one–loop effective potential at finite temperature for bosons is given. As we will see, the finite temperature effective potential consists of the effective potential at $T = 0$ and a temperature dependent term. In this section, we will closely follow discussions laid out [57, 342].

From statistical mechanics, it is known that a thermal average of any set of operators $A...Z$ can by calculated by:

$$\langle A...Z \rangle_\beta = \frac{\mathrm{Tr}(e^{-\beta \hat{H}} A...Z)}{\mathrm{Tr} e^{-\beta \hat{H}}}, \tag{C.1}$$

where $\hat{H}$ is a Hamiltonian. By defining these operators in Schrödinger's picture, it is straightforward to show that propagators at finite temperature obey the same equations as those at zero temperature, with the exception that they are periodic in Euclidean time with period β [56, 57]. This implies that the expression for

effective potential at finite temperature can be obtained from the potential at $T = 0$ once the following replacements are done [56]:

$$\int \frac{d^4p}{(2\pi)^3} \to \frac{1}{\beta} \sum_{n=-\infty}^{\infty} \int \frac{d^3p}{(2\pi)^3} \qquad \text{and} \qquad p_0 \to \frac{2\pi n}{\beta}, \tag{C.2}$$

where the sum on the left hand side is for the Euclidean time component and integral remains for spatial coordinates. Taking expression that we derived in Eq. (2.43), and using $p^2 = p_0^2 + \mathbf{p}^2 \to (2\pi n/\beta)^2 + \mathbf{p}^2$ we finally get:

$$V_1^{\beta}(\phi_c) = \frac{1}{2\beta} \sum_{n=-\infty}^{\infty} \int \frac{d^3p}{(2\pi)^3} \ln\left(\frac{4\pi^2 n^2}{\beta^2} + E^2\right), \tag{C.3}$$

where $E^2 = \mathbf{p}^2 + m^2(\phi)$. For the ϕ^4 theory $m^2(\phi_c)$ is given in Eq. (2.34). To evaluate the sum, let us define:

$$v(E) \equiv \sum_{n=-\infty}^{\infty} \ln\left(\frac{4\pi^2 n^2}{\beta^2} + E^2\right), \tag{C.4}$$

which, after differentiating it with respect to energy, becomes:

$$\frac{\partial v(E)}{\partial E} = \sum_{n=-\infty}^{\infty} \frac{2E}{\frac{4\pi^2 n^2}{\beta^2} + E^2}. \tag{C.5}$$

Using the identity:

$$\sum_{n=1}^{\infty} \frac{y}{y^2 + n^2} = -\frac{1}{2y} + \frac{\pi}{2} + \frac{\pi e^{-2\pi y}}{1 - e^{-2\pi y}}, \tag{C.6}$$

Eq. (C.5) can be rewritten as:

$$\frac{\partial v(E)}{\partial E} = 2\beta\left(\frac{1}{2} + \frac{1}{e^{\beta E} - 1}\right). \tag{C.7}$$

Integrating it one gets:

$$v(E) = 2\beta\left(\frac{E}{2} + \frac{\ln(1-e^{-\beta E})}{\beta}\right) + \text{terms independent of } E. \tag{C.8}$$

Plugging this back into Eq. (C.3) we have:

$$V_1^{\beta}(\phi_c) = \int \frac{d^3p}{(2\pi)^3}\left(\frac{E}{2} + \frac{\ln(1-e^{-\beta E})}{\beta}\right). \tag{C.9}$$

The first integral is one–loop effective potential at $T = 0$. To see that we use identity from residue theorem:

$$-\frac{i}{2}\int_{-\infty}^{\infty}\frac{dy}{2\pi}\ln(-y^2+E^2-i\epsilon) = \frac{E}{2} + \text{infinite constant}, \tag{C.10}$$

where $y \equiv -\sqrt{E^2 - i\epsilon}$. The first integral can therefore be written as:

$$\int \frac{d^3p}{(2\pi)^3}\frac{E}{2} = -\frac{i}{2}\int\frac{d^4p}{(2\pi)^4}\ln(-p_0^2+E^2-i\epsilon). \tag{C.11}$$

After using a Wick rotation it becomes:

$$\int \frac{d^3p}{(2\pi)^3}\frac{E}{2} = \frac{1}{2}\int\frac{d^4p}{(2\pi)^4}\ln(p^2+m^2(\phi_c)), \tag{C.12}$$

which is the same as what we found in Eq. (2.35). To evaluate temperature dependent integral we define $x \equiv \beta p$, which allows to write:

$$\int d^3p = \int p^2\sin\theta d\theta d\phi = 4\pi\int p^2dp = \frac{4\pi}{\beta^3}\int dx x^2. \tag{C.13}$$

Finally, the temperature dependent one–loop contribution to the effective poten-

tial in Eq. (C.9) can then be expressed as:

$$V_1^{\beta}(\phi_c) = \frac{1}{2\pi^2\beta^4}\int_0^{\infty} dx x^2 \ln\left(1 - e^{-\sqrt{x^2+\beta^2 m^2(\phi_c)}}\right), \tag{C.14}$$

per bosonic degree of freedom. Just as it should be, the temperature dependent contribution to the total effective potential at the one–loop level switches off as $\beta = 1/T \to \infty$. This integral doesn't have a closed form solution, but in the high temperature limit can be expanded as [350]:

$$V_1^{\beta}(\phi_c) \backsimeq \frac{\pi^2 T^4}{90} + \frac{m^2(\phi_c)T^2}{24} + \ldots . \tag{C.15}$$

A calculation for fermions is analogous.

The generating functional of correlation functions at finite temperature, $Z^{\beta}[J]$, can be obtained from a corresponding generating functional at zero temperature, $Z[J]$, (which was first introduced in Section (2.4)) by taking into account that at finite temperatures we are dealing with fields which in Euclidean space are periodic in time i.e., $\phi(it = 0, \mathbf{x}) = \phi(it = \beta, \mathbf{x})$. As discussed in the beginning, this translates into making replacements in the standard path integral expression for $Z[J]$, as outlined in Eq. (C.2) [353]. After obtaining expression for $Z^{\beta}[J]$, the free energy of the scalar field can be calculated using a well known statistical mechanics relation:

$$F = -\frac{1}{\beta}\ln Z^{\beta}[J]. \tag{C.16}$$

A simple calculation of the free energy of field ϕ is given in refs. [353, 354], and turns out to be the same as the expression for the one–loop effective potential at finite temperature. Therefore, the effective potential of the scalar field at finite temperature is interpreted as a free energy of the that field. In thermal equilibrium, the free energy is at minimal with respect to all macroscopic parameters,

including the expectation value of the field ϕ. Hence, $\langle\phi\rangle$ is the minimum of the one–loop effective potential at finite temperature.

References

[1] The ATLAS Collaboration, ATLAS-CONF-2012-170. 1, 28, 129

[2] The CMS Collaboration, CMS-PAS-HIG-12-045. 1, 28, 129

[3] Y. Fukuda et al., Phys. Rev. Lett. **81**, 1158 (1998). 1, 31, 96

[4] B. T. Cleveland, T. Daily, R. Davis, Jr., J. R. Distel, K. Lande, C. K. Lee, P. S. Wildenhain and J. Ullman, Astrophys. J. **496**, 505 (1998). 1, 31

[5] R. Davis, Jr., D. S. Harmer and K. C. Hoffman, Phys. Rev. Lett. **20**, 1205 (1968). 1, 31

[6] A. H. Guth, Phys. Rev. D **23**, 347 (1981). 1, 4

[7] A. D. Linde, Phys. Lett. B **108**, 389 (1982). 1, 4

[8] A. Albrecht and P. J. Steinhardt, Phys. Rev. Lett. **48**, 1220 (1982). 1, 4

[9] F. Zwicky, 1933, Helv. Phys. Acta 6, 110 1, 26, 90

[10] Y. Sofue and V. Rubin, Ann. Rev. Astron. Astrophys. **39**, 137 (2001) [astro-ph/0010594]. 1, 2, 26, 90

[11] A. D. Sakharov, Pisma Zh. Eksp. Teor. Fiz. **5**, 32 (1967) [JETP Lett. **5**, 24 (1967)] [Sov. Phys. Usp. **34**, 392 (1991)] [Usp. Fiz. Nauk **161**, 61 (1991)]. 1, 28, 164

[12] B. Fields and S. Sarkar, astro-ph/0601514. 1

[13] G. Degrassi, S. Di Vita, J. Elias-Miro, J. R. Espinosa, G. F. Giudice, G. Isidori and A. Strumia, JHEP **1208**, 098 (2012) [arXiv:1205.6497 [hep-ph]]. 1, 23, 24, 25

[14] R. D. Peccei and H. R. Quinn, Phys. Rev. Lett. **38**, 1440 (1977). 1, 30, 100

[15] F. Wilczek, Phys. Rev. Lett. **40**, 279 (1978). 1

[16] N. Kaiser and G. Squires, Astrophys. J. **404**, 441 (1993). 2, 27, 91

[17] P. Schneider, Mon. Not. Roy. Astron. Soc. **283**, 837 (1996) [astro-ph/9601039]. 2, 27, 91

[18] D. Clowe, M. Bradac, A. H. Gonzalez, M. Markevitch, S. W. Randall, C. Jones and D. Zaritsky, Astrophys. J. **648**, L109 (2006) [astro-ph/0608407]. 2, 27, 91

[19] N. A. Bahcall and L. M. Lubin, Astrophys. J. **426**, 513 (1994) [astro-ph/9311061]. 2, 26, 91

[20] S. F. Kasun and A. E. Evrard, Astrophys. J. **629**, 781 (2005) [astro-ph/0408056]. 2, 26, 91

[21] Struble, M., & Rood, H. 1991, ApJS, 77, 363 2, 26

[22] M. Markevitch, A. H. Gonzalez, L. David, A. Vikhlinin, S. Murray, W. Forman, C. Jones and W. Tucker, Astrophys. J. **567**, L27 (2002) [astro-ph/0110468]. 2, 27, 91

[23] M. Markevitch, A. H. Gonzalez, D. Clowe, A. Vikhlinin, L. David, W. Forman, C. Jones and S. Murray *et al.*, Astrophys. J. **606**, 819 (2004) [astro-ph/0309303]. 2, 27, 91

[24] S. W. Randall, M. Markevitch, D. Clowe, A. H. Gonzalez and M. Bradac, Astrophys. J. **679**, 1173 (2008) [arXiv:0704.0261 [astro-ph]]. 2, 27, 91

[25] G. W. Angus, H. Shan, H. Zhao and B. Famaey, Astrophys. J. **654**, L13 (2007) [astro-ph/0609125]. 3, 92

[26] G. R. Blumenthal, S. M. Faber, J. R. Primack and M. J. Rees, Nature **311**, 517 (1984). 3, 27, 32, 96

[27] A. Jenkins *et al.* [Virgo Consortium Collaboration], Astrophys. J. **499**, 20 (1998) [astro-ph/9709010]. 3, 27, 96

[28] R. Allahverdi, K. Enqvist, J. Garcia-Bellido and A. Mazumdar, Phys. Rev. Lett. **97**, 191304 (2006) [hep-ph/0605035]. 4, 146, 147, 148, 149

[29] R. Allahverdi, K. Enqvist, J. Garcia-Bellido, A. Jokinen and A. Mazumdar, JCAP **0706**, 019 (2007) [hep-ph/0610134]. 4, 146, 147, 148, 149, 150, 152

[30] M. S. Carena and C. E. M. Wagner, hep-ph/9704347. 4, 28

[31] https://twiki.cern.ch/twiki/bin/view/AtlasPublic/SupersymmetryPublicResults 4, 5, 134, 179

[32] https://twiki.cern.ch/twiki/bin/view/CMSPublic/PhysicsResultsSUS 4, 5, 134, 179

[33] N. Cabibbo, Phys. Rev. Lett. **10**, 531 (1963). 4, 29

[34] M. Kobayashi and T. Maskawa, Prog. Theor. Phys. **49**, 652 (1973). 4, 29

[35] S. Ambrosanio and B. Mele, Phys. Rev. D **55**, 1399 (1997) [Erratum-ibid. D **56**, 3157 (1997)] [hep-ph/9609212]. 5

[36] S. Ambrosanio, G. L. Kane, G. D. Kribs, S. P. Martin and S. Mrenna, Phys. Rev. D **55**, 1372 (1997) [hep-ph/9607414]. 5

[37] S. P. Martin, In *Kane, G.L. (ed.): Perspectives on supersymmetry II* 1-153 [hep-ph/9709356]. 5, 47, 48, 49, 50, 51, 53, 54, 55, 56, 57, 58, 59, 60, 61, 63, 64, 65, 66, 67, 70, 71, 72, 74, 75, 77, 78, 81, 82, 83, 86, 87, 88, 98, 122

[38] H. Baer, C. h. Chen, M. Drees, F. Paige and X. Tata, Phys. Rev. Lett. **79**, 986 (1997) [Erratum-ibid. **80**, 642 (1998)] [hep-ph/9704457]. 5

[39] G. L. Bayatian *et al.* [CMS Collaboration], J. Phys. G **34**, 995 (2007). 5

[40] G. Aad *et al.* [ATLAS Collaboration], Phys. Lett. B **710**, 67 (2012) [arXiv:1109.6572 [hep-ex]]. 5

[41] S. Abdullin *et al.* [CMS Collaboration], J. Phys. G **28**, 469 (2002) [hep-ph/9806366]. 5

[42] J. Abdallah *et al.* [DELPHI Collaboration], Eur. Phys. J. C **38**, 395 (2005) [hep-ex/0406019]. 5, 179

[43] CDF Collaboration, http://www-cdf.fnal.gov/physics/exotic/exotic.html 5, 134

[44] D0 Collaboration, http://www-d0.fnal.gov/d0_publications/d0_pubs_list_runII_bytopic.html 5, 134

[45] C. Cheung, L. J. Hall, D. Pinner and J. T. Ruderman, JHEP **1305**, 100 (2013) [arXiv:1211.4873 [hep-ph]]. 5

[46] S. L. Glashow, Nucl. Phys. **22**, 579 (1961). 7

[47] S. Weinberg, Phys. Rev. Lett. **19**, 1264 (1967). 7

[48] A. Salam, Conf. Proc. C **680519**, 367 (1968). 7

[49] F. Bezrukov, M. Y. Kalmykov, B. A. Kniehl and M. Shaposhnikov, JHEP **1210**, 140 (2012) [arXiv:1205.2893 [hep-ph]]. 8

[50] F. Jegerlehner, Acta Phys. Polon. B **45**, 1167 (2014) [arXiv:1304.7813 [hep-ph]]. 8

[51] P. W. Higgs, Phys. Lett. **12**, 132 (1964). 10, 11

[52] F. Englert and R. Brout, Phys. Rev. Lett. **13**, 321 (1964). 10

[53] G. S. Guralnik, C. R. Hagen and T. W. B. Kibble, Phys. Rev. Lett. **13**, 585 (1964). 10

[54] http://pdg.lbl.gov/2014/reviews/rpp2014-rev-phys-constants.pdf 12

[55] S. R. Coleman and E. J. Weinberg, Phys. Rev. D **7**, 1888 (1973). 13, 14, 15, 21, 22

[56] M. Sher, Phys. Rept. **179** (1989) 273. 13, 14, 20, 21, 208, 209

[57] M. Quiros, hep-ph/9901312. 13, 14, 16, 18, 164, 169, 170, 173, 174, 208

[58] R. Clarkson and D. McKeon, Lectures on Quantum Field Theory, 266 (2003) 13

[59] V. Branchina, E. Messina and A. Platania, arXiv:1407.4112 [hep-ph]. 24

[60] Y. Tang, Mod. Phys. Lett. A **28**, 1330002 (2013) [arXiv:1301.5812 [hep-ph]]. 25

[61] A. Kobakhidze and A. Spencer-Smith, JHEP **1308**, 036 (2013) [arXiv:1305.7283 [hep-ph]]. 24

[62] E. Witten, Nucl. Phys. B **188** (1981) 513. 25, 48

[63] S. Dimopoulos and H. Georgi, Nucl. Phys. B **193** (1981) 150. 25, 48

[64] R. K. Kaul and P. Majumdar, Nucl. Phys. B **199** (1982) 36. 25, 48

[65] P. J. E. Peebles, Astrophys. J. **263**, L1 (1982). 27, 32

[66] P. Gondolo and G. Gelmini, Nucl. Phys. B **360**, 145 (1991). 27, 102, 106

[67] K. Griest and D. Seckel, Phys. Rev. D **43**, 3191 (1991). 27, 106, 107

[68] V. A. Kuzmin, V. A. Rubakov and M. E. Shaposhnikov, Phys. Lett. **155B** 1 (1985). 28

[69] P. B. Arnold and L. D. McLerran, Phys. Rev. D **36**, 581 (1987). 28

[70] V. A. Rubakov and M. E. Shaposhnikov, Usp. Fiz. Nauk **166**, 493 (1996) [Phys. Usp. **39**, 461 (1996)] [hep-ph/9603208]. 28

[71] P. Huet, hep-ph/9406301. 29

[72] G. Baym, D. Bodeker and L. D. McLerran, Phys. Rev. D **53**, 662 (1996) [hep-ph/9507429]. 29

[73] G. Baym and H. Heiselberg, Phys. Rev. D **56**, 5254 (1997) [astro-ph/9704214]. 29

[74] D.L. Book, NRL Plasma Formulary, Naval Research Laboratory, Washington (1990). 29

[75] J. H. Christenson, J. W. Cronin, V. L. Fitch and R. Turlay, Phys. Rev. Lett. **13**, 138 (1964). 30

[76] K.A. Olive et al. (Particle Data Group), Chin. Phys. C, **38**, 090001 (2014). 30

[77] B. Aubert *et al.* [BaBar Collaboration], Phys. Rev. Lett. **87**, 091801 (2001) [hep-ex/0107013]. 30

[78] D. Buskulic *et al.* [ALEPH Collaboration], Phys. Lett. B **307**, 194 (1993) [Phys. Lett. B **325**, 537 (1994)]. 30

[79] A. Poluektov *et al.*, [Belle Collab.], Phys. Rev. **D 81**, 112002 (2010). 30

[80] R. Aaij *et al.*, [LHCb Collab.], Phys. Lett. **B712**, 203 (2012). 30

[81] R. Aaij *et al.*, [LHCb Collab.], Phys. Rev. Lett. **110**, 221601 (2013). 30

[82] M. Pospelov and A. Ritz, Nucl. Phys. B **573**, 177 (2000) [hep-ph/9908508]. 30

[83] S. A. Thomas, F. B. Abdalla and O. Lahav, Phys. Rev. Lett. **105**, 031301 (2010) [arXiv:0911.5291 [astro-ph.CO]]. 31, 96

[84] P. Minkowski, Phys. Lett. B **67**, 421 (1977). 31

[85] R. N. Mohapatra and G. Senjanovic, Phys. Rev. Lett. **44**, 912 (1980). 31

[86] W. Konetschny and W. Kummer, Phys. Lett. B **70**, 433 (1977). 31

[87] T. P. Cheng and L. F. Li, Phys. Rev. D **22**, 2860 (1980). 31

[88] G. Lazarides, Q. Shafi and C. Wetterich, Nucl. Phys. B **181**, 287 (1981). 31

[89] J. Schechter and J. W. F. Valle, Phys. Rev. D **22**, 2227 (1980). 31

[90] R. Foot, H. Lew, X. G. He and G. C. Joshi, Z. Phys. C **44**, 441 (1989). 31

[91] P. A. R. Ade *et al.* [Planck Collaboration], arXiv:1303.5076 [astro-ph.CO]. 32, 33, 36, 44, 46, 90, 126, 129, 151, 155, 157, 158, 181, 187

[92] R. A. Alpher, H. Bethe and G. Gamow, Phys. Rev. **73**, 803 (1948). 32

[93] S. Sarkar, Rept. Prog. Phys. **59**, 1493 (1996) [hep-ph/9602260]. 32

[94] S. Burles, K. M. Nollett and M. S. Turner, Astrophys. J. **552**, L1 (2001) [astro-ph/0010171]. 32

[95] A. G. Riess *et al.* [Supernova Search Team Collaboration], Astron. J. **116**, 1009 (1998) [astro-ph/9805201]. 32

[96] S. Perlmutter *et al.* [Supernova Cosmology Project Collaboration], Astrophys. J. **517**, 565 (1999) [astro-ph/9812133]. 32

[97] A. G. Riess, L. Macri, S. Casertano, H. Lampeitl, H. C. Ferguson, A. V. Filippenko, S. W. Jha and W. Li *et al.*, Astrophys. J. **730**, 119 (2011) [Erratum-ibid. **732**, 129 (2011)] [arXiv:1103.2976 [astro-ph.CO]]. 32, 36

[98] Albert Einstein. *The Foundation of the General Theory of Relativity.* Annalen Phys.,**49**:769-822, 1916. 33

[99] A. Friedmann, Z. Phys. **10**, 377 (1922). 33

[100] H. P. Robertson, Rev. Mod. Phys. **5**, 62 (1933); 33

[101] A. G. Walker, J. London Math. Soc. **19**, 219 (1944). 33

[102] E. W. Kolb, (Ed.) and M. S. Turner, (Ed.), The Early Universe. Reprints, REDWOOD CITY, USA: ADDISON-WESLEY (1988) 719 P. (FRONTIERS IN PHYSICS, 70); 34, 100, 102, 104, 105, 173

[103] G. Hinshaw *et al.* [WMAP Collaboration], Astrophys. J. Suppl. **208**, 19 (2013) [arXiv:1212.5226 [astro-ph.CO]]. 36

[104] A. A. Costa, X. D. Xu, B. Wang, E. G. M. Ferreira and E. Abdalla, Phys. Rev. D **89**, 103531 (2014) [arXiv:1311.7380 [astro-ph.CO]]. 36

[105] V. Salvatelli, N. Said, M. Bruni, A. Melchiorri and D. Wands, Phys. Rev. Lett. **113**, no. 18, 181301 (2014) [arXiv:1406.7297 [astro-ph.CO]]. 36

[106] D. G. York *et al.* [SDSS Collaboration], Astron. J. **120**, 1579 (2000) [astro-ph/0006396]. 36

[107] Y. B. Zeldovich and M. Y. Khlopov, Phys. Lett. B **79**, 239 (1978). 37

[108] J. Preskill, Phys. Rev. Lett. **43**, 1365 (1979). 37

[109] A. R. Liddle and D. H. Lyth, Cosmological inflation and large-scale structure, Cambridge University Press (2000). 40, 41, 42, 43, 44, 46

[110] A. R. Liddle and D. H. Lyth, Phys. Rept. **231**, 1 (1993) [astro-ph/9303019]. 40, 41, 42, 43, 44, 46

[111] T. S. Bunch and P. C. W. Davies, Proc. Roy. Soc. Lond. A **360**, 117 (1978). 42

[112] D. Baumann, arXiv:0907.5424 [hep-th]. 42

[113] A. R. Liddle and D. H. Lyth, Phys. Lett. B **291**, 391 (1992) [astro-ph/9208007]. 44

[114] E. R. Harrison, Phys. Rev. D **1**, 2726 (1970). 44

[115] Ya.B. Zeldovich, Mon. Not. R. Astron. Soc. 160, **1** (1972). 44

[116] R. Haag, J. T. Lopuszanski and M. Sohnius, Nucl. Phys. B **88**, 257 (1975). 49

[117] J. Wess and J. Bagger, Supersymmetry and supergravity, Princeton, USA: Univ. Pr. (1992) 259 p 49

[118] Poincaré, Henri, Sur la dynamique de le électron, Rendiconti del Circolo matematico di Palermo **21**: 129-176 (1905/6). 50

[119] F. Quevedo, S. Krippendorf and O. Schlotterer, arXiv:1011.1491 [hep-th]. 50, 51

[120] H. P. Nilles, Phys. Rept. **110**, 1 (1984). 50, 51, 71, 152

[121] P. Fayet, Phys. Lett. B **69**, 489 (1977). 53

[122] E. Witten, Nucl. Phys. B **188**, 513 (1981). 53

[123] M. Dine, A. E. Nelson, Y. Nir and Y. Shirman, Phys. Rev. D **53**, 2658 (1996) [hep-ph/9507378]. 53

[124] A. Mazumdar and J. Rocher, Phys. Rept. **497**, 85 (2011) [arXiv:1001.0993 [hep-ph]]. 68, 69

[125] M. Dine, L. Randall and S. D. Thomas, Nucl. Phys. B **458**, 291 (1996) [hep-ph/9507453]. 68, 147

[126] M. Dine, L. Randall and S. D. Thomas, Phys. Rev. Lett. **75**, 398 (1995) [hep-ph/9503303]. 68

[127] T. Gherghetta, C. F. Kolda and S. P. Martin, Nucl. Phys. B **468**, 37 (1996) [hep-ph/9510370]. 68, 147, 148

[128] A. H. Chamseddine, R. L. Arnowitt and P. Nath, Phys. Rev. Lett. **49**, 970 (1982). 71, 84

[129] R. Barbieri, S. Ferrara and C. A. Savoy, Phys. Lett. B **119**, 343 (1982). 71, 84

[130] L. J. Hall, J. D. Lykken and S. Weinberg, Phys. Rev. D **27**, 2359 (1983). 71, 84

[131] M. Dine and W. Fischler, Phys. Lett. B **110**, 227 (1982); 72

[132] C.R. Nappi and B.A. Ovrut, Phys.Lett. B **113**, 175 (1982); 72

[133] L. Alvarez-Gaum e, M. Claudson and M. B. Wise, Nucl. Phys. B **207**,96 (1982). 72

[134] L. Randall and R. Sundrum, Nucl. Phys. B **557**, 79 (1999) [hep-th/9810155]. 73

[135] G. F. Giudice, M. A. Luty, H. Murayama and R. Rattazzi, JHEP **9812**, 027 (1998) [hep-ph/9810442]. 73

[136] http://acfahep.kek.jp/acfareport/node66.html 73

[137] A. Arbey, M. Battaglia, A. Djouadi, F. Mahmoudi and J. Quevillon, Phys. Lett. B **708**, 162 (2012) [arXiv:1112.3028 [hep-ph]]. 73

[138] P. Grothaus, M. Lindner and Y. Takanishi, arXiv:1207.4434 [hep-ph]. 75

[139] M. Perelstein and C. Spethmann, In *Karlsruhe 2007, SUSY 2007* 358-361 [arXiv:0710.4148 [hep-ph]]. 75

[140] J. L. Feng, K. T. Matchev and T. Moroi, Phys. Rev. D **61**, 075005 (2000) [hep-ph/9909334]. 76

[141] J. L. Feng, K. T. Matchev and T. Moroi, Phys. Rev. Lett. **84**, 2322 (2000) [hep-ph/9908309]. 76

[142] A. Djouadi, Phys. Rept. **459**, 1 (2008) [hep-ph/0503173]. 79, 80

[143] A. Arbey, M. Battaglia, A. Djouadi and F. Mahmoudi, JHEP **1209**, 107 (2012) [arXiv:1207.1348 [hep-ph]]. 79, 80

[144] H. E. Haber, hep-ph/9505240. 79

[145] J. F. Gunion, A. Stange and S. Willenbrock, In *Barklow, T.L. (ed.) et al.: Electroweak symmetry breaking and new physics at the TeV scale* 23-145 [hep-ph/9602238]. 79

[146] M. Drees, R. Godbole and P. Roy. Theory and phenomenology of sparticles: An account of four-dimensional N=1 supersymmetry in high energy physics - 2004. World Scientific. (2004) 555 p. 83

[147] http://lepsusy.web.cern.ch/lepsusy/www/inos_moriond01/charginos_pub.html 83, 127, 129

[148] M. Drees and M. M. Nojiri, Phys. Rev. D **47**, 376 (1993) [hep-ph/9207234]. 84

[149] H. Baer and M. Brhlik, Phys. Rev. D **53**, 597 (1996) [hep-ph/9508321]. 84

[150] J. R. Ellis, T. Falk, K. A. Olive and M. Schmitt, Phys. Lett. B **388**, 97 (1996) [hep-ph/9607292]. 84

[151] J. R. Ellis, T. Falk, G. Ganis, K. A. Olive and M. Srednicki, Phys. Lett. B **510**, 236 (2001) [hep-ph/0102098]. 84

[152] K. A. Olive, J. Phys. Conf. Ser. **315**, 012021 (2011) [arXiv:1009.0232 [hep-ph]]. 84, 85

[153] J. Ellis, K. A. Olive and P. Sandick, New J. Phys. **11**, 105015 (2009) [arXiv:0905.0107 [hep-ph]]. 85

[154] J. R. Ellis, T. Falk, K. A. Olive and Y. Santoso, Nucl. Phys. B **652**, 259 (2003) [hep-ph/0210205]. 85

[155] J. R. Ellis, K. A. Olive and Y. Santoso, Phys. Lett. B **539**, 107 (2002) [hep-ph/0204192]. 85

[156] U. Ellwanger, C. Hugonie and A. M. Teixeira, Phys. Rept. **496**, 1 (2010) [arXiv:0910.1785 [hep-ph]] 87, 88, 128, 129

[157] D. J. Miller, R. Nevzorov and P. M. Zerwas, Nucl. Phys. B **681**, 3 (2004) [hep-ph/0304049]. 87

[158] R. Mayle, J. R. Wilson, J. R. Ellis, K. A. Olive, D. N. Schramm and G. Steigman, Phys. Lett. B **203**, 188 (1988). 87

[159] G. G. Raffelt, Phys. Rept. **198**, 1 (1990). 87

[160] R. Barbieri, L. J. Hall, A. Y. Papaioannou, D. Pappadopulo and V. S. Rychkov, JHEP **0803**, 005 (2008) [arXiv:0712.2903 [hep-ph]]. 87

[161] J. E. Kim and G. Carosi, Rev. Mod. Phys. **82**, 557 (2010) [arXiv:0807.3125 [hep-ph]]. 87

[162] A. Vilenkin, Phys. Rept. **121**, 263 (1985). 88

[163] S. A. Abel, S. Sarkar and P. L. White, Nucl. Phys. B **454**, 663 (1995) [hep-ph/9506359]. 88

[164] C. Panagiotakopoulos and K. Tamvakis, Phys. Lett. B **446**, 224 (1999) [hep-ph/9809475]. 88

[165] M. Carena, N. R. Shah and C. E. M. Wagner, Phys. Rev. D **85**, 036003 (2012) [arXiv:1110.4378 [hep-ph]]. 88, 177

[166] K. G. Begeman, Astron. Astrophys. **223**, 47 (1989). 91

[167] [**?**] 92

[168] Ya. B. Zel'dovich, Zh. Eksp. Teor. Fiz. **48**, 986 (1965); Ya. B. Zel'dovich, L. B. Okun, and S.B. Pikelner, Usp. Fiz. Nauk, **84**, 113 (1965); H. -Y. Chiu. Phys. Rev. Lett. **17**, 712 (1966). 93

[169] http://ned.ipac.caltech.edu/level5/Sept05/Gondolo/Gondolo2.html 93

[170] S. Profumo, arXiv:1301.0952 [hep-ph]. 94, 102, 117

[171] X. -l. Chen, M. Kamionkowski and X. -m. Zhang, Phys. Rev. D **64**, 021302 (2001) [astro-ph/0103452]. 94

[172] A. M. Green, S. Hofmann and D. J. Schwarz, JCAP **0508**, 003 (2005) [astro-ph/0503387]. 94

[173] I. M. Shoemaker, Phys. Dark Univ. **2**, no. 3, 157 (2013) [arXiv:1305.1936 [hep-ph]]. 94

[174] F. -Y. Cyr-Racine, S. Profumo and K. Sigurdson, Phys. Rev. D **80** (2009) 081302 [arXiv:0904.3933 [astro-ph.CO]]. 94

[175] N. Arkani-Hamed, A. Delgado and G. F. Giudice, Nucl. Phys. B **741**, 108 (2006) [hep-ph/0601041]. 95, 135, 137

[176] P. A. R. Ade *et al.* [Planck Collaboration], arXiv:1303.5082 [astro-ph.CO]. 95

[177] R. Bernabei *et al.* [DAMA Collaboration], Eur. Phys. J. C **56**, 333 (2008) [arXiv:0804.2741 [astro-ph]]. 95, 111, 113, 114, 129

[178] R. Bernabei *et al.* [DAMA and LIBRA Collaborations], Eur. Phys. J. C **67**, 39 (2010) [arXiv:1002.1028 [astro-ph.GA]]. 95, 111, 114, 129, 182

[179] C. E. Aalseth *et al.* [CoGeNT Collaboration], Phys. Rev. Lett. **106**, 131301 (2011) [arXiv:1002.4703 [astro-ph.CO]]. 95, 111, 113, 129, 182

[180] G. Angloher, M. Bauer, I. Bavykina, A. Bento, C. Bucci, C. Ciemniak, G. Deuter and F. von Feilitzsch *et al.*, Eur. Phys. J. C **72**, 1971 (2012) [arXiv:1109.0702 [astro-ph.CO]]. 95, 111, 115, 129, 182

[181] R. Agnese *et al.* [CDMS Collaboration], Phys. Rev. Lett. **111**, 251301 (2013) [arXiv:1304.4279 [hep-ex]]. 95, 111

[182] R. Becker-Szendy, C. B. Bratton, D. Casper, S. T. Dye, W. Gajewski, M. Goldhaber, T. J. Haines and P. Halverson *et al.*, Phys. Rev. D **46**, 3720 (1992). 97

[183] K. S. Hirata *et al.* [Kamiokande-II Collaboration], Phys. Lett. B **280**, 146 (1992). 97

[184] M. Ambrosio *et al.* [MACRO Collaboration], Eur. Phys. J. C **36**, 323 (2004). 97

[185] G. L. Fogli, E. Lisi and A. Marrone, Phys. Rev. D **64**, 093005 (2001) [hep-ph/0105139]. 97

[186] A. Dighe and S. Ray, Phys. Rev. D **76**, 113001 (2007) [arXiv:0709.0383 [hep-ph]]. 97

[187] A. Merle, Int. J. Mod. Phys. D **22**, 1330020 (2013) [arXiv:1302.2625 [hep-ph]]. 97

[188] A. Boyarsky, D. Malyshev, A. Neronov and O. Ruchayskiy, Mon. Not. Roy. Astron. Soc. **387**, 1345 (2008) 97

[189] A. Boyarsky, O. Ruchayskiy, D. Iakubovskyi and J. Franse, arXiv:1402.4119 [astro-ph.CO]. 98, 121

[190] E. Bulbul, M. Markevitch, A. Foster, R. K. Smith, M. Loewenstein and S. W. Randall, arXiv:1402.2301 [astro-ph.CO]. 98, 121

[191] T. Falk, K. A. Olive and M. Srednicki, Phys. Lett. B **339**, 248 (1994) [hep-ph/9409270]. 98

[192] G. Belanger, J. Da Silva and A. Pukhov, JCAP **1112**, 014 (2011) [arXiv:1110.2414 [hep-ph]]. 98

[193] R. Allahverdi, B. Dutta and A. Mazumdar, Phys. Rev. Lett. **99**, 261301 (2007) [arXiv:0708.3983 [hep-ph]]. 98

[194] R. Allahverdi, B. Dutta and K. Sinha, Phys. Rev. D **86**, 095016 (2012) [arXiv:1208.0115 [hep-ph]]. 99

[195] T. Moroi, hep-ph/9503210. 99

[196] H. Baer, arXiv:1310.1859 [hep-ph]. 100

[197] T. Appelquist, H. -C. Cheng and B. A. Dobrescu, Phys. Rev. D **64**, 035002 (2001) [hep-ph/0012100]. 101

[198] K. Kong and K. T. Matchev, JHEP **0601**, 038 (2006) [hep-ph/0509119]. 101

[199] W. Hu, R. Barkana and A. Gruzinov, Phys. Rev. Lett. **85**, 1158 (2000) [astro-ph/0003365]. 101

[200] C. Boehm and P. Fayet, Nucl. Phys. B **683**, 219 (2004) [hep-ph/0305261]. 101

[201] H. M. Hodges, Phys. Rev. D **47**, 456 (1993). 101

[202] R. Foot, Phys. Rev. D **78**, 043529 (2008) [arXiv:0804.4518 [hep-ph]]. 101

[203] J. L. Feng, A. Rajaraman and F. Takayama, Phys. Rev. Lett. **91**, 011302 (2003) [hep-ph/0302215]. 101

[204] J. L. Feng, A. Rajaraman and F. Takayama, Phys. Rev. D **68**, 063504 (2003) [hep-ph/0306024]. 101

[205] E. W. Kolb, D. J. H. Chung and A. Riotto, In *Heidelberg 1998, Dark matter in astrophysics and particle physics 1998* 592-614 [hep-ph/9810361]. 101

[206] D. J. H. Chung, P. Crotty, E. W. Kolb and A. Riotto, Phys. Rev. D **64**, 043503 (2001) [hep-ph/0104100]. 101

[207] A. Kusenko and M. E. Shaposhnikov, Phys. Lett. B **418**, 46 (1998) [hep-ph/9709492]. 101

[208] A. Kusenko, V. Kuzmin, M. E. Shaposhnikov and P. G. Tinyakov, Phys. Rev. Lett. **80**, 3185 (1998) [hep-ph/9712212]. 101

[209] K. Enqvist and J. McDonald, Phys. Lett. B **440**, 59 (1998) [hep-ph/9807269]. 101

[210] D. N. Spergel and P. J. Steinhardt, Phys. Rev. Lett. **84**, 3760 (2000) [astro-ph/9909386]. 101

[211] J. R. Ellis, G. B. Gelmini, J. L. Lopez, D. V. Nanopoulos and S. Sarkar, Nucl. Phys. B **373**, 399 (1992). 101

[212] K. Benakli, J. R. Ellis and D. V. Nanopoulos, Phys. Rev. D **59**, 047301 (1999) [hep-ph/9803333]. 101

[213] P. H. Frampton, M. Kawasaki, F. Takahashi and T. T. Yanagida, JCAP **1004**, 023 (2010) [arXiv:1001.2308 [hep-ph]]. 101

[214] M. R. S. Hawkins, Mon. Not. Roy. Astron. Soc. **415**, 2744 (2011) [arXiv:1106.3875 [astro-ph.CO]]. 101

[215] K. M. Belotsky *et al.*, Mod. Phys. Lett. A **29**, 1440005 (2014) [arXiv:1410.0203 [astro-ph.CO]]. 101

[216] http://home.physics.ucla.edu/ arisaka/home/Dark_Matter/files/dm-candidates.png 101

[217] T. Schwetz-Mangold talk "The Dark side of the Universe", MPIK Heidelberg, ISAPP 2011. 104, 105

[218] B. Dutta, arXiv:1403.6217 [hep-ph]. 108

[219] G. Aad *et al.* [ATLAS Collaboration], Phys. Rev. Lett. **109**, 211802 (2012) [arXiv:1208.1447 [hep-ex]]. 108, 109

[220] G. Aad *et al.* [ATLAS Collaboration], arXiv:1403.5294 [hep-ex]. 110, 111

[221] G. Aad *et al.* [ATLAS Collaboration], arXiv:1403.4853 [hep-ex]. 108

[222] R. Agnese *et al.* [CDMS Collaboration], Phys. Rev. D **88**, 031104 (2013) [arXiv:1304.3706 [astro-ph.CO]]. 111, 129, 182

[223] E. Aprile *et al.* [XENON100 Collaboration], Phys. Rev. Lett. **109**, 181301 (2012) [arXiv:1207.5988 [astro-ph.CO]]. 111, 113, 129

[224] D. S. Akerib *et al.* [LUX Collaboration], arXiv:1310.8214 [astro-ph.CO]. 111, 129

[225] P. Cushman *et al.*, arXiv:1310.8327 [hep-ex]. 112

[226] G. Angloher *et al.* [CRESST Collaboration], arXiv:1509.01515 [astro-ph.CO]. 112, 115, 116

[227] J. L. Feng, J. Kumar, D. Marfatia and D. Sanford, Phys. Lett. B **703**, 124 (2011) [arXiv:1102.4331 [hep-ph]]. 112, 113, 143

[228] J. Angle *et al.* [XENON10 Collaboration], Phys. Rev. Lett. **107**, 051301 (2011) [Phys. Rev. Lett. **110**, 249901 (2013)], 10.1103/PhysRevLett.107.051301 [arXiv:1104.3088 [astro-ph.CO]]. 113

[229] D. S. Akerib *et al.* [CDMS Collaboration], Phys. Rev. D **82**, 122004 (2010) [arXiv:1010.4290 [astro-ph.CO]]. 113

[230] Z. Ahmed *et al.* [CDMS-II Collaboration], Phys. Rev. Lett. **106** (2011) 131302 [arXiv:1011.2482 [astro-ph.CO]]. 113

[231] M. C. Smith, G. R. Ruchti, A. Helmi, R. F. G. Wyse, J. P. Fulbright, K. C. Freeman, J. F. Navarro and G. M. Seabroke *et al.*, Mon. Not. Roy. Astron. Soc. **379**, 755 (2007) [astro-ph/0611671]. 113, 127

[232] K.A. Drukier et al., Phys. Rev. D **33** (1986) 3495; K. Freese et al., Phys. Rev. D **37** (1988) 3388. 113

[233] N. Fornengo, R. A. Lineros, M. Regis and M. Taoso, JCAP **1201**, 005 (2012) [arXiv:1110.4337 [astro-ph.GA]]. 117

[234] T. Delahaye, R. Lineros, F. Donato, N. Fornengo and P. Salati, Phys. Rev. D **77**, 063527 (2008) [arXiv:0712.2312 [astro-ph]]. 117

[235] T. Lacroix, C. Boehm and J. Silk, Phys. Rev. D **89**, 063534 (2014) [arXiv:1311.0139 [astro-ph.HE]]. 117

[236] O. Adriani *et al.* [PAMELA Collaboration], Nature **458**, 607 (2009) [arXiv:0810.4995 [astro-ph]]. 117, 119

[237] T. Delahaye, F. Donato, N. Fornengo, J. Lavalle, R. Lineros, P. Salati and R. Taillet, Astron. Astrophys. **501**, 821 (2009) [arXiv:0809.5268 [astro-ph]]. 118

[238] J. Lavalle, J. Pochon, P. Salati and R. Taillet, Astron. Astrophys. **462**, 827 (2007) [astro-ph/0603796]. 118

[239] J. Lavalle, Q. Yuan, D. Maurin and X. J. Bi, Astron. Astrophys. **479**, 427 (2008) [arXiv:0709.3634 [astro-ph]]. 118

[240] L. Pieri, J. Lavalle, G. Bertone and E. Branchini, Phys. Rev. D **83**, 023518 (2011) [arXiv:0908.0195 [astro-ph.HE]]. 118

[241] C. R. Chen and F. Takahashi, JCAP **0902**, 004 (2009) [arXiv:0810.4110 [hep-ph]]. K. Ishiwata, S. Matsumoto and T. Moroi, Phys. Lett. B **675**, 446 (2009) [arXiv:0811.0250 [hep-ph]]. A. Ibarra and D. Tran, JCAP **0902**, 021 (2009) [arXiv:0811.1555 [hep-ph]]. C. R. Chen, M. M. Nojiri, F. Takahashi and T. T. Yanagida, Prog. Theor. Phys. **122**, 553 (2009) [arXiv:0811.3357 [astro-ph]]. E. Nardi, F. Sannino and A. Strumia, JCAP **0901**, 043 (2009) [arXiv:0811.4153 [hep-ph]]. 118

[242] M. Ibe, H. Murayama and T. T. Yanagida, Phys. Rev. D **79**, 095009 (2009) [arXiv:0812.0072 [hep-ph]]. 118

[243] M. Cirelli, Pramana **79**, 1021 (2012) [arXiv:1202.1454 [hep-ph]]. 118

[244] D. J. Phalen, A. Pierce and N. Weiner, Phys. Rev. D **80**, 063513 (2009) [arXiv:0901.3165 [hep-ph]]. 118

[245] P. J. Fox and E. Poppitz, Phys. Rev. D **79**, 083528 (2009) [arXiv:0811.0399 [hep-ph]]. 118

[246] P. Blasi and E. Amato, arXiv:1007.4745 [astro-ph.HE]. 118

[247] C. S. Shen, Astrophys. J., **162** , L181 (1970). 118

[248] S. Profumo, Central Eur. J. Phys. **10**, 1 (2011) [arXiv:0812.4457 [astro-ph]]. 118, 119

[249] J. Chang, J. H. Adams, H. S. Ahn, G. L. Bashindzhagyan, M. Christl, O. Ganel, T. G. Guzik, J. Isbert, K. C. Kim, E. N. Kuznetsov, et al., Nature (London) **456**, 362 (2008) 118

[250] A. A. Abdo *et al.* [Fermi LAT Collaboration], Phys. Rev. Lett. **102**, 181101 (2009) [arXiv:0905.0025 [astro-ph.HE]]. 119

[251] M. Aguilar *et al.* [AMS Collaboration], Phys. Rev. Lett. **110**, no. 14, 141102 (2013). 119

[252] M. Ackermann *et al.* [Fermi LAT Collaboration], Phys. Rev. Lett. **108**, 011103 (2012) [arXiv:1109.0521 [astro-ph.HE]]. 119

[253] R. L. Golden *et al.* [WIZARDS Collaboration], Astrophys. J. **457**, L103 (1996). 119, 120

[254] S. W. Barwick *et al.* [HEAT Collaboration], Astrophys. J. **482**, L191 (1997) [astro-ph/9703192]. 119, 120

[255] I. V. Moskalenko and A. W. Strong, Astrophys. J. **493**, 694 (1998) [astro-ph/9710124]. 119, 120

[256] M. Aguilar *et al.* [AMS Collaboration], Phys. Rev. Lett. **113**, 121102 (2014). 120

[257] M. Boudaud, S. Aupetit, S. Caroff, A. Putze, G. Belanger, Y. Genolini, C. Goy and V. Poireau *et al.*, arXiv:1410.3799 [astro-ph.HE]. 120

[258] G. Tomar, S. Mohanty and S. Rao, arXiv:1306.3646 [hep-ph]. 120, 181

[259] C. Weniger, JCAP **1208**, 007 (2012) [arXiv:1204.2797 [hep-ph]]. 120, 181

[260] E. Tempel, A. Hektor and M. Raidal, JCAP **1209** (2012) 032 [Addendum-ibid. **1211** (2012) A01] [arXiv:1205.1045 [hep-ph]]. 120

[261] M. Su and D. P. Finkbeiner, arXiv:1206.1616 [astro-ph.HE]. 120

[262] A. Hektor, M. Raidal and E. Tempel, Astrophys. J. **762**, L22 (2013) [arXiv:1207.4466 [astro-ph.HE]]. 120

[263] T. Bringmann, X. Huang, A. Ibarra, S. Vogl and C. Weniger, JCAP **1207**, 054 (2012) [arXiv:1203.1312 [hep-ph]]. 120

[264] S. Profumo and T. Linden, JCAP **1207**, 011 (2012) [arXiv:1204.6047 [astro-ph.HE]]. 120

[265] D. P. Finkbeiner, M. Su and C. Weniger, JCAP **1301**, 029 (2013) [arXiv:1209.4562 [astro-ph.HE]]. 120

[266] A. Hektor, M. Raidal and E. Tempel, Eur. Phys. J. C **73**, 2578 (2013) [arXiv:1209.4548 [astro-ph.HE]]. 120

[267] D. Whiteson, Phys. Rev. D **88**, no. 2, 023530 (2013) [arXiv:1302.0427 [astro-ph.HE]]. 120

[268] M. Su and D. P. Finkbeiner, arXiv:1207.7060 [astro-ph.HE]. 120

[269] T. E. Jeltema and S. Profumo, Mon. Not. Roy. Astron. Soc. **450**, no. 2, 2143 (2015) [arXiv:1408.1699 [astro-ph.HE]]. 121

[270] T. Higaki, K. S. Jeong and F. Takahashi, arXiv:1402.6965 [hep-ph]. 121

[271] K. Kong, J. -C. Park and S. C. Park, arXiv:1403.1536 [hep-ph]. 121

[272] K. Nakayama, F. Takahashi and T. T. Yanagida, arXiv:1403.1733 [hep-ph]. 121

[273] R. Krall, M. Reece and T. Roxlo, arXiv:1403.1240 [hep-ph]. 121

[274] A. Djouadi *et al.* [MSSM Working Group Collaboration], hep-ph/9901246. 122

[275] S. S. AbdusSalam, B. C. Allanach, F. Quevedo, F. Feroz and M. Hobson, Phys. Rev. D **81**, 095012 (2010) [arXiv:0904.2548 [hep-ph]]. 122

[276] P. Bechtle, K. Desch, W. Porod and P. Wienemann, Eur. Phys. J. C **46**, 533 (2006) [hep-ph/0511006]. 122

[277] F. Gabbiani, E. Gabrielli, A. Masiero and L. Silvestrini, Nucl. Phys. B **477**, 321 (1996) [hep-ph/9604387]. 123

[278] G. Belanger, F. Boudjema, A. Pukhov and A. Semenov, Comput. Phys. Commun. **176**, 367 (2007) [hep-ph/0607059]; Nuovo Cim. C **033N2**, 111 (2010) [arXiv:1005.4133 [hep-ph]]; G. Belanger, F. Boudjema, P. Brun, A. Pukhov, S. Rosier-Lees, P. Salati and A. Semenov, Comput. Phys. Commun. **182**, 842 (2011) [arXiv:1004.1092 [hep-ph]]. 123, 196

[279] G. Belanger, F. Boudjema and A. Pukhov, arXiv:1402.0787 [hep-ph]. 124, 125

[280] J. S. Lee et al., Comput. Phys. Commun. **156**, 283 (2004). 124

[281] N. D. Christensen and C. Duhr, Comput.Phys.Commun. 180, 1614 (2009). 124

[282] F. Staub, Comput. Phys. Commun. **182**, 808 (2011) [arXiv:1002.0840 [hep-ph]]. 124

[283] F. Staub, Comput. Phys. Commun. **185**, 1773 (2014) [arXiv:1309.7223 [hep-ph]]. 124

[284] U. Ellwanger and C. Hugonie, Comput. Phys. Commun. **175**, 290 (2006) [hep-ph/0508022]. 124

[285] J. Da Silva, arXiv:1312.0257 [hep-ph]. 126

[286] E. Aprile [XENON1T Collaboration], arXiv:1206.6288 [astro-ph.IM]. 127

[287] R. Aaij *et al.* [LHCb Collaboration], arXiv:1211.2674 [hep-ex]. 127, 129

[288] Y. Amhis *et al.* [Heavy Flavor Averaging Group Collaboration], arXiv:1207.1158 [hep-ex]. 127, 129

[289] A. Menon, D. E. Morrissey and C. E. M. Wagner, Phys. Rev. D **70**, 035005 (2004) [hep-ph/0404184]. 128, 129

[290] J. Abdallah *et al.* [DELPHI Collaboration], Eur. Phys. J. C **31**, 421 (2003) [hep-ex/0311019]. 127, 130, 134, 138

[291] The LEP Electroweak Working Group (http://lepewwg.web.cern.ch/LEPEWWG/) 129

[292] J. Beringer *et al.* (Particle Data Group), Phys. Rev. D **86**, 010001 (2012). 130

[293] H. K. Dreiner, S. Heinemeyer, O. Kittel, U. Langenfeld, A. M. Weber and G. Weiglein, Eur. Phys. J. C **62**, 547 (2009) [arXiv:0901.3485 [hep-ph]]. 130

[294] D. Hooper, T. Plehn, Phys. Lett. B562, 18 (2003) [hep-ph/0212226]. 130

[295] A. Bottino, F. Donato, N. Fornengo and S. Scopel, Phys. Rev. D **68**, 043506 (2003) [hep-ph/0304080]. 131

[296] G. Belanger, F. Boudjema, A. Cottrant, A. Pukhov and S. Rosier-Lees, JHEP **0403**, 012 (2004) [hep-ph/0310037]. 131

[297] J. S. Lee and S. Scopel, Phys. Rev. D **75**, 075001 (2007) [hep-ph/0701221 [hep-ph]]. 131

[298] G. Aad *et al.* [ATLAS Collaboration], Phys. Lett. B **716**, 1 (2012) [arXiv:1207.7214 [hep-ex]]. 131

[299] S. Chatrchyan *et al.* [CMS Collaboration], Phys. Lett. B **716**, 30 (2012) [arXiv:1207.7235 [hep-ex]]. 131

[300] P. Grothaus, M. Lindner and Y. Takanishi, arXiv:1207.4434 [hep-ph]. 131

[301] J. R. Ellis, S. F. King and J. P. Roberts, JHEP **0804**, 099 (2008) [arXiv:0711.2741 [hep-ph]]. 131

[302] D. Horton and G. G. Ross, Nucl. Phys. B **830**, 221 (2010) [arXiv:0908.0857 [hep-ph]]. 131

[303] M. Perelstein and B. Shakya, JHEP **1110**, 142 (2011) [arXiv:1107.5048 [hep-ph]]. 131

[304] A. Arbey, M. Battaglia and F. Mahmoudi, Eur. Phys. J. C **72**, 1847 (2012) [arXiv:1110.3726 [hep-ph]]. 131

[305] A. Arbey, M. Battaglia and F. Mahmoudi, Eur. Phys. J. C **72**, 1906 (2012) [arXiv:1112.3032 [hep-ph]]. 131

[306] M. W. Cahill-Rowley, J. L. Hewett, A. Ismail and T. G. Rizzo, arXiv:1211.1981 [hep-ph]. 131

[307] S. Amsel, K. Freese and P. Sandick, JHEP **1111**, 110 (2011) [arXiv:1108.0448 [hep-ph]]. 131

[308] P. Bechtle *et al.*, JHEP **1206**, 098 (2012) [arXiv:1204.4199 [hep-ph]]. 131

[309] M. W. Cahill-Rowley, J. L. Hewett, A. Ismail and T. G. Rizzo, Phys. Rev. D **86**, 075015 (2012) [arXiv:1206.5800 [hep-ph]]. 131

[310] M. Perelstein and B. Shakya, arXiv:1208.0833 [hep-ph]. 131

[311] H. Baer, V. Barger, P. Huang, D. Mickelson, A. Mustafayev and X. Tata, arXiv:1210.3019 [hep-ph]. 131

[312] S. Antusch, L. Calibbi, V. Maurer, M. Monaco and M. Spinrath, JHEP **1301**, 187 (2013) [arXiv:1207.7236 [hep-ph]]. 131

[313] I. Gogoladze, F. Nasir and Q. Shafi, arXiv:1212.2593 [hep-ph]. 131

[314] G. Aad *et al.* [ATLAS Collaboration], Phys. Lett. B **718**, 879 (2013) [arXiv:1208.2884 [hep-ex]]. 138

[315] C. Boehm, P. S. B. Dev, A. Mazumdar and E. Pukartas, JHEP **1306**, 113 (2013) [arXiv:1303.5386 [hep-ph]]. 142

[316] A. Arbey, M. Battaglia and F. Mahmoudi, Eur. Phys. J. C **72**, 2169 (2012) doi:10.1140/epjc/s10052-012-2169-9 [arXiv:1205.2557 [hep-ph]]. 144, 190

[317] A. Arbey, M. Battaglia and F. Mahmoudi, Phys. Rev. D **88**, 095001 (2013) [arXiv:1308.2153 [hep-ph]]. 144, 190

[318] R. Allahverdi, A. Kusenko and A. Mazumdar, JCAP **0707**, 018 (2007) [hep-ph/0608138]. 146

[319] R. Allahverdi, B. Dutta and A. Mazumdar, Phys. Rev. D **75**, 075018 (2007) [hep-ph/0702112]. 147, 152

[320] R. Allahverdi, B. Dutta and Y. Santoso, Phys. Rev. D **82**, 035012 (2010) [arXiv:1004.2741 [hep-ph]]. 147

[321] K. Enqvist, A. Mazumdar and P. Stephens, JCAP **1006**, 020 (2010) [arXiv:1004.3724 [hep-ph]]. 149

[322] J. C. Bueno Sanchez, K. Dimopoulos and D. H. Lyth, JCAP **0701**, 015 (2007) [hep-ph/0608299]. 149, 150

[323] D. H. Lyth, JCAP **0704**, 006 (2007) [hep-ph/0605283]. 149

[324] R. Allahverdi, A. Ferrantelli, J. Garcia-Bellido and A. Mazumdar, Phys. Rev. D **83**, 123507 (2011) [arXiv:1103.2123 [hep-ph]]. 151

[325] A. Chatterjee and A. Mazumdar, JCAP **1109**, 009 (2011) [arXiv:1103.5758 [hep-ph]]. 163

[326] R. Allahverdi, B. Dutta and A. Mazumdar, Phys. Rev. Lett. **99**, 261301 (2007) [arXiv:0708.3983 [hep-ph]]. A. Mazumdar and S. Morisi, arXiv:1201.6189 [hep-ph]. 163

[327] A. Riotto and M. Trodden, Ann. Rev. Nucl. Part. Sci. **49**, 35 (1999) [hep-ph/9901362]. 164

[328] A. D. Dolgov, and Ya. B. Zeldovich, Rev. Mod. Phys.**53**, 1 (1981). 165

[329] H. Murayama, Phys. Lett. B **597**, 73 (2004) [hep-ph/0307127]. 165

[330] J. M. Cline, hep-ph/0609145. 165

[331] K. Enqvist and A. Mazumdar, Phys. Rept. **380**, 99 (2003) [hep-ph/0209244]. 167

[332] R. H. Brandenberger, A. C. Davis, T. Prokopec and M. Trodden, Phys. Rev. D **53**, 4257 (1996) [hep-ph/9409281]. 167

[333] R. H. Brandenberger and A. C. Davis, Phys. Lett. B **308**, 79 (1993) [astro-ph/9206001]. 167

[334] M. Carena, G. Nardini, M. Quiros and C. E. M. Wagner, JHEP **1302**, 001 (2013) [arXiv:1207.6330 [hep-ph]]. 167, 185

[335] G. 't Hooft, Phys. Rev. Lett. **37**, 8 (1976). 168, 170

[336] https://en.wikipedia.org/wiki/Gauge_anomaly 168

[337] M. van der Meulen, D. Sexty, J. Smit and A. Tranberg, JHEP **0602**, 029 (2006) [hep-ph/0511080]. 169

[338] V. A. Kuzmin, V. A. Rubakov and M. E. Shaposhnikov, Phys. Lett. B **155**, 36 (1985). 170

[339] P. B. Arnold and L. D. McLerran, Phys. Rev. D **37**, 1020 (1988). 170

[340] M. Dine and A. Kusenko, Rev. Mod. Phys. **76**, 1 (2003) doi:10.1103/RevModPhys.76.1 [hep-ph/0303065]. 170

[341] P. B. Arnold, D. Son and L. G. Yaffe, Phys. Rev. D **55**, 6264 (1997) doi:10.1103/PhysRevD.55.6264 [hep-ph/9609481]. 170

[342] L. Dolan and R. Jackiw, Phys. Rev. D **9** 12 (1974) 171, 208

[343] D. E. Morrissey and M. J. Ramsey-Musolf, New J. Phys. **14**, 125003 (2012) [arXiv:1206.2942 [hep-ph]]. 172, 174

[344] K. Fanakubo, Progress of Theoretical Physics, Vol. 96, No. 3, (1996). 171

[345] V. A. Kuzmin, V. A. Rubakov, and M. E. Shaposhnikov, Phys. Lett. **155B**, 36 (1985); A. G. Cohen, D. B. Kaplan, and A. E. Nelson, Nucl. Phys. B **349**, 727 (1991); M. Joyce, T. Prokopec, and N. Turok, Phys. Lett. B **339**, 312 (1994). 172

[346] P. Huet and A. E. Nelson, Phys. Rev. D **53**, 4578 (1996); V. A. Rubakov and M. E. Shaposhnikov, Usp. Fiz. Nauk **166**, 493 (1996) [Phys. Usp. 39, 461 (1996)]; M. S. Carena and C. E. M. Wagner, arXiv:hep-ph/9704347; A. Riotto and M. Trodden, Annu. Rev. Nucl. Part. Sci. **49**, 35 (1999). 172

[347] J. M. Cline, M. Joyce, and K. Kainulainen, Phys. Lett. B **417**, 79 (1998); J. M. Cline, M. Joyce, and K. Kainulainen,J. High Energy Phys. **07** (2000) 018; M. Quiros, Acta Phys. Pol. B 38, **3661** (2007) . 172

[348] K. Kajantie, M. Laine, K. Rummukainen, and M. E. Shaposhnikov, Nucl. Phys. B **466**, 189 (1996). 172

[349] M. Carena, N. R. Shah and C. E. M. Wagner, Phys. Rev. D **85**, 036003 (2012) 175, 187, 192

[350] L. Dolan and R. Jackiw, Phys. Rev. D **9**, 3320 (1974). 176, 211

[351] http://oeis.org/A001620 176

[352] S. Abel, S. Khalil and O. Lebedev, Nucl. Phys. B **606**, 151 (2001) [hep-ph/0103320]. 179

[353] D. Bailin and A. Love, *Cosmology in Gauge Field Theory and String Theory*, IOP Publishing, 2004. 211

[354] J. Kapusta and C. Gale, *Finite temperature field theory*, Cambridge Univ. Press, 2006. 211